IRE Transactions

on ANTENNAS and PROPAGATION

Volume AP-4 **OCTOBER 1956** **Number 4**
Published Quarterly

TABLE OF CONTENTS

PUBLISHED BY THE
Professional Group on Antennas and Propagation

IRE TRANSACTIONS® PGAP IS A QUARTERLY PUBLICATION DEVOTED TO EXPERIMENTAL AND THEORETICAL PAPERS ON ANTENNAS AND WIRELESS PROPAGATION OF ELECTROMAGNETIC WAVES

MANUSCRIPTS should be submitted to John B. Smyth, Editor, SRA, 3930 4th Avenue, San Diego 3, California. Manuscripts should be original typewritten copy, double spaced, plus one carbon copy. References should appear as footnotes and include author's name, title, journal, volume, initial and final page numbers, and date. Each paper must have an abstract of not more than 200 words. News items concerning PGAP members and group activities should be sent to the News Editor, Mr. H. A. Finke, Polytechnic Research and Development Company, 55 Johnson Street, Brooklyn, New York.

ILLUSTRATIONS should be submitted as follows: All line drawings (graphs, charts, block diagrams, cutaways, etc.) should be inked uniformly and ready for reproduction. If commercially printed grids are used in graph drawings, author should be sure printer's ink is of a color that will reproduce. All half-tone illustrations (photographs, wash, airbrush, or pencil renderings, etc.) should be clean and ready to reproduce. Photographs should be glossy prints. Call-outs or labels should be marked on a registered tissue overlay, not on the illustration itself. No illustration should be larger than 8 x 10 inches.

Copies can be purchased from
THE INSTITUTE OF RADIO ENGINEERS
1 East 79 St., New York 21, N.Y.

PRICE PER COPY: members of the Professional Group on Antennas and Propagation, $2.10; members of the IRE, $3.15; nonmembers, $6.30.

ANNUAL SUBSCRIPTION PRICE: IRE members, $8.50; Colleges and public libraries, $10.00; nonmembers, $17.00.

Entered as second-class matter, at the post office at Menasha, Wisconsin, under the act of August 24, 1912. Acceptance for mailing at a special rate of postage is provided for in the act of February 28, 1925, embodied in Paragraph 4, Section 412, P. L. & R., authorized October 26, 1927.

A Notice to Readers

Because the cost of publishing the proceedings of the Electromagnetic Wave Theory Symposium (vol. AP-4, no. 3; July, 1956) exceeded expectations, the funds of the PGAP were temporarily depleted. As a result, six papers originally scheduled to appear in the present issue had to be withdrawn in order to maintain the year-end treasury balance in the black. The withdrawn papers will be added to the January, 1957 issue. We apologize to the authors for this unavoidable and unexpected delay.

—*The Editor*

news and views

Message from the Secretary

I would like to report several items pertaining to our present activity. Each year there are, of course, several changes in the membership of the PGAP Administrative Committee. The following is a list of members with their responsibilities and the dates at which the various terms of office expire.

Honorary Member

Lester C. Van Atta, Hughes Research Laboratory, Culver City, Calif. (Indefinite term: an honor accorded the PGAP founder)

Members Ex-Officio—(Past chairmen continue as members ex-officio for three years after their term.)

Philip S. Carter, Radio Corporation of America, Rocky Point, N.Y.—*Development of PGAP* (1957).

Delmer C. Ports, Jansky and Bailey, Washington, D.C. —*Development of PGAP* (1959).

Regular Members

John I. Bohnert, Naval Research Laboratory, Washington D.C.—*Vice-Chairman* (1958).

Henry C. Booker, Cornell University, Ithaca, N. Y.—*Chairman* (1958).

Arthur Dorne, Dorne and Margolin, Inc., 30 Sylvester Street, Westbury N. Y.—*News and Views Editor and PGAP Representative to National Convention Program Committee.*

Frederick T. Haddock, University of Michigan, Ann Arbor, Mich.—*Not yet assigned* (1959).

Robert A. Helliwell, Stanford University, Stanford, Calif.—*Membership* (1957).

Jack W. Herbstreit, National Bureau of Standards, Boulder, Colo.—*Not yet assigned* (1959).

Donald D. King, Radiation Laboratory, Johns Hopkins University, Baltimore, Md.—*Promotion of Local Chapter Organization and Activity* (1958).

Robert L. Mattingly, Bell Telephone Laboratory, Whippany, N. J.—*Secretary-Treasurer and Public Relations Man Responsible for Publication of Promotional Information in Other Technical Journals* (1959).

Victor H. Rumsey, University of Illinois, Urbana, Ill.—*Propagation Papers Procurement* (1957).

John B. Smyth, Smyth Research Associates, 3930 Fourth Avenue, San Diego, Calif.—Transactions *Editor* (1958).

Roy C. Spencer, Sylvania Electric Products, 100 First Street, Waltham, Mass.—Transactions-Proceedings *Liaison* (1957).

Archie W. Straiton, University of Texas, Austin, Tex.—*Antenna Papers Procurement* (1957).

A recent ruling of the Administrative Committee will make available the roster of the PGAP membership (2211, of which 276 are students as of September 30) to any organization which is currently subscribing to a year's institutional listing in our Transactions. The charge for this information will be nominal.

Our PGAP local chapters are continuing to grow in number. At present there are eight in existence and two more sections, Syracuse, N. Y. and Akron, Ohio, have expressed an interest in this affiliation. Items from six of these chapters will be found in the next section, "Chapter News." The other two sections are Albuquerque, N. M. and Orange Belt, Calif. The chairmen of these chapters from whom information regarding their activity may be obtained are respectively, G. Oltman, Sandia Corporation, Albuquerque, N. M. and T. J. Gibban, 204 Princeton Avenue, Claremont, Calif.

We have received many acknowledgments from foreign libraries attesting to the effectiveness of our policy of introducing our TRANSACTIONS into these libraries on a complementary basis.

ROBERT L. MATTINGLY

CHAPTER NEWS

Chicago Section

The first meeting for the 1956–1957 season of the Chicago Chapter of the PGAP was held on Friday, October 19, at the Western Society of Engineers Building, 84 East Randolph Street. This was a field trip through WGN-TV's new television station on top of the Prudential Building. They are operating at maximum power of 316kw erp or as they say "the highest power from the highest tower."

The next meeting of the chapter will be November 16 at the Western Society of Engineers Building at which time Dr. R. F. H. Yang of Andrew Corporation will give a talk on "The Development of Microwave Antennas."

Denver-Boulder Chapter

On May 23, 1956, the Denver-Boulder Chapter of the PGAP celebrated the completion of its first operating year.

The activities marking the anniversary began with a technical meeting, open to the public, held at the Radio Building of the NBS, Boulder Laboratories, and concluded with an annual meeting and evening banquet for members at the Memorial Building of the University of Colorado. A reception was held between the two events for members of the PGAP and their friends, at the home of Dr. and Mrs. E. K. Smith.

The technical session featured Dr. A. D. Wheelon of the Ramo-Wooldridge Corporation of Los Angeles. Dr. Wheelon spoke on the subject of certain theoretical aspects of scatter propagation. The meeting concluded with the showing of slides taken during visits to England and other European countries by Drs. Wait and Cottony.

The chapter has held meetings frequently since then at the National Bureau of Standards with Dr. James Wait of NBS, Chapter Chairman, presiding. The most recent of these were as follows:

July 19, 1956—A paper entitled, "A Survey of Current Ionospheric Research at the Cavendish Laboratory," was presented by Dr. Glenn Keitel, physicist, recently Fulbright Fellow at Cavendish Laboratory, Cambridge University, England.

August 8, 1956—"Recent RDF Research at the University of Illinois," a paper by Dr. Harold D. Webb, Associate Professor and Co-Supervisor of RDF Research, University of Illinois, was presented.

August 28, 1956—A paper entitled, "Turbulence in the Ionosphere" was presented by Dr. H. G. Booker, Professor of Electrical Engineering, at Cornell University.

Los Angeles Chapter

The Los Angeles Chapter of the PGAP held its September meeting jointly with the General IRE Section meeting for which it provided the speaker, Dr. L. C. Van Atta of Hughes Aircraft Company, who spoke on "Microwave Antenna Problems."

The newly elected officers of the group, Robert Elliott (Rantec Corp.), *Chairman;* Robert Spegen, *Vice-Chairman;* and Thomas Kinaga, *Secretary-Treasurer,* met with committee chairmen at an organizational meeting on October 11 to plan activities for the coming year.

Philadelphia Chapter

The first meeting of the Philadelphia Chapter will be held November 28, 1956. C. T. McCoy, of Philco, Research Division, will present a paper, entitled "Principals of Low Noise Microwave Receiver Design" with emphasis upon the microwave properties of crystals and their significance to antenna problems.

San Diego Chapter

An election was held for the next year's officers of the newly formed San Diego combined Professional Group of Antennas and Propagation and Microwave Theory and Techniques. Those elected were the following: Dr. John B. Smyth, *Chairman;* R. E. Honer, *Vice-Chairman;* W. L. Teeter, *Secretary.* Dave Proctor was temporary chairman.

Washington Chapter

The Washington Chapter of the Professional Group on Antennas and Propagation announces the election of the following officers for the 1956–1957 year: William W. Balwanz, of Naval Research Laboratory, *Chairman;* Harry Fine, of Federal Communications Commission, *Vice-Chairman;* Herschel T. Ward, of Melpar, Inc., *Secretary.* Terms of office will run concurrently with those of the Washington Section Officers.

RECENT MEETINGS

URSI

The Fall Meeting of the U.S.A. National Committee, URSI, was held October 11 and 12, 1956 at the University of California, Berkeley, Calif. The participating URSI National Commissions were: Commission 2, Radio and Troposphere—*Chairman,* Dr. J. B. Smyth; Commission 3, Ionospheric Radio—*Chairman,* Dr. M. G. Morgan; Commission 4, Radio Noise of Terrestrial Origin—*Chairman,* Prof. A. W. Sullivan.

There were three sessions held each day with a dinner and social evening on October 11 and a U.S.A. National Committee meeting on the evening of October 12.

Symposium on Optics and Microwaves

In cooperation with George Washington University, the Optical Society of America, and the Office of Naval

Research, the IRE Professional Group on Antennas and Propagation again presented an outstanding technical symposium in Lisner Auditorium, George Washington University, Washington, D. C., on November 14–16, 1956. Devoted to the subject of "Optics and Microwaves" the program comprised 24 papers and was arranged to emphasize many significant aspects of the two fields so that it might be clearly seen where they differ and where they are alike.

CCIR

The Eighth Plenary Assembly of the International Radio Consultative Committee (CCIR) was held in Warsaw, Poland, between August 9 and September 13, 1956.

It was well-attended and much good work was accomplished. There were in attendance some 400 delegates and supporting personnel from 41 countries which participate in this work.

The members of the United States delegation were designated from the representatives of government agencies and private companies and organizations who had participated in the preparatory work in the United States for the Eighth Plenary Assembly and are as follows: J. S. Cross, *Chairman;* E. W. Allen, *Vice-Chairman;* D. K. Bailey; E. W. Bemis; J. B. Coleman; W. Q. Crichlow; H. E. Dinger; Mrs. F. T. Dowling; L. W. Garvey; W. D. George; Miss Gertrude Grabowska; Mrs. J. G. Harris; J. W. Herbstreit; A. G. Jensen; Miss E. K. Kraft; W. Mason; A. G. Skrivseth; G. S. Turner; A. P. Walker; N. White, and F. H. Willis.

The scene of the conference was the Palace of Culture and Science, the 750-foot skyscraper which dominates the Warsaw skyline, in which excellent facilities were provided for the plenary sessions, for the meetings of the Study Groups which dealt with the specific technical questions considered by the Conference, and for the personal comfort and convenience of those in attendance at the Conference.

No attempt will be made here to discuss in detail the many technical questions which were considered, but some idea of their scope and significance can be obtained by referring to the titles of the fourteen Study Groups which have been organized to deal with them. In order they are: I—Transmitters; II—Receivers; III—Fixed Systems; IV—Ground-Wave Propagation; V—Tropospheric Propagation; VI—Ionospheric Propagation; VII—Standard Frequency and Time Signals; VIII—Monitoring; IX—Radio Relay Systems; X—Broadcasting; XI—Television; XII—Tropical Broadcasting; XIII—Mobile Systems, and XIV—Vocabulary.

The work of these committees has been steadily increasing over the last few years to the extent that it was becoming difficult for the Study Groups to resolve the large number of problems confronting them during the short period of time available to them during the Plenary Assemblies. Consequently, it was agreed to reorganize the work so as to spread a large portion of the load to the three-year intervals between assemblies. This, together with some rearrangement of work assignments to the various Study Groups, should result in more effective operation of the committee.

The present Director of the CCIR, Dr. Balth van der Pol, is scheduled to retire on December 31, 1956. Six applications for the position were accepted and Dr. E. Metzler of Switzerland was elected as the new Director.

An invitation was extended to the CCIR to hold its Ninth Plenary Assembly in the United States and was accepted by acclamation. Although the exact time and place was not fixed, it will probably be held in either 1959 or 1960.

On the whole the contributions of the United States were well-received by the Assembly and served as the basis for many of the final documents adopted. The continued participation of the United States in future CCIR work will have a profound influence on telecommunication developments in other countries and will thus benefit the United States in the final analysis. The value of the CCIR as a forum for the exchange of views and information among the most qualified engineers and scientists of this and other countries should be recognized, and to this end, the CCIR should be supported by all those in the United States—both government and industry—concerned with the over-all improvement and advancement of communications.

E. W. Allen, Ch. Eng.
Federal Communication Commission
Washington D. C.

Future Meetings

Symposium on Very-Low-Frequency Propagation

This symposium, sponsored by the National Bureau of Standards and the Professional Group on Antennas and Propagation of the IRE, at NBS, Boulder, Colo. is to be held January 23–25, 1957. The following committees and their respective chairmen are responsible for its presentation:

Steering Committee—J. R. Wait
Local Arrangements—R. Silberstein
Finance—J. R. Johler
Publicity—C. H. Bragaw
Panel Discussions—T. N. Gautier and R. A. Helliwell
Regular Technical Papers—J. M. Watts and J. R. Wait.

F. W. Brown, K. A. Norton, and R. J. Slutz will be acting in an advisory capacity.

Persons wishing to attend this meeting should notify Mrs. M. Halter, NBS, Boulder, Colo., as soon as possible. Although papers will still be accepted until November 30, the program is essentially frozen now. The papers which have been accepted so far are listed on the next page. No more than one or two changes or additions are anticipated.

1) "Some Physical Problems in the Generation and Propagation of VLF Radiation" by E. L. Hill, Department of Physics, University of Minnesota.
2) "Studies of High Power VLF Antennas" by W. Gustafson and E. Devaney, U. S. Navy Electronics Laboratory, San Diego.
3) "Some Properties and Applications of Magneto-Ionic Theory at VLF" by R. A. Helliwell, Radio Propagation Laboratory, Stanford University.
4) "The Relation Between Group Delay of a Whistler and the Distribution of Ionization Along the Ray Path" by R. L. Smith, Radio Propagation Laboratory, Stanford University.
5) "Measurement and Interpretation of the Polarization and Angle of Arrival of Whistlers" by J. H. Crary, Radio Propagation Laboratory, Stanford University.
6) "The Effect of the Earth's Magnetic Field on the Transmission and Reflection of VLF Waves at the Lower Edge of the Ionosphere" by I. Yabroff, Radio Propagation Laboratory, Stanford University.
7) "Records of VLF Hiss at Boulder, Colorado, During 1956" by J. M. Watts, National Bureau of Standards, Boulder.
8) "Extra-Terrestrial Origins of VLF Signals" by R. Gallet, National Bureau of Standards, Boulder.
9) "Extensions to the Geometrical Optics of Sky Wave Propagation at VLF" by J. R. Wait and A. Murphy, National Bureau of Standards, Boulder.
10) "Wave Guide Mode Calculations for VLF Ionospheric Propagation Including the Influence of Ground Conductivity" by J. R. Wait and H. H. Howe, National Bureau of Standards, Boulder.
11) "A Study of Signal-Versus-Distance Data at VLF" by J. L. Heritage and S. Weisbrod of Smyth Research Associates and J. E. Bickel of U. S. Navy Electronics Laboratory.
12) "Basic Experimental Studies of the Magnetic Field of Electromagnetic Sources Immersed in a Semi-Infinite Conducting Medium" by M. B. Kraichman, U. S. Navy Ordnance Laboratory, White Oak, Silver Spring, Md.
13) "A Technique for the Rapid Analysis of Whistlers" by J. K. Grierson and L. R. O. Storey, Radio Physics Laboratory, Ottawa, Canada.
14) "A Method to Interpret the Dispersion Curves of Whistlers" by L. R. O. Storey, Radio Physics Laboratory, Ottawa, Canada.
15) "Relations Between the Character of Atmospherics and Their Place of Origin" by J. Chapman and E. T. Pierce, Cavendish Laboratory, Cambridge, England.
16) "Survey of Investigations of VLF Propagation at Cambridge" by K. G. Budden, Cavendish Laboratory, Cambridge, England.
17) "A Study of VLF Ground Wave Propagation in Alaska" by G. M. Stanley, Geophysical Institute, College, Alaska.
18) "The Phase and Group Velocity of the VLF Ground Wave" by J. R. Johler, National Bureau of Standards, Boulder.
19) "Polarization of the Ground Wave of a Radio Atmospheric" by A. W. Sullivan, University of Florida.
20) "Noise Investigation at VLF by the National Bureau of Standards" by W. O. Crichlow, National Bureau of Standards, Boulder.
21) "Spectrum Analysis of Spherics" by W. Taylor, National Bureau of Standards, Boulder.
22) "Statistical Descriptions of Atmospheric Radio Noise" by A. D. Watt, National Bureau of Standards, Boulder.
23) "On the Polarization of Spherics" by A. G. Jean, National Bureau of Standards, Boulder.
24) "The Effect of Receiver Band Width on the Amplitude Distribution of VLF Atmospheric Noise" by F. F. Fulton, Jr., National Bureau of Standards, Boulder.
25) "Our Present State of Knowledge of the Lower Ionosphere" by A. H. Waynick, Ionospheric Research Laboratory, State College, Pa.
26) "Heavy Ion Effects in Audio-Frequency Propagation" by C. O. Hines, Radio Physics Laboratory, Ottawa, Canada.
27) "Some Recent Measurements of Atmospheric Noise in Canada" by C. A. McKerrow, Radio Physics Laboratory, Ottawa, Canada.
28) "Performance and Design Criteria for High Power VLF Antennas" by W. M. Brown, Bureau of Ships, Washington, D. C.
29) "Ionospheric Irregularities Causing Random Fading of VLF " by S. A. Bowhill, Pennsylvania State University, University Park, Pa.
30) "75 Kc/Sec Pulsed Normal Incidence Ionospheric Sounding" by A. J. Ferraro, J. J. Gibbons, R. E. Houston, W. J. Ross, and E. R. Schmerling, Pennsylvania State University, University Park, Pa.
31) "A VLF Antenna for Generating a Horizontally Polarized Radiation Field" by R. S. Macmillan, R. M. Golden, and W. V. T. Rusch, California Institute of Technology, Pasadena, Calif.
32) "Artificial Generation of Low-Frequency Atmospheric Pulses" by M. M. Newman, Lightning and Transients Research Institute, Minneapolis, Minn.
33) "The Numerical Solution of the Differential Equations Governing the Reflexion of Long Radio Waves from the Ionosphere" by K. G. Budden, Cavendish Laboratory, University of Cambridge, Cambridge, England.

Symposium on Communication Theory and Antenna Design

The Air Force Cambridge Research Laboratories are co-sponsoring a Symposium on Communication Theory and Antenna Design with the Boston University, Physical Research Laboratories, to be held at Hillel House, Boston University, Boston, Mass., on January 9–11, 1957.

For further information write to: Miss Alice Cahill, CRRD, Hq. Air Force Cambridge Research Center, Air Research and Development Command, Laurence G. Hanscom Field, Bedford, Mass.

Following is the tentative program. There will probably be some additions, and there are two changes possibly to be made.

January 9, 1957

Morning

Registration: 9:00–9:30 A.M.

Opening Address: 9:30–9:45 A.M.—Dr. Duncan MacDonald, Boston University, Dr. L. M. Hollingsworth, AFCRC.

Keynote Talk—Dr. Roy C. Gunter, Jr., ARCRC-Clark University.

Mathematical Introduction I—Dr. Charles Bumer, Clark University.

Mathematical Introduction II—Dr. F. Sheppard Holt, AFCRC-Tufts University.

Afternoon

Application to Electronics I—Dr. Arthur Kohlenberg, Melpar, Inc.

Application to Electronics II—Dr. Peter Elias, Massachusetts Institute of Technology.

Evening

Symposium Banquet at Laurence G. Hanscom Field, Bedford, Mass.: 7:30 P.M.

Speaker: Col. Gordon T. Gould, Jr., Director, Communications and Electronics Division, Hq. Air Research and Development Command.

January 10, 1957

Morning

Application to Optics I—Dr. Edward O'Neill, Boston University.

Application to Optics II—Lt. George B. Parrent, Jr., AFCRC.

Afternoon

Electro-Optical Systems in Cascade—Dr. Otto Schade, Radio Corp. of America.

Application to Radio Astronomy I—Dr. R. N. Bracewell, Div. of Radio Physics, the Commonwealth Scientific and Industrial Research Organization, Australia.

Application to Radio Astronomy II—To be announced.

Evening

7:00 P.M. Discussion Group on the Application of Antenna Problems: Group Leader: Dr. Roy C. Spencer, Sylvania Electric Cor Products Corp.

January 11, 1957

Morning

Antennas I—Dr. John Ruze, AFCRC-Radiation Engineering Laboratory.

Antennas II—Dr. W. H. Stell, Div. of Physics, the Commonwealth Scientific and Industrial Research Organization, Australia.

Antennas III—To be announced.

Afternoon

Classified—Contributed Papers on Special Antenna Problems.

Other Notes

There is still time to select topics for a PGAP symposium at the IRE National Convention in March. Dr. J. T. Bolljahn, of Stanford Research Institute, who continues as PGAP Meetings Chairman, although he is no longer a member of the Administrative Committee, urges anyone with suggestions for suitable topics to communicate them to him as soon as possible.

The membership is reminded that material for publication in this department is always welcome. News about PGAP members, special events, activities, or University courses, as well as comments or opinions on PGAP affairs are all solicited. Such items should be sent to Arthur Dorne, News and Views Editor, Dorne and Margolin, 30 Sylvester St., Westbury, N. Y.

contributions

Circularly-Polarized Biconical Horns*

C. GOATLEY† AND F. D. GREEN†

Summary—A new technique is described for obtaining circular polarization from a biconical horn. This polarization is obtained through use of a spatial array of thin conducting elements between the cone faces; orientation of the elements varies with distance from the feed. The method has been used successfully at *S* band and *X* band.

This technique was applied to horns which have maximum radiation intensity in the plane normal to the cone axes as well as to other horns with beams tilted out of this plane. The beam tilt was obtained by an appropriate choice of cone configurations.

General Description

Feed System

THE BICONICAL horn is among the most versatile of omnidirectional antennas because of its simplicity of design and, with the appropriate type of feed, its excellent broadband characteristics. Early work on the antenna[1] showed that it could be designed for either horizontal or vertical polarization, the choice of which largely determines the type of feed required.

Excitation of the antenna to produce vertical polarization (TEM mode) requires the least complex feed arrangement. This feed is easily formed by flaring the inner and outer conductors of a coaxial transmission line so that the inner conductor joins the upper cone and the outer conductor joins the lower cone.

Horizontally polarized (TE_{01} mode) versions of the antenna can be obtained by utilizing feeds such as the loop, slotted waveguide, or tridipole. The remaining possibility to be discussed is that of producing circular or elliptical polarization.

The most straightforward approach to producing circular polarization would suggest the design of a circularly-polarized feed. The complexity of adaptable feed types made it desirable to find a simpler method. Accordingly, use was made of the flared coaxial feed, which is mechanically simple and inherently broadband, and the antenna was altered between the feed and the aperture to obtain circular polarization.

Depolarizing Elements

The method of obtaining elliptical and circular polarization is somewhat unconventional. It consists basically of interposing a dense array of thin, conducting elements on cylindrical plastic forms between the faces of the cones. Fig. 1 shows an *S*-band model of the antenna disassembled to view the array configuration. This model is 12 inches in diameter and 6 inches high. The cylinders are formed from thin polyethylene sheet material; the conducting elements are of silver paint applied with a Speedball pen.

Conducting elements on the innermost cylinder of the array are in a plane normal to the common axis of the cones, and those on succeeding cylinders are inclined in

* Manuscript received by the PGAP, October 27, 1955; revised manuscript received, July 16, 1956. Presented at the National Electronics Conference, Chicago, Ill., October, 1955.

† Melpar, Inc., Falls Church, Va.

[1] W. L. Barrow, L. J. Chu, and J. J. Jansen, "Biconical electromagnetic horns," PROC. IRE, vol. 27, pp. 769–779; December, 1939.

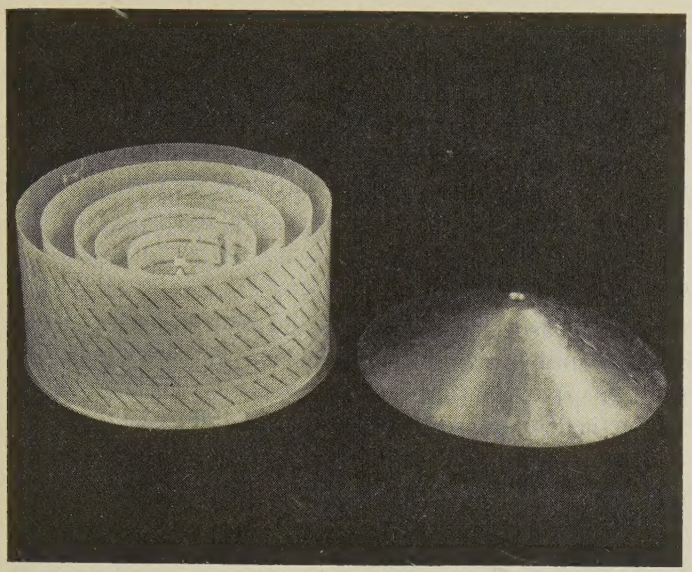

Fig. 1—*S*-band horn with depolarizing elements.

Experimental Data

Polarization

The alteration of the electric field caused by insertion of the elements is such that elliptical polarization of voltage axial ratio less than 5:1 is obtained over the frequency band from 2000–5200 mc and the polarization is very nearly circular over a limited frequency band centering at 3500 mc.

Polarization patterns of the antenna were measured by rotating a pyramidal waveguide horn in a plane normal to the direction of maximum radiation. This arrangement permits only the measurement of the polarization pattern and did not provide information on the relative phase of the field components to determine the sense of rotation of the resultant field vector.

Polarization patterns of the *S*-band horn measured at 3000 and 5000 mc are shown in Fig. 2(a) and 2(b). Characteristic of the patterns is a clockwise rotation of the

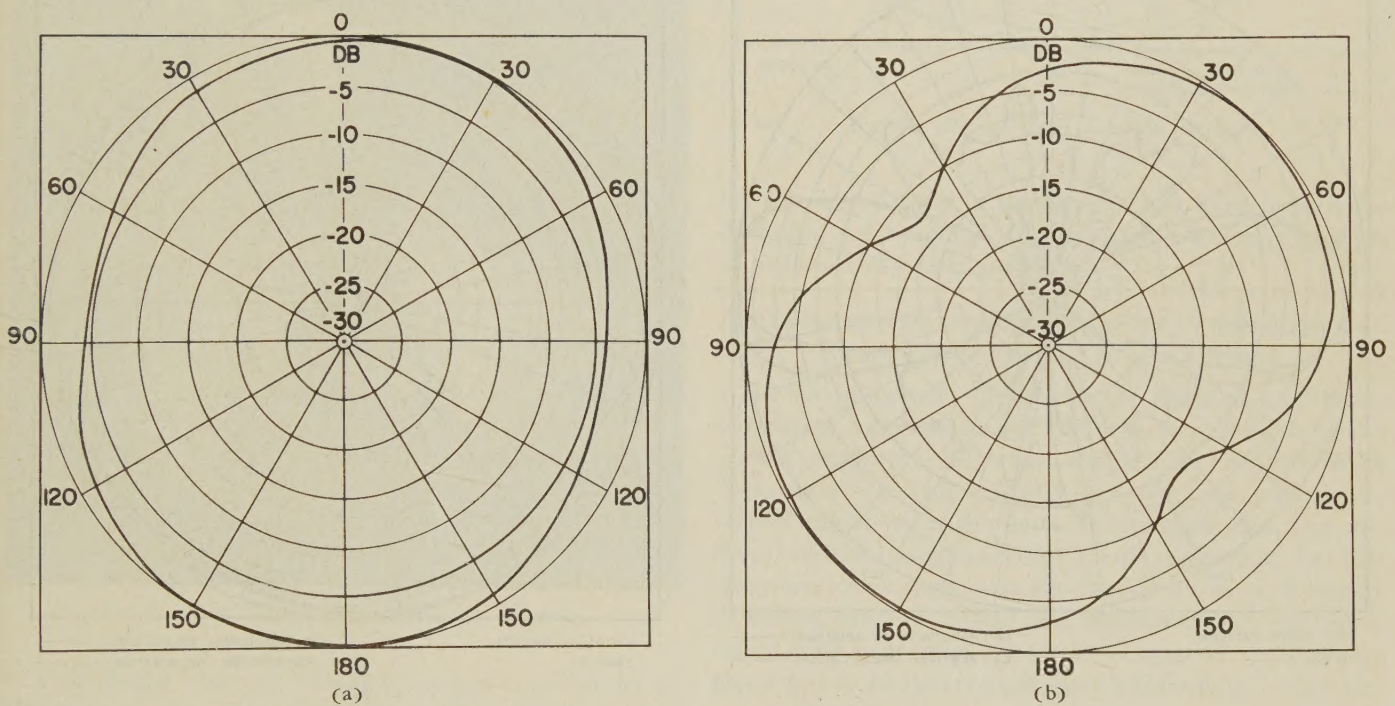

Fig. 2—(a) Polarization pattern—3000 mc. (b) Polarization pattern—5000 mc.

equal increments at progressively greater angles so that the elements on the outer cylinder are at 45°. The elements are one inch long (one-quarter wavelength at 3000 mc) and are evenly spaced about each row. The rows are symmetrically disposed above and below a centerline about the circumference of each cylinder. Center-to-center spacing between adjacent elements in a row is $\frac{3}{4}$ inches on the outer three cylinders and, to accommodate the desired element length, is extended to approximately twice that on the inner two cylinders. Radial spacing between each of the five cylinders is one inch.

axis with increasing frequency and a smooth variation in the axial ratio as a function of frequency. A graph of the axial ratio variation over a limited frequency band is shown in Fig. 3 and indicates the close approach to circular polarization at 3500 mc as measured in the plane of maximum radiation.

Radiation Patterns

Radiation patterns measured in the vertical and azimuth planes at 3500 mc are shown in Fig. 4(a) and 4(b) for both vertical and horizontal polarization. Patterns in the vertical plane showed slightly narrower

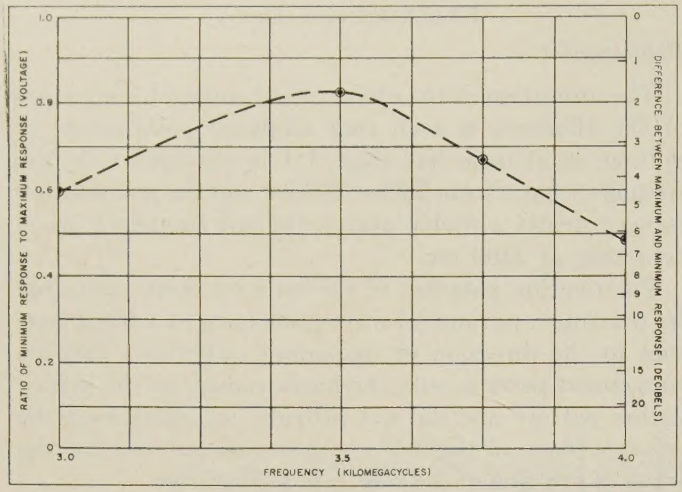

Fig. 3—Axial ratio variation with frequency.

Asymmetry in the patterns is believed to be largely due to imperfections in the experimental model such as joints in the plastic cylinders, irregularities in the metal cones, and slight eccentricities in the coaxial feed at the flare joints. These irregularities also show up as slight variations in the polarization patterns as measured at different azimuth positions around the horn.

Gain Measurement

Gain measurements were made on the antenna for vertical and horizontal polarization at three azimuth positions spaced 120° apart about the horn. The results for vertical polarization are given in Table I as measured at one azimuth position. Differences in the measured gain occur at different azimuth positions, as would be expected from an examination of the radiation patterns.

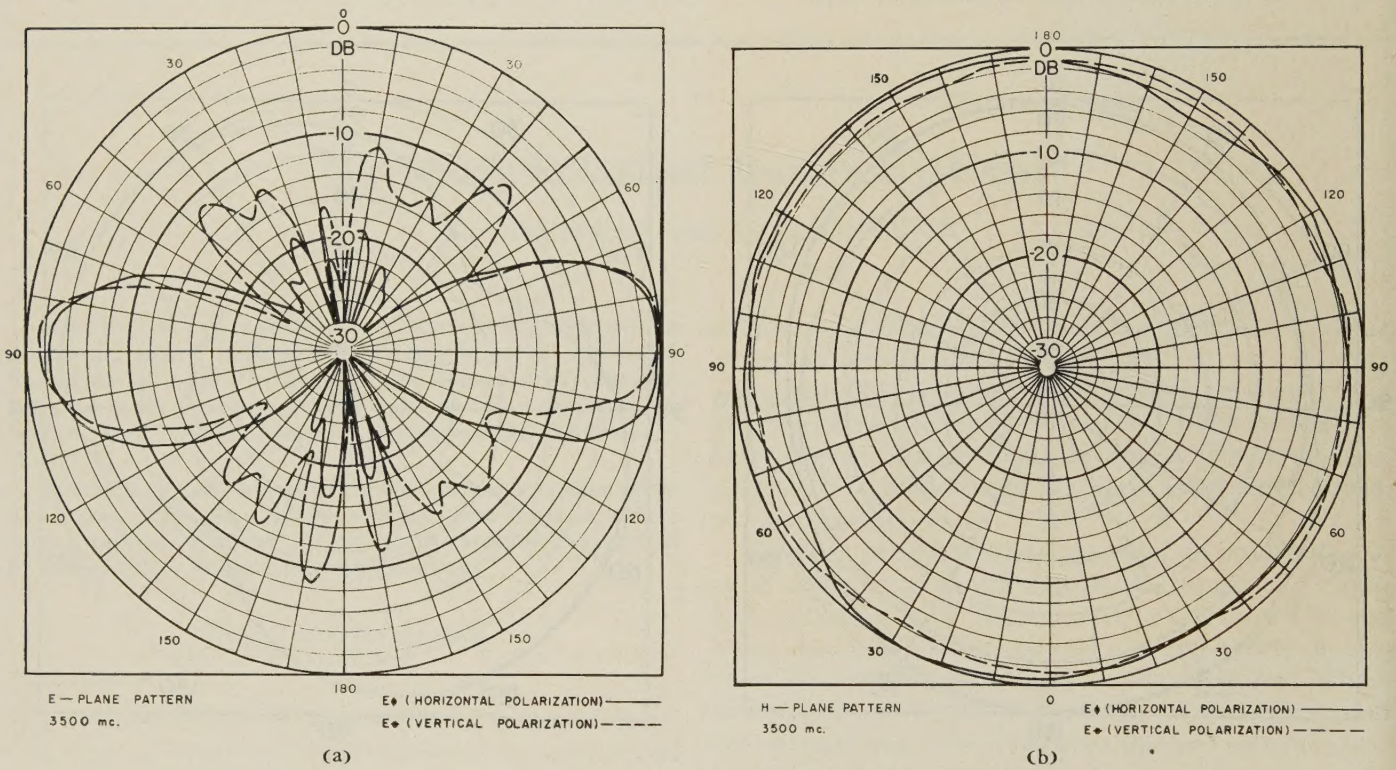

Fig. 4—(a) Vertical plane radiation pattern. (b) Azimuth plane radiation pattern.

beamwidths at all frequencies for vertically-polarized radiation than for horizontally-polarized radiation. Similarly, the sidelobe level is consistently lower for horizontal polarization over the entire frequency range. The narrower beamwidths, and to some extent the lower sidelobe level, can be attributed to the difference in aperture illumination for the two fields. The field producing vertical polarization illuminates the aperture of the horn uniformly while the field producing horizontal polarization is distributed sinusoidally across the aperture.

The values given in Table I are representative of values obtained at all three azimuth positions.

TABLE I

GAIN OF ANTENNA FOR VERTICALLY POLARIZED SIGNAL

Frequency (mc)	Gain Over Isotropic (db)
3000	1.46
3500	0.70
4000	−1.03
4500	1.20
5000	2.80
5500	2.05

Match characteristics of the *S*-band antenna are indicated by the vswr which remains less than 2:1 over a 2:1 frequency band.

Scaling and Beam Tilting

In order to achieve full utilization of the antenna, it was desirable to investigate the feasibility of tilting the beam out of the horizontal plane and scaling for use at other frequencies. Both endeavors were successful in scaling the antenna for use at *X* band, and the experimental model is shown in Fig. 5. When assembled, it is 10 inches in diameter and $2\frac{1}{2}$ inches high. The lower cone is replaced with a disk to achieve beam tilting.

Fig. 5—*X*-band horn with depolarizing elements.

This model also contains 5 cylinders constructed in the same manner as those used in the *S*-band model. The cylinders are separated radially by 0.3 inches. There are 5 rows of elements on the outer cylinder, 4 rows on each of the next 2, and 3 rows on each of the last 2 cylinders. Each element is 0.35 inches long, and center-to-center spacing between the elements is approximately 0.4 inches on all cylinders except the inner one where the spacing is increased to 0.5 inches. Vertical plane radiation pattern of the scaled model is shown in Fig. 6 as measured at 10,000 mc. Use of a single cone with a circular plate in place of the lower cone was sufficient to tilt the beam approximately 15° out of the horizontal plane. Polarization patterns show the same general characteristics as those measured with the *S*-band model, but it was found that element densities appreciably lower than used in this model tend to introduce undesirable variations in the polarization characteristics at different azimuth positions.

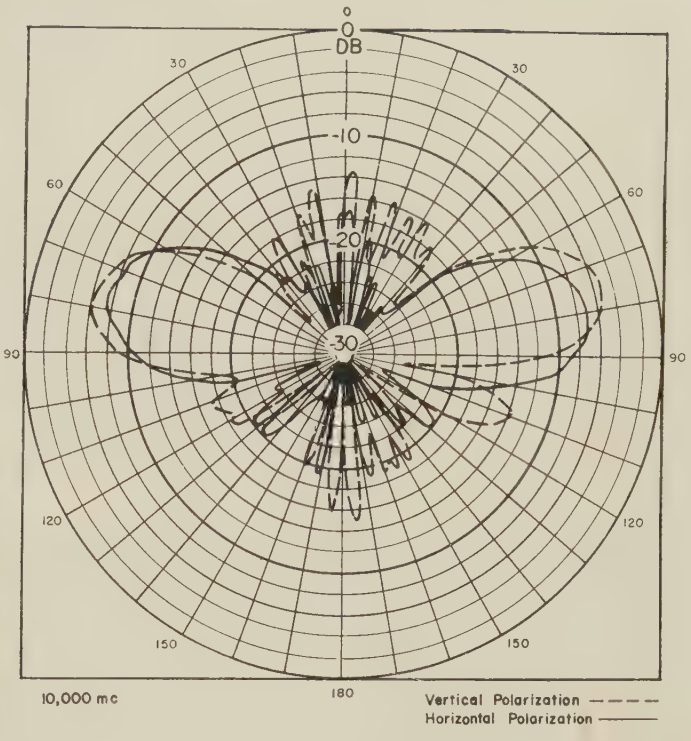

Fig. 6—Vertical plane radiation patterns.

Analysis of Phase Difference Between Vertical and Horizontal Field Components

All of the present designs of the antenna have been developed experimentally. Information which would permit design of a horn with predictable characteristics depends on knowing considerably more about the function of the array of elements. It is evident that the elements induce horizontal components of the field, but the complete array must also be considered as an artificial dielectric medium filling the space between the cone faces. The properties of certain types of artificial dielectrics can be determined analytically with a high degree of exactness. Such is not the case with an artificial dielectric consisting of thin conducting pins.[2] Empirical data on such a medium is available, but it does not appear to be directly applicable to the case where the pins vary in orientation through the medium. For this reason, an exact analysis of the mechanisms producing elliptical polarization from the antenna appears impractical. However, a qualitative analysis is useful to demonstrate why a phase difference is introduced between horizontal and vertical components of the field, and the concept of optical path length is convenient for this purpose. Fig. 7 shows a cross section of

[2] S. A. Schelkunoff and H. T. Friis, "Antenna Theory and Practice," John Wiley and Sons, Inc., New York, N. Y., pp. 577–579; 1952.

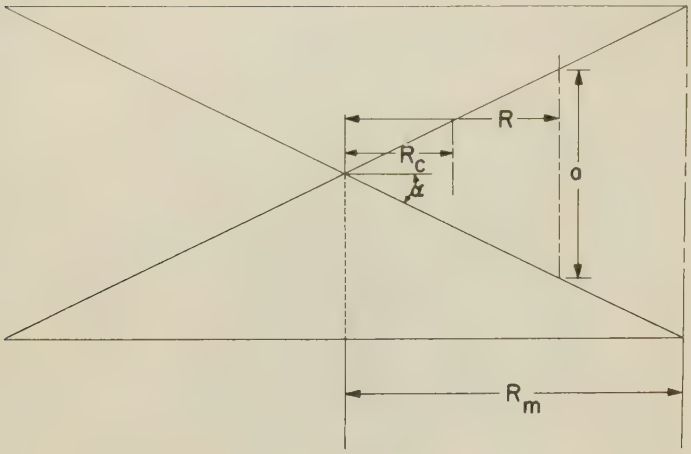

Fig. 7—Cross section of biconical horn.

the horn. R_c is the radius at which the cross section height, a, becomes too small to propagate the horizontal field components. Let n_H be the effective index of refraction[3] for the horizontally-polarized field component. For this component it may be shown that $n_H = \lambda_g/\lambda_e$ where λ_g is in effect the guide wavelength, and λ_e is the wavelength in a medium of index n_h. The value of n_h is assumed to vary as a function of radius because of the changing orientation of the elements forming the dielectric medium. From these considerations a general expression for n_h can be given in the form

$$n_h = f_h(R). \tag{1}$$

It follows immediately that

$$\lambda_e = \frac{\lambda}{f_h(R)} \tag{2}$$

where λ is the free-space wavelength.

The cutoff wavelength λ_c may also be obtained in terms of R from Fig. 7 and (1). Where $a = 2R \tan \alpha$, $\lambda_c = [4R \tan \alpha][f_h(R)]$, and

$$\frac{\lambda_g}{\lambda_e} = \frac{1}{\sqrt{1 - \left(\frac{\lambda_e}{\lambda_c}\right)^2}}, \tag{3}$$

the expression for the total index of refraction becomes

$$n_H = \frac{1}{\sqrt{1 - \left(\frac{\lambda}{[4R \tan \alpha][f_h(R)]^2}\right)^2}}. \tag{4}$$

The propagation velocity of the vertical field component depends only on the index of refraction of the dielectric medium. The index for that polarization can be immediately written in a general form as a function of R so that

$$n_v = f_v(R). \tag{5}$$

[3] The index of refraction equals the square root of the dielectric constant.

Since the optical path length is defined as $\int n\, dR$, the phase difference between the components can be obtained in the form

$$\theta = \frac{2\pi}{\lambda}\left(\int_0^{R_m} f_v(R)dR - \int_{R_c}^{R_m} \frac{dR}{\sqrt{1 - \left(\frac{\lambda}{[4R \tan \alpha][f_h(R)]^2}\right)^2}}\right). \tag{6}$$

Although the functions describing the effective index of refraction for either polarization are not explicitly defined, the form of (6) suggests that a phase difference should exist and that it will vary with frequency.

Some question must exist regarding the choice of R_c as the lower limit of the second integral since it involves the assumption that the horizontal field component is generated at R_c. Such an assumption must be considered to have limited validity, but investigation has not been extensive enough to determine an apparent phase-center for the horizontal component.

The relative amplitude of the field components is also dependent on the configuration of the array of elements, and it seems reasonable to expect that both orientation and density of the elements play a significant part. No investigation of this has been made experimentally or otherwise.

Applications of the Antenna

One of the most interesting possible uses for the depolarized horn was discussed in a recent paper by Kelleher and Morrow.[4] Their particular application consisted of employing the horn to feed a symmetrical toroidal lens which can be designed to shape the beam in the vertical plane. The probable appearance of such a system is shown in Fig. 8. At present its practicability seems limited only by the weight of the lens material.

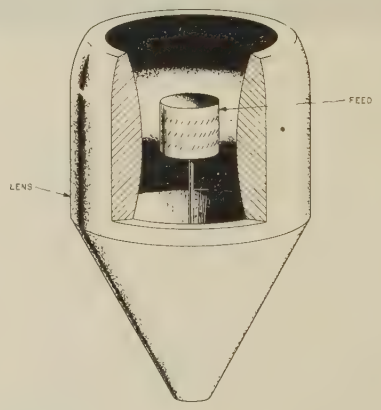

Fig. 8—Toroidal lens with horn feed.

Acknowledgment

The authors wish to thank K. S. Kelleher for his suggestions in the preparation of this paper.

[4] K. S. Kelleher and C. W. Morrow, "Omnidirectional circularly polarized antennas," 1955 IRE Convention Record, Part I, pp. 28–31.

Phase Centers of Microwave Antennas*

DAVID CARTER†

Summary—**This paper is concerned with the location of the phase centers of microwave antennas. The inadequacy of conventional aperture theory for the accurate description of phase centers is discussed. Formulas are developed and, for numerical indications, calculations are made for paraboloidal reflectors of different f/D ratios and a class of primary patterns which provide an approximate representation of a great many common feeds. The results are presented in graphical form to provide useful design information and show the dependence of principal E- and H-plane phase center location on feed and dish parameters. Contrary to the prediction of aperture theory, it is shown that the phase centers of axially symmetric antennas are not in the aperture plane, but they are dispersed about it.**

THERE IS a good deal of ambiguity on the location of the phase centers of microwave antennas. Different answers are obtained depending on the approach used. For some purposes, where antennas are rotated or used in interferometric systems, knowledge of phase center location is desirable and often necessary. For small antennas this information is rather easily measured in the laboratory. However, the large ranges required for the measurement of large aperture antennas at small wavelengths make such measurements exceedingly difficult. Reflections in the range, mechanical inaccuracies, etc., may well make accurate measurements impossible.

Theoretical calculations have been made to obtain phase distribution over the main lobe.[1] These calculations are based on the aperture distribution method of calculating far-field patterns[2–4] and show the phase and amplitude distributions in the far field for different assumed aperture-field distributions. While this theory satisfactorily predicts the far-field amplitude distributions for small angles off-axis, it cannot accurately locate the phase centers of real antennas.

The major difficulty is the fact that the total aperture-field distribution is generally not known and not used in the formulations referred to above. To obtain these formulations from information that might usually be known in microwave antennas, such as feed patterns (amplitude, phase and polarization) and reflector geometry, approximations are made which seriously affect the location of the phase center. In the first place the location of the "aperture" plane is somewhat arbitrary.[5]

If one employs the usual methods of geometrical optics, for example, to obtain the aperture-phase and amplitude distributions from a point source feed pattern and a paraboloid reflector,[6] one obtains the same distributions on any two parallel planes which are perpendicular to the axis of the reflector. Calculations of the far-field patterns from these aperture distributions by means of the Fraunhofer field approximation,[7]

$$U_p \simeq \frac{je^{-jkR}}{\lambda R} \int_A F(\xi, \eta) e^{j(k_x\xi + k_y\eta)} d\xi d\eta,$$

then would be identical and one would obtain phase centers differing in location by the axial separation of these two arbitrarily chosen planes. The notation used here is the same as that of S. Silver.[4] (See Fig. 1.)

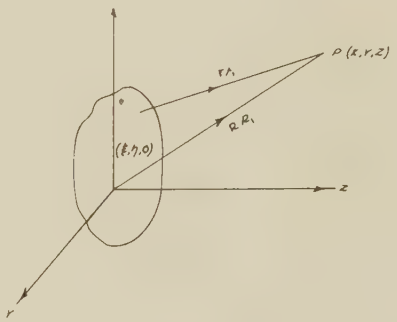

Fig. 1—Coordinate system. The origin is at the focal point of the reflector.

A second significant discrepancy occurs in the fact that there is no counterpart of the longitudinal component of reflector current in the aperture distribution.[8] This longitudinal component of current makes no significant contribution to the amplitude patterns at angles near the axis, and it has generally been neglected. However, it does contribute to the curvature of the far-field phase pattern and is, therefore, significant in the calculation of phase centers. For this reason, phase centers derived from the far-field patterns of representative aperture distributions,[9] will not coincide with the actual phase centers of the antennas represented by these aperture distributions. In fact it will be shown that paraboloids illuminated by point source feeds with axial symmetric patterns have principal plane phase centers which are not coincident and whose location depends on the feed and dish parameters. This is in contrast to the results of aperture theory which would pre-

* Manuscript received by the PGAP, November 10, 1955; revised manuscript received, July 30, 1956.

† San Jose State College, San Jose, Calif.

[1] C. C. Allen, "Radiation patterns for aperture antennas with nonlinear phase distributions," 1953 IRE Convention Record, Part 2, pp. 9–12.

[2] R. C. Spencer, "Fourier Integral Methods of Pattern Analysis," R. L. Rep. No. 762-1; January 21, 1956.

[3] H. T. Friis and W. D. Lewis, "Radar antennas," *Bell Sys. Tech. J.*, vol. 26, pp. 232–246; April, 1947.

[4] Silver, S., "Microwave Antenna Theory and Design," McGraw-Hill Book Co., Inc., New York, N. Y., 1949.

[5] *Ibid.*, p. 158.

[6] *Ibid.*, p. 419.

[7] *Ibid.*, p. 173.

[8] *Ibid.*, p. 420.

[9] Allen, *op. cit.*, p. 9.

dict coincident phase centers located in the aperture plane in such cases.

This latter statement follows directly from the fact that the Fourier transform of an even function is real. Thus the Fraunhofer field of an aperture distribution, $F(\xi, \eta)$, is given by[10]

$$U_p = \frac{j}{\lambda R} e^{-jkR} \int_{-\infty}^{\infty} \int_{-\infty}^{\infty} u(\xi, \eta) e^{j(k_x \xi + k_y \eta)} d\xi d\eta$$

where $u(\xi, \eta)$ vanishes everywhere except inside the aperture area, wherein it coincides with the aperture distribution. Since the integral is real if $u(\xi, \eta)$ is a real (except for an arbitrary complex constant) function even with respect to both of its arguments, the phase of U_p will be independent of direction, (θ, ϕ), except for discrete points when U_p passes through zero making the phase change by π radians. In the case of the paraboloid illuminated by a point source feed with axial symmetric patterns, having negligible cross-polarization component of reflected field, the aperture distribution of the principal polarization component is axially symmetric and phase constant.[11] Therefore the corresponding aperture distribution representation, $u(\xi, \eta)$ possesses more than enough symmetry to make its Fourier transform real. Hence the equiphase surface in the region of the main lobe in the Fraunhofer field is given by $kR =$ constant, which is a sphere with center at the origin of coordinates. Thus, for this example, the aperture distribution approximation predicts that there will be a single point phase center located at the origin which is taken at the center of the aperture plane.

To obtain a more accurate description of the phase center of such antennas, the phase distribution in the far field will be calculated from the current distribution over the reflector. Inclusion of the longitudinal component of reflector current will be seen to separate the principal E- and H-plane centers of phase. In addition this approach will locate these phase centers with respect to the vertex of the paraboloid. This will be done in terms of a primary feed gain parameter, and the paraboloids angular aperture to show the variation of these phase center locations with feed and dish parameters.

Choosing a class of primary patterns which provide an approximate representation of a great many common feeds, the axially symmetric point source primary feed gain function will be taken as (see Fig. 2)

$$G_p(\psi) = G(0) \cos^n \psi = G(0) \left(\frac{1 - x^2}{1 + x^2} \right)^n.$$

Then assuming as before that for most feeds of interest the cross polarization component of reflected field may be neglected in calculating the principal polarization diffraction patterns, it has been shown that

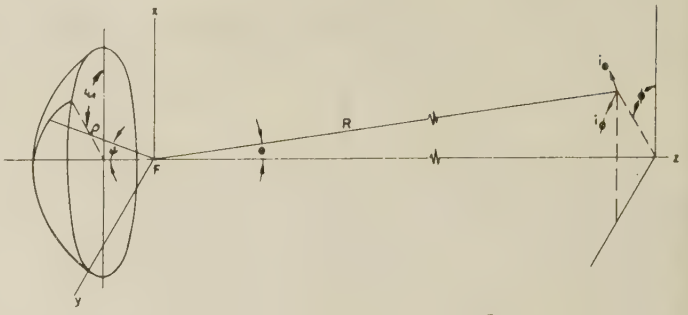

Fig. 2—Coordinate system. The aperture is in the $x=y$ plane.

principal E- and H-plane patterns of the radiation field of such a paraboloid antenna is given by[12]

$$\vec{E}(\theta) = C \frac{e^{-j(kR + 2kf \cos^2 (\theta/2))}}{R} \cdot \begin{cases} \vec{i}_\theta [I_{z2} \sin \theta - I_{x1} \cos \theta + j(I_{z1} \sin \theta + I_{x2} \cos \theta)] & \text{in the } E\text{-plane} \\ \pm \vec{i}_\phi (I_{x1} - jI_{x2}) & \text{in the } H\text{-plane} \end{cases}$$

where

$$I_{x1} = \int_0^X \left(\frac{1 - x^2}{1 + x^2} \right)^{n/2} \frac{x}{1 + x^2} \cdot \cos \left(2kfx^2 \sin^2 \frac{\theta}{2} \right) J_0(2kfx \sin \theta) dx,$$

$$I_{x2} = \int_0^X \left(\frac{1 - x^2}{1 + x^2} \right)^{n/2} \frac{x}{1 + x^2} \cdot \sin \left(2kfx^2 \sin^2 \frac{\theta}{2} \right) J_0(2kfx \sin \theta) dx,$$

$$I_{z1} = \int_0^X \left(\frac{1 - x^2}{1 + x^2} \right)^{n/2} \frac{x^2}{1 + x^2} \cdot \cos \left(2kfx^2 \sin^2 \frac{\theta}{2} \right) J_1(2kfx \sin \theta) dx,$$

$$I_{z2} = \int_0^X \left(\frac{1 - x^2}{1 + x^2} \right)^{n/2} \frac{x^2}{1 + x^2} \cdot \sin \left(2kfx^2 \sin^2 \frac{\theta}{2} \right) J_1(2kfx \sin \theta) dx,$$

$$x = \tan \frac{\psi}{2}$$

and C is a constant equal to

$$-4j\omega\mu f \left[\frac{n+1}{\pi} \left(\frac{\epsilon}{\mu} \right)^{1/2} P_T \right]^{1/2}.$$

[10] Silver, *op. cit.*, p. 174.
[11] *Ibid.*, p. 419.

[12] D. Carter, "Wide angle radiation in pencil beam antennas," *J. Appl. Phys.*, vol. 26, pp. 645–652; June, 1955.

The notation here is the same as Carter's,[12] and the origin of coordinates is taken at the focus of the paraboloid. From this expression for the principal E- and H-plane patterns, it can be seen that the equiphase contours are given by

$$R = \begin{cases} \text{const.} - 2f\cos^2\dfrac{\theta}{2} + \dfrac{1}{k}\tan^{-1}\dfrac{I_{z1}\sin\theta + I_{x2}\cos\theta}{I_{z2}\sin\theta - I_{x1}\cos\theta} & \text{in the } E\text{-plane} \\ \text{const.} - 2f\cos^2\dfrac{\theta}{2} - \dfrac{1}{k}\tan^{-1}\dfrac{I_{x2}}{I_{x1}} & \text{in the } H\text{-plane} \end{cases}$$

Here one can see the effect of the longitudinal component of reflector current in separating the principal E- and H-plane phase centers. Thus if I_{z1} and I_{z2} were negligible the equiphase contour in the E plane would reduce to the same expression as obtained for the H plane. The fact that the longitudinal component of reflector current contributes to the principal E-plane equiphase contour and does not contribute in the H plane is not surprising. Consideration of the distribution of this component on the paraboloid as represented in Fig. 3 shows that it has odd symmetry about the H plane and the contributions from both sides of this plane cancel everywhere in the plane. This does not happen in the principal E plane because the longitudinal component of reflector current has even symmetry about that plane.

Fig. 3—Longitudinal component of reflector current. The distribution of this current component is represented by the horizontal arrows and the dots and crosses to illustrate the symmetry about the principal E and H planes. The vertical arrow at the focus indicates the polarization of the feed.

To obtain the phase centers, the radius of curvature of the equiphase contours will be evaluated on the axis of the main lobe. If $R(\theta)$ is the equiphase contour, the radius of curvature, ρ, is given by

$$\rho = R\,\frac{\left[1 + \dfrac{1}{R^2}\left(\dfrac{dR}{d\theta}\right)^2\right]^{3/2}}{1 + \dfrac{2}{R^2}\dfrac{dR}{d\theta} - \dfrac{1}{R}\dfrac{d^2R}{d\theta^2}}.$$

The phase patterns of axially symmetric antennas are axially symmetric and have continuous first derivatives. Therefore, on the axis, the first derivative of R with respect to θ vanishes and

$$\rho(0) = \frac{R(0)}{1 - \left(\dfrac{1}{R}\dfrac{d^2R}{d\theta^2}\right)_{\theta=0}} \simeq R(0) + \left[\frac{d^2R}{d\theta^2}\right]_{\theta=0}.$$

in the far zone. Hence the phase center lies behind the origin a distance equal to

$$\rho(0) - R(0) = \left[\frac{d^2R}{d\theta^2}\right]_{\theta=0}.$$

It will be convenient to express the phase center locations as fractions of the focal length in front of the vertex of the paraboloid. Calling this normalized distance ζ, it can be seen that

$$\zeta = \frac{f - [\rho(0) - R(0)]}{f} = 1 - \frac{1}{f}\left[\frac{d^2R}{d\theta^2}\right]_{\theta=0}.$$

Performing the somewhat laborious operations indicated it can be shown that for $\theta = 0$,

$$\frac{\partial I_{x2}}{\partial\theta} = I_{x2} = I_{z1} = I_{z2} = 0$$

$$\frac{\partial^2 I_{x2}}{\partial\theta^2} = \frac{\partial I_{z1}}{\partial\theta} = kf\int_0^X \left(\frac{1 - x^2}{1 + x^2}\right)^{n/2} \frac{x^3}{1 + x^2}\,dx$$

and

$$\zeta = \frac{\displaystyle\int_0^X \left(\frac{1 - x^2}{1 + x^2}\right)^{n/2} \frac{x^3}{1 + x^2}\,dx}{\displaystyle\int_0^X \left(\frac{1 - x^2}{1 + x^2}\right)^{n/2} \frac{x}{1 + x^2}\,dx} X \quad \begin{matrix} 1 & \text{in the } H\text{-plane} \\ \text{or} & \\ 3 & \text{in the } E\text{-plane.} \end{matrix}$$

This last formula locates the phase centers as a function of the primary feed gain parameter, n, and the angular aperture of the paraboloid, $\Psi = 2\tan^{-1} x$. Choosing a range of the parameters n and Ψ to obtain representations of the most common configurations, the phase center locations were evaluated and plotted in Figs. 4 and 5. For purposes of comparison a plot of aperture plane location vs angular aperture was added to Fig. 5.

Contrary to the prediction of aperture theory, Figs. 4 and 5 indicate that the phase centers are not in the aperture plane, but they are dispersed about it. For the most part, they lie between the aperture plane and the vertex which is the region to the left of the aperture plane locus in Fig. 5. The H-plane phase centers always lie behind the aperture plane, near the vertex. This is also true for the E-plane phase centers in most cases. However, the axial component of reflector current, which does contribute in the E plane, pushes the phase centers further ahead of the vertex than their corresponding location in the principal H plane. The reason for this is that the reflector's curvature forces the axial component of current distribution to lie ahead of the vertex, producing a maximum of this component distribution near the aperture plane. In some cases of low primary feed gain and small angular aperture, Fig. 5 indicates that the principal E-plane phase centers are located in front of the aperture plane.

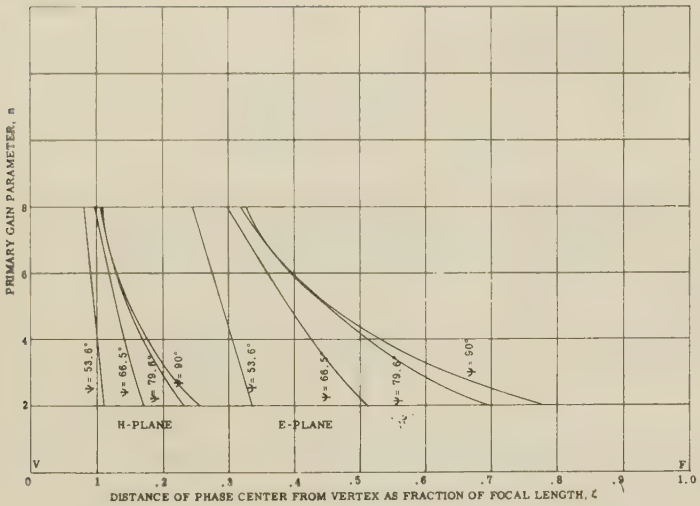

Fig. 4—Principal plane phase centers. These curves show the variation of the phase center locations with primary feed gain in the principal E and H planes of a paraboloid reflector fed by a primary having a gain function.

$$G_p = \begin{cases} 2(n+1)\cos^n \psi & \text{for } 0 \leqq \psi \leqq \dfrac{\pi}{2} \\ 0 & \text{for } \dfrac{\pi}{2} \leqq \psi \leqq \pi. \end{cases}$$

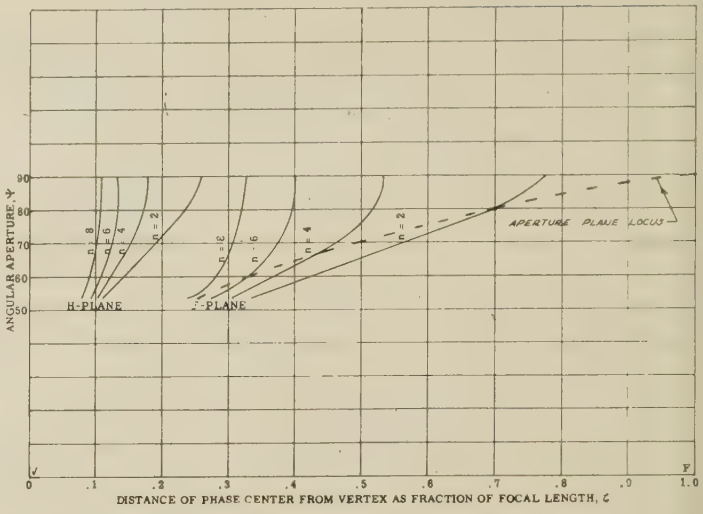

Fig. 5—Principal plane phase centers. These curves show the variation of the phase center locations with angular aperture in the principal E and H planes of a paraboloid reflector fed by a primary having a gain function,

$$G_p = \begin{cases} 2(n+1)\cos^n \psi & \text{for } 0 \leqq \psi \leqq \dfrac{\pi}{2} \\ 0 & \text{for } \dfrac{\pi}{2} \leqq \psi \leqq \pi. \end{cases}$$

Finally it should be noted from Figs. 4 and 5 that, in general, decreasing the paraboloid angular aperture and increasing primary feed gain moves both principal E- and H-plane phase centers towards the vertex of the paraboloid. This was to be expected since either of these two variations tends toward the limiting case of reflection by a plane mirror of a point source, a case in which image theory tells us that the phase center is located in the reflecting plane. Thus decreasing the angular aperture means either decreasing the paraboloid diameter for a fixed focal length or increasing the focal length for a fixed diameter. In the former case the aperture plane is moved back toward the vertex and in the latter case the vertex is moved forward toward the aperture plane, both variations effectively producing a flatter reflector. Similarly increasing primary feed gain increases the current in the zero curvature vertex region at the expense of the currents near the aperture plane, effectively producing a flatter current distribution. Since either of these variations produces a flatter current distribution located near the vertex, the phase centers should move together toward the vertex.

In conclusion, it should be stressed that these results apply strictly only for feeds which are axially symmetric point sources located at the focus of the paraboloid. This provides an approximation for a great many common feeds. However, the phase centers of the reflected radiation field can be varied and even pushed behind the dish by defocusing and separating the primary feed phase centers.

A New Method for the Measurement of the Average Dielectric Constant of the Underground Medium on Site*

MOHAMED A. H. EL-SAID†

Summary—**An electromagnetic interference pattern[1] in the far-distance condition is utilized to determine the average dielectric constant of the underground propagational medium. The method depends upon the determination of the surface wave velocity by means of measuring the first self-resonance frequency of a dipole wire laid on the earth's surface.**

Introduction

THE TECHNIQUE of sending radio waves to large distances into the interior of the earth has recently become important to the art of geophysical prospection.[1] The dielectric constant of the underground material over the propagational path is one of the important parameters of this technique and a knowledge of its magnitude is essential both from the viewpoint of quantitative understanding of the propagation of em waves into the earth's interior, and also for prospecting purposes. Direct methods depending upon laboratory measurements on rock samples from the site are not indicative of the conditions prevailing in the underground propagational medium. This paper provides a new method for the determination of the dielectric constant of a site with good accuracy.

Average Dielectric Constant

The inhomogeneity of the underground material causes the dielectric constant to vary from point to point along a propagational path. This will cause the phase velocity and the wavelength to vary as the wave progresses into the material. However, an average value of the wave velocity and wavelength may be envisaged if we consider an average value for the dielectric constant. This is true as long as the wavelength is many times greater than the variational distances, which is the case in the operating frequency range utilized for prospecting.

When a dipole is laid on the earth's surface and is excited by a voltage, the wave which is set up will have in the far-zone three so-called fundamental components: one traveling and expanding into the upper space, another into the interior of the earth, and a third along the earth's surface so that the boundary condition is satisfied. In the presence of an underground reflecting surface such as a water layer or a metallic ore, the underground wave will be reflected back to the earth's surface thus interfering with the surface wave. It is known[1] that the resulting em interference pattern at distances on the earth's surface which are much larger than the depth of the reflecting surface is characterized by fringes occurring at regular intervals given by:

$$\text{Delay frequency } F_0 = c/d\left(\sqrt{\epsilon_g} - \frac{I}{\alpha}\right) \tag{1a}$$

$$\text{Delay distance } \quad d_0 = c/f\left(\sqrt{\epsilon_g} - \frac{I}{\alpha}\right) \tag{1b}$$

in the variable frequency and variable distance interference methods respectively, where:

c = velocity of light,
ϵ_g = average dielectric constant of the underground material,
α = ratio of the surface wave velocity to the velocity of light,
f = operating frequency of the transmitter,
d = distance between the transmitting and receiving dipoles.

The values of F_0 and d_0 are independent of the depth h of the reflecting surface provided that $d \gg h$. Also, the product $F_0 d = f d_0$ is substantially constant, a criterion which identifies the so-called "far-distance condition."

Eqs. (1a) and (1b) may also be re-written as:

$$\sqrt{\epsilon_g} = \left(\frac{I}{\alpha} + \frac{c}{F_0 d}\right) = \left(\frac{I}{\alpha} + \frac{c}{f d_0}\right). \tag{1c}$$

This far-distance relationship comprises therefore a method for the determination of ϵ_g if α is known. The measurement of α on site can be effected by means of the following method.

Surface Wave Velocity

A dipole laid on the earth's surface will exhibit a self-resonance frequency which is less than that of the same dipole in free space by virtue of the fact that the dielectric constant of the earth's surface material is greater than that of air. Fig. 1 shows the observed behavior of the driving point impedance of a dipole antenna laid on the ground in the desert land during summertime; r_0 and x_0 are the resistive and reactive series components, respectively. These components were measured by means of a balanced radio frequency bridge placed at the dipole center. It will be seen that these curves have the same general character as those of the same antenna in free space.[2] Further, the first self-resonance frequency of such laid dipole is approximately half that of the first self-antiresonance. This

* Manuscript received by the PGAP, December 28, 1955; revised manuscript received, April 3, 1956.
† Dept. of Engrg., Cairo University, Giza, Egypt.
[1] M. A. H. El-Said, "Geophysical prospection of underground water in the desert by means of electromagnetic interference fringes," PROC. IRE, vol. 44, pp. 24–30; January, 1956.
[2] See Ronald W. King, "Electromagnetic Engineering," McGraw-Hill Book Co., Inc., New York, N. Y.

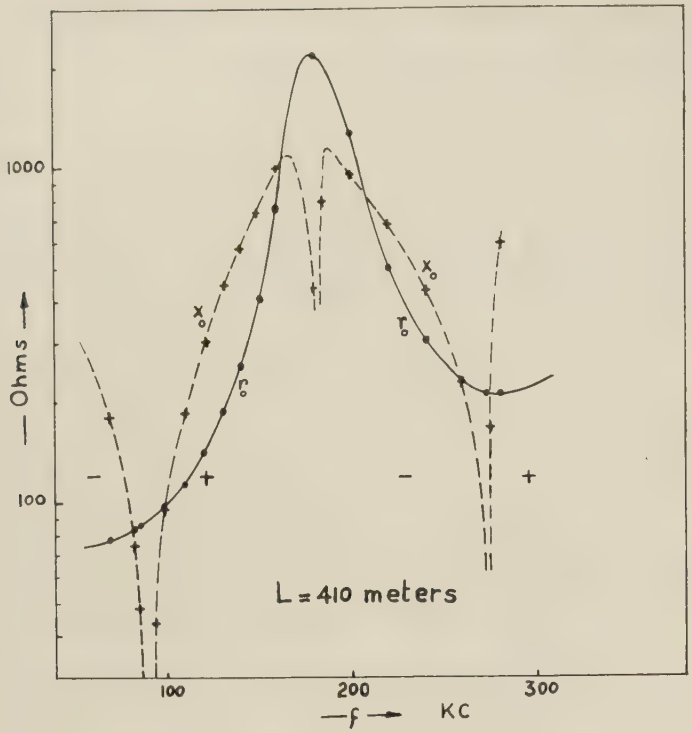

Fig. 1—Observed driving point impedance components of a dipole wire laid on the earth's surface in the desert.

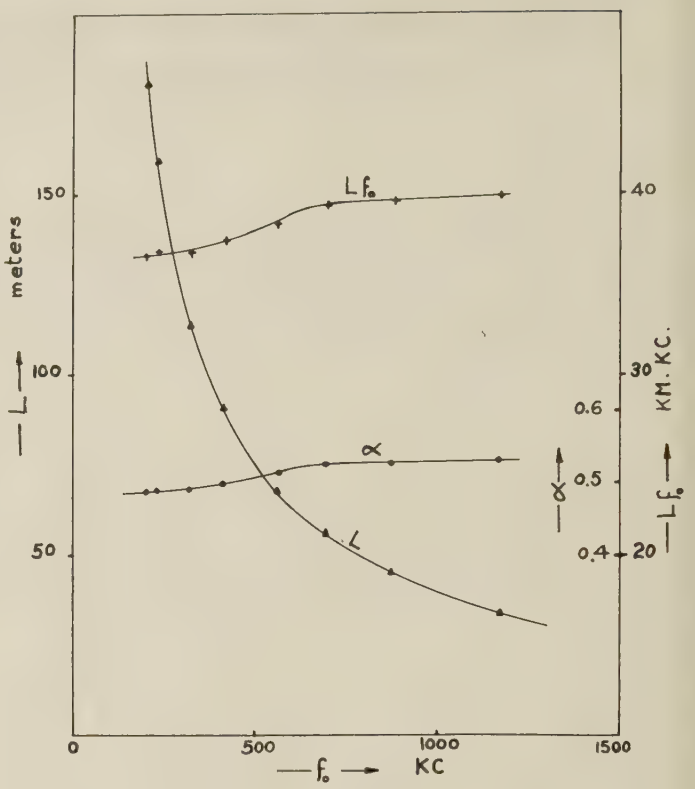

Fig. 2—Parameters of a dipole wire laid on the earth's surface in the desert and excited from the center at its first self-resonance frequency; the deduced surface wave velocity is shown.

denotes that the voltage wave is reflected at the open end with negligible phase-shift. Moreover, the measured current distribution along this dipole wire when excited with a voltage at its first self-resonance frequency indicated a practically sine curve.

In general, the driving point impedance of an excited dipole is a complex quantity, and when the wave set up by such antenna is reflected at the open end and reaches the driving point with a phase retardation of π, the impedance becomes minimum and is resistive. Under this condition, the antenna exhibits its first self-resonance. For a dipole laid on the earth's surface, the phase-shift depends upon the velocity of the wave which is set up by the antenna on the earth's surface. The velocity of propagation may thus be determined by a measurement of the antenna self-resonance frequency. To a first approximation, this is the same velocity with which the surface wave propagates in the far zone, thus $L = \lambda_s/4$ where λ_s is the surface wavelength, from which:

$$\alpha = 4f_0L/c = I/\sqrt{\epsilon_c} \qquad (2)$$

where L is the halflength of the dipole, f_0 is its first self-resonance frequency, and ϵ_c is a so-called "combined dielectric constant" which is between that of air and that of the earth's surface material.

Experimental Work

Fig. 2 shows the observed values of the length L against the first self-resonance frequency f_0 of the dipole; calculated values of the product f_0L and α are also shown. These curves are taken for a dipole wire having a diameter of 1 millimeter covered with rubber insulation whose diameter is 4 millimeters. It will be seen that the product f_0L, and hence also α, are substantially constant over a wide range of frequencies. An investigation of the parameters of the earth's material over this frequency range was made by measurements on sample materials taken at various depths from the surface. These measurements were effected by filling a cylindrical air condenser with the material and measuring the susceptance and conductance components of the sample by means of the radio frequency bridge. Values of the dielectric constant ϵ and the resistivity ρ were calculated accordingly, and the results are shown in Fig. 3. It will be seen that ρ decreases rapidly with depth owing to the increased moisture content which also results in an increased value of ϵ. When the samples were left to dry in the sun, the remeasured constants assumed the values at zero depth. Further, the observed effect of the increase of frequency from 100 kc to 1000 kc on the surface sample was to reduce ϵ from 8.2 to 6.3, that is, a ratio of 1.3. This ratio increases considerably with depth. The observed increase of α by a factor of 1.08 over the frequency range from 200 kc to 1000 kc may be attributed mainly to the above mentioned changes of ϵ with frequency. It should be considered, however, that the relative effects of the large changes in ϵ with depth are very much reduced by virtue of the fact that the energy storage in the material decreases with depth because of increased distances from the antenna wire and increased losses. Observed changes in resistivity will have only a second order effect on the actual value of α.

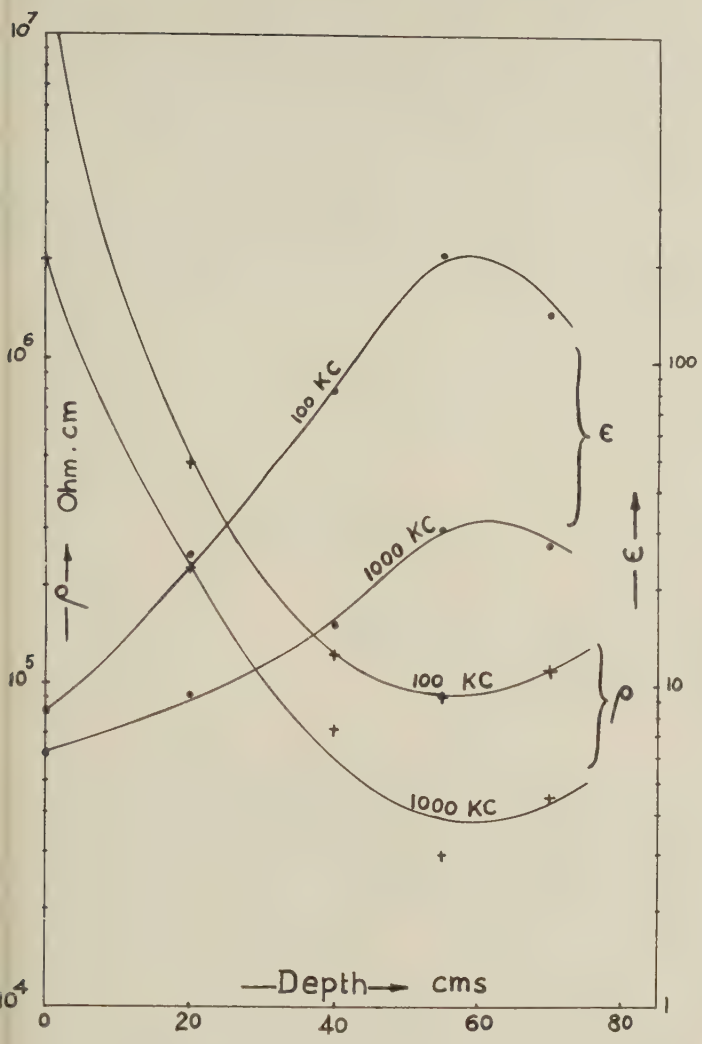

Fig. 3—Dielectric constant and resistivity of sample materials of a desert site against depth at frequencies of 100 kc and 1000 kc.

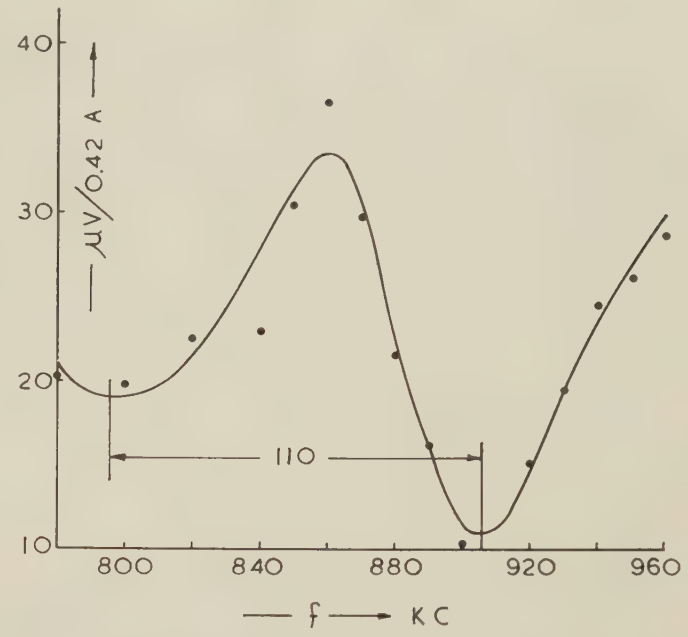

Fig. 4—Sample of the "far-distance" interference patterns of a desert site: Abu-Aweigla-Senai, point 2. $d=2100$ m, $F=110$ kc, $\sqrt{\epsilon_c}=2.68$, $\sqrt{\epsilon_g}=3.58$.

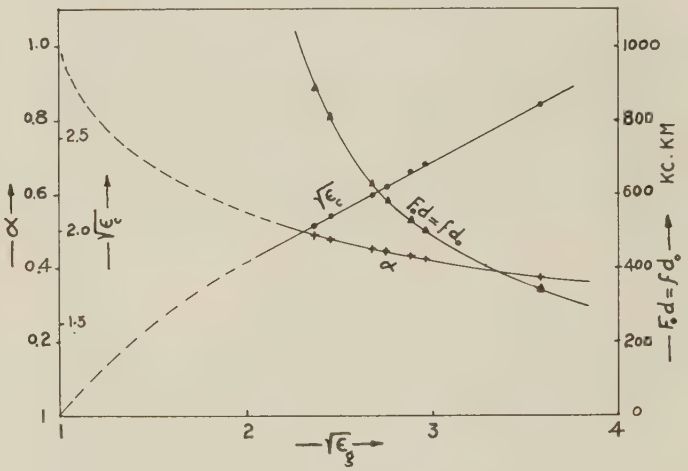

Fig. 5—Parameters for "far-distance" interference patterns, Egyptian desert, summertime.

Fig. 4 shows a sample of the observed far-distance interference patterns obtained at some place in Senai, Egypt, where the water table is at a depth of about 500 meters. It is interesting to observe that the depth of the fringes is large. The distance over which this pattern was taken is $d=2100$ meters, that is, a ratio of $m=d/h=4.2$. Since it is not usually convenient in the field to use distances of the order of 10 times the depth, it can be shown that (see Appendix) for $m\geq 2$ we have:

$$\sqrt{\epsilon_g} \cong \left(\frac{I}{\alpha}+\frac{c}{F_0 d}\right)\Big/\left(I+\frac{2}{m^2}\right)$$

$$\cong \left(\frac{I}{\alpha}+\frac{c}{f d_0}\right)\Big/\left(I+\frac{2}{m^2}\right). \qquad (1d)$$

In the experiment of Fig. 4, observed $F_0=110$ kc, measured $\sqrt{\epsilon_c}=I/\alpha=2.68$, and the calculated value of $\sqrt{\epsilon_g}$ is 3.58 for that particular site.

The results established here were primarily intended for use in the determination of the water table in the desert by means of the electromagnetic interference fringe method. For this purpose the proper procedure for prospecting would be as follows:

1) Determine α of the site.
2) Obtain two interference patterns, one at an appropriate distance and the other at a far-distance.
3) Estimate $\sqrt{\epsilon_g}$ from (1c).
4) Determine the approximate value of h from the information contained in the appropriate distance pattern and from this estimate m.
5) From (1d) and the information contained in the far-distance pattern, obtain the correct value of $\sqrt{\epsilon_g}$.
6) Repeat 4) to determine the correct value of h if necessary.

Typical values of the product $F_0 d=f d_0$ and α are shown in Fig. 5 against $\sqrt{\epsilon_g}$, for the Egyptian desert during summertime.

Acknowledgment

The author wishes to express gratitude to H. Mahmoud, Professor of Radio and Electronics, Cairo University, for many helpful suggestions. Thanks are also due to Mohamed Y. Ibiary, Lecturer, for genuine assistance during the execution of the field work and for many helpful discussions.

Appendix

Let $d=mh$, where $m\gg 1$ at far distances. We then have

$$D = d\left(1+\frac{2}{m^2}\right),$$

and it can be shown that in the variable frequency interference method we get

$$\sqrt{\epsilon_g}\cong\left(\frac{1}{\alpha}+\frac{c}{F_0 d}\right)\Big/\left(1+\frac{2}{m^2}\right).$$

In the variable distance interference method, at far distances we have: $d_{n+1}-d_n\cong d_o$ and if $m\gg 1$ we can say that $m_{n+1}\cong m_n=m$. With these approximations, it can be shown that

$$\sqrt{\epsilon_g}\cong\left(\frac{1}{\alpha}+\frac{c}{fd_0}\right)\Big/\left(1+\frac{2}{m^2}\right).$$

The Image Method of Beam Shaping*

PAUL T. HUTCHISON†

Summary—**The image scheme of beam shaping for use at microwave frequencies is described. Cosecant-squared radiation patterns are obtained with parabolic reflectors no larger than those required to give pencil beams of commensurate beam widths. Radiation patterns calculated using diffraction theory are compared with measured patterns of a paraboloidal dish fed by a horn feed and one image horn. Experimental patterns are included to show the effects of variation of all parameters. A qualitative analysis of a paraboloid fed by a horn and several images is shown to agree with measured results.**

Introduction

MICROWAVE antennas having a so-called "cosecant-squared" radiation pattern[1] in the vertical plane and a uniformly narrow beam in the other plane are in widespread use for airborne mapping and other radar applications. One scheme that has been used to obtain such a radiation pattern is the multiple feed type antenna.[2] This paper describes the image scheme of beam shaping which employs a section of a paraboloidal reflector fed by an electromagnetic horn and an image of the horn provided by a flat conducting ground plane below the axis of the reflector. Because of the similarity of these systems, a brief description of the former will be included.

A paraboloidal reflector or dish has the property of transforming a spherical wave into a plane wave if the spherical wave source is placed at the focal point of the dish. If a small horn feed which closely approximates a spherical wave source is displaced from the axis of the dish, the resulting secondary beam will be displaced on the opposite side of the axis by an angle proportional to the feed displacement. This property of the paraboloid is the basic principle in the design of the image and the multiple feed antennas.

If a paraboloidal reflector is fed by two horns, one of which is displaced from the axis, there will be two secondary beams with an angular displacement determined by the angular separation of the horns. The amplitude of each beam is approximately proportional to the square root of the power fed to each horn. If the horns are spaced and fed properly, the combination of the beams will give a smooth cosecant-squared pattern over limited angles.

A side view of an image type antenna employing a flat ground plane and a cut paraboloid of focal length F is shown in Fig. 1. The rays that are reflected from the ground plane seemingly come from a point $d/2$ below the ground plane. The feed below the ground plane is an image of the main horn, and its directivity is a function of the main horn radiation pattern. The waves apparently emanating from the image are the waves that are reflected from the ground plane, so the power division between the main and image horns is determined by the tilt angle ϕ. If the wave is horizontally polarized, the rays undergo a 180° phase-reversal at the ground plane, so effectively the horn and its image are fed 180° out of phase. The image horn causes a secondary beam displaced from the axis of the paraboloid by an angle proportional to d/F and having an amplitude determined by the tilt of the horn feed.

* Manuscript received by the PGAP, July 7, 1955; revised manuscript received January 31, 1956.

† Georgia Inst. Tech., Atlanta, Ga. Formerly with Raytheon Mfg. Co., Newton 58, Mass.

[1] S. Silver, "Microwave Antenna Theory and Design," McGraw-Hill Publishing Co., Inc., New York, N. Y., pp. 465–471; 1949.

[2] *Ibid.*, p. 473.

The problem is to find the radiation pattern of this image type antenna and to show how to control it. The discussion will be divided into the following categories: 1) theoretical analysis, 2) the effects of variation of parameters and a comparison of calculated and measured results, and 3) modifications of the ground plane to give cosecant squared coverage over wider angles.

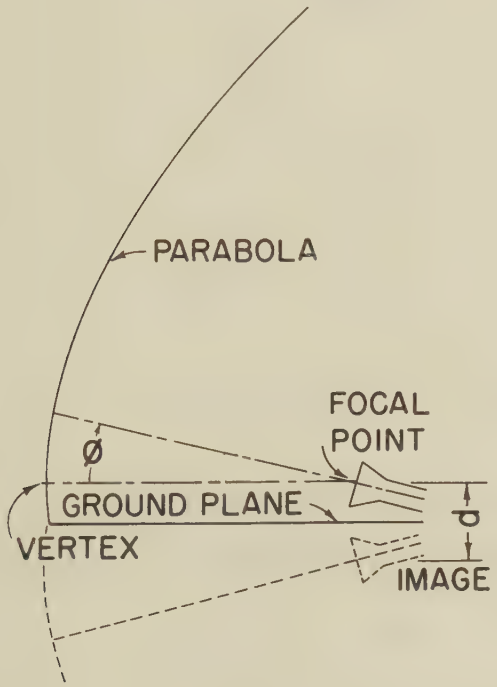

Fig. 1—Cross section of image type antenna with flat ground plane.

Theoretical Beam Shape

The antenna to be analyzed is a cut paraboloid of revolution with a flat ground plane displaced from the axis of the dish by a distance $d/2$. The small horn feed, horizontally polarized, is at the focal point and tilted an angle ϕ above the axis of the dish. The problem of finding the resultant radiation pattern of this antenna will be solved by finding first the secondary beams produced by the main and image horns individually and combining the beams using the principle of superposition. An intermediate step will be an analysis of the amplitude and phase variations of the field intensity across the mouth of the dish.

The field distribution over the aperture of the dish due to the main feed, $F(y)$, is determined by the radiation pattern and tilt of the horn. In Fig. 2(b) the amplitude and phase of the field intensity across the aperture due to illumination by the main feed are plotted as a function of y. Since the horn is at the focal point, the phase of the intensity is constant over the aperture $y=-B$ to $y=A$. The origin is arbitrarily placed at the point of maximum intensity to simplify the integrals encountered later.

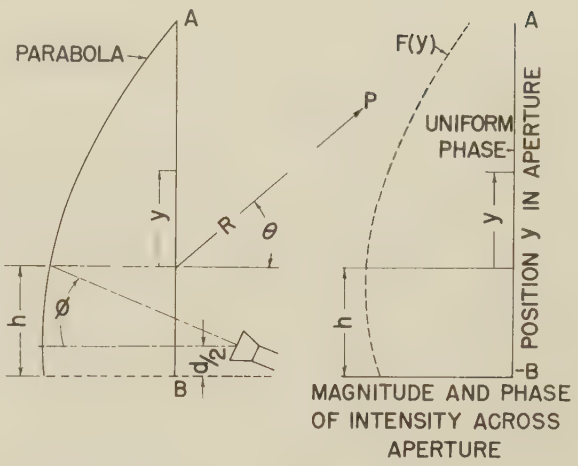

Fig. 2—Horn and reflector relationship and illumination of reflector by main horn.

The field distribution over the aperture due to illumination of the dish by the image, $G(y)$, is a function of the main horn radiation pattern as well as the displacement of the ground plane. $G(y)$ will be maximum at the intersection of the ground plane and the parabola, and $G(-B)$ is approximately equal to $F(-B)$ in magnitude. The image is at a distance d below the focal point, and since an off-axis fed paraboloid is not a perfect beam forming element, the phase of $G(y)$ varies with y. The phase is determined by the method of ray tracing as shown in Fig. 3. The total path of a ray from the image

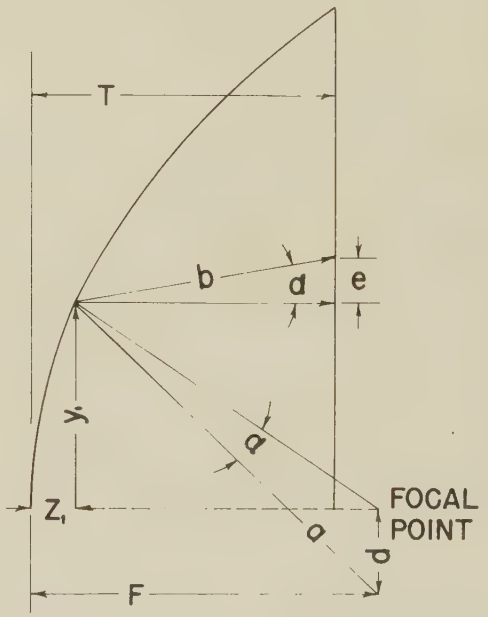

Fig. 3—Geometry for calculating pathlengths of rays from image.

to the aperture is $a+b$. All rays emanating from the main feed travel $F+T$ before reaching the aperture of the dish, so $2\pi/\lambda\,[(a+b)-(F+T)]\pm\pi$ will be the phase angle of $G(y)$ relative to $F(y)$. The expressions for a and b are:

$$a = \frac{1}{4F}\left[(4F^2 + y_1^2)^2 + 16F^2d(d + 2y_1)\right]^{1/2} \quad (1)$$

$$b = a\left[\frac{(4F^2 + y_1^2)(4FT - y_1^2)}{(4F^2 + y_1^2)^2 + 16F^2dy_1}\right]. \quad (2)$$

Fig. 4 shows the pathlength variation for one particular setting of the ground plane. For small values of d/F, this curve can be closely approximated by the straight dashed lines shown in Fig. 4. This approximation simplifies the problem of finding the shape of the secondary beam due to illumination of the aperture by the image.

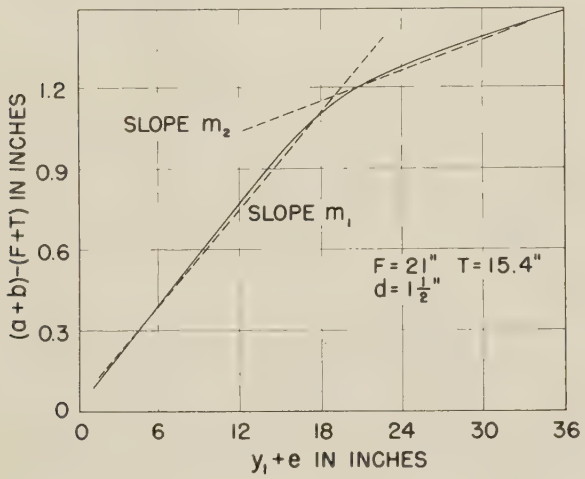

Fig. 4—Pathlength variation as a function of position across mouth of reflector.

In Fig. 5 the amplitude and phase of the field intensity due to illumination by the image are plotted as a function of y. The phase difference of $F(y)$ and $G(y)$ at the origin is $\beta c \pm \pi$, where c is the difference in pathlengths in centimeters if β is in radians per centimeter.

The resultant field intensity at any point is the combination of $F(y)$ and $G(y)$, taking into consideration their time phase difference. The total intensity at $y = -B$ is small since $F(-B)$ and $G(-B)$ are almost equal in magnitude and nearly 180° out of phase. As the tilt of the horn is changed, the magnitudes of $F(y)$ and $G(y)$ change, but the phases are unaltered. As d is increased, the slopes m_1 and m_2 are changed, so the phase of $G(y)$ is changed, but the other functions are constant.

The next step in the solution of the problem is to calculate the secondary radiation pattern. By using Huygen's Principle,[3] the secondary pattern in the yz or vertical plane can be expressed in terms of $F(y)$ and $G(y)$ over the rectangular aperture.

[3] Bell Laboratories Staff, "Radar Systems & Components," D. Van Nostrand Co., Inc., New York, N. Y., p. 476; 1949.

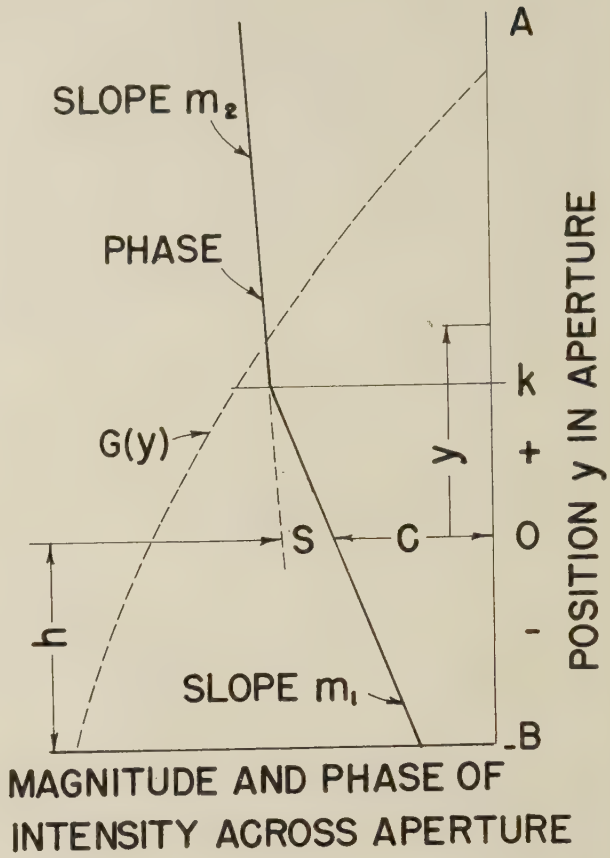

Fig. 5—Illumination of the reflector by the image horn.

$$E = \frac{K\epsilon^{-j\beta R}}{R}\left[\int_{y=-B}^{y=A} F(y)\epsilon^{j\beta y \sin\theta}\,dy + \epsilon^{-j(\beta C \pm \pi)}\int_{y=-B}^{y=k} G(y)\epsilon^{j\beta y(\sin\theta - m_1)}\,dy + \epsilon^{-j[\beta(C+S)\pm\pi]}\int_{y=k}^{y=A} G(y)\epsilon^{j\beta y(\sin\theta - m_2)}dy\right]. \quad (3)$$

E is the electric field intensity at any point in the yz plane.

K is a constant of proportionality.

$\beta = 2\pi/\lambda$ where λ is the wavelength.

$F(y)$ is the illumination of the aperture by the main horn.

$G(y)$ is the illumination of the aperture by the image horn.

m_1 and m_2 are slopes of the phase variation curve as shown in Fig. 4.

c, s, A, B, and k are points or distances shown in Fig. 5.

The first term in (3) represents the radiation pattern of the antenna when no ground plane is used. This pattern due to illumination of the reflector by the main feed will be called the main beam and will be maximum along the axis of the dish regardless of $F(y)$. The re-

maining terms give the radiation pattern of the dish illuminated by the image. This secondary beam, called the image beam, will have maximum radiation at some angle above the axis of the paraboloid. Since the value of $G(y)$ is comparatively small in the region of the aperture $y=k$ to $y=A$, the image beam peak will be determined by the second term in (3) which gives maximum radiation at an angle $\theta=\arcsin m_1$. The factor $\beta C \pm \pi$ gives the phase difference of the real components of the field intensities in the main and image beams. Because of the positioning of the origin, the quadrature components of field intensity are small compared to the real components, so $\beta C \pm \pi$ gives a good indication of the total phase difference of the intensities. This analysis of a three-dimensional problem by a two-dimensional approach is obviously in error unless the variation of the field intensity across the aperture has the same variation in y for all parts of the aperture. This assumption was made and a comparison of the calculated and measured results shows that this is justifiable in most cases. Probably the main source of error in this analysis is the assumption that the horn feed is a point source.

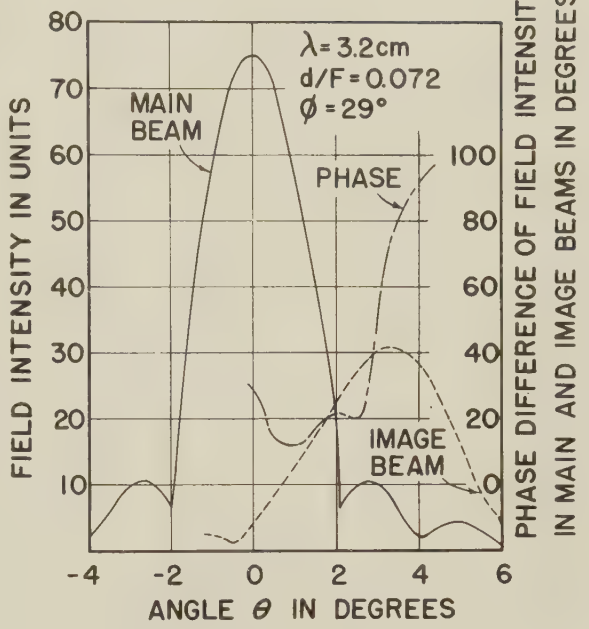

Fig. 6—Relative amplitude and phase of field intensities in main and image secondary beams.

Experimental Results

The reflector used in this experiment was a rectangular section of a spun aluminum paraboloid having a 21-inch focal length and vertical and horizontal dimensions of 36 and 72 inches. The horizontal half-power beam width at the peak of the beam was 1.4° and the absolute gain 40 db operating at a wavelength of 3.2 cm. In calculating the radiation patterns of the antenna employing a flat ground plane, both $F(y)$ and $G(y)$ were assumed sinusoidal since the feed produced almost this type of illumination. The calculated patterns of the main and image beams and the phase difference of the field intensities in the two beams are shown in Fig. 6 for $d/F=0.072$ and $\phi=29°$. The phase difference of the field intensities at the origin due to the main and image horns is 36°. However, the phase difference of the radiation fields will not be exactly 36° since the relative phase of the intensity in each beam varies with θ. This phase difference is never greater than about 30° in the region where a deep null might occur, that is the region of approximately equal intensities. If a cosecant-squared pattern is desired, the two beams must add so the power at any angle θ is varied as cosecant-squared theta, so any dip or irregularity in the pattern would ruin it. The theoretical and measured radiation patterns for this setting of the ground plane are shown in Fig. 7(a). As will be shown later, the phase relationships will not be so favorable for other values of d/F.

Variation of Parameters

To get a clear picture of the operation of this antenna, it will be helpful to observe the changes in beam shape as the following parameters are changed: 1) ground plane level, 2) tilt of the feed, and 3) frequency.

As the ratio d/F is increased, the position of the image and hence the image beam is displaced further from the axis of the paraboloid. If the main and image beams are far enough apart, 7 or 8° in this case, there will be a distinct null about midway between them since neither radiation pattern shows any appreciable energy in this region. Experiments show the presence of a deep null (25 decibels) when d/F is greater than 0.143. When d/F is between 0.072 and 0.12, the beams are positioned so the radiation pattern could be smooth similar to Fig. 7(a) if the phase relationships between the beams are correct. Calculations show a deep null is likely when d/F is 0.12 since $\beta C \pm \pi$ for this setting is 180°. As discussed previously, the intensities are nearly in phase when $\phi=29°$ and d/F is 0.072. For the intermediate setting of d/F equal to 0.095, the phase difference is 108°, so a slight dip is observed between the two beams. Figs. 7(a) and 7(b) (next page) show the behavior of the radiation patterns as d/F is changed.

As the tilt ϕ of the horn feed is changed, effectively the power division between the main and image horns is changed. The relative magnitudes of the two secondary beams will change, but their positions will not. As the horn is tilted, $\beta C \pm \pi$ changes from 36° when $\phi=29°$ to 80° when $\phi=40°$, but the relative magnitudes of the real and quadrature components in each beam also change. Calculations show that changing the tilt of the feed has some small effect on the phase relationships, but the change in the relative magnitudes of the secondary beams is the predominant effect. Fig. 8 shows the measured patterns for several values of ϕ when d/F is

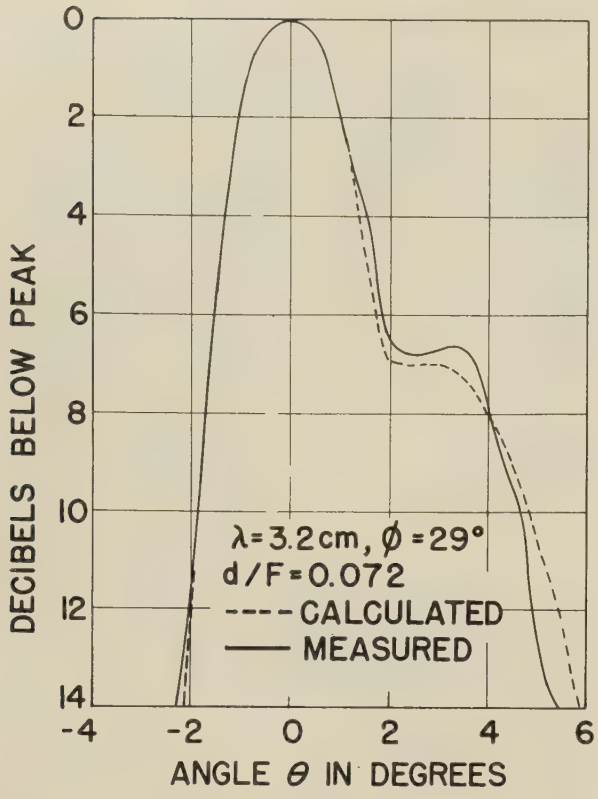

(a)

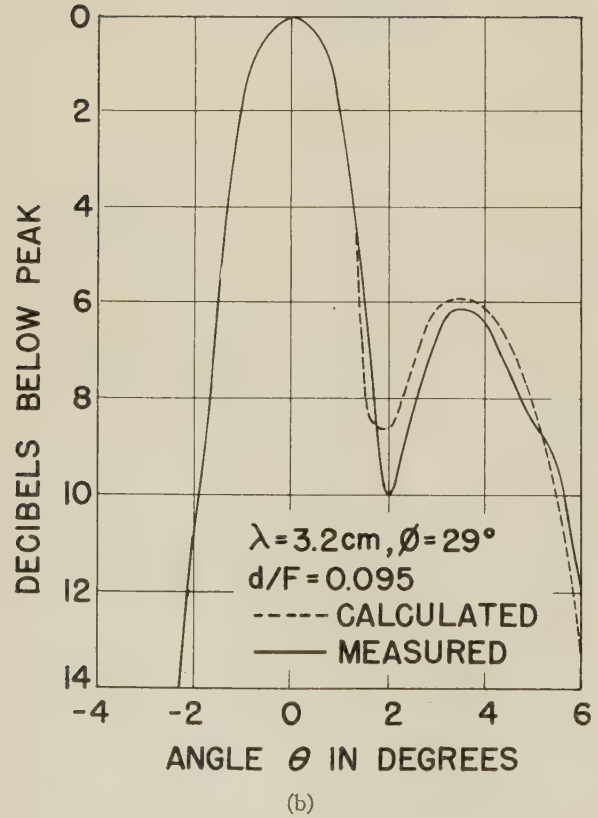

(b)

Fig. 7—Calculated and measured radiation patterns of image type antenna for different values of d/F.

0.072. Changing the magnitude of the image beam by a large per cent usually requires changing the radiation pattern of the horn feed.

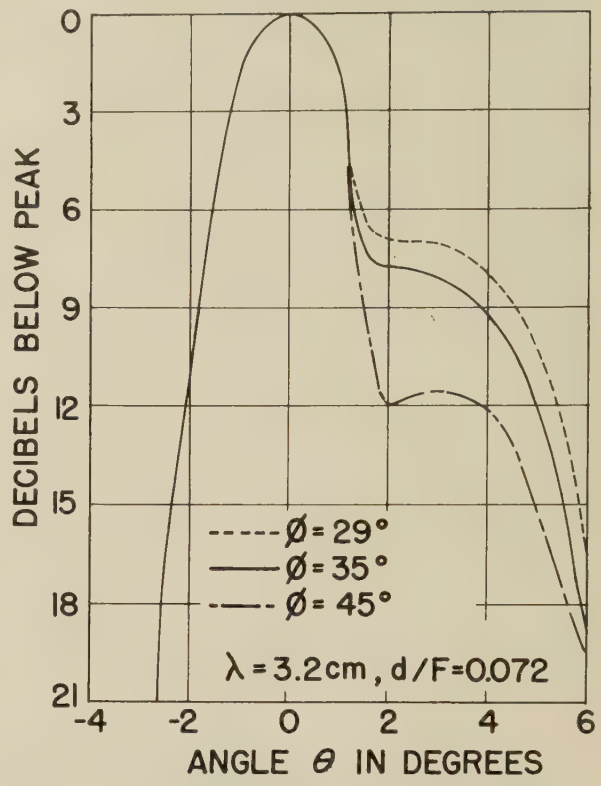

Fig. 8—Measured radiation patterns of image type antenna for several tilt angles of the horn feed.

As the frequency is changed, say ±5 per cent, the only change in the beam shape that should be observed is the usual change in beamwidths. If the ground plane is $\frac{3}{4}$ inch, $d/F=0.072$, below the axis of the dish, $\beta C \pm \pi$ varies from 25 to 47° at the two extreme frequencies, which may cause the beam shape to change a few per cent, but not enough to cause a noticeable dip or null. This antenna was tested over a 10-per-cent band, and the radiation patterns were almost identical except for side lobe levels.

Selection of Focal Length

The phase difference of the field intensities in the main and image beams is determined by d, F, and the wavelength λ, and the angular position of the image beam depends on the ratio d/F.

The position of the image beam must be close enough to the main beam to make the radiation pattern a smooth curve similar to Fig. 7(a). From the calculated beamwidths of the main and image beams, the desired angular position of the image beam can be determined. The ratio d/F is then determined from the empirical expression:

$$O(d/F) = \tan \theta_0. \tag{4}$$

O is the beam deviation factor[4] which is defined as the ratio of the angular displacement of the secondary beam from the axis to the angular displacement of the

[4] Silver, *op. cit.*, p. 488.

feed from the axis. θ_0 is the desired position of the lobe or beam due to the offset horn or image.

In most cases the antenna will have the horn tilted so the peak illumination from the main feed is about $D/3$ above the bottom of the dish. D is the vertical height of the dish. If some value of F is assumed and the values of d and $y_1=D/3$ are substituted into (1) and (2), the value of $a+b$ for this tilt angle can be calculated. In order to satisfy the phase relationships for a smooth pattern, $a+b$ should be about one-half wavelength greater than $F+T$.

Multiple Images

The addition of the main beam and the beam due to a single image gives very limited cosecant-squared coverage especially when the main beam is narrow. By shaping the ground plane as shown in Fig. 9, two images are

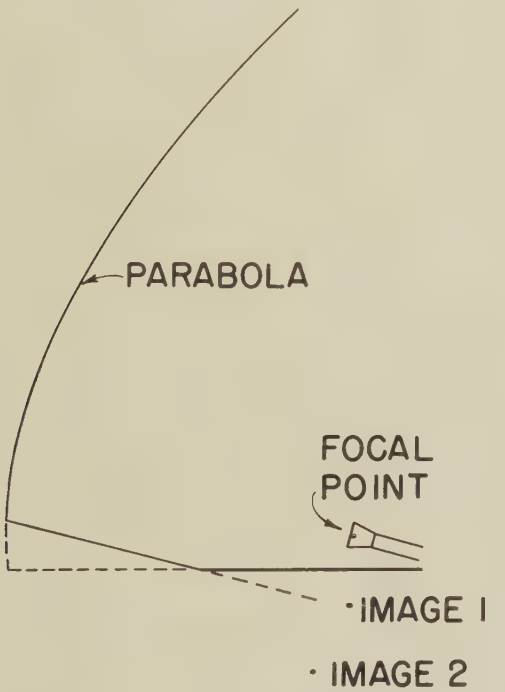

Fig. 9—Image antenna using ground plane to provide two images.

provided. In the two-image system, each image effectively illuminates only a portion of the reflector, so the vertical beamwidths of the image beams are wider than beamwidths of the single-image system. By use of the dual image ground plane, the coverage was increased from about 5° as shown in Fig. 7(a) to about 16°. Changing the shape of the ground plane to a curved surface in

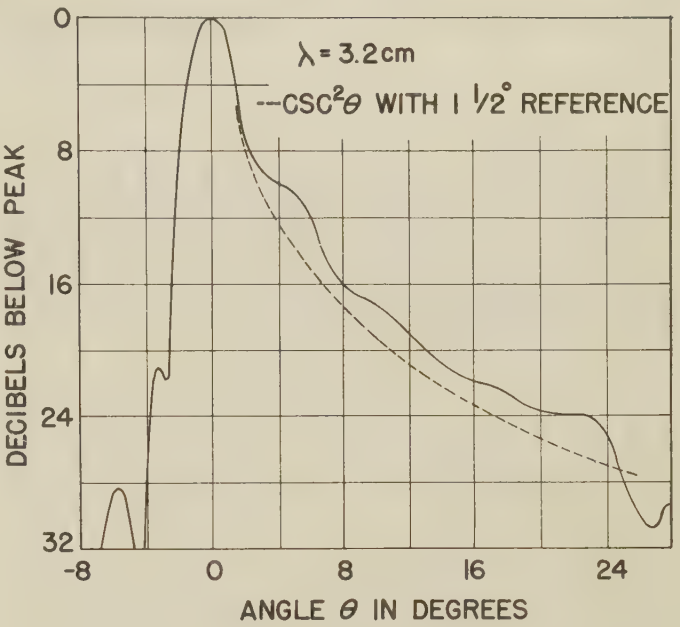

Fig. 10—Radiation pattern of an image type antenna using a ground plane curved in one plane to provide multiple images.

the vertical plane feeds the paraboloid with a series of images which gives a smooth pattern as shown in Fig. 10.

One advantage of this antenna is the high gain obtained because the presence of the ground plane allows more nearly constant illumination of the aperture in the vertical plane, without spillover. Also, reflections from the reflector back into the horn feed are a minimum since the horn is at a point of low intensity due to cancellation of the fields from the main and image horns.

Conclusion

The well-known image principle used in optics is applied to microwave antennas for the purpose of beam shaping. A method of calculating the radiation pattern of a paraboloidal dish fed by a horn and its image and the ways of controlling this pattern have been presented. Measured radiation patterns of the antenna fed by a horn and one image are shown to agree with the theoretical patterns. A qualitative analysis of a ground plane which provides several images is substantiated by actual patterns which show this type antenna provides good cosecant-squared coverage over limited angles.

The flat ground plane was first used by Paul Hines, of the Raytheon Manufacturing Company, to provide shaped beams from a horn feed of pillbox construction. The author is indebted to Dr. L. J. Chu, of the Massachusetts Institute of Technology, for his helpful discussions during the preparation of this paper.

Loop Antenna Measurements*

PHYLLIS A. KENNEDY†

Summary—**Experimental measurements on three loop antenna configurations are presented. The technique for obtaining impedance and current distributions using a single-wire transmission line over an image plane is described with particular attention given to the difficulties encountered. The results are reproduced in graphical form, and for loops where theoretical results are available, curves comparing theory and experiment are presented.**

Introduction

THE CLOSED thin-wire transmitting loop in its various configurations has been useful for some time because of its valuable directional properties and broad-band operational characteristics. Several theoretical studies have been made on the circular loop,[1–3] but due to the difficulties encountered in obtaining solutions for the current distribution and input impedance, and the complicated numerical evaluation involved, only approximate theoretical results which agree qualitatively with experiment have been obtained.

Recent solutions for the circular and square loops have been found respectively by Storer[4] and King.[5] Storer has used a variational method in which Hallén's Fourier-series solution for the current has been modified to avoid the difficulties of convergence previously encountered and hence facilitate the numerical computations. As a result, a series of tables and curves has been compiled of impedance and current distribution on circular loops of circumference up to 2.5 wavelengths for several thicknesses of wire. Theoretical data obtained by Storer provide a quantitative comparison in this paper. King has applied an iteration method to the problem of the square loop driven from one corner or driven from the center of one side. By superimposing the solutions of four independent integral equations representing four-phase sequences when the loop is driven at each corner by arbitrary voltages, a general solution for the current distribution is obtained. A similar solution will result for the square loop driven at the center of a side. Numerical evaluation of the results is in process.

Image-Plane Measuring Technique

By the theorem of images a single conductor over an infinite, perfectly conducting ground plane produces fields identical to those of a single conductor and its image. If the conditions of a plane surface, perfect conductivity, and infinite extent are satisfactorily approximated for the ground plane, very good experimental results can be obtained by the image-plane technique. In addition to simplicity of construction, other advantages of the system are 1) that it is inherently balanced and thus a high degree of electrical symmetry obtains, and 2) the presence of the image plane serves as an electrical shield to isolate operator and measuring equipment from the antenna.

The square and circular loops of interest are used to terminate a single wire transmission line mounted over an image plane. The input impedance of the loop is measured by sampling the rf signal along the driven transmission line with a small movable probe. The standing-wave-ratio or width-of-the-minimum method is used to determine impedance. The amplitude and phase of the current are obtained with a similar probe moved along the loop itself. The phase is determined by mixing the signal picked up on the loop with that from a matched transmission line and varying the position of the probe on the matched line to give a minimum signal.

Transmission-Line Description

The image plane used in this investigation (see Fig. 1) is of $\frac{1}{8}$-inch duralium and measures 12 feet by 10 feet. The center section, comprised of a two-foot strip, is highly polished and divided into four removable panels for easy adaptation to other measuring techniques. In the near vicinity of the transmission line and antenna it was found necessary to provide a smooth, highly conducting transition from one panel to another with the aid of silver paint and aluminum foil.

A single-wire transmission line of $\frac{1}{4}$-inch brass tubing is mounted over part of the polished section of the image plane. A coaxial driving unit incorporating an ordinary type-*N* connector is soldered directly to the line. An inner line conductor terminated in a small search probe serves as a means of moving the probe along a 1/16-inch slot in the outer conductor as well as transmitting the rf signal to the detecting system. A rack-and-pinion device of fine pitch provides an accurate method of meas-

* Manuscript received by the PGAP, October 5, 1955; revised manuscript received, January 31, 1956. Paper given at the 1955 National Conference on Aeronautical Electronics, Dayton, Ohio. Published as Cruft Lab. Tech. Rep. No. 213, Harvard Univ., Cambridge, Mass., May, 1955. This research was made possible through the joint support of the Navy Department (Office of Naval Research), the Signal Corps of the U. S. Army, and the U. S. Air Force, under ONR Contract N5ori-76, T. O. 1.

† Gordon McKay Lab., Harvard Univ., Cambridge, Mass.

[1] E. Hallén, "Theoretical investigations into the transmitting and receiving qualities of antennae," *Nova Acta Upsala*, ser. IV, vol. 11, pp. 1–44; 1938.

[2] G. Glinski, "Note on circular loop antennas with non-uniform current distribution," *J. Appl. Phys.*, vol. 18, pp. 638–644; July, 1947.

[3] H. C. Pocklington, "Electric oscillation in wires," *Proc. Camb. Phil. Soc.*, vol. 9, p. 324; 1897.

[4] J. E. Storer, "Theoretical Discussion of Circular Loops," Cruft Lab. Tech. Rep. No. 212, Harvard Univ., Cambridge, Mass.; 1955.

[5] R. King, "Theory of the Square-Loop Antenna," Cruft Lab. Tech. Rep. No. 222, Harvard Univ., Cambridge, Mass., 1955 and IRE Trans., vol. AP-4, pp. 393–407; July, 1956.

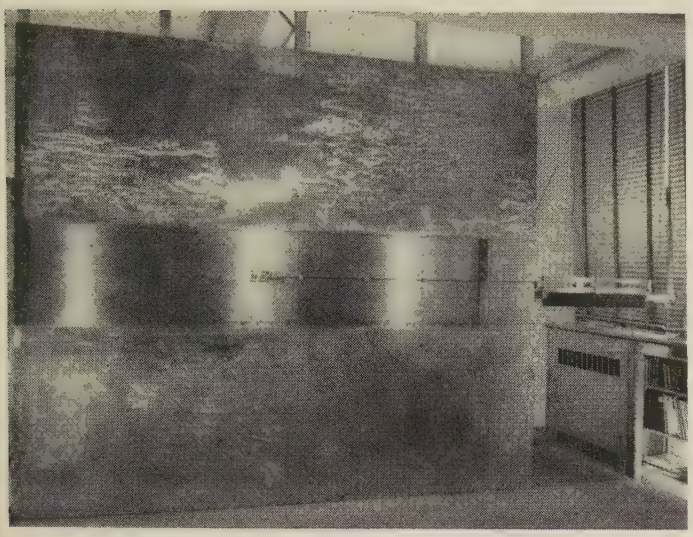

Fig. 1—Vertical image plane.

uring the motion of the probe. Adjustments on the carriage allow for a wide range of line spacings and for rotation of the slot through 180°. For the measurements described in this report a full line spacing of 1.246 cm was maintained, establishing a transmission-line characteristic resistance of

$$R_c \doteq 120 \cosh^{-1}\left(\frac{b}{2a}\right) = 155.4 \text{ ohms},$$

where b is the distance between centers of the line and its image, and a is the radius of the conductor.

The transmission line is supported at a position $\lambda/4$ behind the driving point by a short-circuiting plate. This quarter-wave section presents a high impedance to the generator. However, the distance from driving point to the load is nearly $1\frac{1}{2}$ meters long and additional support is needed. It was established experimentally that the smallest usable bead of polyfoam (that which would adequately support and space the line) had the effect of an added shunt capacitance across the line. The effect could be minimized by placing the beads at positions of minimum impedance along the line where the shunt effect would be small. However, for measurements involving continual end-load variation, it was not feasible to reposition the supporting beads for each new measurement. Therefore, the use of a single polyfoam strip supporting and spacing the entire length of line was decided upon (see Fig. 2). With such a strip, uniform and consistent measurements were made along the line and the results were interpreted in terms of the *measured* transmission-line wavelength, λ''. The wavelength in a medium of polyfoam, λ_p, was calculated as follows:

$$\frac{\lambda}{\lambda_p} = \sqrt{\frac{\epsilon_p}{\epsilon}}$$

where $\epsilon_p/\epsilon = 1.05 =$ the relative dielectric constant of polyfoam

$$\lambda_p = \frac{40}{1.025} = 39.02 \text{ cm}$$

$\lambda =$ free space wavelength.

The measured λ'' must be between the values for free space and polyfoam; that is $39.02 \text{ cm} < \lambda'' < 40$ cm as only a small portion of the space between line and image plane is filled with polyfoam. The measured value of λ'' was 39.62. The values of phase constant, β, and characteristic resistance, R_c, were adjusted to the following new values for use in computing impedance.

$$\beta = \frac{2\pi}{\lambda''} = 0.158; \qquad R_c = \frac{120}{\sqrt{\epsilon_{\text{eff}}}} \cosh^{-1}\left(\frac{b}{2a}\right) = 154.1$$

where

$$\frac{\epsilon_{\text{eff}}}{\epsilon} = \left(\frac{\lambda^2}{\lambda''^2}\right) = \text{relative effective dielectric constant.}$$

These new values apply to impedance measurements for the circular loop. The square loops were not supported in this way and the original values of $\beta = 0.157$ and $R_c = 155.4$ ohms apply to them. The image-plane system described above is a modification of that discussed by Angelakos[6] and Conley.[7]

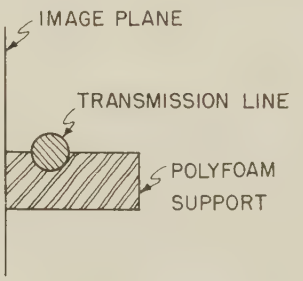

Fig. 2—Cross section of supported transmission line.

Measuring Equipment

The arrangement of the measuring equipment is shown in the block diagram of Fig. 3. A standard frequency generator (Measurements Corporation, Boonton, N. J., Model 84) having a maximum output power of 200 milliwatts was used to produce a frequency of 750-mc. A double-stub tuner and a single-tube tuner are attached to the output. At the correct 750 mc setting the generator was found to produce a substantial 520-mc signal in addition to the desired 750 mc. The single stub is used to detune the 520-mc signal and the double stub as a matching device for the 750-mc signal.

[6] D. J. Angelakos, "Current and Charge Distributions on Antennas and Open-Wire Lines," Cruft Lab. Tech. Rep. No. 98, Harvard University, Cambridge, Mass., 1950.

[7] P. Conley, "Impedance Measurements With Open-Wire Lines," Cruft Lab. Tech. Rep. No. 35, Harvard Univ., Cambridge, Mass., March, 1948.

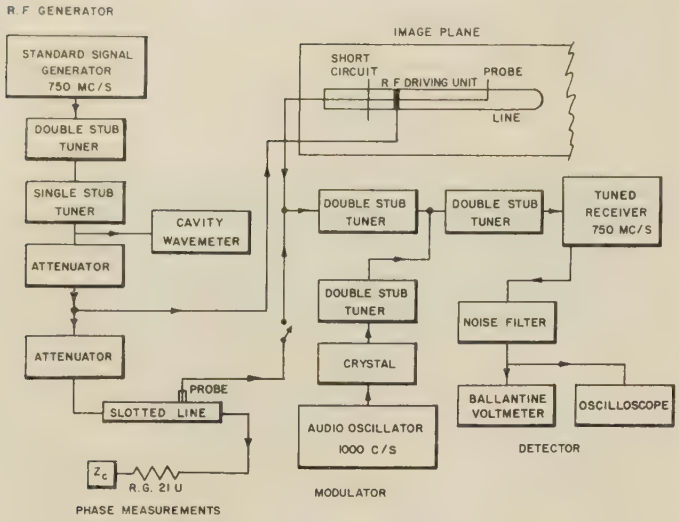

Fig. 3.

A waveguide-beyond-cutoff attenuator is used to vary the power fed to the line. The rf signal is picked up from the transmission line by a charge or current probe and mixed with a 1000-cps modulation signal through a crystal. A U. S. Navy Radio Receiver Model RDO tuned to 750 mc is used as an amplifier and detector. The detecting system was calibrated and all meter readings corrected against the calibration curve. The 1000-cps output from the receiver was filtered through a noise filter and observed on a Ballantine voltmeter and an oscilloscope.

Measuring Procedure

Impedance measurements[8] were made using the standing-wave ratio method for antennas which were well matched; the width-of-the-minimum method was used when twice-the-minimum power point could be located accurately. The hyperbolic solution of the transmission-line equations shows that

$$\sinh(\alpha d + \rho) = \sin\beta\left(\frac{\delta l}{2}\right)$$

and

$$\coth \rho = \text{vswr}$$

where

$\gamma = \alpha + j\beta$ = propagation constant
δl = width of the minimum at twice the minimum power point
d = distance from line termination to probe
ρ = terminal attenuation function.

For high standing-wave ratios it is apparent that αd and ρ are of the same order of magnitude, and that attenuation must be considered. A half-line attenuation constant of 2.57×10^{-5} nepers/cm was calculated and used in many of the final computations. All measurements were made on a half-loop configuration which, when referred to the characteristic resistance of the full transmission line, resulted in the input impedance of the complete loop.

Current distribution measurements were not made on square loops, since it was not feasible to maneuver a probe around a series of right-angle bends. Distributions on circular loops involved slotting these loops parallel to the plane of the loop and moving a shielded-loop probe[6,9] around the loop contour. Measurements near the junction were avoided since errors due to coupling to the transmission line currents would be involved.

The slotted line shown in the block diagram of Fig. 3 was used for phase measurements. If this line is well matched, the error due to vswr > 1 is kept at a minimum. A signal is picked up by the search probe at an arbitrary point on the loop and mixed with a signal similarly coupled out of the matched line. If the probe position on the matched line is varied to give a minimum signal on the Ballantine voltmeter and oscilloscope, the two signals are 180° out of phase. For a new position of the antenna probe another position of the matched-line probe will give a similar minimum signal. The difference in position of probe along the matched line from some arbitrary reference position may be expressed in degrees and is a measure of the difference in phase between signals at the two positions on the image line. The position of the minimum can only be obtained accurately if the minimum is sharp. Therefore the amplitude of the signal from the matched line must be very nearly that of the signal from the search probe on the antenna itself. This was most easily done by varying the probe depth in the phase line and calibrating this change directly in degrees of phase shift. A small correction was then applied to the phase angle.

Antenna Construction

Loop antennas of $\frac{1}{4}$-inch brass tubing (radius = 0.318 cm) were designed to cover a range of circumference or perimeter from $\lambda/2$ to 3λ. The conventional parameter for the thickness of an antenna is

$$\Omega = 2 \ln \frac{2h}{a},$$

where

$2h$ = circumference or perimeter of loop
a = radius of conductor.

With constant radius the longer antennas are electrically thinner. One set of data was taken on square loops of 0.106 inch conductor diameter driven from one corner. The physical thickness of these loops was such that the conductor could be readily shortened and rebent from the 2λ to the $\lambda/2$ loop size, and from the re-

[8] D. D. King, "Impedance measurements on transmission lines," Proc. IRE, vol. 35, pp. 509–513; May, 1947.

[9] R. King, "Theory of Linear Antennas," Harvard University Press, Cambridge, Mass., pp. 129–131, 1956.

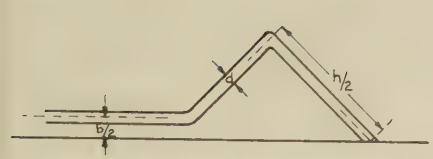

A SQUARE LOOP DRIVEN FROM ONE CORNER

b = 1.246 cm
a = d/2 = .318 cm
$h = \frac{\text{perimeter}}{2}$
$h' = \frac{\text{actual conductor length}}{2}$
$= h - .881$ cm

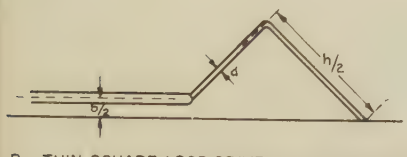

B THIN SQUARE LOOP DRIVEN FROM ONE CORNER

b = 1.246 cm
a = d/2 = .134 cm
$h = \frac{\text{perimeter}}{2}$
$h' = \frac{\text{actual conductor length}}{2}$
$= h - .881$ cm

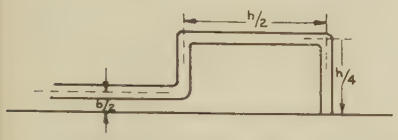

C. SQUARE LOOP DRIVEN FROM CENTER OF ONE SIDE

b = 1.246 cm
a = d/2 = .318 cm
$h = \frac{\text{perimeter}}{2}$
$h' = \frac{\text{actual conductor length}}{2}$
$= h - \frac{b}{2}$ cm

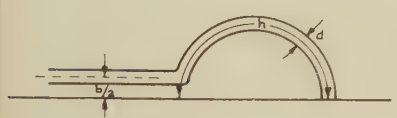

D. CIRCULAR LOOP

b = 1.246 cm
c = d/2 = .318 cm
$h = \frac{\text{circumference}}{2}$
$h' = \frac{\text{actual conductor length}}{2}$
$= h - \frac{b}{2}$ cm

Fig. 4—Loop configuration and notation (image-plane method).

sults a fairly accurate prediction could be made about the input impedances of thin loops.

The critical dimensions and mounting procedures are given in Fig. 4. Although all loops were constructed on the basis of loop size representing the complete square or circular configuration, it was decided to let the antenna size be determined by the actual length of conductor. In the loop case this implies an effective perimeter or circumference slightly smaller than the actual one. Results obtained will be referred to these *effective* dimensions.

Both types of square loops were constructed using a set of angle bends to which various lengths of tubing could be fitted. Contact to the image plane was made by tapping holes in the plane and screwing a slotted brass plate directly to it. A few sets of holes permitted the mounting of the complete set of antennas and neither the holes in the ground plane nor the screw heads extending slightly above the surface of the plate were found to have any effect on the measurements. To avoid further defacing of the ground plane the circular loops were mounted at a single contact point by a screw from the back of the screen, and connection to the transmission line was made by a series of appropriate lengths of tubing supported by strips of polyfoam. Had the extent of the undertaking been realized at the beginning of experimentation, more consistent mounting methods could have been used.

Presentation of Data

Input Impedance

Impedance data have been obtained for several loop sizes between $\lambda/2$ and 3λ. These experimental results are available in tabulated form but appear here in Figs. 5 through 11. The procedure for procuring the final impedance values is partially mathematical and partially graphical. Standard Smith chart representations of the normalized impedances were obtained from measurements of standing-wave ratio and position of voltage minimum. Fig. 5 (next page) compares impedance spirals for loops of two different conductor sizes which, for purposes of comparison, may be described as thick and thin. Another Smith chart, Fig. 6, compares loop measurements for three loop configurations, keeping the conductor size constant.

The actual plotting of impedances in Smith chart representation is facilitated by the spiral form which individual curves take. The need for a vast number of experimental points in the vicinity of peaks and dips is eliminated. The normalized values of resistance and reactance can be read directly from the Smith chart, and when multiplied by the characteristic resistance of the transmission line along which the measurements were made, produce the impedance of each antenna measured. In addition, values are easily extrapolated to yield additional $\beta_0 h' = 2\pi h'/\lambda$ or $\beta_0'' h' = 2\pi h'/\lambda''$ values. The linear or semilog plots of the final impedances were obtained by this partially graphical method, the irregularities of the curves requiring some extrapolated values. Reading directly from a Smith chart in regions of high standing-wave ratio can produce errors caused by the limited accuracy of that part of the circle diagram. For such values it is better to plot the normalized admittance and compute the impedance from it.

As a supplement to the Smith charts curves have been plotted for the thin square loop driven from one corner in Fig. 7 (p. 616); the thicker square loop driven from one corner in Fig. 8; the square loop driven from the center of one side in Fig. 9; and the circular loop in Figs. 10 and 11. Figs. 10 and 11 also contain the theoretical impedances and admittances for antennas of comparable dimensions obtained by Storer.[4]

Current Distribution

Current distributions on circular loops have been plotted as a function of probe position around the loop. The distance around the half-circumference of each loop is calibrated in degrees (the angle which the probe position forms with the image plane) with the driving point being considered as $\Phi = 0°$ and the short circuit $\Phi = 180°$. The distance around the half-loop is also calibrated in fractions of a wavelength.

The search probe used to determine the amplitude and phase of the current was mounted in a slot in the plane of the loop. Therefore measurements very near

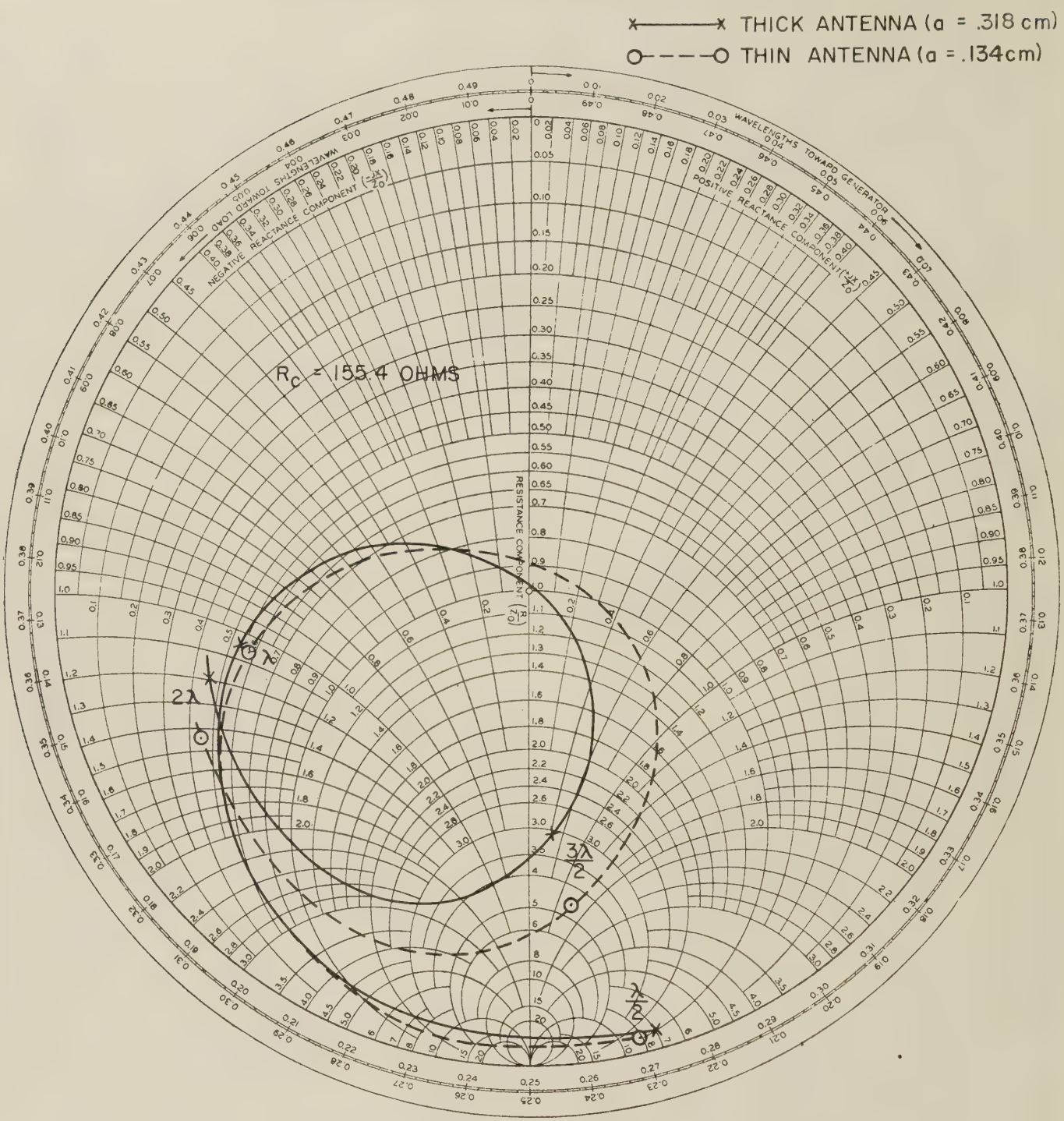

Fig. 5—Impedance of square loop driven from one corner.

$\Phi = 180°$ were not considered accurate due to the small circular short-circuiting plate and the coupling of the probe to its own image. Measurements near the driving point were even less reliable since the orientation of the probe was such that a maximum of coupling to the transmission line occurred (see Fig. 12, p. 617). The apparent distribution then was a result of a combination of currents on both antenna and transmission line. Quite arbitrarily, results obtained by the probe within 2 cm of the junction were ignored, and where feasible the curves were extrapolated to $\Phi = 0°$.

The most reasonable way of presenting the amplitude of the current would be to assume a driving voltage of 1 volt and normalize $|I|$ in amperes/volt to the input admittance of each antenna. Since the reliability of the input current data was known to be quite poor, the current amplitude curves were presented as relative to the current maximum obtained at $\Phi = 180°$. In Fig. 13 (p. 618) this maximum was arbitrarily given the value of one. In Fig. 14 where comparison with theory is possible, a more reliable current maximum was available, and two sets of experimental data were normalized to the theory at $\Phi = 90°$.

The position $\Phi = 90°$ is equally distant from both the

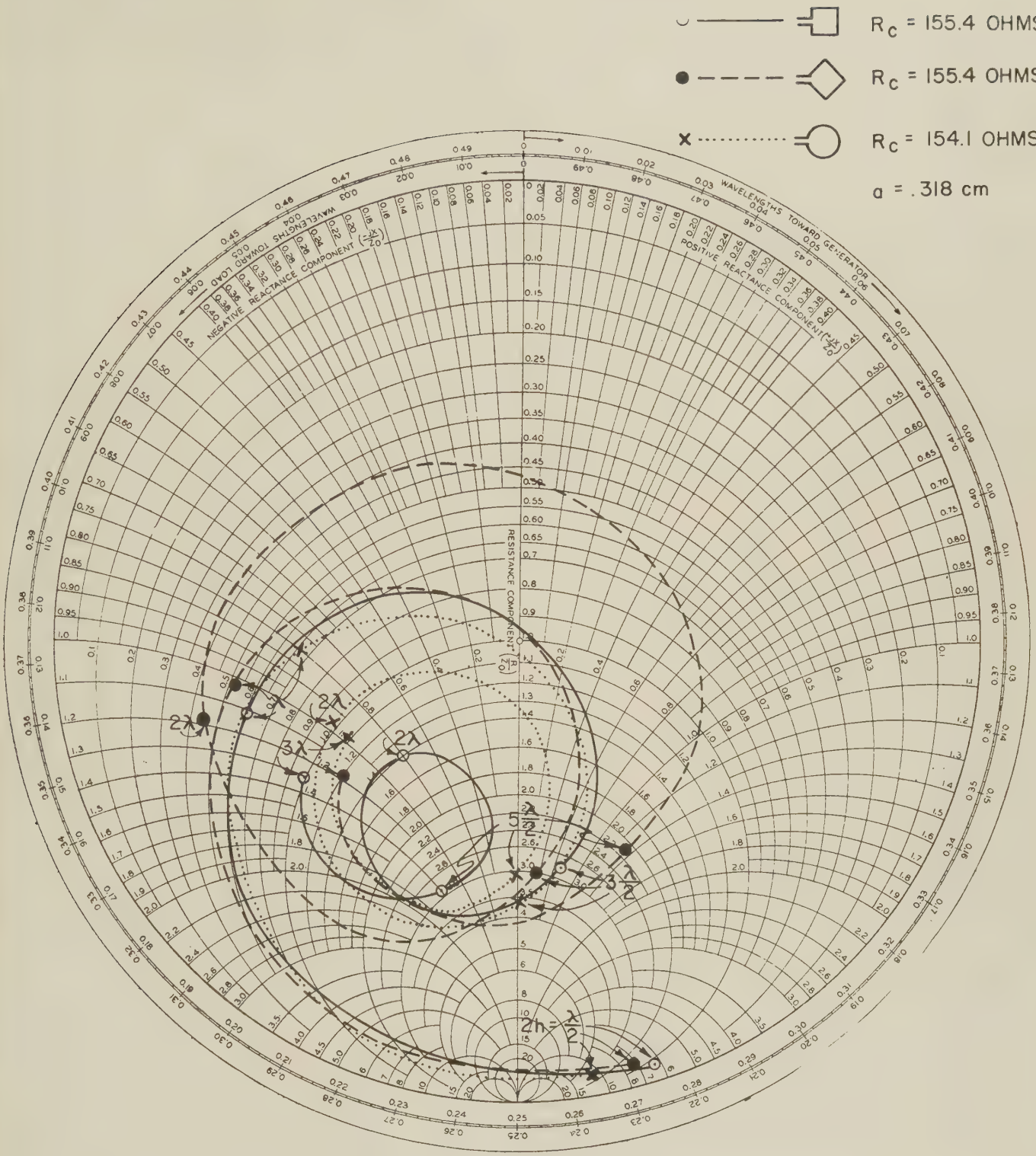

Fig. 6—Impedance of three-loop configurations.

driving point and the short circuit and is likely to provide the most reliable data. This point was taken as a reference for the phase measurements and, for purposes of presentation, the phase angle, θ, is set equal to 0° at $\Phi = 90°$.

Conclusion

The input impedances of the square loops of different thickness shown in Fig. 5 provide a basis for a general statement about the effect of conductor size on the impedance of loop antennas. It is apparent that the thinner antenna has a higher input impedance at antiresonance than the thicker antenna, and its resonance occurs for a smaller loop perimeter. A superposition of the semilog plots of Figs. 7 and 8 would illustrate this more clearly.

It is interesting to compare the input impedance of a loop antenna with a dipole of corresponding length and

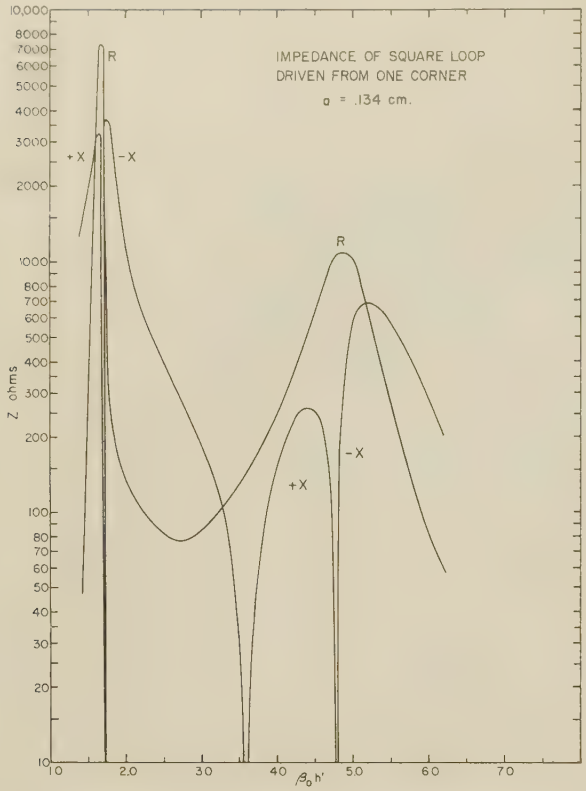

Fig. 7—Impedance of square loop driven from one corner.

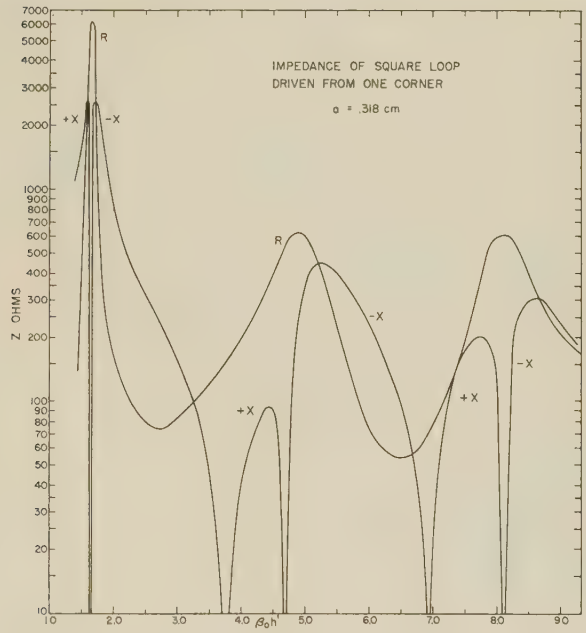

Fig. 8—Impedance of square loop driven from one corner.

conductor size. Kennedy and King[10] include circle diagrams and linear plots which should be compared with the experimental results from this paper and the circular-loop theory of Storer.[4] The resonant and antireso-

[10] P. A. Kennedy, and R. King, "Experimental and Theoretica Impedances and Admittances of Center-Driven Antennas," Cruft Lab. Tech. Rep. No. 155, Harvard Univ., Cambridge, Mass., April, 1953.

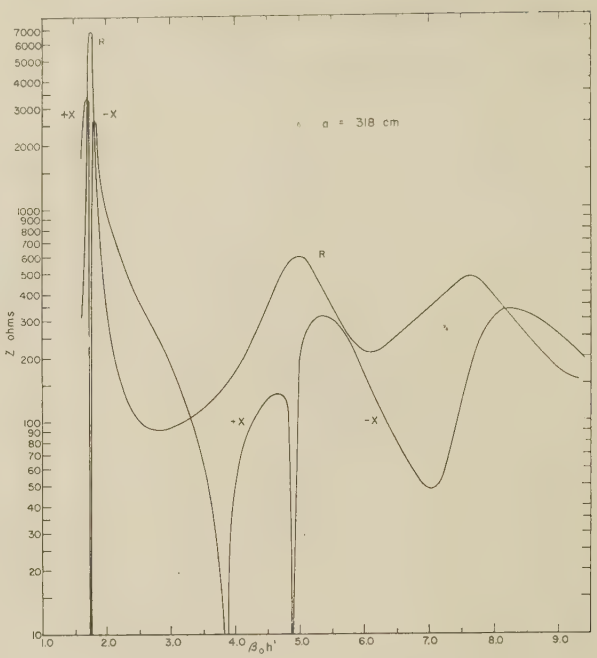

Fig. 9—Impedance of square loop driven from center of one side.

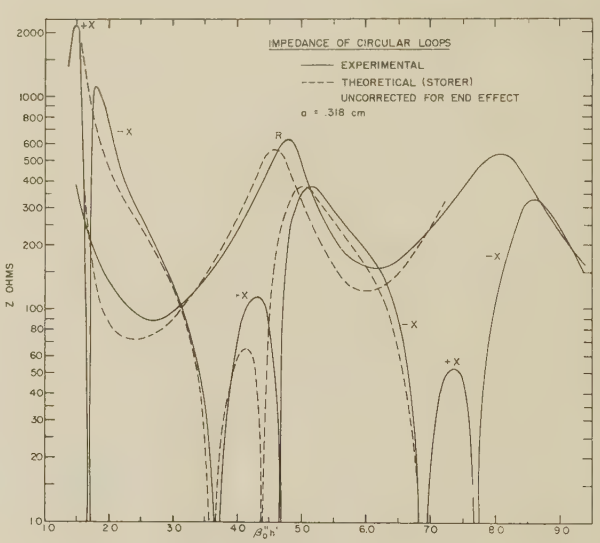

Fig. 10—Impedance of circular loops.

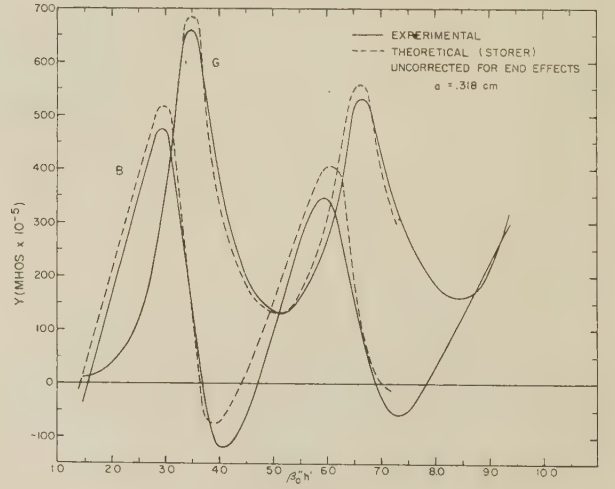

Fig. 11—Admittance of circular loops.

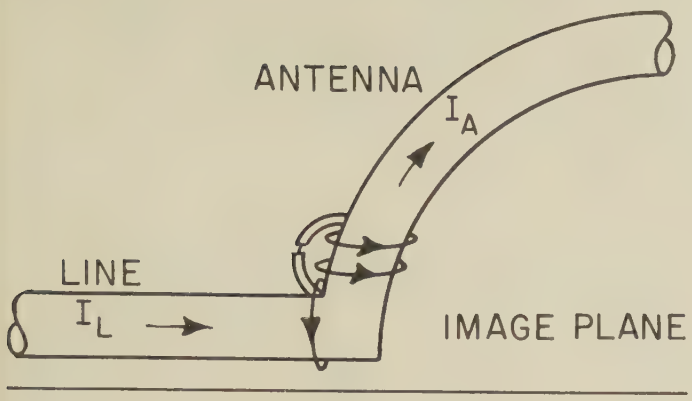

Fig. 12—Probe orientation.

nant antenna sizes compare in the following way: the first antiresonant loop has a resistance and reactance of very large magnitude, and a comparison of the input impedance spiral of the loop with that of the dipole shows the sequence of resonance and antiresonance to be interchanged, but to be quite comparable in general outline. Note, however, that the loop antennas are more capacitive than dipole antennas of corresponding size.

A comparison of loop antennas of all three configurations is found in the Smith chart of Fig. 6. It is apparent that the curves lie quite close together when $2h=\lambda/2$, λ, and $3\lambda/2$. When $2h=2\lambda$, there is a wide spread in input impedance for the three configurations—the square loop driven from the center of one side having the largest impedance, the square loop driven from one corner having the smallest impedance, and the circular loop falling in between. The curves approach each other again at $5\lambda/2$ and are close at 3λ.

A plausible explanation is found for this curve separation if a cosinusoidal distribution of the current about each of these contours is considered as in Fig. 15. For the loop size $2h=2\lambda$, configuration (a) has a current minimum at all four corners. Therefore, a maximum concentration of charge exists at these points. Configuration (b) represents the opposite condition and (c) can be said to have a maximum concentration of charge in several bent regions. The condition in (a) and to a lesser extent in (c) can be interpreted as an effective lengthening of the antenna or compression in the distribution pattern.

The amount of compression is then a measure of the capacitive loading at the corners or bends. The input current will be affected by the compression in distribution pattern, and the input impedance will vary inversely as the current.

A plot of current distribution (Fig. 16) obtained experimentally by Kaliszewski[11] is of value. The compression in distribution pattern is discernible from the shifted minima—the "center-driven" square loop being shifted the most and the "corner-driven" square loop being shifted the least. The currents at the driving point then differ by an amount proportional to the shift. The shift of the circular loop is exaggerated since the only available data are for a loop of circumference 2.2λ. The relative values of the input current from Fig. 16 mean little since there is some error in the peak voltages. However, a qualitative estimate of $|I_0|$ can be made from the shifted peaks.

More could be said about this corner effect if each antenna size measured could be examined for the relationship between current minima and bends in the antenna. In some cases such a combination of current minima and current maxima at the corners will occur that all three loop configurations will have distributions shifted essentially by the same amount, and no appreciable separation in the impedance spirals will be noticeable. It would be hard to say anything quantitative about small effects which are of the same order of magnitude as the experimental error, so only the antenna size for which the corner effect is greatest has been considered.

Comparison with Theory

In Fig. 10, the experimental input impedances of a set of circular loops are compared with Storer's theoretical results. No attempt has been made in the theory to consider the actual driving conditions, but, nevertheless, fairly good agreement exists. A plot of the admittance in Fig. 11 is perhaps more revealing. The conductances appear to be in good agreement, but some discrepancy exists in the susceptance terms. By adding a constant negative capacitance to the theoretical susceptance, the effect of coupling between line and termination can be taken into account. An exact determination of this quantity has not been made, but a qualitative estimate using data available from the corresponding problem in the dipole suggests that the correction involved would promote better agreement between theoretical and experimental susceptance curves.

A comparison with theory of amplitude and phase of the current on a circular loop of particular circumference is provided in Fig. 14. There is some scatter of experimental points, but in general good agreement with theory exists for both amplitude and phase. The curve of a cosine distribution is superimposed and it appears to be a reasonable approximation of the actual distribution.

General Observations

If the curves of Figs. 7, 8, 9, and 10 are observed near resonance, an estimated bandwidth of 150 mc with standing-wave ratio $\leqq 1.5$ can be calculated. (For this estimate a constant antenna length was chosen and resistance was plotted as a function of frequency.)

The current amplitudes for the large loops of Fig. 13 show a similarity to a traveling wave form for $\Phi<90°$.

[11] T. Kaliszewski, "Complementary Loop Antennas," Cruft Lab. Tech. Rep. No. 241; February, 1956.

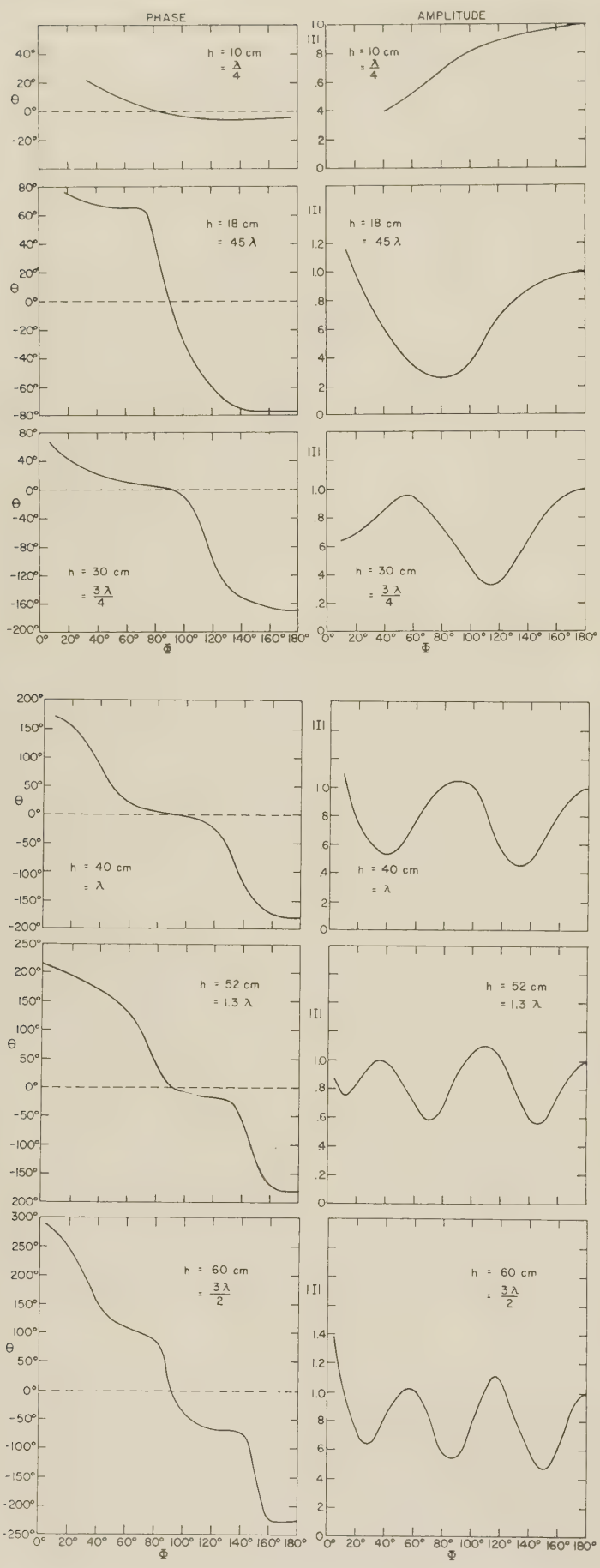

Fig. 13—Current distribution on circular loops.

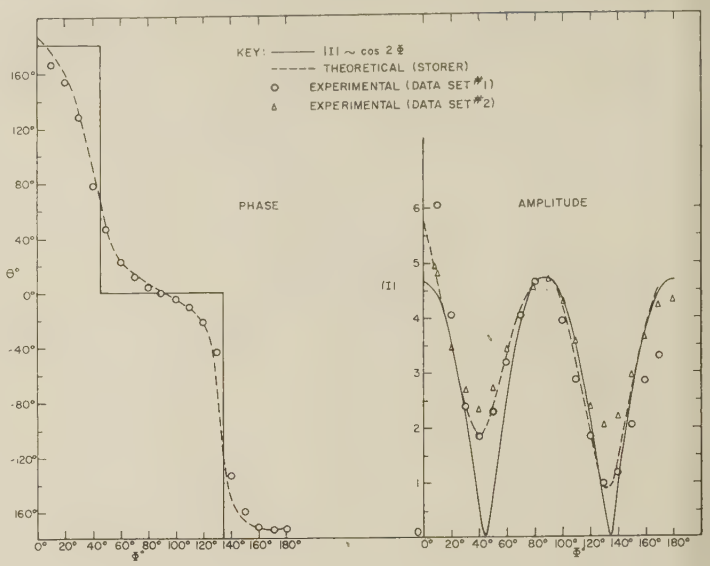

Fig. 14—Current distribution on circular loop ($h=40$ cm $=\lambda$; $\Omega=11$).

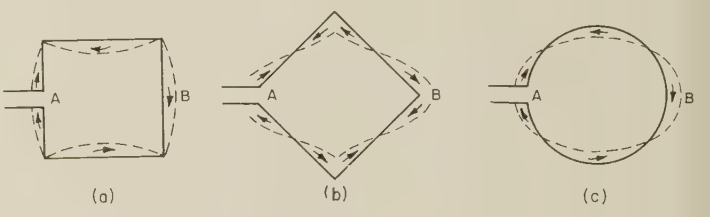

Fig. 15—Assumed consinusoidal current distribution ($2h=2\lambda$).

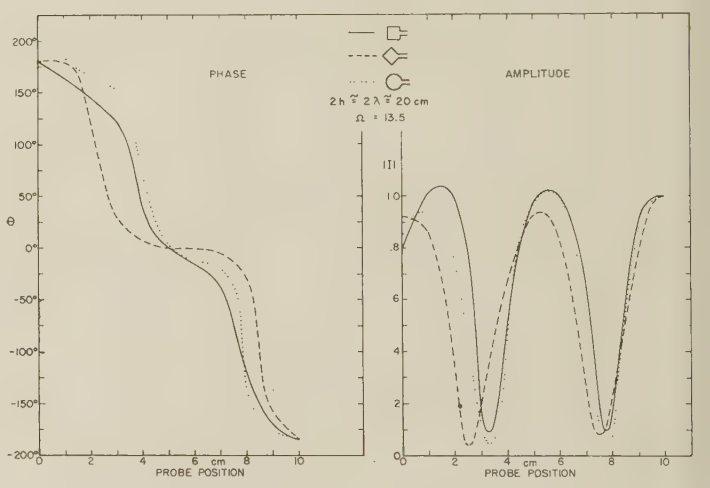

Fig. 16—Current distribution—comparison of three configurations (complementary slot methods).

The current at points far from the short circuit resembles that of an infinitely long transmission line. A similar observation has been made by Storer[4] from his theoretical solution of the current distribution on large loops.

Acknowledgment

Thanks are due to Prof. Ronold King for his aid in interpreting the experimental results and to Prof. James E. Storer for the use of his theory.

Systematic Errors Caused by the Scanning of Antenna Arrays: Phase Shifters in the Branch Lines*

L. A. KURTZ† AND R. S. ELLIOTT†

Summary—**By choosing a suitable equivalent circuit representation for an array-type scanning antenna with the phase shifters in its branch lines, a general expression is derived for the radiation pattern in terms of the active impedances of the radiating elements, the incremental phase shift between elements, and the desired aperture distribution. If the active impedances of the radiating elements vary with beam position as a result of mutual coupling, or if the active impedances are constant, but different from the characteristic impedances of the branch lines, then an infinite series is required to represent the radiation pattern. The first term of the series is the desired pattern and the remainder can be defined as the systematic error. Individual terms of the series represent beams with relative angular positions which correspond to multiples of the interelement phase shift and with relative magnitudes which are dependent upon the deviation from a match of the active impedance of the radiators. The systematic error, if uncontrolled, can prevent the achievement of low sidelobe level. Experimental evidence is presented in support of the analysis.**

Introduction

THE RESEARCH reported in this memorandum was initiated by experimental findings with a two-dimensional scanning array. This antenna was fed by a standing wave through shunt coupling to a main line and the beam was scanned away from broadside by inserting phase shifters in the branch lines. It was noticed that the pattern steadily and seriously deteriorated with increasing scan angle, and developed high, unwanted sidelobes. The hypothesis was made that this deterioration was caused by the changing mutual coupling between elements in the array. A theory was evolved, based on this hypothesis, which satisfactorily explained the principal perturbations in the pattern and linked pattern degradation to variations in the branch line impedances.

To test the theory, a versatile array was constructed for which mutual coupling in the plane of scan was virtually eliminated. Mutual coupling was then simulated by a range of controlled impedances achieved by varying the number of radiating elements in each stack of the array. Adjustable phase shifters were inserted in the branch lines, and radiation patterns were measured as functions of active impedance and scan angle. Subsequent sections of this report will be devoted to a development of the theory, discussion of the experiment, and a comparative analysis. One significant outgrowth of the analysis will be seen to be the specification of a tolerable mismatch for a prescribed sidelobe level.

* Manuscript received by the PGAP, November 25, 1955; revised manuscript received, April 16, 1956. This research was performed while the authors were members of the Hughes Research Labs., Culver City, Calif.

† Rantec Corp., Calabasas, Calif.

Theory

The theory to be presented will be limited to arrays which are fed by a standing wave in the main line, which contain phase shifters only in the branch lines, and which are scanned in a plane parallel to the main line. The radiating elements can be either slots or dipoles; any polarization is permissible, and the coupling between the main line and a branch line can be either series or shunt. For shunt coupling, an adequate equivalent circuit is suggested by Fig. 1. In Fig. 1, the junctions are spaced 180 electrical degrees apart and the degree of coupling of the mth branch is controlled by A_m, the turns ratio of the coupling transformer. The phase shifters are represented as variable lengths of transmission line of characteristic impedance Z_0. The fixed electrical length of the first branch line is θ_1 and $(\theta_1+m\theta)$ is the variable electrical length of the mth branch line. Thus $\theta=0$ corresponds to broadside operation.

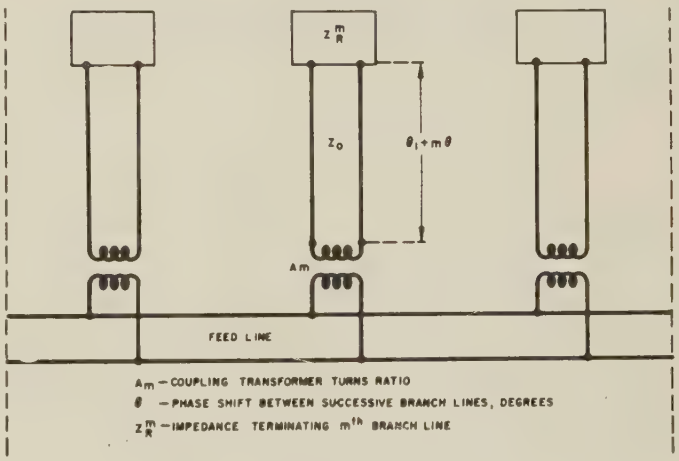

Fig. 1—Simplified equivalent circuit of scanning array.

The active impedance terminating each branch line, $Z_R{}^m$, may consist of mutual-impedance as well as self-impedance. The principal mutual contributions come from the two adjacent neighbors. For long arrays with conventional aperture distributions, the magnitude of a given radiating current, $I_R{}^m$ differs only slightly from the neighboring values $I_R{}^{m-1}$ and $I_R{}^{m+1}$. If a uniform progressive phase shift is employed to scan the beam, the phase of $I_R{}^m$ is approximately halfway between that of $I_R{}^{m-1}$ and $I_R{}^{m+1}$. Therefore, $Z_R{}^m$ does not differ greatly from one branch line to another, if the self-impedances are alike, which is usually the case. This

argument becomes weak for the branch line impedances near either end of the array, but for long arrays the influence of the end elements is relatively slight. Hence, the assumption is made that $Z_R{}^m$ is the same for all m and the superscript will be dropped in the ensuing analysis.

The additional assumption is made that all system components are perfect, with the one exception that Z_R may not necessarily be equal to Z_0. Thus all junctions are assumed precisely placed, all transformers exact, all phase shifters lossless and perfectly matched.

Let E_s be the main line voltage common to all junctions, and let $I_R{}^m$ be the current flowing through the active impedance, Z_R, of the mth branch line. Using conventional transmission line theory, the relation between current and voltage is found to be

$$I_R{}^m = \frac{A_m E_s}{Z_R \cos(\theta_1 + m\theta) + jZ_0 \sin(\theta_1 + m\theta)} . \quad (1)$$

If d is the spacing between radiators and ϕ is the azimuthal angle measured from broadside, the array factor in the plane of scan is proportional to $F(\phi)$, where

$$F(\phi) = \sum_{m=1}^{M} I_R{}^m e^{jmkd \sin \phi} \quad (2)$$

and M is the number of branch lines in the array.

If the reflection coefficient, Γ, is defined by the relation

$$\Gamma = \frac{Z_R - Z_0}{Z_R + Z_0}, \quad (3)$$

(1) may be rewritten

$$I_R{}^m = \frac{2E_s A_m}{Z_R + Z_0} \frac{e^{-j(\theta_1 + m\theta)}}{1 + \Gamma e^{-2j(\theta_1 + m\theta)}} . \quad (4)$$

By expanding the factor $[1+\Gamma e^{-2j(\theta_1+m\theta)}]^{-1}$ in a binomial series, the expression for $I_R{}^m$ becomes

$$I_R{}^m = \frac{2A_m E_s}{Z_R + Z_0} \sum_{n=0}^{\infty} (-1)^n \Gamma^n e^{-j(2n+1)(\theta_1 + m\theta)} \quad (5)$$

and, therefore, the field pattern is given by

$$\begin{aligned} F(\phi) = {} & B \sum_{m=1}^{M} A_m e^{jm[kd \sin \phi - \theta]} \\ & - (\Gamma e^{-j2\theta_1}) B \sum_{m=1}^{M} A_m e^{jm[kd \sin \phi - 3\theta]} \\ & + (\Gamma e^{j2\theta_1})^2 B \sum_{m=1}^{M} A_m e^{jm[kd \sin \phi - 5\theta]} \\ & - \cdots \cdots \cdots \cdots \end{aligned} \quad (6)$$

or

$$F(\phi) = B \sum_{n=0}^{\infty} (-1)^n \Gamma^n e^{-j2n\theta_1} \sum_{m=1}^{M} A_m e^{jm[kd \sin \phi - (2n+1)\theta]} \quad (7)$$

in which

$$B = \frac{2E_s e^{-j\theta_1}}{Z_R + Z_0} .$$

Eq. (7) is quite general even though it was derived for the specific case of shunt loading of the feed line with the amount of loading being controlled by ideal transformers. A similar expression can be obtained for shunt loading of the feed line wherein the coupling is controlled by quarter wave transformers of characteristic impedance, $Z_0{}^m$. In this case, the term $(-j)^{2n+1}$ would replace the term $(-1)^n$ and $Z_0{}^m$ would replace A_m. If series loading of the feed line were employed, then I_s, the common feed line current, would replace E_s, all else remaining unchanged. Essential features of (7) are independent of the type of loading of the feed line.

Eq. (6) can be interpreted generally in terms of multiple reflections within the branch lines. Successive terms of (6) are reduced in magnitude by $|\Gamma|$, the reflection coefficient of the impedance terminating the branch lines. *Eq. (6) implies that the effective sidelobe level cannot be less than* $|\Gamma|$.[1] In addition, successive terms differ in interelement phase shift by 2θ, twice the interelement phase shift introduced into the branch lines. Therefore, the second term in (6) represents that energy which travels out along the branch lines, is reflected by the mismatch of Z_R, travels back along the branch lines, to be reflected again because of the small coupling between branch line and main line, travels out along the branch lines again to Z_R, where it is radiated. Similarly, the third term in (6) represents that energy which requires two round trips in the branch lines before being radiated, etc. Hence, the array factor given by (6) represents many individual beams. Successive beams arise from the proper aperture distribution but have successively smaller magnitudes and spatial positions which are successively shifted relative to the main or zero order beam. All beams except the $n=0$ beam constitute the systematic error.

Certain special cases are of interest. For instance, if $\Gamma=0(Z_R=Z_0)$, then there will be only one beam for all values of interelement phase shift. Likewise, if $\theta=0$, there will be only one beam for all values of Γ. In the region between these two extremes, (6) is of value in interpreting measured radiation patterns in terms of the design aperture distribution, the reflection coefficient, and the interelement phase shift.

[1] When the phase shift is so small that the principal lobe of the first error pattern overlaps the main beam of the desired pattern, the definition of sidelobe level becomes tenuous. What is observed is a shoulder on the main beam. At broadside, the principal lobes of all error patterns coincide with the desired main beam. Although the systematic error is still present, it is undetectable and the sidelobe level reverts to its design value.

Experimental Array

Experimental verification of (6) requires an array in which the interelement phase shift, θ, and the active impedances, Z_R, can be independently and accurately controlled. Such control has been obtained with the two-dimensional array of edge slots shown in Fig. 2. The main line waveguide contains a linear array of edge slots cut to yield a 32-db Dolph-Tschebyscheff pattern. These slots are coupled to the branch line waveguides as shown. Each branch line contains a standing-wave fed array of edge slots, also cut to give a 32-db Dolph-Tschebyscheff pattern.

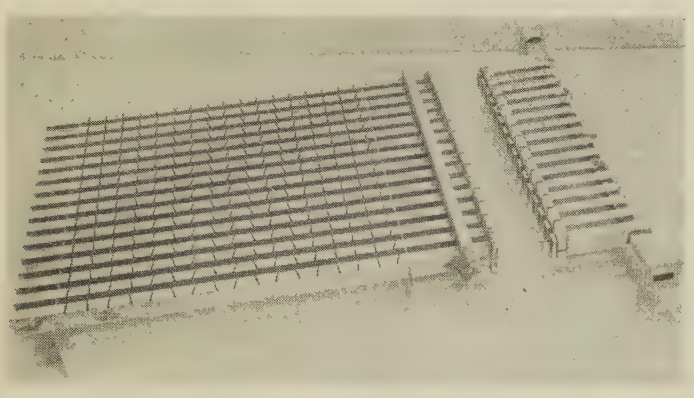

Fig. 2—Experimental array with dielectric plugs inserted in the branch lines to provide the required phase shift.

The required phase shift, $m\theta$, was introduced into each branch line by inserting a block of polystyrene in the waveguide. Quarter wave transformers in the form of notches were cut in the ends of the polystyrene blocks to reduce the discontinuity at the dielectric interface. The phase shifting blocks introduced a vswr of less than 1.10 and the error in phase shift was less than three degrees. With all blocks positioned for $\theta=0°$, the E-plane and H-plane patterns of the array are shown in Fig. 3. The deviations of these patterns from those having uniform 32-db sidelobes characteristic of the Dolph-Tschebyscheff aperture distribution result from the random errors in the construction of the array and from the element factor.

The impedance, Z_R, terminating each of the branch lines is that of a linear array of edge slots, and since these slots are standing-wave fed, Z_R can be varied by covering groups of slots with metal-foil tape. The range of impedances which were used is shown in Fig. 4, (next page) where the numbers indicate which rows of slots are radiating. The impedance values of Fig. 4 are the averages of the sixteen individual branch line impedances. These values do not include the effects of mutual coupling between arrays. This mutual coupling, however, has been reduced to a negligible value by chokes located between array waveguides. These chokes reduce the cross polarization in the radiation patterns by more than 15 db, and the same surface currents which produce cross polarization also produce mutual coupling between waveguides.

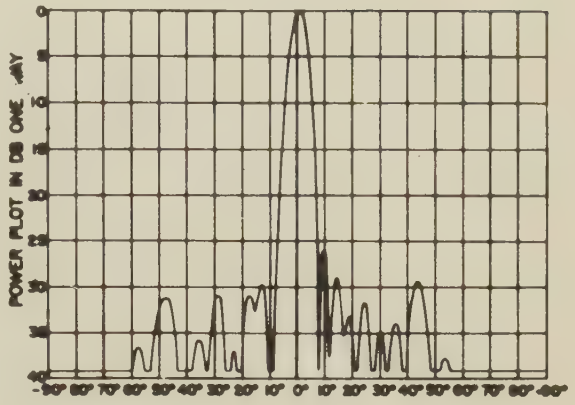

A) H-plane

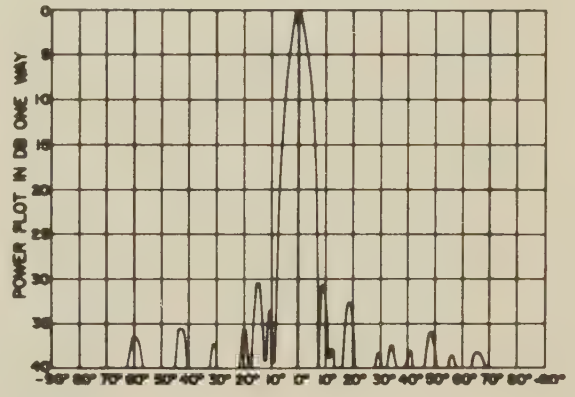

B) E-plane

Fig. 3—Measured radiation patterns $f=9375$ mc.

A measured radiation pattern is represented by the product of the array factor given by (7) and an element factor. Fig. 5 shows the element pattern (H plane) of one of the center linear arrays of the two-dimensional array of Fig. 2. Out to an angle of $\pm 70°$ this pattern represents, within ± 1 db, all the element patterns except the outside halves of the end element patterns.

Measured Radiation Patterns

Measured H-plane radiation patterns for the range of impedances shown in Fig. 3 and for increments of 20° in θ have been recorded, and representative[2] patterns are given in Figs. 6 through 9 (pp. 623–626). Relative gains are not shown because all patterns are normalized. The beams are numbered to correspond to the terms in (7); $n=0$ corresponds to the main beam. The primed numbers indicate the second occurrence of a given beam due to the element spacing of $0.70\lambda_0$ in the H plane. The best example of this recurrence of a beam is shown in Fig. 9 where $\theta=140°$.

[2] For a complete set of patterns the reader is referred to Tech. Memo. No. 359, Hughes Res. Lab.; May, 1955.

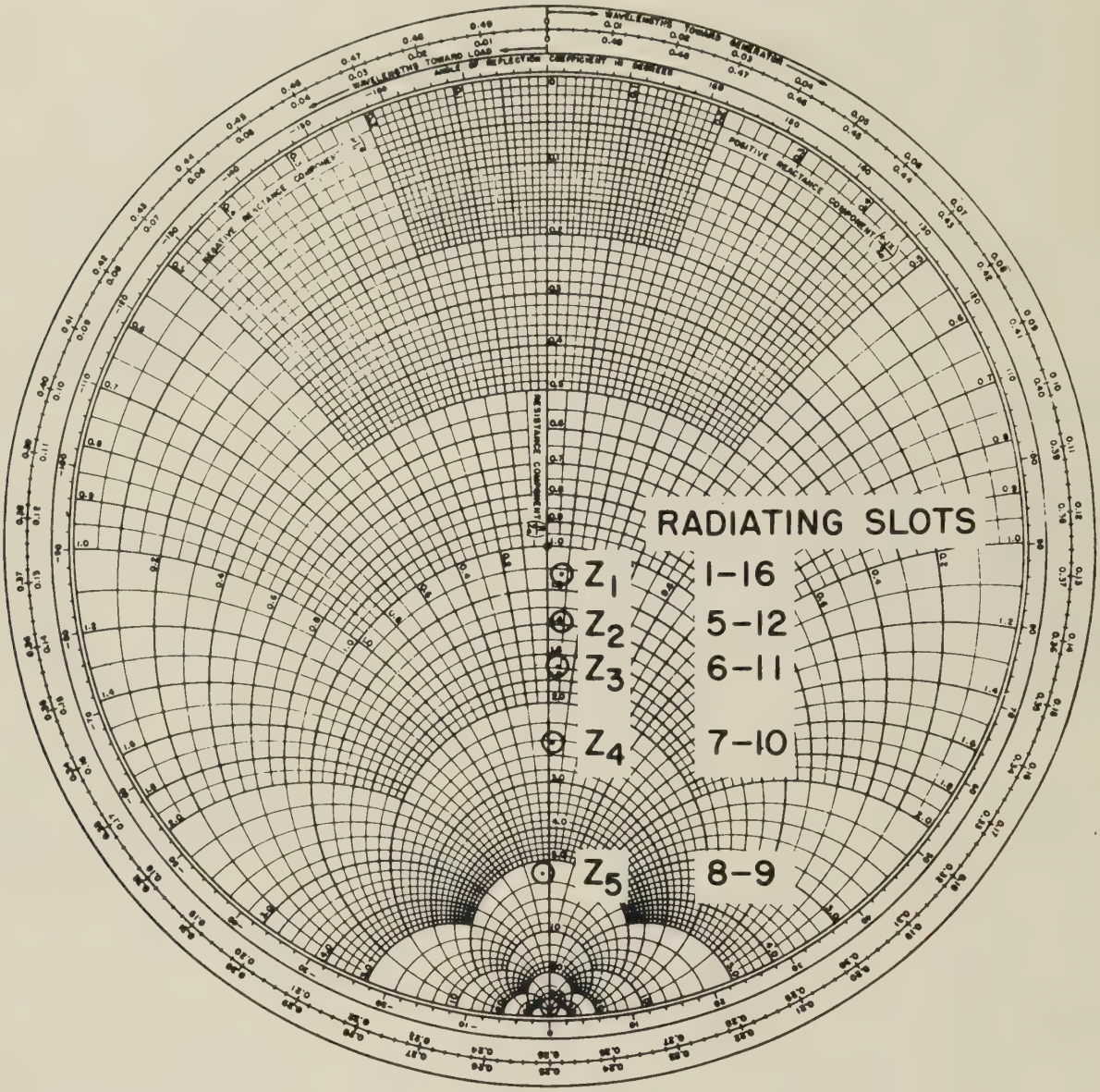

Fig. 4—Average impedance (Z_R) of branch line arrays.

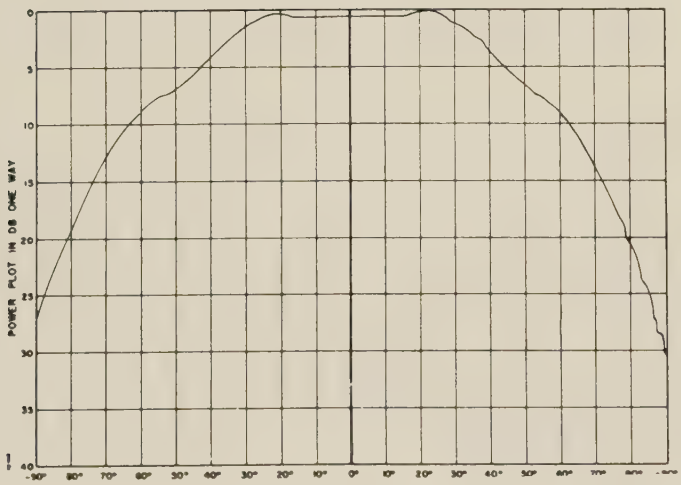

Fig. 5—Measured element pattern of individual linear array of Fig. 2.

Comparisons of Theory and Experiment

The positions and relative magnitudes of the various beams shown in Figs. 6 through 9 can be predicted from (7) through the knowledge of Γ and θ. Both Γ and θ are determinable quantities for the array described above. The average values of Γ can be computed from the data in Fig. 3 and θ can be deduced from the physical dimensions of the dielectric which is inserted in the branch line waveguides.

Using (7), the *position* of a beam is given by the following equation:

$$kd \sin \phi - (2n + 1)\theta = 2\pi p \qquad (8)$$

with p an integer. A curve of ϕ vs $(2n+1)\theta+2\pi p$ for $d=0.70\lambda_0$ is shown in Fig. 10. A precision measurement of beam positions seemed unwarranted because of the shifting effect which is a consequence of the partial

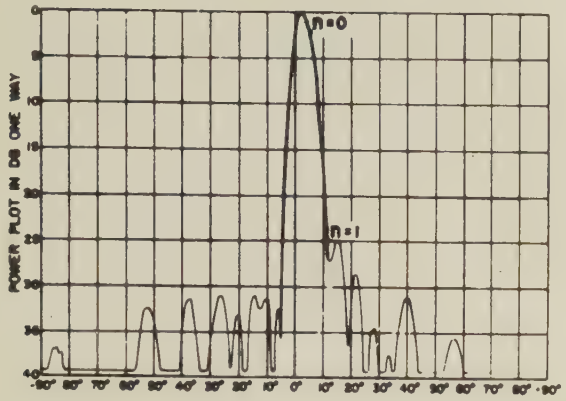

A) $Z_R = Z_1$

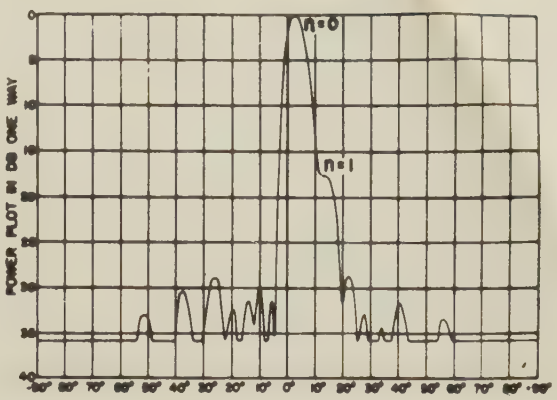

B) $Z_R = Z_2$

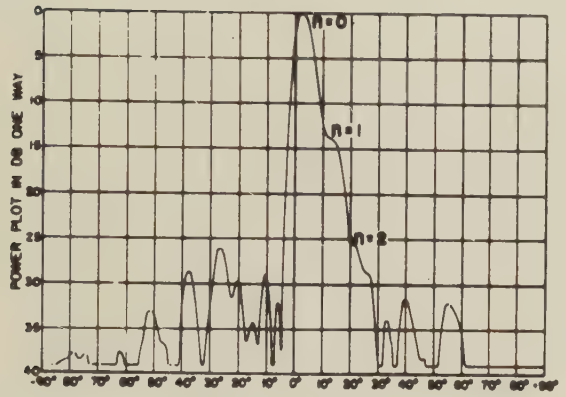

C) $Z_R = Z_3$

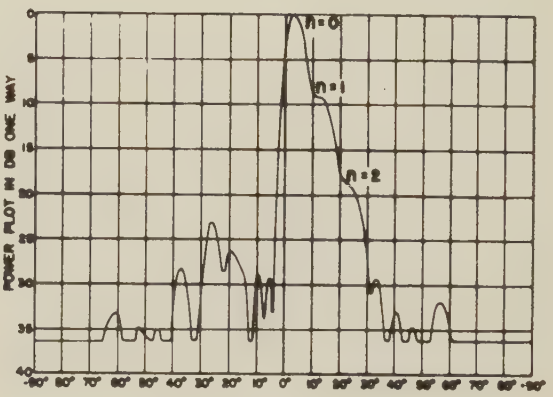

D) $Z_R = Z_4$

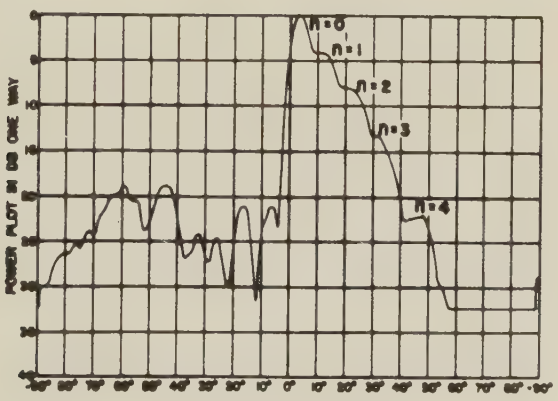

E) $Z_R = Z_5$

Fig. 6—Measured radiation patterns vs Z_R; $\theta = 20°$; $f = 9375$ mc.

superposition of lobes of patterns of different orders. However, when beam positions are read from the patterns of which Figs. 6 through 9 are representative, and compared with the values predicted, a remarkably close agreement is noticed. This is evidenced by Table I (p. 627).

Comparison of the measured *magnitudes* of the beams with the magnitudes predicted from (7) has been made by the following procedure. First, the beam magnitudes in the measured patterns such as those in Figs. 6 through 9 were adjusted to remove the effect of the element factor given in Fig. 5. Second, the average difference between successive beams in a given pattern was determined and entered in Table II (p. 627). As an example, in Fig. 8(D), corrections of $\frac{1}{2}$ db, $\frac{3}{4}$ db, and $3\frac{1}{2}$ db are necessary for beams 0, 1′, and 2′, respectively. With

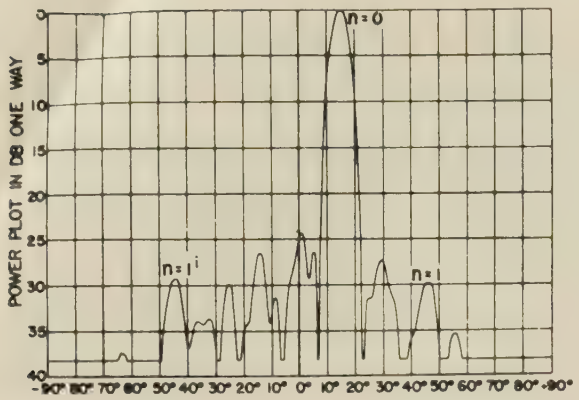

A) $Z_R = Z_1$

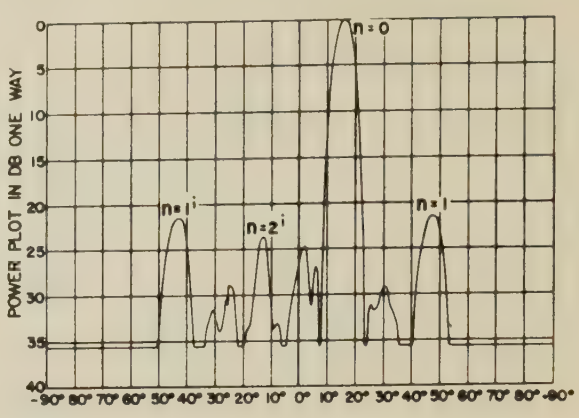

B) $Z_R = Z_2$

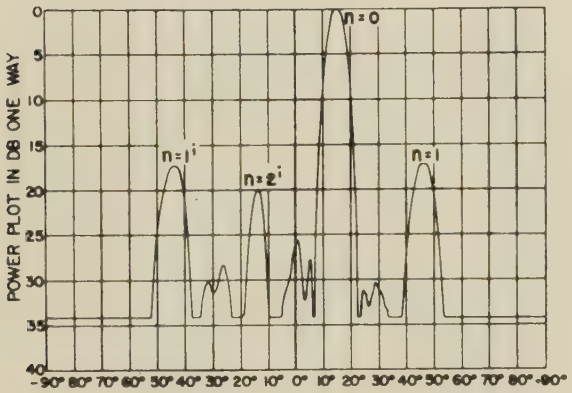

C) $Z_R = Z_3$

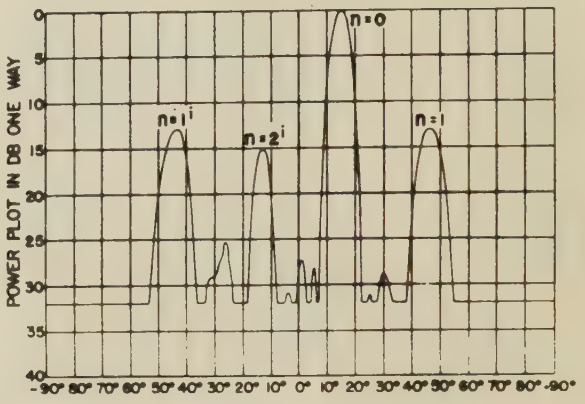

D) $Z_R = Z_4$

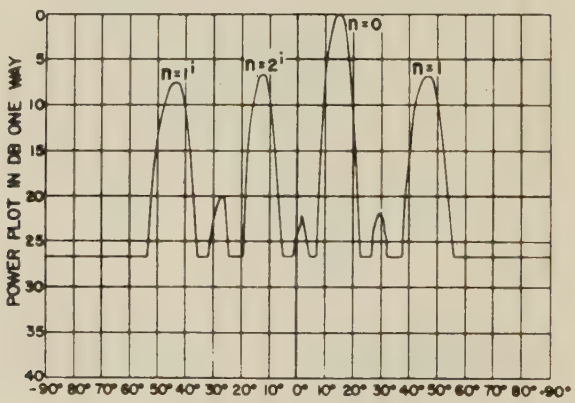

E) $Z_R = Z_5$

Fig. 7—Measured radiation patterns vs Z_R; $\theta = 60°$; $f = 9375$ mc.

the element factor removed, beam 1′ is $8\frac{1}{2}$ db below beam 0 and beam 2′ is $2(9\frac{3}{4}) = 19\frac{1}{2}$ db below beam 0. Therefore, the average value 9 db is entered in Table II for this case ($\theta = 100°$ and $Z_R = Z_4$).

The last step in the procedure was the conversion of the average values of Table II from decibel to voltage ratios and the comparison of these ratios with the reflection coefficients obtained from Fig. 4. This comparison is made in Table III (p. 627). The agreement between the measured reflection coefficient and the reflection coefficient inferred from the radiation patterns is quite satisfactory. This agreement, together with the accurate prediction of the beam positions, provides strong support for the theory embodied in (7).

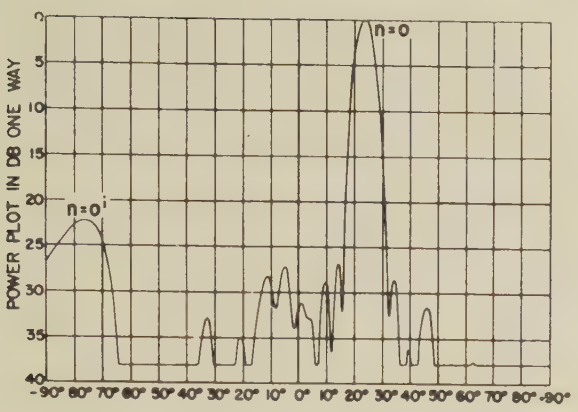

A) $Z_R = Z_1$

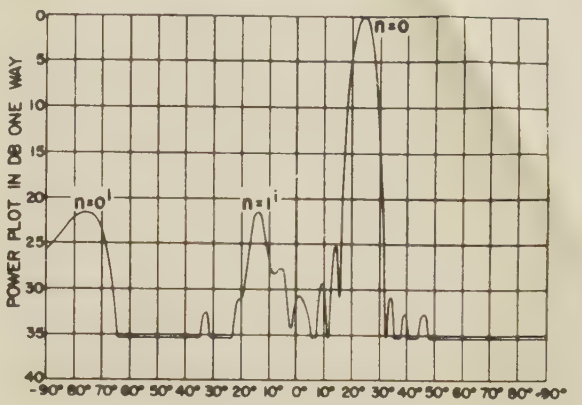

B) $Z_R = Z_2$

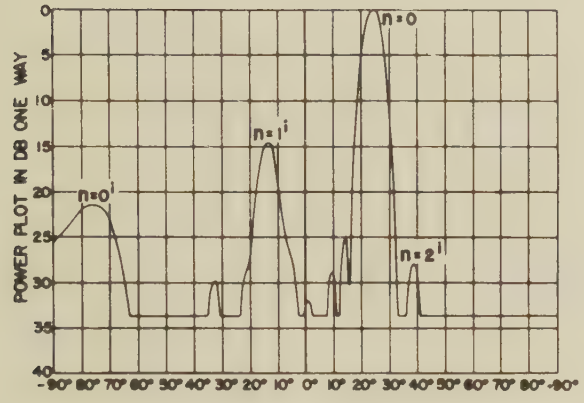

C) $Z_R = Z_3$

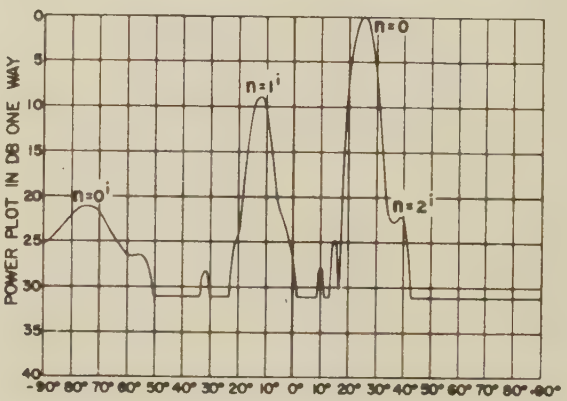

D) $Z_R = Z_4$

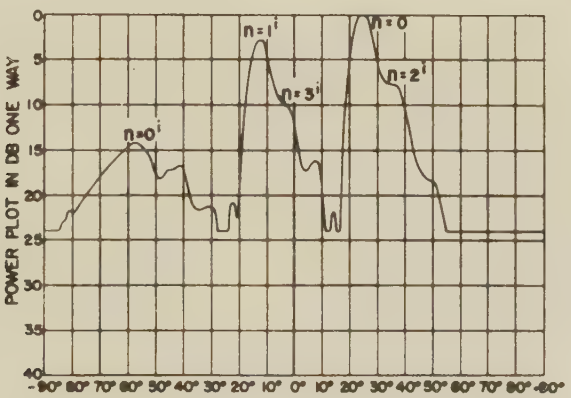

E) $Z_R = Z_5$

Fig. 8—Measured radiation patterns vs Z_R; $\theta = 100°$; $f = 9375$ mc.

Discussion

This study of resonantly spaced arrays with phase shifters in the branch lines has revealed several new ideas. The most important of these has already been mentioned, namely, that the effective sidelobe level cannot be less than $|\Gamma|$. In many two-dimensional arrays, the mutual coupling between branch line radiators is not so small as it is in the array of Fig. 2, especially if the other polarization is being employed. With increased mutual coupling, the active impedances of the branch lines are strongly affected by the interelement phase shift. Thus, in many two-dimensional arrays, as the phase shift increases so does the reflection coefficient. The influence this has on the systematic error is equivalent to moving diagonally across Table II and indicates a progressive deterioration of the sidelobe

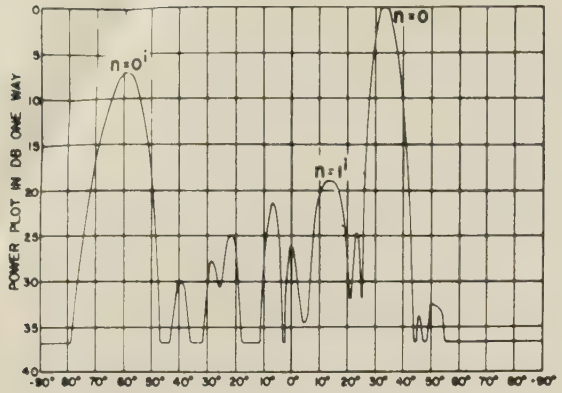

A) $Z_R = Z_1$

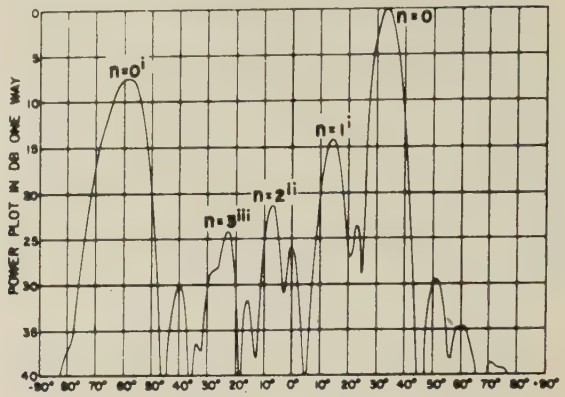

B) $Z_R = Z_2$

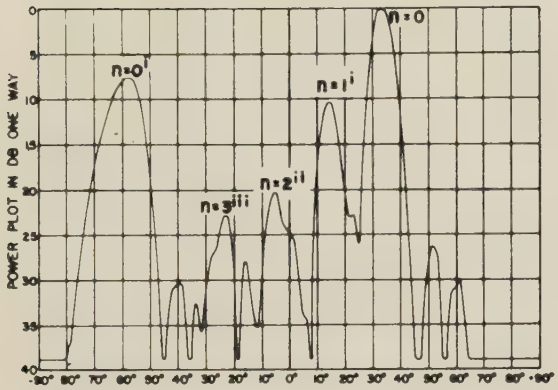

C) $Z_R = Z_3$

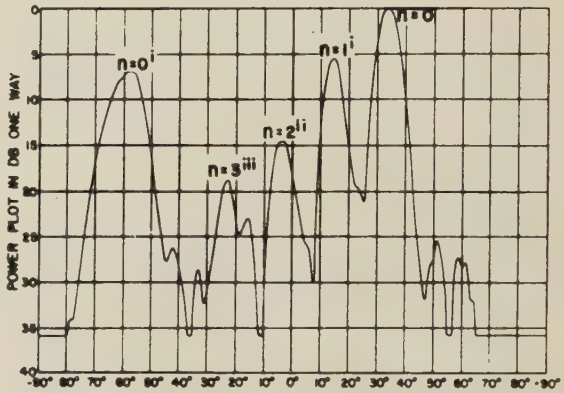

D) $Z_R = Z_4$

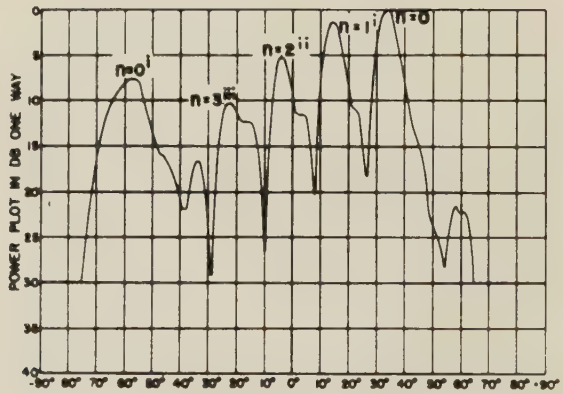

E) $Z_R = Z_5$

Fig. 9—Measured radiation patterns vs Z_R; $\theta = 140°$; $f = 9375$ mc.

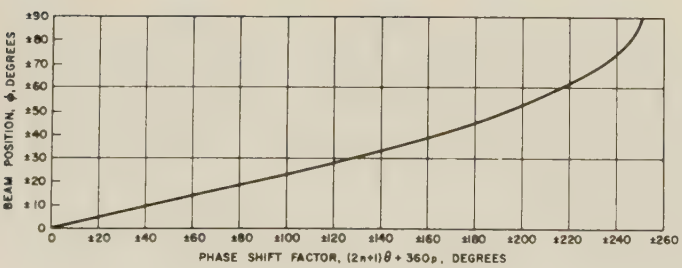

Fig. 10—Beam position vs phase shift.

level as the beam is scanned further away from its central position. Several ways have been found to overcome this defect. One method places the phase shifters in the main line whereas another maintains the phase shifters in the branch lines but uses a traveling wave to excite the branch line radiators instead of a standing wave. Both of these methods have been tried experimentally and gave excellent results. The sidelobe level remained acceptably low over a wide angle of scan. The

TABLE I

Progressive Phase Shift $\theta°$	Beam No. n	Beam Position $\theta°$ Calculated	Beam Position $\theta°$ Measured	Progressive Phase Shift $\theta°$	Beam No. n	Beam Position $\theta°$ Calculated	Beam Position $\theta°$ Measured
20°	0	4.50	3.0	100°	0	23.40	24.1
	1	13.75	14.1		1^{i}	−13.75	−12.9
	2	23.40	23.7		2^{i}	33.75	37.8
	3	33.75	32.0		3^{i}	− 4.55	− 3.0
	4	45.60	48.0	120°	0	28.45	27.4
40°	0	9.15	10.4		0^{i}	−72.25	−69.5
	1	28.45	29.0		1^{i}	0.00	− 1.0
	2	52.50	53.5		2^{ii}	−28.45	−29.0
	1^{i}	−72.25	−67.3	140°	0	33.75	34.0
	2^{i}	−40.05	−38.2		0^{i}	−60.80	−57.4
	3^{i}	−18.51	−19.0		1^{i}	13.75	14.8
60°	0	13.75	15.2		2^{ii}	− 4.55	− 4.5
	1	45.60	46.4		3^{iii}	−23.40	−22.4
	1^{i}	−45.60	44.1	160°	0	40.05	37.7
	2^{i}	−13.75	−13.3		0^{i}	−52.50	−52.7
80°	0	18.50	19.1		1^{i}	28.45	26.3
	1	72.25	69.7		2^{ii}	18.50	18.0
	3	−40.05	−38.0		3^{iii}	9.15	8.5
	4	0.00	1.0		4^{iv}	0.00	− 1.5
	1^{i}	−28.45	−27.5		5^{v}	− 9.15	− 9.0
	2^{i}	9.15	9.8		6^{vi}	−18.50	−19.0
	3^{i}	52.50	52.0				

TABLE II

Z_R	Average Difference of Beam Level—DB								
	$\theta=20°$	$\theta=40°$	$\theta=60°$	$\theta=80°$	$\theta=100°$	$\theta=120°$	$\theta=140°$	$\theta=160°$	Average
Z_1	25	22.5	24.5	31	28	21.5	20.5	19	24
Z_2	17.5	16	16	19	21.5	15.5	16	15	17
Z_3	13	12	12	13	14	11.5	12	11	12.5
Z_4	9	8	8	8.5	9	7.5	8	8	8
Z_5	4	3.5	3	3	2.5	3.5	3.5	3.5	3.5

TABLE III

Z_R	Reflection Coefficients, Γ Impedance Measurements (Fig. 4)	Pattern Measurements (Table II)
Z_1	0.060	0.063
Z_2	0.17	0.14
Z_3	0.26	0.24
Z_4	0.42	0.40
Z_5	0.70	0.67

traveling-wave feeds gave a slightly lower efficiency but provided the added improvement of an increased bandwidth. These results will be reported in detail at a later date.

Several additional features of interest were uncovered. For example, contrary to anticipation, the systematic error is commonly observed in a direction quite different from that of the main beam. Eq. (7) is useful in predicting this direction. It is also possible that the reflection coefficient may be inferred from the radiation pattern in cases where it is otherwise unobtainable.

Conclusion

For resonantly fed scanning arrays with phase shifters in the branch lines, the sidelobe level has been found to depend on the interelement phase shift and the impedance mismatch in the branch lines. Spurious lobes created by multiple reflections in the branch lines are the controlling factor in the sidelobe level. A theory has been evolved to explain this phenomenon and has been corroborated by extensive experiments. These findings have a practical application to arrays in which mutual coupling causes the active impedances of the branch lines to depend on scan angle. For such arrays a serious deterioration of the sidelobe level can result with scan and other feeding methods are preferred.

A High-Performance Conically-Scanning X-Band Antenna of Novel Design*

J. G. McCANN† AND R. J. STEGEN†

Summary—A conically-scanning antenna is described which consists of a scanner mechanism, rear feed, and 8-foot diameter paraboloid producing a pencil beam having equal *E*- and *H*-plane beamwidths. The polarization may be quickly changed from linear to circular to vertical polarization. The sense of the polarization is readily changed from left-hand to right-hand. The replacement of one section of transmission line by a half-wave plate changes the unit from a nutating polarization scanner to a twice-scan-speed rotating polarization scanner. The scanner incorporates some novel features such as a symmetrical rear feed having equal *E*- and *H*-plane patterns, high-power quarter-wave and half-wave plates, and an orthogonal mode absorber.

This paper describes the techniques which were employed to obtain the above mentioned performance. The problems encountered and their solutions are described.

Introduction

THE DESIRABILITY of maintaining accurate tracking information on missiles and aircraft has resulted in a demand for better radar sets. These improved radar sets must function as both beacon and skin trackers with improved sensitivities and accuracies. Modified or newly designed antennas which are a part of the new radars must handle higher powers and be more versatile than formerly available types. The improved performance of nutating polarization antennas over the rotating polarization types in general dictates their use. Circular polarization and also other types are quite desirable for certain applications. Vibration free scanning is most desirable so that units which are dynamically balanced must be used.

The antenna to be described here operates from 9100 to 9600 mc and includes two interchangeable circularly symmetric feeds which radiate linear or circular polarization equally well. The transmission line contains components which may be readily adjustable to provide for either horizontal, vertical, right-hand circular, left-hand circular, or twice can speed rotating linear polarization. The complete antenna system is designed to handle 250 kw peak power unpressurized. Round waveguide is used throughout most of the transmission line so that a rotating feed may be used. Because the moving parts rotate rather than nutate, the mechanical components are simplified and near perfect dynamic balancing is achieved, thereby minimizing vibration and reducing the attendant "noise."

Design

General

The conically scanning antenna consists of a waveguide transmission line, torque tube, feed, scanner assembly with drive motor, and reference generator. The complete unit is shown in Figs. 1 and 2 and is to be mounted in an 8-foot diameter paraboloid whose focal length is 27.5 inches. The transmission line and torque tube include taper sections, orthogonal mode absorber, quarter- and half-wave plates, and rotary joints. On transmitting, the rf energy enters the rectangular waveguide at the rear of the unit; passes, in order, through a taper section from rectangular to round waveguide, an orthogonal mode absorber, a rotary joint, a quarter-wave plate section, and a second rotary joint. At this point the rf either passes through a half-wave plate section or a hollow waveguide, and then through a taper section to dielectric loaded round waveguide. A splash plate directs the energy through a pressurizing cover and onto the paraboloid which colli-

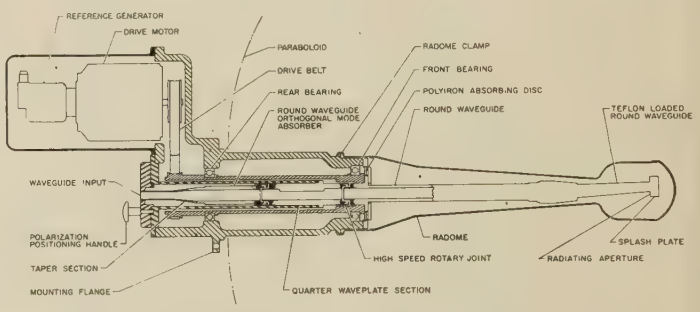

Fig. 1—Cutaway drawing of the complete unit and paraboloid.

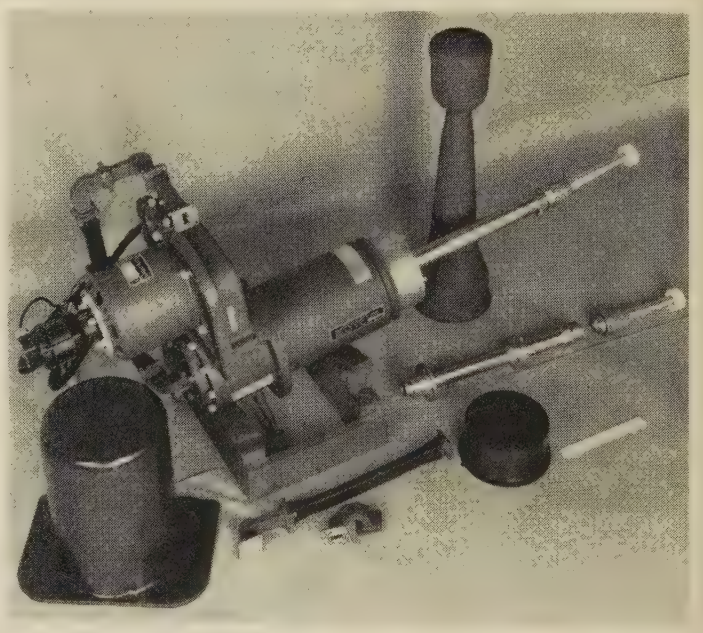

Fig. 2—Conical scanning unit including two feeds, half-wave plate and pressurizing hood.

* Manuscript received by the PGAP, October 3, 1955; revised manuscript received February 23, 1956.

† Canoga Corp., Van Nuys, Calif.

mates it into a beam. The circularly symmetric splash plate of the feed is offset from the axis of the paraboloid so that the center of radiation is displaced from the axis of rotation. This displacement causes the center of radiation to move in a circle about the focal point of the reflector, the radiated beam of the antenna describing a corresponding circular motion in space. By using either of two feed units one may obtain a 3-db or 1-db crossover. The complete unit including the radome may be pressurized to 30 psi absolute. This technique eliminates the need for a rotating pressure seal. The various types of polarizations are obtained by simple adjustments of parts of the unit.

Polarizations Available

The rf input waveguide, taper section, and orthogonal mode absorber may be rotated to any one of four positions. Vertical polarization is obtained by positioning the rectangular waveguide so that the electric vector is vertical. The quarter-wave plate section is horizontal and, therefore, is normal to the electric field and consequently has no effect on the linearity of polarization. Rotating the input waveguide 90° results in horizontal polarization. The quarter-wave plate section being parallel to the electric field again does not effect the linearity of the polarization.

If the rectangular waveguide is rotated to a position 45° from the vertical, the polarization will be circular. Right-hand polarization[1] results when the electric vector, as viewed from the rear of the unit, is up to the left; left-hand, when the E vector is up to the right.

Linear polarization rotating at twice the scan speed may be achieved by use of a half-wave plate rotating with the feed. The rf input waveguide is positioned so as to result in linear polarization leaving the quarter-wave plate. This linear polarization, on propagating through the rotating half-wave plate, will be converted to linear polarization rotating at twice the scan rate. It appears that twice scan rate rotating polarization may provide better tracking of a linearly polarized beacon than ordinary rotating polarization.

Microwave Components

Input Section

The input section consists of an inductive iris, a taper section from rectangular to round waveguide, an orthogonal mode absorber, and one-half of a rotary joint. The function of the inductive iris is to match out the inherent discontinuity of the taper section and orthogonal mode absorber. The maximum vswr of the input section over the band 9.0 to 9.7 kmc without the iris was 1.20 and with the iris was 1.08.

If it is assumed that a maximum value for the axial ratio is 0.6 db and the antenna vswr is under 1.4 then it is easily shown that the vswr of the orthogonal mode absorber must be less than 1.5. The absorber must dissipate all of the reflected power from the feed which, for 250 watts average power and a vswr of 1.4, would be 10.5 watts. After considering the relative advantages and disadvantages of a number of different types of absorbers, it was decided that a polyiron loaded slot should be used. Measurements indicated that a long axial polyiron loaded slot in round waveguide would have very low loss (less than 0.1 db for 12 inches of slot) and reflection when oriented so as not to couple to the incident wave. The polyiron is placed on the outside of the round waveguide, thereby minimizing attenuation of the incident wave. When oriented for maximum coupling the reflection from the device was still very small. The attenuation was about 1.1 db per inch. Two slots each 3.5 inches long and diametrically opposite each other are used. The total one-way attenuation is 7.7 db which represents a vswr of 1.46 to the reflected wave. The polyiron is in contact with the brass waveguide and can therefore adequately handle the power to be dissipated.

The rotary joint is a half wavelength folded coaxial type in which the break in the metal occurs at a current minimum. The characteristic impedances of the two quarter-wavelength sections are designed to give broadband performance.

Quarter-Wave Plate Section

The quarter-wave plate consists of a length of guide having circular cross section at either end and departing from circular symmetry in the intermediate section. This part was broached from a thick walled tube using a special broach having a circular cross section with a flat side. After broaching, the ends of the tube were turned to a circular cross section. The ends of the flat portion were turned to a diameter less than the tube diameter to provide a matching section. The length of the matching section was determined experimentally, being about a quarter guide wavelength. The length of the center section was adjusted to obtain 90° of relative phase shift between the two orthogonal modes normal to and parallel to the flat portion. The axial ratios as a function of frequency for three different length quarter-wave plates are shown in Fig. 3.

Half-Wave Plate Section

The design and fabrication of the half-wave plate is similar to that of the quarter-wave plate. The center section is made longer so that there is a differential phase shift of 180° between the principal orthogonal modes. Fig. 4 shows the axial ratio as a function of frequency.

Feed Unit

The feed unit shown in Fig. 5 consists of a section of air-filled round waveguide, a taper section to teflon-loaded waveguide, and a teflon supported metal splash plate.

[1] The sense of polarization is defined by IRE Standards, for an observer watching the departing wave: The polarization is "right-handed" or "left-handed" according to whether the E-vector traces out the ellipse in the clockwise or counterclockwise sense, respectively.

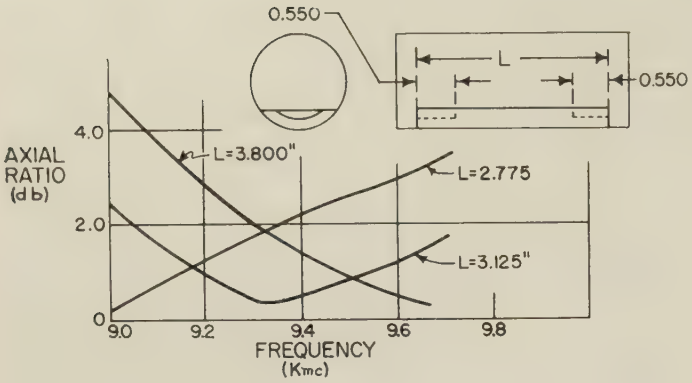

Fig. 3—Axial ratios for three different length plates.

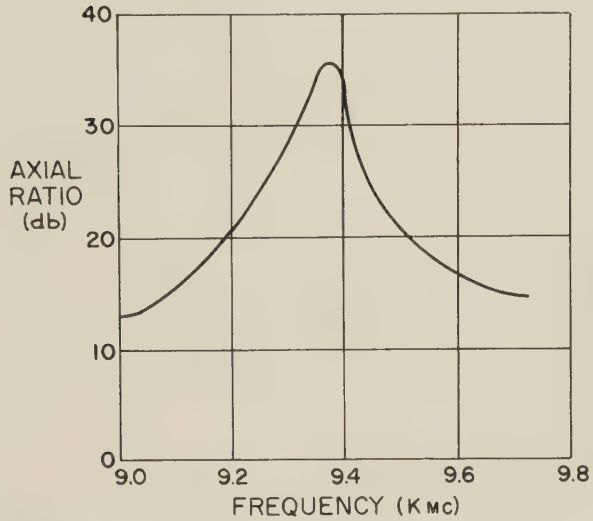

Fig. 4—Axial ratio vs frequency for half-wave plate.

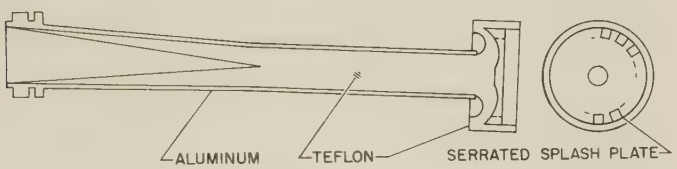

Fig. 5—Section view of feed.

The first section of air-filled guide is cut at a small angle with the normal to the axis of the waveguide. Rotation of the torque tube causes the center of radiation to describe a circle about the axis of the paraboloid. The collimated beam from the paraboloid traces out a similar path in space.

The teflon taper begins at the outer wall of the larger diameter round waveguide for several reasons. This construction, in conjunction with the splash plate support, is used to hold the complete feed unit together. The outside taper also reduces the fields at the air-dielectric interfacial space, thereby reducing the possibility of corona or arc-over. The length of the taper is adjusted so that the mismatch due to incremental changes in cross section are minimized.

The teflon loaded round waveguide was designed to have the same cutoff wavelength as the air-filled waveguide. Teflon is used to reduce the diameter of the ring source as well as for strength. Since a ring source has different centers of radiation in the E and H planes it cannot be focused properly in a paraboloid. This defocusing results in poorer beam formation than with a point source feed. The diameter of the teflon loaded waveguide is made as small as possible to minimize this defocusing.

The radiating portion of this feed is a modification of a Naval Research Laboratory design.[2] The teflon in the waveguide is extended beyond the end of the tube and supports the serrated splash plate. The depth of the serrations may be adjusted to control the H-plane primary patterns. These serrations have little effect on the E-plane pattern, the outer diameter of the splash plate determining its shape. The match of the feed to its transmission line has been optimized over the band by properly shaping and positioning the various parts. The matching of the feed was obtained chiefly by adjusting the distance from the splash plate to the end of the metal tube and by introducing additional reflections from the flat at the center of the splash plate. These reflections are at a position which tends to cancel other reflections over the complete band. The splash plate support and the waveguide dielectric are threaded and screwed together. Teflon pins are inserted axially to lock the parts together. The splash plate retains these pins, the splash plate being held in by a teflon nut.

Radome

The pressurizing hood is a thin wall type which has been designed to allow the wave to pass through at or near normal incidence. The hood is fabricated of a fiberglas cloth impregnated with a low-loss polyester resin and will withstand 30 psi pressure. The radiation pattern is only very slightly affected by the presence of the hood. The signal loss at the peak of the main beam due to the hood is 0.5 db.

Polyiron Absorbing Disk

The polyiron disk shown in Fig. 1 absorbs any power that may tend to leak into the region of the front bearing, thereby minimizing the possibility of bearing burnout due to rf arcing.

Secondary Radiation Patterns and VSWR and Power

The maximum vswr of the complete unit for twice scan speed rotating linear polarization is 1.32. The maximum vswr's when radiating nutating linear and circular polarizations are 1.32 and 1.17 respectively. The vswr of the circularly polarized feeds are obviously better than the linearly polarized units because reflected energy from beyond the quarter-wave plate is returned as an orthogonal mode and dissipated in the absorber.

The measured beam crossover levels for the two different offsets are 3.2 ± 0.4 db and 1.0 ± 0.2 db. The offset

[2] F. L. Hennessey, "A Broad Band Axially Symmetric Vertex Feed," *Naval Res. Lab. Rep.* No. 4071; October 22, 1952.

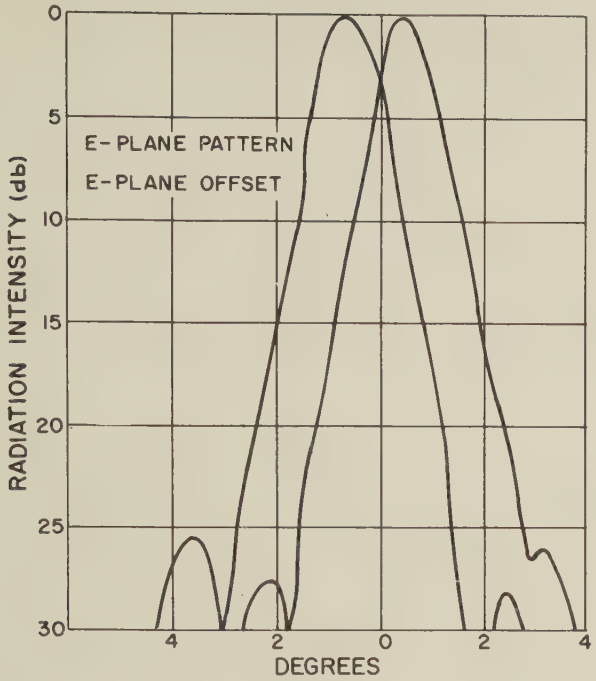

Fig. 6—Offset plane patterns showing beam crossover (frequency 9100 mc).

plane secondary radiation patterns are shown in Fig. 6. All side lobes were below 25 db. The patterns were measured with a transmitter-receiver distance of 1600 feet. The complete unit was high power tested without pressurization. There was no sign of arcing or corona at the maximum available power of 250 kw.

Drive System

The conical scanner is driven by a synchronous motor rated at $\frac{1}{3}$ hp, 115 v, 60 cycles, 3 phase, 1800 rpm. This drive motor is connected by means of a Gilmer "Timing" belt to the choke and sprocket assembly of the torque tube section as shown in Fig. 1. The use of this belt drive system insures quiet, vibrationless operation. The need for periodic lubrication, oil and grease seals, and other difficulties associated with gear drives is eliminated. The belt and sprockets have teeth which eliminate slippage and insure that conical scanning occurs at the synchronous motor speed. An idler pulley is provided for adjusting belt tension.

Reference Generator

The reference generator is a two-pole generator delivering 67 v into an 1800 ohm load. It may be electrically phased by loosening base clamping screws.

Conclusion

A high-performance conically scanning antenna has been designed for use in conjunction with a high-precision, high-power, *X*-band tracking radar. The antenna provides a variety of different types of polarization, with two different beam crossover levels. The feed elements rotate and therefore may be completely dynamically balanced, thereby providing vibration free operation. Highly precise tracking is achieved because of the reduction in error due to vibration of the antenna. High power components are used throughout and it is believed that this unit will handle one megawatt when pressurized to 30 psi absolute.

Acknowledgment

The work described in this report was performed under Signal Corps Contract DA 36-039 SC-52625. The authors would like to acknowledge the contributions of G. Hewitt, W. Falstrom, and L. Woodford for the mechanical design of the antenna. R. R. Higgins and G. Hammond performed many of the radiation pattern and impedance measurements.

Slot Admittance Data at K_a Band*

MAURICE G. CHERNIN†

Summary—**Admittance data on transverse edge slots in RG-96/U waveguide can be obtained by a technique called the moving lossy short technique. By this technique the radiation attenuation of a test section of identical slots can be determined. It is then possible to specify both the slot inclination angle and the slot depth of cut required to yield any conductance within the range of measurements. These data were used to design an experimental 30-slot array with a 25-db Taylor aperture distribution. This array was successful, yielding sidelobes near −23 db. Subsequently, the same data were used in designing an 8-foot array with 432 edge slots having the same aperture distribution. This array had a half-power beamwidth of 14 minutes and sidelobes of the order of −24 db. These results compared favorably with design objectives.**

Introduction

RECENT developments in system components at K_a band have made the need for antennas in this frequency band more pronounced. The long, linear array with transverse edge slots is an antenna type which has had successful use at the lower frequencies, for example at X band. To construct similar linear arrays at K_a band, it is necessary to obtain information on the electrical characteristics of the slots which are to be used. Such information can be obtained by scaling data obtained at X band, although this method is not entirely satisfactory due to the dimensional differences of the waveguide used at the two frequencies. A second method is to measure the slots at K_a band as they are to be used. Since this method does not require the extrapolation of data from other frequencies, it offers a more direct approach to the problem.

An adaptation of a measuring technique suggested by Oliner[1] was used to measure the radiation and dissipative attenuation of sections of K_a-band waveguide with identical transverse edge slots in one of the narrow walls. This technique, called the moving lossy short technique, has as its principal advantage over the standard slot measurement procedure the fact that the vswr which is being measured can be adjusted over a wide range by varying the loss in the movable short. The characteristics of the unknown to be measured determine the optimum amount of loss to be incorporated in the short. Another advantage over the standard slot measurement procedure is that the moving lossy short technique "automatically" averages 8 to 10 (or more) data points, compared with the one datum point per frequency which is usually taken with the standard technique.

* Manuscript received by the PGAP, October 3, 1955; revised manuscript received, April 18, 1956.

† Hughes Aircraft Co., Inc., Culver City, Calif.

[1] H. M. Altschuler and A. A. Oliner, "Microwave measurements with a lossy variable short circuit," Res. Rep. R-399-54, Polytech. Inst. of Brooklyn, Bklyn., N. Y., September 16, 1954.

It should be noted that the determination of the attenuation of a slot or group of slots requires no knowledge of the admittance of the slot. Hence, it is not necessary to know if a slot is resonant to determine the frequency at which radiated power is maximized. However, since the conductance of a slot is a more common reference term, the data are presented in this form.

Theory

The philosophy behind the moving lossy short technique is that the attenuation produced by a test section is related to certain of its scattering matrix elements and can be determined more precisely from the scattering matrix elements than directly. The total attenuation (A_t) of a test section is equal to the dissipative attenuation (A_d) plus the reflective attenuation (A_r). The dissipative attenuation includes both radiation and wall loss. If the assumption is made that the test sections are symmetrical, then these attenuations can be expressed in decibels as follows:

$$A_t = -10 \log_{10}\left[\frac{\rho}{|\Gamma_s|}(1 - |S_{11}|^2)\right]$$

$$A_r = -10 \log_{10}\left[1 - \frac{|S_{11}|^2}{|\Gamma_s|^2}\right]$$

$$A_d = -10 \log_{10}\left[\frac{\rho}{|\Gamma_s|}\,\frac{1 - |S_{11}|^2}{1 - \dfrac{|S_{11}|^2}{|\Gamma_s|^2}}\right]. \qquad (1)$$

These equations can be developed in the following manner. Network theory defines the matrix element S_{12} as the transmission coefficient from terminal 1 to terminal 2.

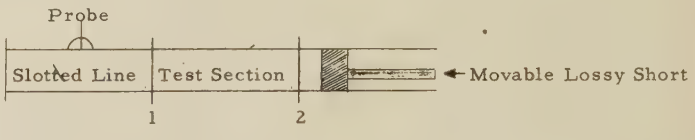

The insertion loss is then equal to $-20 \log_{10} |S_{12}|$ in decibels. However, when there is loss present in the short circuit, one half of this loss appears in the insertion loss as determined from $|S_{12}|$. Hence, to determine the insertion loss of the given test section only, the effect of the lossy short must be accounted for; that is,

$$A_t = \text{total insertion loss} - 1/2 \text{ loss in termination}$$
$$= -20 \log_{10} |S_{12}| + 10 \log_{10} |\Gamma_s|$$

where $|\Gamma_s|$ is the reflection coefficient of the short.

$$A_t = -10 \log_{10} \frac{|S_{12}|^2}{|\Gamma_s|}.$$

From Deschamps' construction technique[2]

$$\rho = \frac{|S_{12}|^2}{[1 - |S_{11}|^2]}.$$

From physical symmetry

$$|S_{11}| = |S_{22}|.$$

Substituting for $|S_{12}|$ in the expression for A_t

$$A_t = -10 \log_{10} \left[\frac{\rho}{|\Gamma_s|} (1 - |S_{11}|^2) \right]. \quad (2)$$

This equation is the expression for the total attenuation of a test section and represents attenuation due to radiation, dissipation, and reflection. The reflected power from the discontinuities of the slots is proportional to the square of the reflection coefficients. Since the reflection coefficient of a discontinuity is the first element in its scattering matrix, the reflected power from the test section is proportional to $|S_{11}|^2$. The power that is not reflected is $1 - |S_{11}|^2$. The attenuation of the section due to reflection is

$$A_r = 10 \log_{10} \frac{1}{1 - |S_{11}|^2} = -10 \log_{10} [1 - |S_{11}|^2]. \quad (3)$$

Since the reflected power is the entire reflected power (that is, includes power reflected from the lossy short), (3) for A_r must be corrected.

If the reflection coefficient of the test section is designated as $|S'_{11}|$, then[3]

$$|S'_{11}|^2 = \frac{|S_{11}|^2}{|\Gamma_s|^2}$$

and

$$A_r = -10 \log_{10} \left[1 - \frac{|S_{11}|^2}{|\Gamma_s|^2} \right]. \quad (4)$$

The equation for the dissipative attenuation may be obtained by algebraic manipulation of (2) and (4) in $A_t = A_r + A_d$.

Experimental Procedure

To apply the moving lossy short technique, numerous test sections were manufactured, each with twenty identical slots. The sections differed from each other in slot inclination angle or in depth of cut. The slot spacing was chosen in such a manner that the same admittance data might be used in the design of a long array which would meet small "squint angle" requirements. The waveguide wall in which the slots were cut was milled to a 0.015-inch thickness before the slots were cut. The milling made it possible to control the wavelength at which a test section displayed its maximum attenuation by varying the slot depth of cut.

Two sets of data were taken at each frequency for each test section measured. The first measurements were taken with the movable lossy short connected directly to a slotted line. The test section to be measured was then inserted between the slotted line and the lossy short. For both measurement runs, the movable lossy short was moved to eight equally-spaced positions[4] so that the term S_{11} (an element of the scattering matrix of the test section) could be obtained. The position of the voltage minimum and the vswr in the slotted line were recorded for each position of the short. The eight positions of the short covered a movement of exactly one-half guide wavelength. For optimum accuracy, the guide wavelength was measured by the short driving mechanism with the slotted line probe fixed.

From these data, the amplitude and phase of the reflection coefficient, Γ, were calculated for each position of the lossy short and plotted on standard polar coordinate paper. When the calculations for the data obtained with the test section absent were plotted, a circle resulted which has its center at or very near the origin of the plane. If the circle is centric, the radius is equal to $|\Gamma_s|$. This circle is, in effect, a calibration of the lossy short at that particular frequency. The corresponding calculations when the test section was present in the setup yielded a circle in the reflection coefficient plane which has a radius and displacement from the center of the plane related to both the power being radiated by the slots and the power being dissipated in wall losses. The radius of this circle is ρ.

The term $|S_{11}|$, an element of the scattering matrix of the test section, is then obtained by geometric constructions on the Γ-plane circles resulting from the data recorded with the test section present. The method of constructions is illustrated in Fig. 1. The underlying theory, as well as the procedures for obtaining the other elements of the scattering matrix (amplitude and phase), is presented by Deschamps.

Through the use of (1) through (4), the measurements made on each test section were translated into attenuation per section. The attenuation in turn was converted into conductance per slot in this manner.

Each test section is considered as

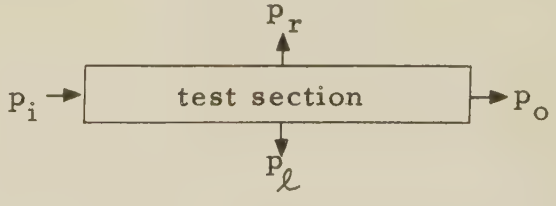

[2] G. A. Deschamps, "Determination of reflection coefficients and insertion loss of a waveguide junction," *J. Appl. Phys.*, vol. 24, pp. 1046–1050; August, 1953.

[3] H. M. Altschuler and A. A. Oliner, *op. cit.*,

[4] Equal spacing of the measurement positions is not necessary when the movable lossy short is connected directly to the slotted line (test section absent). However, in the experimental work the positions used were equally spaced for both sets of measurements because the data taking was facilitated by maintaining the same test setup for all runs.

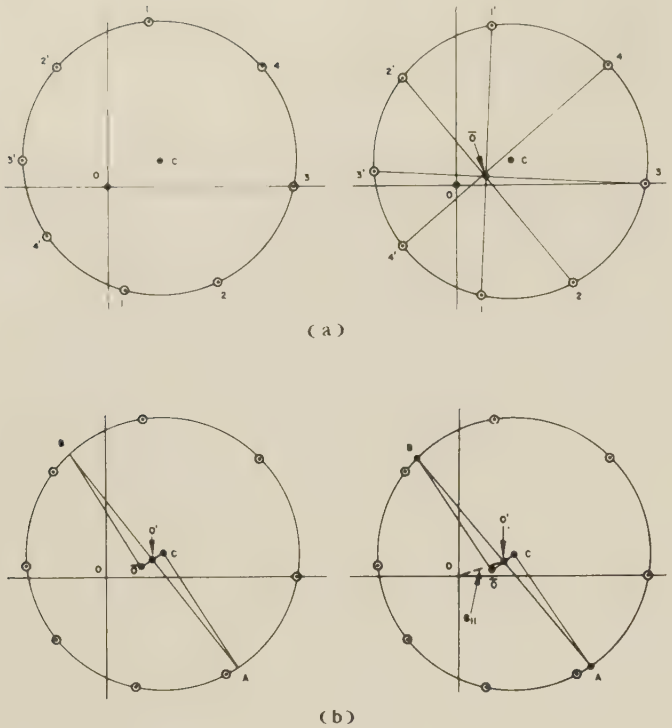

Fig. 1—Method of construction of Γ-plane circles.

(a) 1) Plot reflection coefficients on polar coordinate paper (always an even number of points) and draw best circle through all points.
2) Number points to give two equal groups of points.
3) Label center of circle C and intersection of polar coordinates O.
4) Connect points 1 with 1′, 2 with 2′, etc.
5) Label intersection of chords $\bar{O}$.

(b) 1) Connect C and $\bar{O}$.
2) Raise perpendiculars at C and $\bar{O}$ to intersect circle periphery at opposite sides. Label one point of intersection A, and the other B.
3) Draw AB.
4) O' is the intersection of $C\bar{O}$ and AB.
5) Draw OO'. Line OO' is S_{11}.

where

p_i = power input to section,

p_o = power output from section,

p_r = power radiated from section,

p_l = power dissipated in wall losses.

From an energy conservation outlook, it may be said that

$$p_i = p_o + p_l + p_r$$

or

$$1 = \frac{p_o}{p_i} + \frac{p_l}{p_i} + \frac{p_r}{p_i}$$

$$\frac{p_r}{p_i} = 1 - \frac{p_o}{p_i} - \frac{p_l}{p_i} = g \qquad (5)$$

where

$$\frac{p_l}{p_i} = \frac{\beta - 1}{\beta} \qquad (6)$$

and β is the wall loss attenuation factor of the waveguide without slots (expressed as a power ratio). Eq. (5) may be applied to elements of the test section, each element extending from midway between two slots to the next adjacent midway position as shown below.

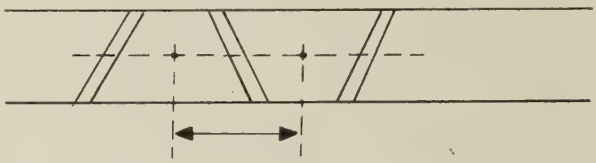

Since g, the conductance per slot, is equivalent to the ratio of the power radiated by a slot to the power in the guide at that point, the value of g can be calculated from (5) if the ratios p_o/p_i and p_l/p_i for each slot and its associated spacing are known. The test section factor p_o/p_i, or rather its inverse, is the dissipative attenuation and is determined from the measurements. It is expressed in decibels and represents the dissipative attenuation of twenty slots and their associated slot-to-slot spacings. Dividing this attenuation figure in decibels by 20 and converting it to a power ratio make it suitable for insertion into (5) for the calculation of conductance per slot. The wall loss factor, p_l/p_i, the remaining term which must be determined, can be calculated from (6) if β is known. This term can be read from a handbook and converted into the expression for one-slot spacing. The conductance per slot, g, can then be calculated from (5).

Results

For each test section a set of circles in the reflection coefficient plane was plotted over a frequency range from 8.2 to 8.9 millimeters. Since each test section was unique in slot inclination angle or in slot depth of cut, complete information was acquired on the effect of these parameters on the admittance characteristics of slots at K_a band. From these Γ-plane circles "resonance" graphs similar to that shown in Fig. 2 were constructed with conductance per slot plotted vs wavelength for both fixed slot inclination angle and different slot depths of cut. The information from these "resonance" graphs were compiled in a "summary" graph to show the manner in which the conductance per slot vs wavelength varied as *both* the slot inclination angle and depth of cut were changed. Finally, it was possible to obtain two curves from which the slot inclination angle and depth of cut could be specified to yield a certain conductance at a particular frequency. Once an array has been designed and the individual slot conductances determined which are required to produce the desired aperture distribution, then the necessary slot angles and depths of cut may be read off the pertinent graphs.

A 30-slot, nonresonant linear array which would yield a −25 db sidelobe level was constructed to test the data. Transverse slots were cut in the edge of RG-96/U waveguide and spaced 0.2424 inch apart. The slot wall

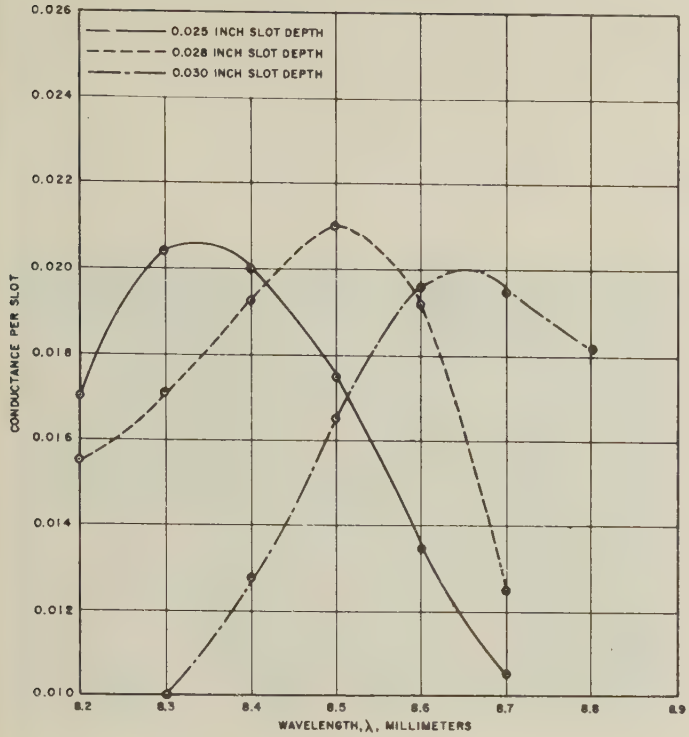

Fig. 2—Sample "resonance" graph plotted from Γ-plane circles with conductance per slot vs wavelength for slot inclination angle of 10 degrees and slot depths of 0.025, 0.028, and 0.030 inch.

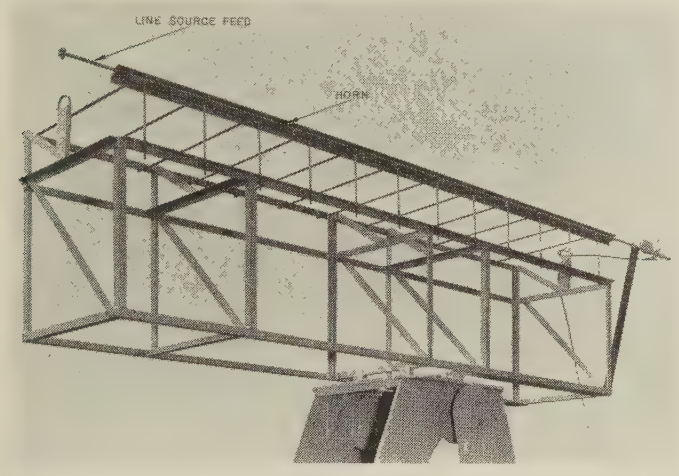

Fig. 3—432-slot array.

was milled to a thickness of 0.015 inch. The array was designed to deliver 30 per cent of the input power to the load. Radiation patterns of the array, taken with a horn, show 23-db sidelobes, close enough to the design objective to satisfy the experimental requirements. The vswr of this array was under 1.12 over the entire frequency band of 8.3 to 8.8 millimeters.

An 8-foot, nonresonant array with 432 transverse edge slots was subsequently designed as a line source. It had been decided that this array was to have a 25-db Taylor[5] aperture distribution, and 5 per cent of the array

[5] T. T. Taylor, "Design of line sources for narrow beamwidth and low sidelobes," Tech. Memo. No. 316, Res. and Dev. Labs., Hughes Aircraft Co., July 31, 1953.

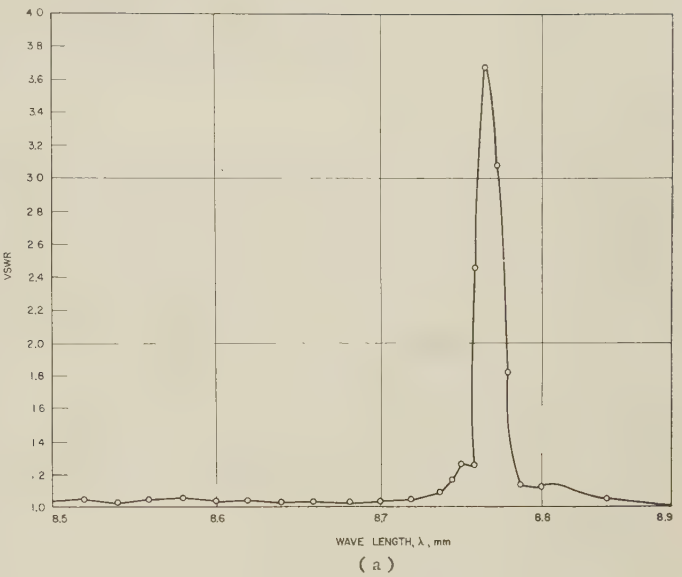

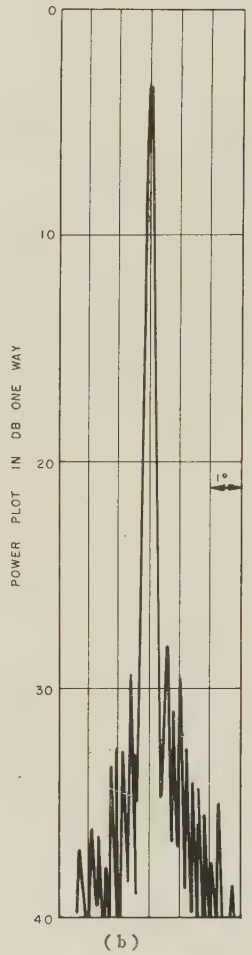

Fig. 4—Electrical characteristics of 432-slot array. (a) VSWR. (b) *E*-plane radiation pattern.

input power was to be delivered to a matched load. As with the experimental 30-slot array, the slot wall was milled to a thickness of 0.015 inch. This array is shown in Fig. 3 in a support on the pattern range. The vswr vs wavelength and the *E*-plane radiation pattern are shown in Fig. 4. The half-power beamwidth is approxi-

mately 14 minutes, as measured with a precision rotary table. Both the sidelobe level of the array and the half-power beamwidth compare favorably with the design objectives.

In the interests of improved accuracy, modifications had to be made to existing laboratory and machining equipment. In the measuring setup, the slotted line was modified to enable the position of the carriage to be measurable as close to 0.0001 inch as possible. This accuracy was accomplished by providing a 40-thread-per-inch drive with a 0.0001-inch least count Ames gauge attached to the carriage. The moving lossy short was also modified for a more controlled positioning of the short by replacing the standard micrometer drive with a unique driving mechanism plus an Ames gauge with a least count of 0.0001 inch.

Machining problems arose as a result of the tight tolerances necessary at such high frequencies as those in the K_a band, where, for example, a 0.0012-inch error in slot spacing can cause a phase error of 1 degree. Precision waveguide milled from coin silver (90 per cent silver and 10 per cent copper) was used in preference to brass waveguide with an internal silver lining, the only other waveguide available for the specific frequency. The silver lining tended to delaminate during milling operations. The actual cutting of the slots to tolerance with the exact design spacing between them was accomplished through the use of a specially designed holding fixture. The device forced a precision-milled gib against one of the wide dimensions of the guide and enabled it to be stressed equally during the cutting process (Fig. 5). The slots were undercut several thousandths of an inch. To finish the slots, the guide section was mounted on the table of a precision traveling-microscope and the slots were brought into tolerance and into shape (sharp, square corners) by hand with the aid of small, specially designed files.

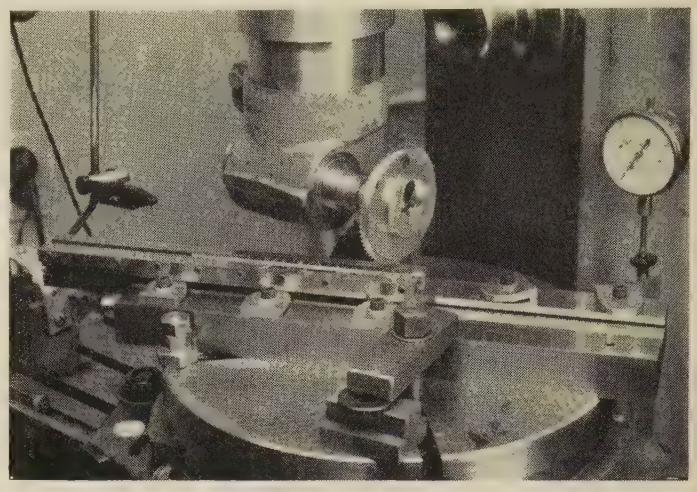

Fig. 5—Slot milling operation.

Acknowledgment

The author wishes to express his appreciation to Drs. R. W. Bickmore and R. S. Wehner for their assistance and direction in this project. The author is also very much indebted to R. G. Giles and T. A. Crail who performed the measurements.

Radiation by Disks and Conical Structures*

A. LEITNER† AND C. P. WELLS†

Summary—**The Lebedev integral transform is applied to a class of boundary value problems in the theory of diffraction and antennas, including circular disks, apertures and hollow conical structures. It is found that the conventional Wiener-Hopf technique, together with this transform, does not explicitly solve these problems. Instead, one is led to an infinite system of linear equations for the representation of the unknown transform function.**

Introduction

IN THIS PAPER, we study the use of the method of integral transforms in a class of radiation and antenna problems involving mixed boundary conditions on coordinate surfaces of the spherical system. The radiating objects of principal interest in this class are the hollow circular cone and the biconical antenna, both of finite slant height and arbitrary apex angle. If these electromagnetic radiation problems possess azimuthal symmetry, they are reducible to scalar form. Let θ_0 be the half-apex angle of the cone. The problems can be formulated as two-part boundary value problems on the surface $\theta=\theta_0$. It was hoped that the use of the appropriate integral transform theorem combined with the Wiener-Hopf technique could produce an explicit solution as was demonstrated in the electrostatic problem of the conducting cone.[1] Here we use the word "explicit" in the sense that the coefficients in the series of wave functions representing the solution can be determined without recourse to an infinite system of linear equations.

The transition from the electrostatic to the wave problem involving conical structures is tantamount to transition from the Mellin to the Lebedev transform. It appears that this extension is of considerable interest among applied mathematicians.

We find that the method "fails" in the sense that the conventional Wiener-Hopf technique also leads to an infinite system of linear equations, although we find it to be of particularly simple form involving factorials only. In the following sections we present a test of these methods on a simpler acoustic problem involving the circular disk. The disk is a cone of half-apex angle $\pi/2$, and Karp[1] has shown that problems involving cones of arbitrary angle can be solved by the Wiener-Hopf technique if this can be done for the disk; also, the wave functions of the azimuthally symmetric electromagnetic field are essentially the same as those for acoustic fields of like symmetry. One may conclude that the solution for conical structures may produce an infinite linear system of a form much simpler than those obtained with other techniques. We hope to present these results in a later paper.

Statement of the Problem

We seek solutions of $\nabla^2 u+k^2u=0$, $k=2\pi/\lambda$ where λ is the wavelength and u the velocity potential. We impose the radiation condition, $r(\partial u/\partial r+iku)\to 0$, ru bounded, as $r\to\infty$.

The problem is that of the radiation by the freely vibrating rigid circular disk

$$(\partial u/\partial z)_{\theta=\pi/2} = v, \qquad r \leqq a, \tag{1}$$

$$(u)_{\theta=\pi/2} = 0, \qquad r \geqq a. \tag{2}$$

The function u also represents the wave scattered by a stationary rigid circular disk from a normally incident plane wave.

This problem has been explicitly solved by use of the oblate spheroidal wave functions, (cf. Bouwkamp and other authors[2]). It has also been treated in cylindrical coordinates, using the Hankel transform and the exact inversion of a certain infinite linear system, by Sommerfeld.[3]

In spherical coordinates the above function u can be represented as a series of the type

$$\sum_{n=0}^{\infty} g_n r^{-1/2} Z_{n+1/2}(kr) P_n(\cos\theta)$$

where $Z_{n+1/2}$ are cylinder functions, P_n Legendre functions and g_n unknown coefficients. These series may be converted to contour integrals surrounding the positive real axis of the complex order plane. The next step is to deform this contour into one lying inside an infinite strip of finite width surrounding the imaginary axis, but it can be shown that this leads to divergent integrals in the problem stated above. However, if we use the device of transforming $k\to -i\gamma$, with γ real and positive, this deformation is permissible without incurring change in value of the integrals involved. The transformation leads to modified Bessel functions of real, positive argument. The Wiener-Hopf technique can now be applied.

* Manuscript received by the PGAP, November 30, 1955; revised manuscript received June 18, 1956. This work was performed under sponsorship of the Office of Ordnance Research, U. S. Army.

† Mich. State Univ., Lansing, Mich.

[1] S. N. Karp, "Natural Charge Distribution and Capacitance of a Finite Conical Shell," Res. Rep. EM-35, Math. Res. Group, N. Y. Univ., New York, N. Y., 1951.

[2] C. F. Bouwkamp, "Theoretische en numerieke behandeling van de buigung door een ronde opening," Dissertation, Groningen; 1941. See also: "Diffraction Theory," Reps. Progr. Phys., Phys. Soc., Gt. Brit., vol. 17, pp. 35–100; 1954.

[3] A. Sommerfeld, "Die frei schwingende kolbenmembran," *Ann. Phys.*, vol. 42, pp. 389–420; 1942.

The idea is to solve the intermediate problem with pure imaginary k, then to reconvert the contour around the real axis and, finally, to transform to real positive k. This device was first used by Oberhettinger[4] in a similar approach to the problem of diffraction by a wedge.

The transformation to modified Bessel functions alters the radiation condition, stated above, to exponential decay of the function like $e^{-\gamma r}/r$ as $r \to \infty$.

Solution

We represent $u(\gamma r, \theta)$ as follows:

$$r^{1/2}u(\gamma r, \theta) = \int_L \mu g(\mu) P_{-1/2+\mu}(|\cos\theta|) I_{-\mu}(\gamma r)\, d\mu, \quad (3)$$

where $I_{-\mu}$ is the modified Bessel function and $g(\mu)$ the unknown function to be determined by boundary conditions (1) and (2); L is a contour inside an infinitely long strip of finite width about the imaginary μ axis from $Im\mu = -\infty$ to $Im\mu = +\infty$; $P_{-1/2+\mu}(\cos\theta)$ is the Legendre function, the appropriate angular function when $\theta \leqq \pi/2$, but, when $\pi/2 \leqq \theta \leqq \pi$, $P_{-1/2+\mu}(-\cos\theta)$ must be used.

Imposing the boundary conditions (1) and (2):

$$r \leqq a\colon\ r^{3/2}v = \int_L \mu g(\mu) P_{-1/2+\mu}'(0) I_{-\mu}(\gamma r)\, d\mu, \quad (4)$$

$$r \geqq a\colon\quad 0 = \int_L \mu g(\mu) P_{-1/2+\mu}(0) I_{-\mu}(\gamma r)\, d\mu. \quad (5)$$

This is a set of dual integral equations for $g(\mu)$. Their form can be simplified by use of the Lebedev transform theorem,[5]

$$\phi(\gamma r) = \int_L \mu \Lambda(\mu) I_{-\mu}(\gamma r)\, d\mu, \quad (6a)$$

$$\pi i \Lambda(\mu) = \int_0^\infty \phi(\gamma r) K_\mu(\gamma r)\, dr/r, \quad (6b)$$

where K_μ is "the modified Hankel" or MacDonald function. The theorem is valid provided both integrals converge and provided $\Lambda(\mu)$ is an even function of μ, analytic in a strip of finite width containing L and the imaginary axis, with decay at least as rapid as $e^{-\pi|\tau|/2}/|\tau|^{3/2}$ as τ, the imaginary part of μ, goes to $\pm\infty$ in this strip.

Using this transform theorem we represent the inhomogeneous term in (4) as follows

$$\left.\begin{matrix} r \leqq a\colon r^{3/2}v \\ r \geqq a\colon\ 0 \end{matrix}\right\} = \int_L \mu \Lambda(\mu) I_{-\mu}(\gamma r)\, d\mu, \quad (7a)$$

with the result that

$$\Lambda(\mu) = (\pi i)^{-1} v \int_0^a r^{1/2} K_\mu(\gamma r)\, dr. \quad (7b)$$

The integral in (7b), which defines $\Lambda(\mu)$, converges in the strip $-3/2 < Re\mu < 3/2$ and has the appropriate decay such that the conditions of Lebedev's theorem are satisfied; it can be continued outside this strip by the use of the Lommel functions. It is found that Λ has the growth of $K_\mu(\gamma a)/\mu$ as $|\mu| \to \infty$ and possesses simple poles at $\mu = \pm(2n+3/2)$ with the residues

$$(2^{1/2} i v/\pi\gamma^{3/2})(-)^n \Gamma(n + \tfrac{3}{2})/n!, \quad n = 0, 1, 2, \cdots. \quad (8)$$

The dual integral equations can now be written

$$r \leqq a\colon\ 0 = \int_L \mu [g(\mu) P_{-1/2+\mu}'(0) - \Lambda(\mu)] I_{-\mu}(\gamma r)\, d\mu, \quad (9)$$

$$r \geqq a\colon\ 0 = \int_L \mu g(\mu) P_{-1/2+\mu}(0) I_{-\mu}(\gamma r)\, d\mu, \quad (10)$$

and in this homogeneous form the first step of the Wiener-Hopf technique may be applied: *i.e.*, (9) and (10) will be *formally satisfied*, if it can be demonstrated that the integrands are analytic functions of at least algebraic decay in halfplanes to the left and right, respectively, of the strip containing L, with these halfplanes of analyticity overlapping in the strip.

It is precisely at this point that the method requires modifications of the integral equation, because for the second of them no such halfplane of analyticity can be found in its present form. Since this circumstance is unconventional we present here certain relations on which the proof of the assertion is based: The factors of the kernel $I_{-\mu}(\gamma r)$ are, as is well known, the integral transforms of the boundary values $u(\gamma r, \pi/2)$ when $r \leqq a$, and $\partial u(\gamma r, \pi/2)/\partial n$ when $r \geqq a$. Thus

$$\pi i [g(\mu) P_{-1/2+\mu}'(0) - \Lambda(\mu)] = \int_a^\infty r^{1/2} [\partial u(\gamma r, \pi/2)/\partial n] K_\mu(\gamma r)\, dr,$$

$$\pi i g(\mu) P_{-1/2+\mu}(0) = \int_0^a r^{-1/2} u(\gamma r, \pi/2) K_\mu(\gamma r)\, dr.$$

Although $u(\gamma r, \pi/2)$ and its derivative are unknown, their behavior as functions of r is well known from general diffraction theory, including that of singularities near edges, such as at $r = a$. Thus the functions defined by the integrals and their analytic continuations can be completely analyzed (the first integral above is an entire function of μ). One can show that $g(\mu)$ has simple poles at the points $\mu = \pm(2n+\frac{1}{2})$, $\pm(2n+3/2)$, in fact, the residues at the latter set of points are *known* in terms of the residues of $\Lambda(\mu)$ given in (8). Furthermore, these integrals determine the asymptotic growth of these functions completely as $K_\mu(\gamma a)/\mu^\alpha$ when $|\mu| \to \infty$, where $\alpha > \frac{1}{2}$.

[4] F. Oberhettinger, "Diffraction of Waves by a Wedge," *Comm. Pure Appl. Math.* vol. 7, pp. 551–563; August, 1954.

[5] N. N. Lebedev, "On representation of arbitrary functions as integrals over MacDonald Functions of Complex Order," *Dokl. Ak. Nauk. SSSR (N.S.)* vol. 58, pp. 1007–1010; 1947. (In Russian.)

From these results one may derive that the integrand in (9) is analytic on a *left*-halfplane $\mathrm{Re}\mu < \frac{1}{2}$ with asymptotic behavior $\mu^{1/2-\alpha}(r/a)^{-\mu}$, a *decay* in the strip and on its left side, since $r \leqq a$. However for the integrand of (10), in which $r \geqq a$, no such halfplane of analyticity can be found unless its form is changed, in such a way that the kernel in (10) becomes the modified Hankel function. This can be done by the decomposition

$$g(\mu)P_{-1/2+\mu}(0) = (\pi/2)[h(-\mu) - h(\mu)]/\sin \pi\mu. \quad (11)$$

Substituting into (10), one obtains

$$r \geqq a\colon\ 0 = \int_L \mu\ h\ (\mu)K_\mu(\gamma r)d\mu.^6 \quad (12)$$

where

$$h(\mu) = (\pi i)^{-1}\int_0^a r^{-1/2}u(\gamma r, \pi/2)I_\mu(\gamma r)dr. \quad (13)$$

From this definition of $h(\mu)$ it can be determined that $h(\mu)$ is free of poles on a right halfplane $\mathrm{Re}\mu > -\frac{1}{2}$ with growth $I_\mu(\gamma a)/\mu^{1/2}$ as $|\mu| \to \infty$ in this halfplane; that $h(\mu)$ has simple poles at $\mu = -(2n+\frac{1}{2})$, with unknown residues; and that the integrand in (12) is analytic on this left halfplane with *decay* $\mu^{-1/2}(r/a)^{-\mu}$ as $|\mu| \to \infty$ there (since $r \geqq a$). Overlapping halfplanes are now determined for both integral equations, and (12) is also formally satisfied.

It now remains to determine the unknown function $g(\mu)$ or the related function $h(\mu)$ by function-theoretical means. With this in mind it is convenient to write the integral equations in the form

$$r \leqq a\colon\ 0 = \int_L G^-(\mu)[\Gamma(1-\mu)(\gamma a/2)^\mu I_{-\mu}(\gamma r)]d\mu, \quad (14)$$

$$r \geqq a\colon\ 0 = \int_L H^+(\mu)[(\gamma a/2)^\mu K_\mu(\gamma r)/\Gamma(\mu)]d\mu, \quad (15)$$

where

$$G^-(\mu) = \mu[g(\mu)P'_{-1/2+\mu}(0) - \Lambda(\mu)](\gamma a/2)^{-\mu}/\Gamma(1-\mu), \quad (16)$$

$$H^+(\mu) = \Gamma(1+\mu)(\gamma a/2)^{-\mu}h(\mu). \quad (17)$$

The purpose of introducing these factors is twofold: first, the expressions inside the brackets in (14) and (15) now have the asymptotic behavior $(r/a)^{-\mu}$ in the left and right halfplanes, respectively, and therefore approach at least a constant value (in the strip) or decay exponentially since $r \gtrless a$, resp. At the same time, these brackets are analytic in the respective halfplanes. Secondly, the functions $G^-(\mu)$ and $H^+(\mu)$ are not only analytic in left and right halfplane, respectively, but also possess algebraic *decay* in these halfplanes of analyticity. We shall call such functions + and − functions respectively.

[6] Note that this modification has introduced the Hankel function for the region $r \geqq a$, and that this function explicitly satisfies the radiation condition.

Now, although the functions G^- and H^+ are analytic in two different halfplanes, these two regions overlap in the strip containing L. Furthermore, by virtue of (11), (16), and (17), there is a relation between these functions which is valid at least in the common strip. We now apply the crucial step of the Wiener-Hopf technique, namely, to exploit these relations for the construction of a function which is analytic on the entire μ plane, while at the same time possessing algebraic decay—that is, a function which by Liouville's theorem is identically zero. One finds

$$\frac{\Gamma\left(\frac{1}{4}-\frac{\mu}{2}\right)}{\Gamma\left(\frac{3}{4}-\frac{\mu}{2}\right)}G^-(\mu) = \frac{\Gamma\left(\frac{3}{4}+\frac{\mu}{2}\right)}{\Gamma\left(\frac{1}{4}+\frac{\mu}{2}\right)}\left\{H(\mu) - \frac{\Gamma(1+\mu)}{\Gamma(1-\mu)}\left(\frac{\gamma a}{2}\right)^{-2\mu}H(-\mu)\right\} - \frac{\Gamma\left(\frac{1}{4}-\frac{\mu}{2}\right)}{\Gamma\left(\frac{3}{4}-\frac{\mu}{2}\right)}\frac{\Lambda(\mu)}{\Gamma(1-\mu)}\left(\frac{\gamma a}{2}\right)^{-\mu}. \quad (18)$$

The superscripts +, − are omitted from $H(\mu)$ to avoid confusion. [$H(-\mu)$ is a minus function.]

The term on the left-hand side of (18) is a minus function. The term containing $H(\mu)$ on the right-hand side is a + function. But the remaining two terms are mixed functions, *i.e.*, they possess simple poles on both halfplanes. Inspection shows that, while these two terms do have poles on the negative real axis, their asymptotic behavior as $|\mu| \to \infty$ in other directions in the left halfplane is one of decay. Thus we may extract these poles by Mittag-Leffler series with the same residues. The series themselves are plus functions. The difference between the original functions and the appropriate Mittag-Leffler series, however, are minus functions. Therefore these difference terms may be transposed to the left of (18), which side of (18) will be a minus function; and since this will equal the functions which remain on the right hand side, either side is identically zero by Liouville theorem. Thus one obtains

$$0 = \left[\Gamma\left(\frac{3}{4}+\frac{\mu}{2}\right)\Big/\Gamma\left(\frac{1}{4}+\frac{\mu}{2}\right)\right]H(\mu) - \sum_0^\infty R_n\Big/\left(\mu+2n+\frac{3}{2}\right) - \sum_1^\infty S_n/(\mu+n) - \sum_0^\infty T_n\Big/\left(\mu+2n+\frac{3}{2}\right), \quad (19)$$

where the T_n are the *known* residues at $\mu = -(2n+3/2)$ of the term in (18) involving $\Lambda(\mu)$, *viz.*,

$$T_n = (a^{3/2}v/2\pi i)(-)^n(\gamma a/2)^{2n}/\Gamma\left(2n+\frac{3}{2}\right). \quad (20)$$

The R_n and S_n, however, are the residues, at $\mu=-1, -2, -3, \cdots$, and $\mu=-(2n+3/2)$ of the term in (18) which involves $H(-\mu)$, *i.e.*, they are *unknown*. They have the form

$$R_n = \left[\left(2n+\frac{3}{2}\right)\Gamma\left(n+\frac{3}{2}\right)\Big/ n!\Gamma^2\left(2n+\frac{5}{2}\right)\right] \cdot(\gamma a/2)^{4n+3/2}H(2n+3/2). \quad (21)$$

$$S_n = \left[-n\Gamma\left(\frac{3}{4}+\frac{n}{2}\right)\Big/(n!)^2\Gamma\left(\frac{1}{4}+\frac{n}{2}\right)\right] \cdot(\gamma a/2)^{2n}H(n). \quad (22)$$

If, in (19), we set μ equal to 1, 3/2, 2, 3, 5/2, $\cdots$, we obtain an infinite system for the numbers $H(n)$, $H(2n+3/2)$ whose coefficients are in the ascending powers of γa and otherwise contain only factorials. If determined, then these numbers define H for all other values of μ, through (19).

We have approximated the solution of this system by terminated expansions of the unknowns in the ascending powers of γa and have obtained series expressions for the radiation patterns and scattering cross sections for the diffraction problem of the disk; these check completely with the existing literature on the problem where other techniques of solution were used. We have also solved the problem of the vibrating disk in a rigid baffle, and of transmission of sound waves by the circular aperture.[7] The former can be solved exactly by use of the Lebedev theorem. Extension of this method to the biconical antenna is in progress.

[7] A. Leitner and C. P. Wells, "Radiation by Disks and Conical Structures," Int. Tech. Rep. No. 1. Contract No. DA-20-018-ORD-13354, Michigan State Univ.; 1955.

Diffraction of Microwaves by Tandem Slits*

LEROY R. ALLDREDGE†

Summary—**The diffraction of a plane electromagnetic wave by two identical slits in tandem is investigated for normal incidence with the polarization parallel to the edges of the slits.**

Theory shows that the scattering cross-section coefficient is proportional to the imaginary part of the far field forward scattering factor. The stationary form of the scattering cross section is developed in terms of the incident field and unknown currents on the edges of the conductors forming the slits. Calculations using the Kirchoff-type approximation in this stationary form for a tandem slit separation of 0.157λ are in good agreement with the experimental values for slit widths greater than 0.5λ.

Similar calculations for zero tandem slit separation, corresponding to a single slit, and for slit widths greater than 0.3λ are in good agreement with those of the exact theory of Morse and Ruberstein,[1] and as determined experimentally.

The infinitely long slits are approximated experimentally by use of a parallel plate system described earlier by Row.[2] The experimental results show an interesting resonance effect as the slit width changes.

* Manuscript received by the PGAP, October 6, 1955; revised manuscript received, April 26, 1956. This paper is based on work done in partial fulfillment of the requirements for the Ph.D. in physics at the Univ. of Maryland, College Pk., Md. The experimental part was partially supported by ONR Contract N50ri-76, T.O.1. at Cruft Lab., Harvard Univ., Cambridge, Mass. The theoretical work was done at the Naval Ordnance Lab., White Oak, Md.

† Operations Research Office, Johns Hopkins University, Chevy Chase, Md.

[1] P. M. Morse and P. J. Ruberstein, "The diffraction of waves by ribbons and by slits," *Phys. Rev.*, vol. 54, pp. 895–898; December, 1938.

[2] R. V. Row, "Microwave diffraction measurements in a parallel plate region," *J. Appl. Phys.*, vol. 24, pp. 1448–1452; December, 1953.

Introduction

MOST diffraction problems have been worked out using the classical Kirchoff theory which explains quite well the diffraction of a wave through an aperture in a conducting screen when the dimensions of the aperture are very large in comparison to the wavelength. When microwave techniques are employed it is not difficult to show that in the aperture near an edge of the conducting screen the electric field differs greatly from the incident field and on the shadow side of the screen the magnetic field is not zero near the edge, so the Kirchoff theory cannot be correct.

Most interesting diffraction problems which are amenable to exact analytical solution have been solved. The principal challenge in diffraction theory is the development of sufficiently accurate approximate methods for handling problems involving scatterers of complicated geometric shapes which have dimensions comparable to a wavelength.

The variational procedure introduced by Levine and Schwinger[3] has been applied most successfully to planar diffraction problems where the scatterer consists of one or more apertures in a perfectly conducting plane of infinite extent and where only the total scattering cross

[3] H. Levine and J. Schwinger, "On the theory of electromagnetic wave diffraction by an aperture in an infinite plane conducting screen," *Comm. on Pure & Appl. Math.*, vol. 3, pp. 355-391; December, 1950

section is found. This paper considers an extension of this theory to the case where the scatterer is no longer confined to a single plane. The particular problem treated here is that of a vertically-polarized plane electromagnetic wave falling normally upon a vertical slit of infinite extent in a perfectly conducting plane with another identical slit in another conducting plane directly behind the first and parallel to it. This complicated diffracting obstacle is simply referred to in this paper as tandem slits. The parameters in this investigation are the slit width (same for both slits) and the tandem separation.

Theory

Scattered Field

Consider two parallel infinite planes Γ_a and Γ_b at $z=0$ and $z=a$ as shown in cross section in Fig. 1. Plane

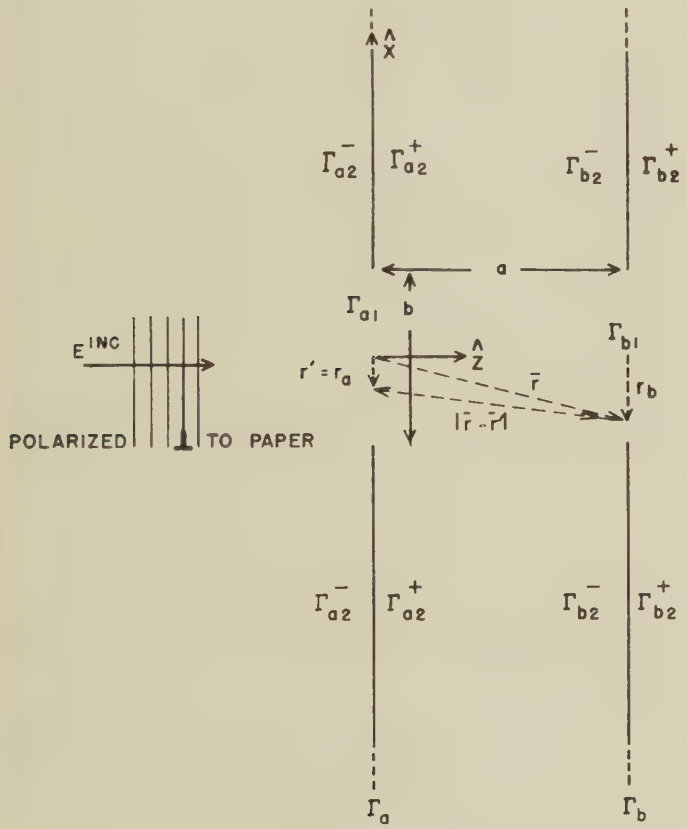

Fig. 1—Cross-sectional view of tandem slit geometry.

Γ_a contains the perfectly conducting infinitely thin screen Γ_{a2} and the slit Γ_{a1} and plane Γ_b contains the screen Γ_{b2} and the slit Γ_{b1}. The parallel edges of the slits are at $x=b/2$, $-b/2$. The resulting problem is one in two dimensions, being independent of y, so that the planes become lines. The plus and minus superscripts indicate respectively the right and left sides of the planes hereafter referred to as lines in the corresponding two-dimensional problem.

A plane electromagnetic wave polarized in the y direction is incident normally on the slit in the half space $z<0$; it is desired to investigate the diffracted field. The incident wave is described by

$$\bar{E}^{\text{inc}}(\bar{r}) = \hat{y} \exp(ik\hat{z}\cdot\bar{r}) = \hat{y} \exp(ikz)$$

$$\bar{H}^{\text{inc}}(\bar{r}) = -\frac{\hat{x}}{Z_0} \exp(ikz) \qquad (1)$$

where $k=2\pi/\lambda$ and λ is the wavelength, $Z_0=376.6$ ohms indicates the impedance of free space, $\hat{x}$, $\hat{y}$, and $\hat{z}$ are unit vectors in x, y, and z directions, and a bar over a letter indicates a vector. The harmonic time dependence, $\exp(-i\omega t)$ is omitted throughout. Rationalized mks units are used.

This incident electromagnetic field will establish certain tangential components of $\bar{E}$ and $\bar{H}$ in the plane $z=0$ on the shadow side of the plane Γ_a. There is a well known existence theorem that the field within a source free region is uniquely determined by either of these tangential components on the bounding surface of the region. If the plane Γ_b did not exist and if we were interested in the field only for $z>0$, we could think of our region as being bounded by Γ_a and a semicircle of infinite radius in the space $z>0$. If this type of approach is attempted useful results can be obtained for the case of a single slit in terms of the transmission coefficient, but this method is no longer of use when the second plane with its slit is introduced.

For this more complicated problem it is profitable to start with a consideration of the field scattered by the conducting screens forming the slits. Since we have postulated perfectly conducting screens, surface current densities $K(\bar{r}')$ will be induced on the screens and will act as the source of the scattered fields. When the general scattering theory[4] is reduced to two dimensions we may write for the y component of the scattered electric field

$$E_y^{SC}(\bar{r}) = -\frac{\omega\mu_0}{4}\int_C H_0^{(1)}(k\,|\,\bar{r}-\bar{r}'\,|)K_y(\bar{r}')d\Gamma' \qquad (2)$$

where $H_0^{(1)}(k|\bar{r}-\bar{r}'|)$, which will usually be indicated by $H_0^{(1)}$ without repeating the argument unless considered necessary to avoid confusion, indicates the zeroth order Jankel function of the first kind, and the integration is over both sides of both conductors as indicated by the notation $C=$ both sides of conductors $\Gamma_{a2}+\Gamma_{b2}=$ b.s. $(\Gamma_{a2}+\Gamma_{b2})$. Write the current as $K_y=K_y^{SC_0}+K_y^P$ and the scattered field as $E_y^{SC}=E_y^{SC_0}+E_y^P$, where the superscripts SC_0 refer to currents and fields corresponding to the case where Γ_{a2} is complete (no slit). The scattered field for an infinite screen is

$$E_y^{SC_0} = -\frac{\omega\mu_0}{4}\int_{\Gamma_a^-} H_0^{(1)}K_y^{SC_0}(\bar{r}')d\Gamma'$$

so we may write for the field scattered by the slit system

[4] S. Silver, "Microwave Antenna Theory and Design," McGraw-Hill Book Co., Inc., New York, N. Y., sec. 3.10; 1949.

$$E_y^P(\bar{r}) = \frac{\omega\mu_0}{4}\int_{\Gamma_{a1}^-} H_0^{(1)} K_y^{SC_0}(\bar{r}')d\Gamma' - \frac{\omega\mu_0}{4}\int_C H_0^{(1)} K_y^P(\bar{r}')d\Gamma'. \quad (3)$$

The surface current density $K_y^P(\bar{r}')$ is the difference between the surface current density which flows when the slits are present and that which would flow if there were no slits in the conductors (infinite conducting planes). For this reason $K_y^P(\bar{r}')$ might be called the perturbation surface current density caused by the slits. Looked at as a boundary value problem it can be said that the driving source for $K_y^P(\bar{r}')$ is localized in a finite area in the slit region, so that $K_y^P(\bar{r}')$ tends to zero with increasing distance from the slits unless special conditions permit a portion of the energy to be carried away from the slit region with no distance attenuation in the energy density. This latter condition may exist if the tandem separation is large enough to permit propagating modes between the conducting planes. Such modes would represent energy scattered into the region between the conducting planes. When these conditions exist the perturbation surface current density between the two planes can be writtten as

$$K_y^P(\bar{r}') = [K_y^P(\bar{r}')]_{\text{w.g.}} + [K_y^P(\bar{r}')]_p$$

where the subscript w.g. indicates that component of the surface current density associated with waveguide modes existing on the inner surfaces of the two conducting plates.

Surface current densities that support propagating modes in perfectly conducting waveguides do not give rise to electromagnetic fields outside the waveguides. Hence the $[K_y^P(\bar{r}')]_{\text{w.g.}}$ contribution to $K_y^P(\bar{r}')$ in (3) can be omitted when calculating $E_y^P(\bar{r})$ for $\bar{r}$ outside the region between the conducting plates or when calculating the energy scattered by the slit system into the space outside of the region between the two conducting plates. The remaining components of $K_y^P(\bar{r}')$ tend to zero with increasing distance from the slit system so that if in (3) it is understood that $K_y^P(\bar{r}')$ does not include the waveguide components the asymptotic expression

$$H_0^{(1)} \underset{r\to\infty}{\cong} \left(\frac{2}{i\pi kr}\right)^{1/2} \exp(ikr) \exp\{-ikr' \cos(\theta - \theta')\}$$

can be used to get an approximation for $E_y^P(\bar{r})$ in the far field outside the region between the conducting plates.

We will use only the special case of forward scattering so θ can be set equal to zero finally resulting in

$$E_y^P(\bar{r}) \cong i\left(\frac{1}{i8\pi kr}\right)^{1/2} \exp(ikr) A(\hat{z}, \hat{z}), \quad (4)$$

where

$$A(\hat{z}, \hat{z}) = i\omega\mu_0\Big[\int_{\text{b.s.}\Gamma_{a2}} K_y^P(\bar{r}')d\Gamma' + \exp(-ika)\int_{\text{b.s.}\Gamma_{a2}} K_y^P(\bar{r}')d\Gamma' - \int_{\Gamma_{a1}^-} K_y^{SC_0}(\bar{r}')d\Gamma'\Big]. \quad (5)$$

These expressions would permit the calculation of the far field forward scattered electric field if the perturbed currents were known over all the conducting screens forming the two slits.

Scattering Cross-Section Coefficient

The total power scattered by the conductors forming the two identical slits must be derived from currents induced on the conductors. Experimentally it is the forward scattered far field as given in (4) that can be readily measured in the laboratory. An interesting relationship can be developed between this far field and a part of the total scattered power.

As indicated earlier some of the scattered energy may propagate down the region between the conducting plates in waveguide fashion. This energy is in no way associated with the forward scattered far field and is therefore omitted from the definition of scattering cross-section coefficient discussed below. In what follows it is understood that the values of the scattered electric field $\overline{E}^{SC}$, the scattered magnetic field $\overline{H}^{SC}$ and the perturbation surface current density $\overline{K}^P$ do not include the components of those factors on Γ_{a2}^+ and Γ_{b2}^- associated with waves being propagated between the conducting screens.

With the above limitations the time average of the power scattered into the space outside the region between the conducting planes can be written as

$$P_{\text{ave}}^{SC} = \frac{1}{2}\,\text{Re}\int_C \hat{n}\cdot(\overline{E}^{SC} \times \overline{H}^{SC*})d\Gamma \quad (6)$$

where Re indicates the real part of the integral, $\hat{n}$ is the outward normal to the conducting surface over which the integral is taken and the * indicates the complex conjugate.

In (6), substitute $\overline{E}^{SC} = \overline{E}^{SC_0} + \overline{E}^P$ and similar expressions for the magnetic field and for the time average of the scattered power, and note that

$$\text{on } \Gamma_{a2}^+, \quad \overline{E}^{SC_0} = -\overline{E}^{\text{inc}}, \quad \overline{H}^{SC_0} = -\overline{H}^{\text{inc}},$$

$$\text{on } \Gamma_{a2}^-, \quad \overline{E}^{SC_0} = -\overline{E}^{\text{inc}}, \quad \overline{H}^{SC_0} = \overline{H}^{\text{inc}},$$

and

$$\text{on } \Gamma_{b2}^+ \text{ and } \Gamma_{b2}^-, \quad \overline{E}^{SC_0} = -\overline{E}^{\text{inc}} \text{ and } \overline{H}^{SC_0} = -\overline{H}^{\text{inc}}.$$

If we further recognize that, since the tangential component of the total electric field must be zero on the perfectly conducting surfaces of Γ_{a2} and Γ_{b2}, the tangential component of E^P must also be zero on these surfaces, and that

$$P_{\text{ave}}{}^{SC_0} = \frac{1}{2}\,\text{Re}\left[\int_{\Gamma_{a_2}{}^- + \Gamma_{a_1}{}^-} \hat{z}\cdot(\overline{E}^{\text{inc}} \times \overline{H}^{\text{inc}*})d\Gamma + \int_{\Gamma_{a_2}{}^+ + \Gamma_{a_1}{}^+} \hat{z}\cdot(\overline{E}^{\text{inc}} \times \overline{H}^{\text{inc}*})d\Gamma,\right.$$

we can obtain from (6)

$$P_{\text{ave}}{}^{P} = -\frac{1}{2}\,\text{Re}\left[\int_{\Gamma_{a_1}{}^-} \hat{z}\cdot(\overline{E}^{\text{inc}} \times \overline{H}^{\text{inc}*})d\Gamma + \int_{\Gamma_{a_1}{}^+} \hat{z}\cdot(\overline{E}^{\text{inc}} \times \overline{H}^{\text{inc}*})d\Gamma - \int_{\Gamma_{a_2}{}^-} \hat{z}\cdot(\overline{E}^{\text{inc}} \times \overline{H}^{P*})d\Gamma + \int_{\Gamma_{a_2}{}^-} \hat{z}\cdot(\overline{E}^{\text{inc}} \times \overline{H}^{P*})d\Gamma - \int_{\Gamma_{b_2}{}^-} \hat{z}\cdot(\overline{E}^{\text{inc}} \times \overline{H}^{P*})d\Gamma + \int_{\Gamma_{b_2}{}^+} \hat{z}\cdot(\overline{E}^{\text{inc}} \times \overline{H}^{P*})d\Gamma\right]. \quad (7)$$

A few additional mathematical manipulations involving the general boundary condition

$$\hat{n} \times \overline{H}^{P} = \overline{K}^{P},$$

the identity

$$\hat{n}\cdot(\overline{E} \times \overline{H}) = -\,\overline{E}\cdot\hat{n} \times \overline{H},$$

the fact that

$$\hat{z} \times \overline{H}^{\text{inc}} = -\frac{\overline{K}^{SC_0}}{2} \text{ over } \Gamma_a{}^-$$

and the numerical value of E^{inc} result in

$$P_{\text{ave}}{}^{P} = \frac{1}{2}\,\text{Re}\left[\int_{\text{b.s.}\Gamma_{a_2}} K^{P*}(\bar{r}')d\Gamma' + \exp(ika)\int_{\text{b.s.}\Gamma_{b_2}} K^{P*}(\bar{r}')d\Gamma' - \int_{\Gamma_{a_1}{}^-} K^{SC_0*}(\bar{r}')d\Gamma'\right], \quad (8)$$

which in accordance with (5) becomes

$$P_{\text{ave}}{}^{P} = \frac{1}{2\omega\mu_0}\,\text{Re}\,[iA^*(\hat{z},\hat{z})] = \frac{\text{Im}\,A(\hat{z},\hat{z})}{2\omega\mu_0}, \quad (9)$$

where Im indicates the imaginary part of $A(\hat{z},\hat{z})$.

The scattering cross-section coefficient σ is defined as the average power $P_{\text{ave}}{}^{P}$ divided by the product of the slit width b and the incident energy per unit area $k/2\omega\mu_0$ and can be written as

$$\sigma = \frac{1}{kb}\,\text{Im}\,A(\hat{z},\hat{z}). \quad (10)$$

This definition of σ might well be called the scattering cross-section coefficient of the slits since $P_{\text{ave}}{}^{P}$ is the difference between the power scattered by the conductors when the slits are present and that which would be scattered if there were no slits in the conductors (infinite conducting planes). It must be remembered that this definition of σ includes only the energy scattered by the slit system into the space outside of the region between the two conducting plates.

The Variational Formulation

The scattering cross-section coefficient cannot be computed accurately using (5) and (10) because the currents are not known, so approximation methods will be required to obtain quantitative answers to any specific problem.

The simple Kirchoff approximation assumes that all of the perturbation currents K^P on the conducting surfaces in (5) are zero. This approximation yields a value of $\sigma = -2$ which is equivalent to assuming that both E and H are unaltered in the first slit and that the second slit plays no part at all. This value approaches the correct value for the case where the slit width is very large compared to the wavelength and where the tandem separation is small.

It is quite obvious that such a simple approximation as this is incapable of predicting any resonant effects with changes in either the slit width or tandem slit separation. In what follows it will be seen that an expression for σ which is stationary with respect to variations in K^P will yield a Kirchoff-type approximation which does predict a resonant effect with changing slit width and changing tandem separation.

Eq. (3) gives the perturbed electric field of the slit system in terms of currents. This expression was developed for a plane wave traveling in the $\hat{z}$ direction. Consider the equation rewritten with additional subscripts $\hat{z}$ on the currents to indicate the direction of the incident field. The limits on the integral containing $[K_y{}^{SC_0}(\bar{r}')]_{\hat{z}}$ can be shown as both sides of $(\Gamma_{a1}+\Gamma_{b1})$, if it is remembered that this factor is zero except over $\Gamma_{a1}{}^-$. This form adds to the apparent symmetry. When the fact that $E_y{}^P(\bar{r})$ is zero for $\bar{r}$ on Γ_{a2} or Γ_{b2} is used we obtain the following integral equation for $[K_y{}^P(\bar{r}')]_{\hat{z}}$;

$$\int_S H_0{}^{(1)}[K_y{}^{SC_0}(\bar{r}')]_{\hat{z}}d\Gamma' = \int_C H_0{}^{(1)}[K_y{}^P(\bar{r}')]_{\hat{z}}d\Gamma' \quad \text{for } \bar{r} \text{ on } \Gamma_{a2} \text{ or } \Gamma_{b2} \quad (11)$$

where the limit S indicates both sides of areas occupied by the slits Γ_{a1} and Γ_{b1}.

So far we have always assumed the incident wave as traveling in the $\hat{z}$ direction in accordance with (1). Now consider the wave as coming from the other direction, that is, assume the incident wave to be

$$[\overline{E}^{\text{inc}}(\bar{r})]_{-\hat{z}} = \hat{y}\exp\{-ik(\bar{r}\cdot\hat{z})\}$$
$$[\overline{H}^{\text{inc}}(\bar{r})]_{-\hat{z}} = \frac{\hat{x}}{Z_0}\exp\{-ik(\bar{r}\cdot\hat{z})\}. \quad (12)$$

For this excitation, different currents will, of course, be

induced on the conducting screen. Multiply (11) by these new perturbation currents $[K_y^P(\bar{r})]_{-\hat{z}}$ and integrate over both sides of $(\Gamma_{a2}+\Gamma_{b2})$ with respect to the variable $(\bar{r})$ obtaining

$$I_1 = \int_C \int [K_y^P(\bar{r})]_{-\hat{z}} H_0^{(1)} [K_y^P(\bar{r}')]_{\hat{z}} d\Gamma' d\Gamma$$

$$= \int_S d\Gamma' \int_C [K_y^P(\bar{r})]_{-\hat{z}} H_0^{(1)} [K_y^{SC_0}(\bar{r}')]_{\hat{z}} d\Gamma, \quad (13)$$

which can be rewritten as

$$I_1 = \int_C \int [K_y^P(\bar{r})]_{-\hat{z}} H_0^{(1)} [K_y^P(\bar{r}')]_{\hat{z}} d\Gamma' d\Gamma$$

$$= \int_{S+C} d\Gamma' \int_C [K_y^P(\bar{r})]_{-\hat{z}} H_0^{(1)} [K_y^{SC_0}(\bar{r}')]_{\hat{z}} d\Gamma$$

$$- \int_C \int [K_y^P(\bar{r})]_{-\hat{z}} H_0^{(1)} [K_y^{SC_0}(\bar{r}')]_{\hat{z}} d\Gamma' d\Gamma. \quad (14)$$

If the excitation is as given in (12) the integral equation for $[K_y^P(\bar{r}')]_{-\hat{z}}$ corresponding to (11) is

$$\int_S H_0^{(1)} [K_y^{SC_0}(\bar{r}')]_{-\hat{z}} d\Gamma' = \int_C H_0^{(1)} [K^P(\bar{r}')]_{-\hat{z}} d\Gamma', \quad (15)$$

for $\bar{r}$ on Γ_{a2} or Γ_{b2}, where it must be remembered that $[K_y^{SC_0}(\bar{r}')]_{-\hat{z}}$ is zero except on $\Gamma_b{}^+$. When this equation is multiplied by $[K_y^P(\bar{r})]_{\hat{z}}$ and integrated over both sides of $(\Gamma_{a2}+\Gamma_{b2})$ we obtain the following alternate form of (13);

$$I_1 = \int_C \int [K_y^P(\bar{r})]_{\hat{z}} H_0^{(1)} [K_y^P(\bar{r}')]_{-\hat{z}} d\Gamma' d\Gamma$$

$$= \int_S d\Gamma' \int_C [K_y^P(\bar{r})]_{\hat{z}} H_0^{(1)} [K_y^{SC_0}(\bar{r}')]_{-\hat{z}} d\Gamma. \quad (16)$$

When (15) is used (14) becomes

$$I_1 = \int_C \int [K_y^P(\bar{r})]_{-\hat{z}} H_0^{(1)} [K_y^P(\bar{r}')]_{\hat{z}} d\Gamma' d\Gamma$$

$$= \int_{S+C} d\Gamma' \int_C [K_y^P(\bar{r})]_{-\hat{z}} H_0^{(1)} [K_y^{SC_0}(\bar{r}')]_{\hat{z}} d\Gamma$$

$$- \int_C d\Gamma' \int_S [K_y^{SC_0}(\bar{r}')]_{\hat{z}} H_0^{(1)} [K_y^{SC_0}(\bar{r})]_{-\hat{z}} d\Gamma. \quad (17)$$

By adding and subtracting a common integral this equation can be rewritten as

$$I_1 = \int_C \int [K_y^P(\bar{r})]_{-\hat{z}} H_0^{(1)} [K_y^P(\bar{r}')]_{\hat{z}} d\Gamma' d\Gamma$$

$$= \int_{S+C} d\Gamma' \int_C [K_y^P(\bar{r})]_{-\hat{z}} H_0^{(1)} [K_y^{SC_0}(\bar{r}')]_{\hat{z}} d\Gamma$$

$$- \int_{S+C} d\Gamma' \int_S [K_y^{SC_0}(\bar{r}')]_{\hat{z}} H_0^{(1)} [K_y^{SC_0}(\bar{r})]_{-\hat{z}} d\Gamma$$

$$+ \int_S \int [K_y^{SC_0}(\bar{r}')]_{\hat{z}} H_0^{(1)} [K_y^{SC_0}(\bar{r})]_{-\hat{z}} d\Gamma' d\Gamma. \quad (18)$$

Consider the scattered field for the case of no aperture in Γ_a (complete screen) for energy incident in the $\hat{z}$ direction. In accordance with (2),

$$[E_y^{SC_0}(\bar{r})]_{\hat{z}} = -\frac{\omega\mu_0}{4} \int_{S+C} H_0^{(1)} [K_y^{SC_0}(\bar{r}')]_{\hat{z}} d\Gamma$$

$$= -\exp(ikz) \text{ for } z \geq 0, \quad (19)$$

where it must be remembered that $[K_y^{SC_0}(\bar{r}')]_{\hat{z}}$ is zero except on $\Gamma_a{}^-$.

Multiply both sides by $[K_y^P(\bar{r})]_{-\hat{z}}$ and integrate over both sides of $(\Gamma_{a2}+\Gamma_{b2})$ to get

$$\int_C \exp(jkz) [K_y^P(\bar{r})]_{-\hat{z}} d\Gamma$$

$$= \frac{\omega\mu_0}{4} \int_{S+C} d\Gamma' \int_C [K_y^P(\bar{r})]_{-\hat{z}} H_0^{(1)} [K_y^{SC_0}(\bar{r}')]_{\hat{z}} d\Gamma,$$

$$\text{for } z > 0. \quad (20)$$

Multiply both sides of (19) by $[K_y^{SC_0}(\bar{r})]_{-\hat{z}}$ and integrate over both sides of $(\Gamma_{a1}+\Gamma_{b1})$ to get

$$\int_S \exp(ikz) [K_y^{SC_0}(\bar{r})]_{-\hat{z}} d\Gamma$$

$$= \frac{\omega\mu_0}{4} \int_{S+C} d\Gamma' \int_S [K_y^{SC_0}(\bar{r})]_{-\hat{z}} H_0^{(1)} [K_y^{SC_0}(\bar{r}')]_{\hat{z}} d\Gamma$$

$$\text{for } z > 0. \quad (21)$$

Employing (13), (16), (18), (20), and (21) the following expression can be obtained:

$$\int_C \int [K_y^P(\bar{r})]_{-\hat{z}} H_0^{(1)} [K_y^P(r')]_{\hat{z}} d\Gamma' d\Gamma$$

$$- \int_S d\Gamma' \int_C [K_y^P(\bar{r})]_{-\hat{z}} H_0^{(1)} [K_y^{SC_0}(\bar{r}')]_{\hat{z}} d\Gamma$$

$$- \int_S d\Gamma' \int_C [K_y^P(\bar{r})]_{\hat{z}} H_0^{(1)} [K_y^{SC_0}(\bar{r}')]_{-\hat{z}} d\Gamma$$

$$= -\frac{4}{\omega\mu_0} \Big[\int_C \exp(ikz) [K_y^P(\bar{r})]_{-\hat{z}} d\Gamma$$

$$- \int_S \exp(ikz) [K_y^{SC_0}(\bar{r})]_{-\hat{z}} d\Gamma \Big]$$

$$- \int_S \int [K_y^{SC_0}(\bar{r}')]_{\hat{z}} H_0^{(1)} [K_y^{SC_0}(\bar{r})]_{-\hat{z}} d\Gamma' d\Gamma. \quad (22)$$

If $\hat{z}$ and $-\hat{z}$ are interchanged this equation will be identical to its present form except for the term in the brackets on the right. Since the rest of the equation is invariant to this change it follows that the term in the bracket must also have the same value when $\hat{z}$ and $-\hat{z}$ are interchanged. When this exchange is made the bracketed term can be expressed in terms of $A(\hat{z}, \hat{z})$ in accordance with (5). If we further define

$$A_k(\hat{z}, \hat{z})$$

$$= -\frac{i\omega^2\mu_0{}^2}{4} \int_S \int [K_y^{SC_0}(\bar{r}')]_{\hat{z}} H_0^{(1)} [K_y^{SC_0}(\bar{r})]_{-\hat{z}} d\Gamma' d\Gamma, \quad (23)$$

then (22) can be written as

$$\frac{i4}{\omega^2\mu_0{}^2}\left[A(\hat{z},\hat{z})-A_k(\hat{z},\hat{z})\right]$$
$$=\int_C\int\left[K_y{}^P(\bar{r})\right]_{-\hat{z}}H_0{}^{(1)}\left]K_y{}^P(\bar{r}')\right]_{\hat{z}}d\Gamma' d\Gamma$$
$$-\int_S d\Gamma'\int_C\left[K_y{}^P(\bar{r})\right]_{-\hat{z}}H_0{}^{(1)}\left[K_y{}^{SC_0}(\bar{r}')\right]_{\hat{z}}d\Gamma$$
$$-\int_S d\Gamma'\int_C\left[K_y{}^P(\bar{r})\right]_{\hat{z}}H_0{}^{(1)}\left[K_y{}^{SC_0}(\bar{r}')\right]_{-\hat{z}}d\Gamma. \quad (24)$$

Thus we have an expression which yields $A(\hat{z},\hat{z})$ and hence σ if we know the perturbation currents that flow on the conducting screens forming the slits first for an excitation field traveling in the $\hat{z}$ direction and secondly for an excitation field traveling in the $-\hat{z}$ direction.

Eq. (5) which is much simpler also gave an expression for $A(\hat{z},\hat{z})$ in terms of the currents. The special value of (24) over (5) is that the former is stationary with respect to changes in K^P provided $[K^P]_{\hat{z}}$ and $[K^P]_{-\hat{z}}$ are chosen so that (11) and (15) are satisfied. It follows that if $\delta A(\hat{z},\hat{z})$ is made equal to zero then K^P must satisfy the proper integral equation, that is, in principle, (24) provides a method of determining K^P.

Experimental Work

The microwave parallel-plate system built by Row[2] was available. With the plates closed a region is formed which is bounded on the top and bottom by plates of aluminum 4 feet by 8 feet. These plates are separated vertically by a distance less than one-half wavelength so that only the TEM mode can propagate if all source currents are in the vertical direction.

The parallel-plate region was excited at one end by an open-ended waveguide. This gives, in effect, a line excitation and a corresponding cylindrical wave so that corrections must be made in the resulting data or the diffracting objects and the measurements must be restricted to a small region in which a plane wave approximation is accurate. In this investigation only data for slit widths less than 1.5 λ were used to obtain scattering cross-section coefficients, except for some phase information for slit widths out of 2.0 λ as described later. The apparent line source was found to be 106 cm in front of the leading slit, which means that for a slit width of 1.5λ the amplitude was constant to within 0.014 per cent across the slit and the phase was constant to within 3.4 degrees.

The desired fields were measured by using a small vertical probe 101.3 cm in back of the slit nearest the source which was insulated from and extended up through the bottom plate. The signal from this probe excited a waveguide and this signal was then used in various standard ways for the determination of phase and amplitude of the original signal.

Construction of the tandem slits used in the parallel-plate region presented several difficult problems; the diffracting edges forming the slits should be very thin compared to a wavelength, should make good contact with the top and bottom plates, and should be quickly and accurately adjustable in tandem separation and slit width. The requirements appear to be mutually exclusive, and it is true that compromises must be made in all of them. The final design used 0.003-inch thick silver foil for the leading edge of the slits but used a thicker construction back from the edges to facilitate the mechanical adjustment of slit width and tandem separation.

Fig. 2 (next page) is a photograph of one of the diffracting edges used to form the slits. Fig. 3 shows the tandem slits in position on the bottom plate of the parallel-plate system. In this photograph, the top plate is in the open position. In this position major adjustments can be made in the diffracting region.

Five watts of microwave power at a free space wavelength of 3.182 cm from an X-21 two-cavity klystron was modulated at 1000 cps by a ferrite Faraday rotation switch. Amplitude measurements of the field were made by feeding the rectified 1000 cps signal into the input of a tuned audio-amplifier. The output of this amplifier was connected to a Ballantine vacuum-tube voltmeter. In making phase measurements, the phase of the signal picked up by the probe was compared with the phase of the known, but adjustable, reference signal selected from a terminated slotted guide. The location of the probe in the slotted guide was measured to 0.001 inch by an Ames gauge.

Experimentally it would be very difficult to make the absolute phase measurements called for by the theory. Most of the difficulty regarding the phase reference for the far field factor can, however, be dispelled by observing for a single slit ($a=0$) both the way in which the phase changes as the slit separation is increased and how the resulting scattering cross-section coefficients, computed by assuming various zero phase reference points, compare with the exact theoretical values.[1] Experimentally it was found that the best fit occurred when the far-field factor was taken as imaginary for the most extreme slit width used (2λ). This procedure was adopted for all the calculations made.

The above procedure for choosing the zero phase angle is justified by the agreement with the theoretical curve for a single slit. When the experimental and theoretical curves for the single slit are compared for large slit widths, however, discrepancies begin to appear for slit widths greater than 1.3λ. These discrepancies are not of the type that can be corrected by changing the zero-phase angle-reference-point, without causing major discrepancies for small slit widths. For this reason it seems proper to conclude that at these large slit widths, the undesirable effects of a cylindrical incident wave and of the probe being too close to the slits are becoming important in determining the amplitude of the signal. Because of this, the final results given here do not show data for slit widths greater than 1.4λ.

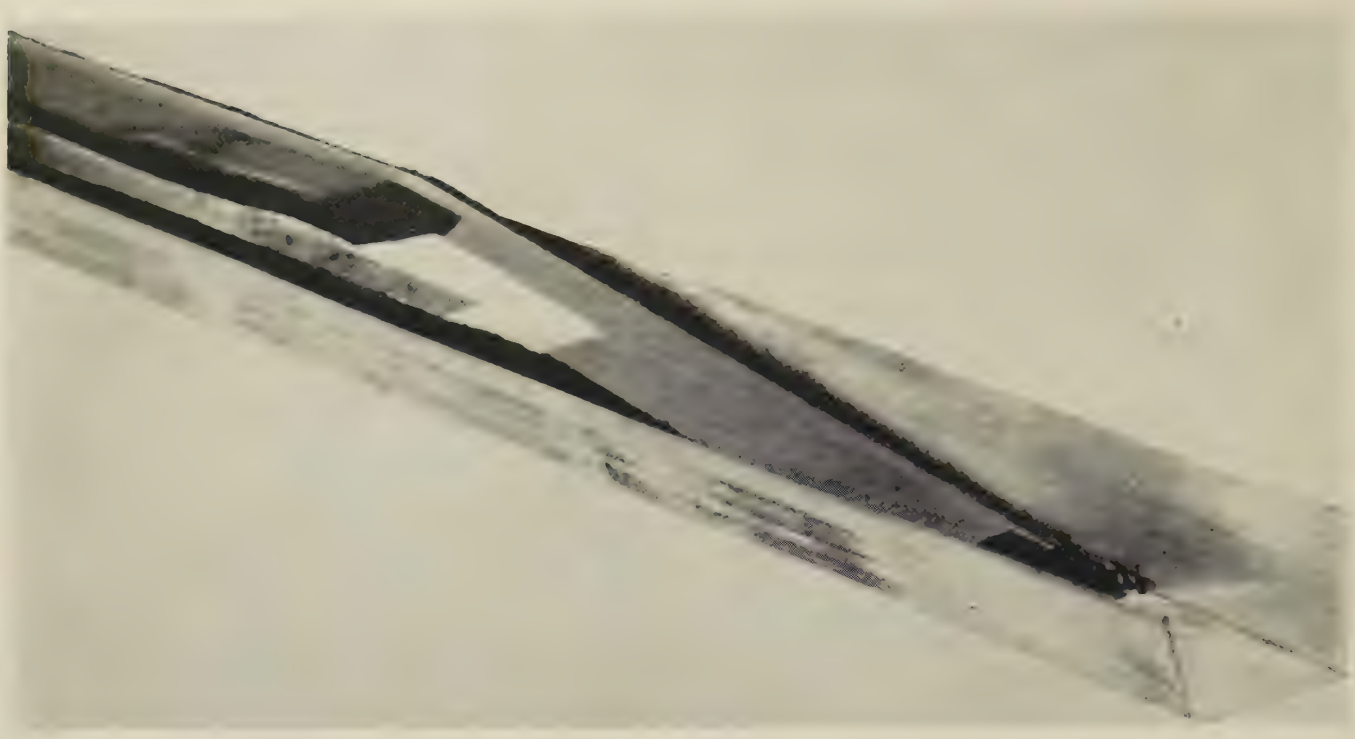

Fig. 2—One of diffracting edges used to form slits.

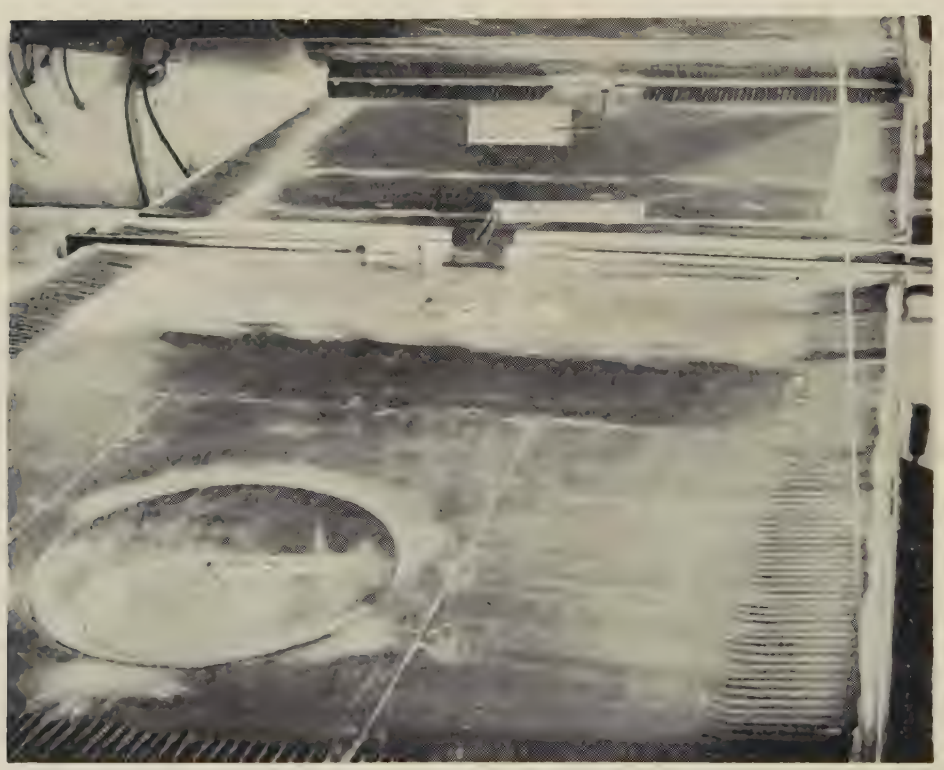

Fig. 3—Tandem slits in parallel-plate region with plates in open position.

The final results are displayed in Fig. 4, where both the amplitude of the received signal divided by slit width and the scattering cross-section coefficients are plotted as functions of the slit width for a variety of tandem slit separations. All of the experimental data has been normalized to fit the Morse-Rubenstein theoretical values for the single slit at $b/\lambda = 1$. Actually the absolute value of the scattering cross section divided by two is plotted so as to be comparable with existing theoretical data for the transmission coefficient, $t = -\sigma/2$, for the single slit.

The experimental result for the magnitude of one-half the scattering cross section (or the transmission) coefficient for zero tandem separation (single slit) are seen

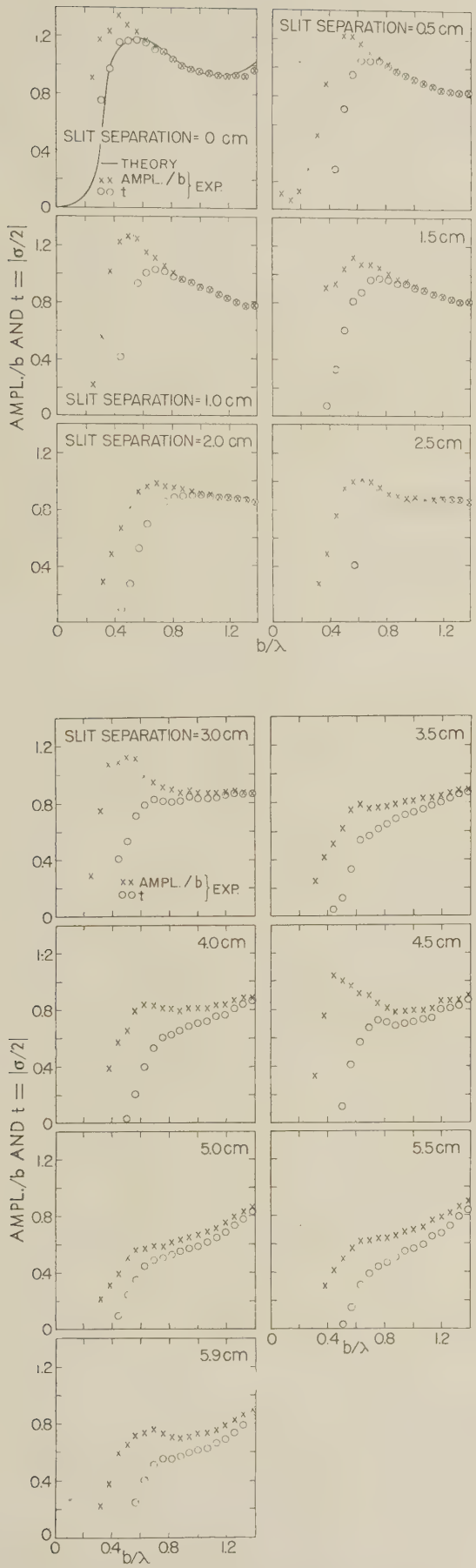

Fig. 4—Scattering cross-section coefficient σ and normalized amplitude in far zone for tandem slit diffraction.

to agree quite well with the Morse-Rubenstein computed values. As the tandem separation increases, the primary peak in the scattered cross-section coefficient decreases and moves toward larger slit widths. The curve changes quite markedly when the tandem separation goes from 1.5 cm to 2.0 cm. This change may be associated with the fact that at 2.0 cm separation the space between the planes forming the slits can now act as a waveguide for the H_{10} mode. Similar changes seem to occur at each new tandem separation that can permit the next higher mode to propagate between the conductors forming the slits. This change in behavior, which seems to be associated with the modes that can be propagated between the conductors, appears in greater relief in the amplitude data. Large peaks in the amplitude have developed for tandem separations of 1.5 cm, 3.0 cm, and 4.5 cm. These peaks are greatly reduced when the slit separations increase respectively to 2.0 cm, 3.5 cm, and 5.0 cm. It would be interesting to investigate this effect in detail to determine how sharp the transition is. It might be caused by a large amount of energy being coupled into the waveguide formed by the slit assembly or it may be that the incident wave sees a greatly modified input impedance at the leading slit.

Comparison of Theory and Experiment

In general when trial functions are used in a variational formula there is no direct way to determine the limits of error that will result. Therefore, it seems wise to first use an approximate current distribution for the case of a single slit, where an exact answer is available and hence the error can be determined, before time is spent trying to work out the more complicated tandem slit problem with similar types of current distribution.

To do this we start with the variational form of $A(\hat{z}, \hat{z})$ given in (24). When this equation is reduced to the case of a single slit, we get

$$A(\hat{z},\hat{z}) = -i\omega^2\mu_0^2 \int_{\Gamma_{a_2}^-}\int [K_y^P(\bar{r})]_{\hat{z}} H_0^{(1)} [K_y^P(\bar{r}')]_{\hat{z}} d\Gamma' d\Gamma + 2i\omega^2\mu_0^2 \left(\frac{\epsilon_0}{\mu_0}\right)^{1/2} \int_{\Gamma_{a_1}^-} d\Gamma' \int_{\Gamma_{a_2}^-} [K_y^P(\bar{r})]_{\hat{z}} H_0^{(1)} d\Gamma - i\omega^2\mu_0\epsilon_0 \int_{\Gamma_{a1}^-}\int H_0^{(1)} d\Gamma' d\Gamma. \quad (25)$$

The simplest approximation is to set the current density equal to zero. This is a Kirchoff-type approximation which becomes

$$A(\hat{z},\hat{z}) \cong A_k(\hat{z},\hat{z}) = -i\omega^2\mu_0\epsilon_0 \int\int_{\Gamma_{a_1}^-} H_0^{(1)} d\Gamma' d\Gamma. \quad (26)$$

Referring to Fig. 1, we can write

$$\mathrm{Im}\, A_k(\hat{z},\hat{z}) = -\omega^2\mu_0\epsilon_0 \int_{-b/2}^{b/2}\int J_0(k|\bar{r}-\bar{r}'|)\, dr' dr. \quad (27)$$

The Bessel function $J_0(k|\bar{r}-\bar{r}'|)$ is an even function so the absolute sign indication on $|\bar{r}-\bar{r}'|$ can be removed

since the vectors $\bar{r}$ and $\bar{r}'$ are collinear. By using a change in variable and the integral formula[5]

$$\int J_p(x)dx = 2\sum_{\nu=0}^{\infty} J_{p+2\nu+1}(x)$$

we get the double infinite sum

$$\operatorname{Im} A_k(\hat{z}, \hat{z}) = -8\sum_{\nu,p=0}^{\infty} J_{2\nu+2p+2}(kb).$$

It can be shown that for a single slit the transmission coefficient t is equal to minus one-half the scattering cross-section coefficient, so we have

$$t_k = -\frac{\sigma_k}{2} = \frac{4}{bk}\sum_{\nu,p=0}^{\infty} J_{2\nu+2p+2}(kb). \tag{28}$$

This double infinite sum is amenable to numerical calculations for relatively small values of b/λ. This numerical calculation is shown in Fig. 5, where it can be readily compared with the exact calculations of Morse and Rubenstein and the experimental value.

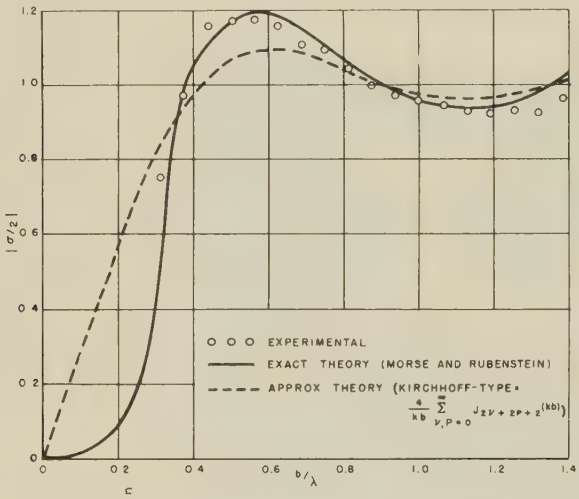

Fig. 5—Scattering cross-section coefficient σ for single slit.

culation are very striking. The currents on the edges of the slit, which have been assumed zero, should play a lesser part for larger values of b/λ so the approximation should be better as b/λ increases to values beyond those shown. The currents on the edges should be relatively more important as b/λ is made very small so it is not at all surprising that the Kirchoff-type approximation is less accurate for small slit widths.

The agreement between the Kirchoff approximation and the exact theory for the single slit is good enough to encourage one to attempt the more tedious calculations required for a similar approximation for the case of tandem slits.

Setting K^P equal to zero in (24) and employing (23) we get for the Kirchoff-type approximation for tandem slits

$$A_k(\hat{z}, \hat{z}) = -\frac{i\omega^2\mu_0^2}{4}\int_S\int [K_y^{SC_0}(\bar{r})]_{\hat{z}} H_0^{(1)}[K_y^{SC_0}(\bar{r}')]_{-\hat{z}} d\Gamma' d\Gamma.$$

When we apply the conditions

$$[K_y^{SC_0}]_{\hat{z}} = -2[H_x^{\text{inc}}]_{\hat{z}} = 2\left(\frac{\epsilon_0}{\mu_0}\right)^{1/2} \text{ on } \Gamma_{a1}^-$$

$$= 0 \text{ on } \Gamma_{a1}^+ \text{ and on both sides of } \Gamma_{b1}$$

and

$$[K_y^{SC_0}]_{-z} = 2[H_x^{\text{inc}}]_{-z} = 2\left(\frac{\epsilon_0}{\mu_0}\right)^{\frac{1}{2}} \exp(-ika) \text{ on } \Gamma_{b1}^+$$

$$= 0 \text{ on } \Gamma_{b1}^- \text{ and on both sides of } \Gamma_{a1},$$

the approximation becomes

$$A_k(\hat{z}, \hat{z}) = -ik^2 \cdot \exp(-ika) \int_{\text{one side of } \Gamma_{b_1}} d\Gamma \int_{\text{one side of } \Gamma_{a_1}} H_0^{(1)} d\Gamma', \tag{29}$$

where we have used the equality $\omega^2\mu_0\epsilon_0 = k^2$.

By employing a change in variable (see Fig. 1), integrating by parts to remove a singularity, and rearranging the terms we can finally get

$$A_k(\hat{z}, \hat{z}) = -i2k\exp(-ika)\int_0^{b/2} dr_b \left[H_0^{(1)}\left[k\left\{\left(\frac{b}{2}-r_b\right)^2 + a^2\right\}^{1/2}\right]k\left(\frac{b}{2}-r_b\right)\right.$$
$$+ H_0^{(1)}\left[k\left\{\left(\frac{b}{2}+r_b\right)^2 + a^2\right\}^{1/2}\right]k\left(\frac{b}{2}+r_b\right)$$
$$+ 2\int_{ka}^{k[(b/2-r_b)^2+a^2]^{1/2}} H_1^{(1)}(y)[y^2 - (ka)^2]^{1/2}dy + \left.\int_{k[(b/2-r_b)+a^2]^{1/2}}^{k[(b/2+r_b)^2+a^2]^{1/2}} H_1^{(1)}(y)[y^2 - (ka)^2]^{1/2}dy\right]. \tag{30}$$

The Kirchoff-type approximation is seen to give reasonable agreement with the exact calculations and with the experimental results for b/λ greater than 0.4. The resonant peaks in σ even for the approximate cal-

In this form although the labor involved is very great it is amenable to numerical evaluation using a desk calculator. This calculation has been made for a slit separation of $a = 0.5$ cm ($ka = 0.986$) and for a range of b/λ from 0 to 1.4 to correspond with one of the experimental cases shown in Fig. 4.

A comparison of this theoretical Kirchhoff-type ap-

[5] E. Jahnke and F. Emde, "Tables of Functions with Formulae and Curves," Dover Publications, New York, N. Y.; 4th ed., p. 145, 1945.

proximation with the experimental values is shown in Fig. 6. The agreement is fairly good; it still predicts the resonance effects quite well. The presence of the term exp $(-ika)$ in (30) makes it possible for even this simple approximation to display at least in a qualitative way the resonance effects with changes in slit separation as were noted experimentally.

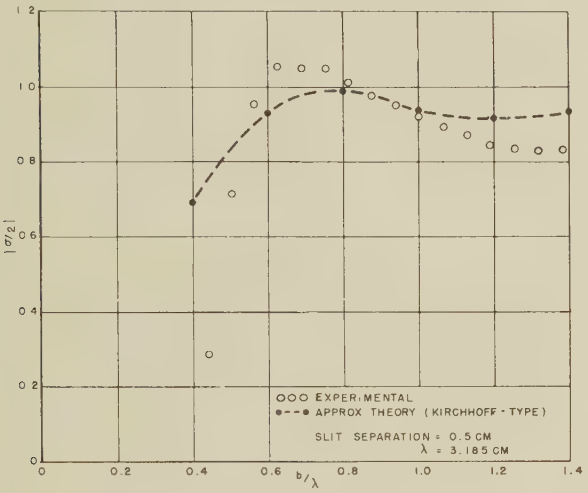

Fig. 6—Scattering cross-section coefficient σ for tandem slits.

It would be desirable to determine the currents on the screen by utilizing the stationary properties of (24), but the work appears very formidable and this is left for future research.

Since the Kirchhoff-type approximation in which all currents have been assumed zero has been shown to be a fairly good approximation it would seem plausible that almost any simple trial function which had the general characteristics of the actual current should yield an improvement. With this thought in mind several attempts were made at using simplified trial functions for the current. The fact that each one tried failed to improve on the original Kirchhoff-type approximation leads to an interesting study in itself.

Moullin and Phillips[6] have discussed the current induced in a conducting ribbon by the incidence of a plane electromagnetic wave. They conclude that the current on one edge is independent of the current on the opposite edge provided the second parallel edge is more distant than $\lambda/2$.

They assumed that for purposes of computing diffraction patterns they could assume a uniform current density extending back from the edge in such a way that its amplitude width integral was equal to the true amplitude width integral.

This type of approximation was tried in (25) for the single slit. The resulting values of the scattering cross-section coefficient were not as close to the Morse-Rubenstein values as was the original Kirchhoff-type approximation. Furthermore the value seemed to depend quite critically on the width of the assumed uniform current density where the amplitude was adjusted each time to preserve the proper amplitude width product.

The stationary characteristics of $A(\hat{z}, \hat{z})$ as given in (24) merely mean that the variations in $A(\hat{z}, \hat{z})$ are independent of the variations in the current density provided K^P obeys the proper integral equation. In general we may write for the variation in $A(\hat{z}, \hat{z})$,

$$\delta A(\hat{z}, \hat{z}) = \alpha \delta K^P + \beta(\delta K^P)^2 + \gamma(\delta K^P)^3 + \cdots .$$

The stationary property of (24) means that the coefficient α is zero, but in general β, γ and the other expansion coefficients are not zero. If a K^P is chosen as a trial function such that δK^P is no longer very small then the higher order terms in the above expansion may make large contributions to $\delta A(\hat{z}, \hat{z})$, thereby resulting in poor approximations to $A(\hat{z}, \hat{z})$. The nature of the complex integrals in (24) involving the imaginary part of $H_0^{(1)}$ which goes to infinity for zero argument seems at least to make it reasonable that an assumed uniform current back from the edge may give a worse approximation than when the current is assumed to be zero.

Acknowledgment

In conclusion I would like to thank R. V. Row and R. D. Kodis of Cruft Laboratory, Harvard University, who suggested this problem and made many helpful suggestions during the experimental part of the work which was done at Harvard University; and to R. K. Wangsness of the University of Maryland who served as advisor.

[6] E. B. Moullin and F. M. Phillips, "On the current induced in a conducting ribbon by the incidence of a plane electromagnetic wave," *Proc. IEE*, vol. 99, pp. 137–150; July, 1952.

Transmission Characteristics of Inclined Wire Gratings*

O. J. SNOW†

Summary—Small diameter parallel wires were imbedded in thin plastic sheets and located closely before an antenna dish receiving plane wave *X* band energy. Polarization was parallel to the wires, and the grating interval was varied between a fifth-wavelength and a whole wavelength for different panels. Received intensity was measured for varied grating tilt angles about an axis lying parallel to the wires and near the center of each panel. Sharp and intense transmission dips were observed for tilt angles at which the parasitic reradiation maxima lay in or near the end-fire direction. The shapes and angular positions of the transmission vs tilt angle curves are approximated by a tentative theory which assumes that the input impedance of the grating is independent of tilt angle and that the apparently absorbed power is proportional to the areas under plots of antenna array patterns. A more precise theory which includes the effect of varying input impedance was required to predict approximate amplitudes as well as sharp transmission dips of smaller magnitude.

Experimental Procedure

THE principal features of the experimental arrangement are illustrated by Fig. 1. The *X* band transmitting antenna was placed at a sufficient distance from the panel to insure a nearly plane incident beam over the grating area, and the receiving dish antenna was placed a few inches behind the panel. The latter was continuously rotatable about an axis lying perpendicular to the plane of the figure. With this configuration, the received intensity was measured vs a varying panel tilt angle θ for several different values of wire separations d, the incident electric vector being maintained parallel to the wires. The effect of interaction between dish and panel on the results was reduced by using as the received intensity the geometric mean of the maximum and minimum intensities as the spacing of the panel center relative to the antenna dish was varied over approximately a half-wavelength. The panel widths as shown in the plane of Fig. 1 were about 4 feet and both 10-inch and 18-inch receiving antenna dishes were used. In all cases a 70 per cent copper–30 per cent zinc brass wire material was used, with sizes in the number 26- to 29-gauge range, although neither small variations in conductivity nor in diameter appeared to affect the results. Except for the case where the wire separation was $\frac{1}{4}$-inch, where the wires alone were used, they were all imbedded near the centers of laminated Fiberglas panels (six piles of number 180 Fiberglas cloth plus Laminac P-43 resin). Since the fabrication details varied somewhat from panel-to-panel, the panel thicknesses varied from 0.044-inch to 0.063-inch as indicated in the upper right hand corner of Fig. 1. The wire spacings chosen were $\frac{1}{4}$-, $\frac{3}{4}$-, 1, and $1\frac{1}{4}$ inch. It was expected that more or less uniform absorption would occur for wire spacings less than about one-half wavelength, therefore, except for the single panel with quarter-inch spacings, spacings greater than one-half wavelength were chosen.

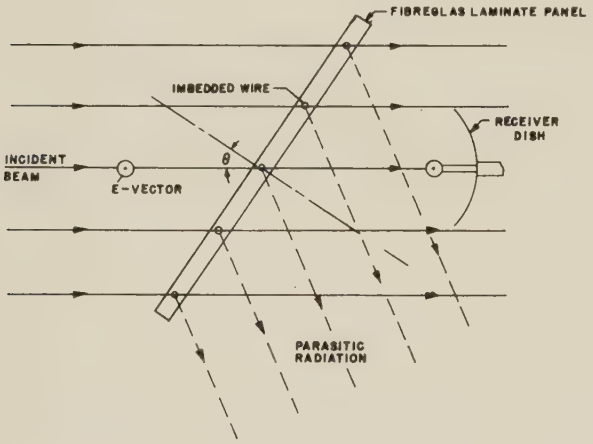

Fig. 1—Experimental arrangement.

Experimental Results

The principal experimental results obtained with such an arrangement are given in Fig. 2. Here per cent power transmission is plotted vs grating tilt angle for four different panels, each with different wire spacings. For simplicity in presentation, only regions of the curves where the variation in transmission is marked are included. The curves are, of course, in all cases approximately symmetrical about the zero tilt position. It is noted that, except for the grating with $\frac{1}{4}$-inch wire spacings, sharp and pronounced transmission dips occur at tilt angles which increase in value as the spacings are decreased.

The separate points which are present in Fig. 2 indicate measured transmissions of wire-free panels of approximately the same construction as those in which the gratings are imbedded. It is observed that these panels exhibit no absorption maxima of their own; also, in some instances, the presence of the wires appears to slightly improve the over-all transmission. Thus the transmission minima may be attributed, primarily, to the effect of the wires alone.

For the case of 1.25-inch wire separation, that is, approximately one wavelength, it may be observed in Fig. 2 that a single major dip occurs at normal incidence. As the wire separation decreases from one wavelength, this single minimum appears to split into two minima as is evidenced by the curve for a 1-inch separation. Here, there are major dips in the neighborhood of plus and minus 15° along with a number of minor variations.

* Manuscript received by the PGAP, September 2, 1955; revised manuscript received, April 9, 1956.

† U. S. Naval Air Dev. Ctr., Aeronautical Elec. and Elect. Lab., Johnsville, Pa.

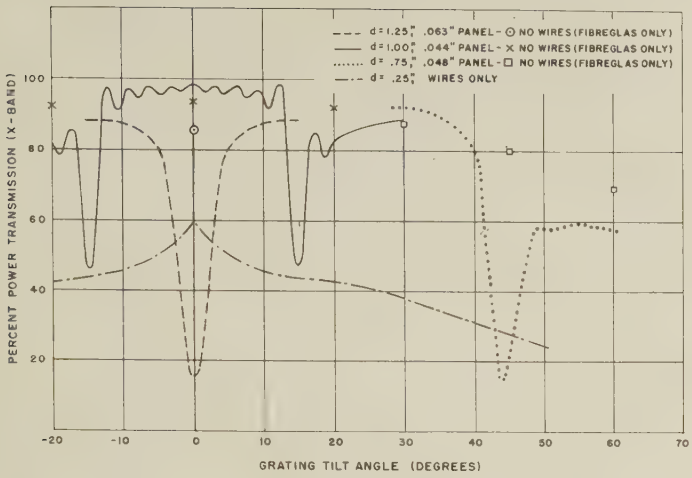

Fig. 2—Experimental transmission curves for four wire gratings.

When the wire separation is reduced to $\frac{3}{4}$-inch, the principal minima have moved to approximately plus and minus 44°. Referring to Fig. 2, it may be seen that these major dips occur at tilt angles which are given, very nearly, by the formula:

$$\sin^{-1}\left(\frac{\lambda}{d} - 1\right).$$

It is immediately apparent that this is also the condition at which the array would be expected to reradiate parasitically in a reverse end-fire direction. In other words, the apparently absorbed energy is reradiated in an end-fire direction when the tilt angle reaches the proper value for this to occur. This relationship is graphically illustrated in Fig. 3. Slight errors in angular measurement, panel flatness, and wire spacings are present such that the measured transmission minima are no more accurate than about one-half of one degree. The extreme differences between the measured values and values computed by the formula above are only slightly higher than this.

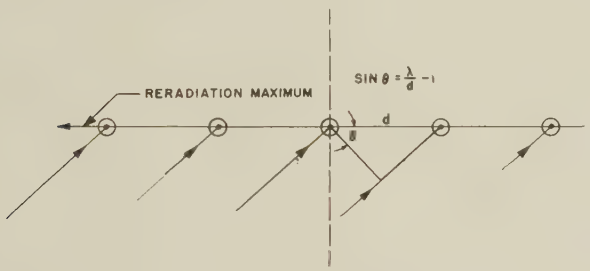

Fig. 3—Observed condition for minimum transmission.

Theory

First, a simple theory which predicts the angular positions and approximate shapes of the transmission curves will be briefly discussed, after which the more complex and accurate theory will be outlined. The simpler tentative theory assumes that the total impedance of each wire is invariant with tilt angle and that the current peak amplitude is identical and uniform over all of them. With these assumptions, it can be stated that the total reradiated power will be proportional to the integral of the power antenna array patterns, where the relative phases between the currents of successive wires is given by $d \sin \theta$ (see Fig. 3). Approximate patterns computed in the plane of the gratings for the case of 1-inch wire spacings (47 wires total), and for three significantly different incident beam directions are plotted in Fig. 4. Note that only reradiated energy is considered here, and that the large effect of the main transmitted beam is not shown. It is observed that radiation peaks are found in the principal transmission or incident beam directions noted by lobes "*a*" in the figure in addition to lobes noted by "*b*" which are peaked in the specular reflection directions. The absolute intensities of these lobes, as well as their widths, change comparatively slowly with changing incident direction, still assuming that the wire current peak amplitudes do not change with incident direction. In pattern "*A*" the incident or tilt angle is appreciably less than 15°, a condition for which the measured transmission is well above 90 per cent, with only minor transmission dips occurring. From the antenna array formula it can be easily shown that, with this condition, the only significant lobe other than those in the main transmission and specular reflection directions is lobe "*c*" which points in an end-fire direction. The amplitude of this lobe grows but remains relatively small until the critical angle of incident beam direction, in this case 15°, is approached. Pattern "*B*" represents the case where the incident beam direction is exactly this critical value. Here the end-fire lobe has grown rapidly to its maximum value, and while its

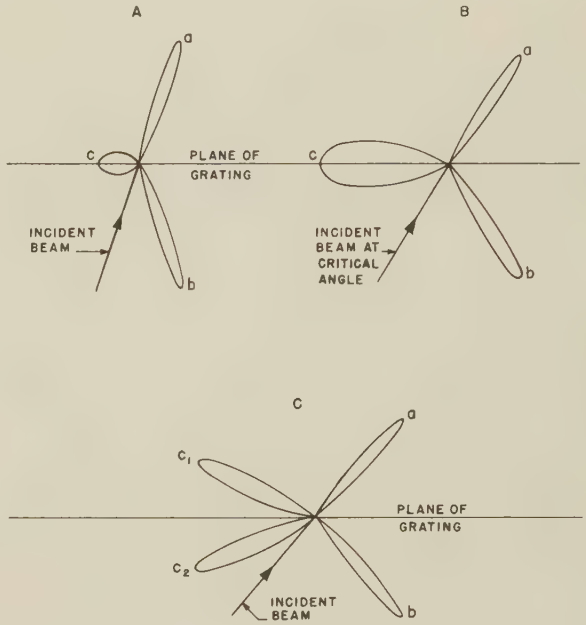

Fig. 4—Approximate parasitic radiation patterns for varying tilt angle (1-inch wire spacing).

amplitude is identical to that of the other two lobes, as given by the antenna array formula, its width is considerably greater, thereby representing a decidedly greater quantity of power. As the incident beam direction angle exceeds the critical angle, the lobe "c" splits into two separate lobes, represented by "c_1" and "c_2" in pattern "C." These two lobes maintain the same amplitude as the others, however, their widths are sufficiently small so that the energy which they represent is significantly less than the energy represented by lobe "c" in pattern "B."

Theoretical Results

Using the simplified assumptions stated above, areas under computed antenna patterns were determined for the case of one-inch wire separation and plotted as a function of grating tilt angle. The detailed results of these calculations are omitted here, but it may be stated that the shape and angular position of major transmission dips were predicted reasonably closely by the computed curve. Of course, nothing could be computed by this simplified method which would give information as to the absolute magnitudes of the transmissions. The minor maxima and minima which lie between the major dips were not predicted at all by the simple theory.

Both in order to investigate the significance of the minor variations and to obtain a theoretical value for the absolute magnitudes of the transmissions, a more thorough examination of this problem was then made. It was assumed that if the absolute magnitudes of the wire currents along with their radiation resistances could be obtained, then the parasitically radiated power could be computed, although omitting the effect of interference between the main transmitted beam and the parasitic lobe radiation which is pointed in the incident beam direction. As a basic reference for this more thorough study, the article by Groves,[1] was used.[2] Although Groves was concerned with the case of pairs of grids with normal incident radiation, he obtains the impedance per meter of the central wire of a single grid as one step in his derivations, still at normal incidence. Following this derivation, it is a relatively simple matter to modify the original equations to make them valid for an arbitrary grid tilt angle and for a finite, rather than an infinite number of wires.

The equation thus obtained was used for the basic computations of the present study. Because of its orthodox nature it is not given here. The formula is composed of two terms which give the self impedance of a single wire, plus terms giving the mutual impedance of the central wire due to each pair of wires located equidistant from it. For the case of the panel with 1-inch wire separations with 47 wires, a total of 25 terms are obtained. This formula also assumes that the wires are of infinite length and that all of them carry the same current. It was known that these assumptions did not hold rigorously for the case under study here, and thus preliminary studies were made to determine approximately the degree to which they did or did not hold. The first assumption was determined to be sufficiently valid, since it was found that changing receiving dish size made no appreciable difference in measured results, indicating a reasonable current uniformity lengthwise over the wires. The second assumption is more critical, since the mutual impedances of the wires near the edges of the grating are obviously quite different from those near the center of the grating. However, the receiving dish sizes were, in practically all cases, of diameters of no more than half of the grating projected widths, indicating that the currents in the wires near to the dish should be relatively uniform. Thus it was concluded that this assumption was probably not a serious one either. The impedances for each of the wires could, of course, be computed by taking the proper summations for each one separately, but this presented a tedious task and it was avoided by accepting this second assumption. Even with the simplifying assumptions, the computations involved are considerable.

Further preliminary investigations were made to determine if computational simplifications could be made by utilizing infinite summation formulas similar to those utilized in Groves' article. To gain information on this subject as well as general knowledge of the phenomenon involved, transmission curves were measured using the 4-foot wide panel with 1-inch wire spacings and with 1 foot of each edge being covered on its front surface with a microwave absorbing material. A 10-inch dish size was used so that more than 6 inches of clear grating beyond the dish edges was maintained. From the results plotted in Fig. 5, with and without the absorber, it appears that the wires beyond the dish edges have an appreciable effect on the measured transmission curve. A similar result was obtained by moving the panel laterally so that its edge which pointed towards the dish was near the dish. Moving the panel laterally in the opposite direction near its extreme caused an appreciable sharpening and deepening of the absorption dip. These results indicate that the grating lengths lying beyond the dish edge in the direction of the end-fire parasitic pattern have no large effect on the transmission curve, while the grating lengths lying beyond the edge in the opposite direction have a significant effect. It implies that the degree of coupling between the wires of one edge to the wires in the central region is appreciable. This also indicates that computations must be based on the impedance formula with the finite number

[1] W. E. Groves, "Transmission of electromagnetic waves through pairs of parallel wire grids," *J. Appl. Phys.*, vol. 24, pp. 845–854; July, 1953.

[2] See also: J. Shmoys, "Diffraction of Electromagnetic Waves by a Plane Wire Grating," Res. Rep. EM-18, Mathematical Research Group, New York University, New York, N. Y.; March, 1950.

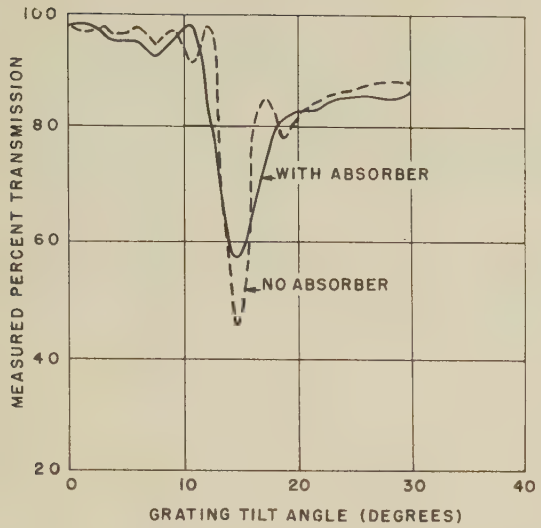

Fig. 5—Measured transmission with and without 1-foot absorber over tilted panel edges.

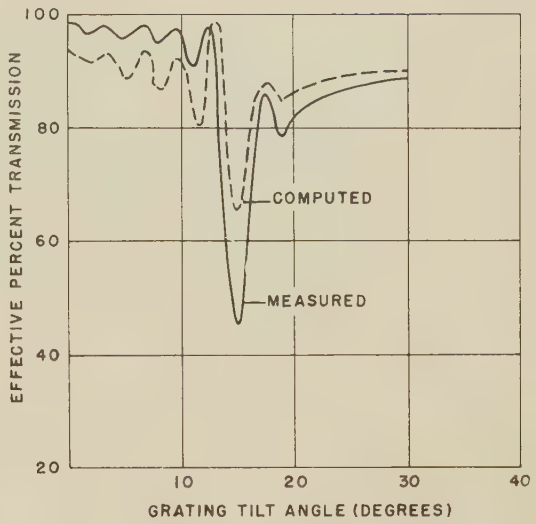

Fig. 6—Measured transmission compared with computed nonradiated energy.

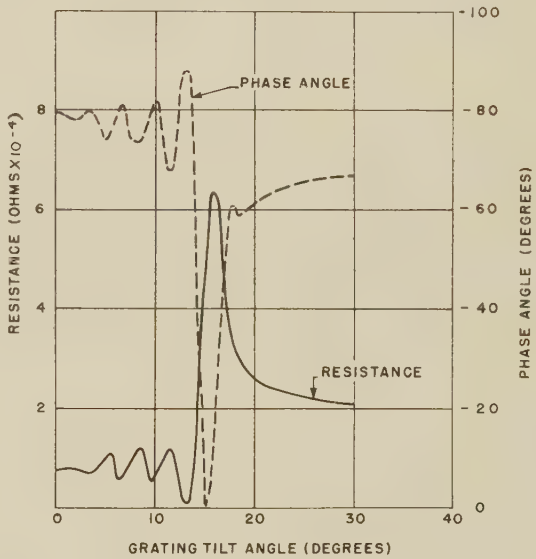

Fig. 7—Resistive component of impedance and phase angle of induced current.

of terms and that use of infinite convergence formulas are not valid in this application.

The microwave power which is parasitically radiated per meter of wire per unit of incident field intensity squared is given by the ratio of the resistive component of the impedance per meter to the square of the magnitude of the total impedance per meter. In the computations for the problem being considered the fraction of energy incident upon the grating, which is parasitically radiated, is assumed to be given by the ratio of the power radiated per meter for the central wire alone to the power per meter per grating interval incident upon the grating. When this radiated fraction is subtracted from unity, the fraction of nonradiated power is obtained. The latter computed value together with the measured transmission percentage is plotted in Fig. 6 as a function of tilt angle for the case of 1-inch wire spacing. Note that both major and minor transmission dips given by the measured data are predicted by the computed results. The amplitudes agree as to order of magnitude, although the discrepancies in this regard are not at all negligible.

The sign and order of magnitude of the discrepancy at the transmission minimum which occurs at a tilt angle of 15° can be explained as due to interference between the transmission beam unaffected by the wires and the parasitic lobe which points in the incident beam direction. That the phasing is correct for this can be seen by an observation of Fig. 7 which gives a plot vs tilt angle of the phase delay of the parasitically induced currents relative to the incident field intensity. Note here that at the angle of 15° where maximum absorption occurs, the phase drops suddenly from a value which is near quadrature to a zero or "in-phase" value. If then, the equivalent current sheet method is applied to the incident field intensity between the wires, it will be found that this equivalent current has a 180° or "out-of-phase" value at a 15° tilt angle, which will cause destructive interference with the fields resulting from the wire currents.

The amplitudes of the minor transmission dips are computed to be greater than the measured values. The phasing between wire fields and incident fields are not destructive as they are in the case of the major dip; however, it appears that they may be slightly constructive which would explain a part of the discrepancy. The remaining part of the differences are probably due to the effect of the assumptions described above, residual experimental errors, and to the presence of the thin Fiberglas laminated sheet which was neglected.

Fig. 7 also gives a plot of the radiation resistance per meter of the central wire as a function of tilt angle. Note that the wiggles in this curve are approximately opposite in phase to those in the transmission and phase

angle curves, as might be expected. The peak of radiation resistance, however, occurs at a tilt angle which is about one degree higher than that for maximum absorption. The total impedance curve, not plotted here, has a shape approximating that of the resistance curve, which indicates that the assumption made previously, that impedances and currents are invariant with tilt angle, are completely invalid. The degree of agreement between theory and experiment obtained when using that assumption may be fortuitous.

Conclusion

In conclusion, the transmission minima introduced by thin wire gratings imbedded in thin plastic sheets with wire spacings lying between a half and one wavelength, when placed close to a receiving antenna dish whose dimensions are smaller than the grating size, have been predicted theoretically with fair results. Sharp transmission dips, accentuated by interference effects, occur at tilt angles where parasitic reradiation is in or near a reverse end-fire direction.

On Resonance in Infinite Gratings of Cylinders*

S. N. KARP† and J. RADLOW†

Summary—**The diffraction by a grating is examined (for spacing large compared to wavelength and dimension of grating element) for wavelengths in the neighborhood of the "Rayleigh" wavelengths. The shape of the elements, and their size in wavelengths is unrestricted. The results, including the effect of interaction, are expressed in terms of quantities relating to single scattering. Some properties of certain determinants formed from single scattered amplitudes are derived. The results are compared with those obtained by other authors, using various restrictions on the parameters.**

I. Introduction

THE PURPOSE of the present work is to present the results of an investigation of the behavior of diffraction gratings of cylinders for wavelengths neighboring certain critical wavelengths, the so-called "Rayleigh Wavelengths." The analysis is based on the results of a previous investigation,[1,2] in which expressions were derived for the Fourier amplitude of the diffracted field of a grating of arbitrary cylinders, subject to the restrictions that the spacing is large as compared to cylinder dimension and wavelength, and that the Rayleigh wavelengths are excluded. The expressions there obtained for the Fourier amplitudes only involved quantities associated with a single scatterer, *in spite of the fact* that interactions were taken into account. The principal result of the present paper is the extension of the conclusions of Karp[2] to the case of critical wavelengths, in which the significance of interaction is maximal. The required results of Karp[1] and Karp[2] are recapitulated in Section II of the present work. They form a special case of a general theory[3] for the calculation of the field scattered by a combination of obstacles in terms of the scattering patterns of the obstacles in isolation. Experience with the case of diffraction by a pair of half planes (*i.e.*, a *slit*)[4] indicates that the accuracy of this kind of calculation is good down to spacings of one wavelength.

In Section III of the present paper we discuss the behavior of the Fourier amplitude of the grating in the limit in which the critical or Rayleigh wavelengths are approached. In this limit the "single scattering" result diverges, while the result given in Section II is indeterminate. However, the limit is evaluated explicitly in the present work. We also include in this section a discussion of certain determinants relating the scattering amplitudes of a single cylinder; the behavior of these determinants is crucial for the limiting process in question.

Section IV is concerned with a brief discussion of energy conservation. It is shown that the "single scattering" result conserves energy with an error which, while small for *general* large spacings, contains a factor which diverges for *critical* spacings. On the other hand the results deduced from Section II are free of this defect.

In Section V we compare our results with those of previous investigators. Most previous work has been based on other types of restrictions than our own. How-

* Manuscript received by the PGAP, January 15, 1956; revised manuscript received, May 18, 1956. The research reported here was performed at the Institute of Mathematical Sciences, New York University, New York, N. Y., and has been made possible through support and sponsorship extended by the U. S. Air Force, AF Cambridge Res. Ctr., under Contract No. AF 19(122)-42.

† Inst. Mathematical Sciences, New York University, New York, N. Y.

[1] S. Karp, "Diffraction by finite and infinite gratings," *Bull. Amer. Phys. Soc., Phys. Rev.*, vol. 86, p. 586; 1952.

[2] S. Karp, "Diffraction by an Infinite Grating of Cylinders," Inst. Math. Sci., New York University, New York, N. Y., Res. Rep. No. EM-85; October, 1955.

[3] S. Karp, "Scattering by a Combination of Obstacles," Symposium, McGill Univ., Montreal, Can.; June, 1953.

[4] S. Karp and A. Russek, "Diffraction by a Wide Slit," Inst. Math. Sci., New York University, Res. Rep. No. EM-75; February, 1955.

ever, Twersky,[5,6] who treated the case of circular cylinders for noncritical spacings obtained equivalent results for the contributions of the individual cylinders in that case, for certain angles of incidence and these results were extended by Magnus (see Appendix)[5,6] to arbitrary angles of incidence, subsequent to the developments by Karp.[1]

A more interesting comparison is made possible by considering the application of our results to the reflection grating, which is the seat of the celebrated "Wood's Anomalies" discussed by Wood,[7] Rayleigh,[8] Fano,[9] and Strong.[10] A definitive theory has been given by Artmann.[11] Since the only restriction of Artmann's analysis is that the corrugations be small compared to wavelength, a comparison with our theory is possible in the case in which corrugations are small and the spacing is large. We specialize our results to small corrugations in Section 5, and, after giving explicit approximate formulas for the scattering amplitudes of a thin strip in the case of when the magnetic vector is parallel to the generators of the grating, we are able to show agreement with the results of Artmann.

On the other hand it is pointed out that both for the resonance and nonresonance cases our results are in disagreement with results given in a new report by Twersky.[12] The nature of the discrepancy is explained, and possibilities for its removal are suggested.

II. Preliminary Results

It is well known that the far field form of every outgoing wave function[13] takes the form

$$H_0(kr)f(\theta) \cong \sqrt{\frac{2}{\pi kr}} \exp\left(ikr - i\frac{\pi}{4}\right) \cdot f(\theta) \qquad (1)$$

where r and θ are polar coordinates. Also, in a problem dealing with diffraction by a combination of obstacles Green's theorem shows that we can regard the scattered field as composed of a sum of outgoing wave functions, each regular in the exterior of one of the scattering bodies. Suppose the bodies in question are far apart, so that all dimensions of each body, and the wavelength as well, are small compared to the distance to any other body in the array. Then it can be shown from (1) that *in the neighborhood of any body in the configuration* the total field is approximately equal to the incident field, plus the field scattered by the body in question, plus a sum of plane waves arriving from the directions of the other bodies. (The complex amplitudes of the latter plane waves are at first unknown.) Consequently the actual field contributed by each body is approximately an unknown linear combination of the fields which that body would scatter when responding to the plane waves in question, in isolation. The necessary coefficients can then be calculated by a consistency argument. For details in the case of $E\|$, see Karp;[2,3] the argument is easily seen to apply for arbitrary boundary conditions, however.

The theory in question can be applied to an infinite grating of cylinders. Before stating the results we recall some formulas from the general theory of infinite gratings.

We consider a grating of congruent cylinders lying in the plane $y=0$. If a plane wave is incident at the angle ϕ, so that

$$u_{\text{inc}} = e^{ik(x\cos\phi + y\sin\phi)} \qquad (2)$$

and if the distance between corresponding points of the grating is d, then the fields contributed by the various cylinders differ among each other only by a translation and by a phase factor $\exp(iknd\cos\phi)$, so that the total field may be written

$$u = u_{\text{inc}} + \sum_{-\infty}^{\infty} \exp(iknd\cos\phi) F(x - nd, y). \qquad (3)$$

Suppose further that the far field form of $F(x, y)$ is given by

$$F(x, y) \sim \sqrt{\frac{2}{\pi kr}} \exp\left(ikr - i\frac{\pi}{4}\right) f(\theta), \qquad (4)$$

where $x = r\cos\theta$, $y = r\sin\theta$. Then in consequence of the regularity of the field in the exterior of a horizontal strip containing the grating elements, the total field can be written as follows

$$u = u_{\text{inc}} + \sum_{-\infty}^{\infty} \frac{2}{kd\sin\theta_\nu} \cdot f(\pm\theta_\nu) \exp ikr\cos(\theta \mp \theta_\nu) \qquad (5)$$

except for values of y in horizontal strips containing the grating elements. The upper sign is to be taken when y is above the strip. In this exact formula the spectral angles θ_ν are given by:

$$k\cos\theta_\nu = k\cos\phi + 2\pi\nu/d$$
$$k\sin\theta_\nu = \sqrt{k^2 - (k\cos\phi + 2\pi\nu/d)^2}. \qquad (6)$$

The infinite grating problem is thus equivalent to the determination of the values of the function $f(\theta)$ for $\theta = \theta_\nu$. A finite number of the quantities θ_ν are real; these lead to propagating waves in (5); *i.e.*, orders of the spectrum.

[5] V. Twersky, "Multiple Scattering of Radiation, Part II (The Grating)," Inst. Math. Sci., New York University, Res. Rep. No. EM-39; December, 1951.

[6] V. Twersky, "Multiple scattering of radiation, part II (the grating)," *J. Appl. Phys.*, vol. 23, p. 1009; 1952.

[7] R. W. Wood, "Anomalous diffraction gratings," *Phys. Rev.*, vol. 48, p. 928; 1935. *Phil. Mag.*, vol. 23, p. 310; 1912; and vol. 4, p. 396; 1902.

[8] Lord Rayleigh, *Proc. Roy. Soc., London*, (*A*), vol. 79, p. 399; 1907.

[9] U. Fano, "Zur Theorie der Intensitats anomalien der Beugung," *Ann. d. Phys.*, (5), vol. 32, p. 393; 1938.

[10] J. Strong, "Effect of evaporation films on energy distribution in grating spectra," *Phys. Rev.*, vol. 39, p. 291; 1936.

[11] K. Artmann, "Zur Theorie des anomalen Reflexion von Optischen Strichgittern," *Z. fur Phys.*, vol. 119, p. 529; 1942.

[12] V. Twersky, "Scattering of Waves by An Infinite Grating," Elec. Defense Lab., Mountain View, Calif., Engrg. Rep. No. EDL-E5; April, 1955.

[13] The result in two dimensions is being stated here. Time dependence $\exp(-i\omega t)$ is assumed.

The function $f(\theta)$ is expressible in terms of the boundary values of $F(x, y)$ by quadratures which are meaningful also for complex θ. We can now state our preliminary formulas, with which we operate in the balance of this paper. We have found (cf. Appendix) using the type of analysis described in the foregoing paragraph, that

$$f(\theta) = f_I(\theta) + A_L f(0) f_L(\theta) + A_R f(\pi) f_R(\theta), \quad (7)$$

$$F(x, y) = F_I(x, y) + A_L f(0) F_L(x, y) + A_R f(\pi) F_R(x, y), \quad (7a)$$

where the functions $f_I(\theta)$, $f_L(\theta)$, and $f_R(\theta)$ are those describing the far field of a single cylinder in the grating, when excited respectively by the incident field, a plane wave coming from $x = -\infty$, and a plane wave coming from $x = +\infty$. The function $F_I(x, y)$, etc., are the corresponding scattered fields defined for all x and y. The constants A_L and A_R are given:

$$A_L = \sqrt{\frac{2}{\pi kd}} \exp\left(-i\frac{\pi}{4}\right) \sum_1^\infty \cdot \exp inkd\,(1 - \cos\phi)/\sqrt{n}$$

$$A_R = \sqrt{\frac{2}{\pi kd}} \exp\left(-i\frac{\pi}{4}\right) \sum_1^\infty \cdot \exp inkd(1 + \cos\phi)/\sqrt{n}. \quad (8)$$

The quantities $f(0)$, and $f(\pi)$, which are obtained from (7) by setting $\theta = 0$ and $\theta = \pi$ respectively, and solving the resulting pair of simultaneous equations, are given by the following:

$$f(0) = \{f_I(0) - A_R\alpha_1\}/\{1 - [A_L F_L(0) + A_R f_R(\pi)] + A_R A_L \alpha_3\}$$

$$f(\pi) = [f_I(\pi) - A_L\alpha_2]/\{1 - [A_L f_L(0) + A_R f_R(\pi)] + A_R A_L \alpha_3\}, \quad (9)$$

in which α_1, α_2, α_3 are given:

$$\alpha_1 = \begin{vmatrix} f_I(0) & f_R(0) \\ f_I(\pi) & f_R(\pi) \end{vmatrix}, \quad \alpha_2 = \begin{vmatrix} f_L(0) & f_I(0) \\ f_L(\pi) & f_I(\pi) \end{vmatrix},$$

$$\alpha_3 = \begin{vmatrix} f_L(0) & f_L(\pi) \\ f_R(0) & f_R(\pi) \end{vmatrix}. \quad (10)$$

This result which is obtained by Karp,[2] holds with the proviso that k, d, and ϕ are such that there is no positive or negative integer ν for which $\sin\theta_\nu$ vanishes. This implies that both A_L and A_R converge. Then A_L and A_R are small quantities for sufficiently large kd, so that the leading term of (7) is $f_I(\theta)$. The approximation $f(\theta) \sim f_I(\theta)$ thus expresses the natural assumption that each grating element responds as if in isolation, when the spacing is very large.

III. The Case of Resonance

Our task in the present work is to discuss the behavior of the solution in the neighborhood of such frequencies or angles of incidence as make $\sin\theta_\nu = 0$. We shall refer to such a situation as a "resonance," and shall discuss the limiting value, of the result of (7), as well as the behavior in the neighborhood of the limit. (We shall not discuss the mathematical question of the existence and properties of the solution at precisely critical frequencies. Such a solution may well differ from the limit of the noncritical solution which it seems to us is the observable quantity here.)

The first thing we shall discuss is the limiting value of the solution given by (5) and (7).

To do so we note that if ν is such that $\sin\theta_\nu$ tends to zero, then the denominator of the νth term of (5) goes to zero. The corresponding exponential factor in this term becomes $\exp(\pm ikx)$. This analytical phenomenon is well known since Rayleigh, who pointed out the connection of grating resonances with the case when a spectral order passes off tangentially. Of course, the approximation $f(\theta) \sim f_I(\theta)$ breaks down completely in this case. However, we shall show that the use of (7) leads to an intelligible result. Our task will be to compute the limit of $f(\theta_\nu)/\sin\theta_\nu$ as $\theta_\nu \to 0, \pi$. In addition it will be noted that all other terms of the series (5) require re-examination in this case. For one or both of the quantities A_L and A_R diverge, and the quantities $A_L f(0)$ and $A_R f(\pi)$ become indeterminate.

In order to proceed it is necessary to scrutinize the manner of divergence of A_L and A_R. This divergence can occur in several ways [cf. (8)], 1) $kd(1-\cos\phi)$ approaches an integral multiple of 2π, 2) $kd(1+\cos\phi)$ approaches such a value, 3) both case 1) and case 2) occur simultaneously. (For the last mentioned case to occur $\tan^2(\phi/2)$ must be rational.) Suppose therefore that there exist positive integers, p_a, p_b such that either

$$kd(1 - \cos\phi) = 2p_a\pi + \delta_a \qquad \delta_a \to 0, \quad (11a)$$

or

$$kd(1 + \cos\phi) = +2p_b\pi + \delta_b, \qquad \delta_b \to 0 \quad (11b)$$

or both. In case 1) the denominator of the term $\nu = p_a$, vanishes in (5) and also A_L diverges. In case 2) it is the term $\nu = -p_b$ which is critical while A_R diverges. It can be shown by comparison with the binomial expansion of $(1-z)^{1/2}$ that for small δ_{ab} we have

$$A_{L,R} \to 2/(2kd\delta_{a,b})^{1/2} \quad (12)$$

where the root is positive, or positive imaginary. In case 3) (11) and (12) show that

$$\lim A_L/A_R = \lim \sqrt{\delta_b/\delta_a}. \quad (13)$$

If we keep ϕ fixed and let k approach a critical value, then the limit is $\cot\phi/2$. If k is a suitably fixed value and ϕ approaches a correspondingly critical value the limit is $+i$. On the other hand, (6) allows us to express $k\sin\theta_\nu$ approximately in terms of δ_a and δ_b, when $\nu = p$ and $\nu = -q$ respectively. Introducing $k_\nu = k\sin\phi_\nu$, we find

$$k_{p_a} \to (2kd\delta_a)^{1/2}/d; \qquad k_{p_b} \to (2kd\delta_b)^{1/2}/d \quad (14)$$

so that

$$\lim k_{pa}A_L = \lim k_{-pb}A_R = \frac{2}{d}$$

$$\lim k_{pa}A_R = \frac{2}{d}\lim (A_R/A_L)$$

$$\lim k_{-pb}A_L = \frac{2}{d} \quad \lim (A_L/A_R). \tag{15}$$

Using (12) to (15) we can pass to the limit in (7). In case 1) we find

$$f(\theta) - f_I(\theta) + \frac{f_I(0) - A_R\alpha_1}{A_R\alpha_3 - f_L(0)} f_L(\theta) - \frac{A_R\alpha_2}{A_R\alpha_3 - f_L(0)} f_R(\theta). \tag{16}$$

We noticed earlier that for large and *noncritical kd* the single scattering hypothesis $f(\theta) = f_I(\theta)$ supplies a first approximation to (7). This is no longer the case as a critical value is approached. Indeed, neglecting the correction supplied by terms of order $A_R = (1/\sqrt{kd})$ in (16) we find

$$f(\theta) \to f_I(\theta) - \frac{f_I(0)}{f_L(0)} f_L(\theta), \tag{17}$$

which differs from $f_I(\theta)$ by a finite amount. In case 2) a similar result is obtained. In this formula it should be noted that the denominator is the forward scattering amplitude of an isolated cylinder. Its negative real part gives the scattering cross section, by a well-known theorem. The vanishing of the cross section implies that

$$\int_0^{2\pi} |f_L(\theta)|^2 d\theta \equiv 0.$$

This in turn implies $f_L(\theta) \equiv 0$ for all θ, whence also the vanishing (everywhere) of the field scattered by the cylinder when excited by the incident field $\exp ikx$. The incident plus scattered field could not then combine so as to fulfill homogeneous boundary conditions. Consequently $f_L(0)$ cannot vanish.

We now consider case 3). In this case we have to consider two possibilities: either α_3 vanishes, or it does not. Both cases are possible for it is easily verified, by calculating the cross section explicitly, that for the case of a circular cylinder α_3 cannot vanish. On the other hand the symmetry of the scattered field for a strip of zero thickness along the y-axis shows that in this case α_3 does vanish.

It is of interest to discuss the determinants α_1, α_2 and α_3. These are properties of a single cylinder. It can be shown that when α_3 vanishes so do α_1 and α_2. To see this define $v = f_L(0)F_R(x, y) - f_R(0)F_L(x, y)$ which is an outgoing wave function. Then form the quantity $E(v) = \mathrm{Im} \int v(\partial\bar{v}/\partial n)ds$ over the body. Then using the boundary condition[14] for F_L and F_R, and the well-known expression for the far field amplitude as a surface integral, we find $E[v] = +4 \mathrm{Re}\{\bar{f}_L(0)\alpha_3\}$. Consequently the vanishing of α_3 implies $E[v] = 0$. Since v is an outgoing wave function, it now follows that v is identically zero. The argument is that used in the proof of the uniqueness theorem for diffracted fields, which actually requires only the vanishing of the energy flux $E(v)$ over the surface. Having now shown that $\alpha_3 \equiv 0$ implies $v \equiv 0$, consideration of the far field form of v shows that

$$f_L(0)f_R(\theta) - f_R(0)f_L(\theta) \equiv 0$$

for all θ. Now by the reciprocity theorem for plane waves, we easily see that $f_I(0) = f_R(\phi + \pi)$, $f_I(\pi) = f_L(\phi + \pi)$, and $f_L(0) = f_P(\pi)$. Recall, for example, that $f_I(0)$ is the far field amplitude in the direction 0 produced by a plane wave incident in direction ϕ while $f_R(\phi + \pi)$ is the far field amplitude resulting in the direction $\phi + \pi$, when a plane wave is incident *from* the direction $\theta =$ zero. Making these substitutions it follows directly that $\alpha_1 = 0$. The vanishing of α_1 implies [by direct substitution of $f_R(\pi)f_I(0)/f_R(0)$ for $f_I(\pi)$] that

$$\alpha_2 = \frac{f_I(0)\alpha_3}{f_R(0)}.$$

Consequently $\alpha_3 \equiv 0$ also implies $\alpha_2 = 0$, as was to be shown. It seems worthwhile to inquire as to when α_3 can vanish. The necessary and sufficient condition (for perfectly conducting bodies) is that the boundary is composed of one or more vertical zero thickness strips, in the case of $E\|$. In the other polarization any number of horizontal strips may be added. The spacing of the vertical strips must be according to half integral multiples of the wavelength. Thus we can have a rectangle of suitable width, in the $H\|$ case. In all these cases the back and forward scattered amplitudes agree, for $E\|$, and differ only in sign, for $H\|$. The result generalizes well-known symmetry properties of a screen of zero thickness. If a general homogeneous boundary condition is to be satisfied, one can derive a differential equation relating the equation of the curve and the coefficients in the boundary condition. These results all follow easily by applying the boundary condition. For the $E\|$ case, for example, we have

$$v \equiv f_L(0)F_R - f_R(0)F_L = -[f_L(0)e^{-ikx} - f_R(0)e^{ikx}]$$

on the boundary. If $\alpha_3 = 0$, v vanishes identically, hence x must be constant on the boundary. Taking the origin of x at a boundary point, we see $f_L(0) = f_R(0)$. Hence at other boundary points $\sin kx = 0$, whence the spacing can be deduced. The sufficiency is shown by defining

$$W \equiv F_L - F_R$$

in the case $E\|$. Then W will be seen to vanish on the boundary and hence $W = 0$, so that $F_L = F_R$. Consequently $f_L(\theta) = f_R(\theta)$ for all θ, whence it is easily shown that α_1, α_2 and α_3 vanish.

[14] Thus, for $F\|$, $F_R = -e^{-ikx}$ on the body.

Returning now to case 3) we first note the result when $\alpha_3 \neq 0$. In this case, we obtain, in the limit

$$f(\theta) = f_I(\theta) - (a_1 f_L(\theta) + \alpha_2 f_R(\theta)]/\alpha_3. \tag{18}$$

If α_3 vanishes, then so do α_1 and α_2, and we obtain in general, using the relation of $f_L(\theta)$ and $f_R(\theta)$

$$f(\theta) = f_I(\theta) + \frac{[A_L + A_R][f_I(0)f_L(\theta)]}{1 - [A_L + A_R]f_L(0)} \tag{19}$$

and therefore in the limit

$$f(\theta) = f_I(\theta) - \frac{f_I(0)}{f_L(0)} f_L(\theta). \tag{20}$$

We have now calculated the limit which $f(\theta)$ approaches.[15] This allows immediate calculation of the complex amplitudes of the noncritical spectra, *i.e.*, the terms in (5) for which the denominator does not tend to zero. We still have to examine the terms $\nu = p_a$, and/or $\nu = -p_b$, where p_a and p_b are given by (11).

In case 1) we find, using (15),

$$\lim \frac{2f(\theta_{pa})}{kd \sin \theta_{pa}} = \left\{ f_I(0) - A_R\alpha_1 - \frac{2}{kd}(f_I'(0)f_L(0) - f_I(0)f_L'(0) - A_R\beta'(0)) \right\} \Big/ [A_R\alpha_3 - f_L(0)] \tag{21}$$

where $-\beta(\theta) = \alpha_3 f_I(\theta) - \alpha_1 f_L(\theta) - \alpha_2 f_R(\theta)$ (note that $\beta(0) = 0$). Since kd is large in any case, this simplifies to

$$\lim \frac{2}{kd} \frac{f(\theta_{pa})}{\sin \theta_{pa}} \to -\frac{f_I(0)}{f_L(0)} \tag{22}$$

the result of (21) furnishes a correction to this formula.

Thus the *total* coefficient in the last spectrum tends to a *finite* quantity as this spectrum tends to the horizontal.

In case 2) we find, for the critical term $\nu = -p_b$, the corresponding approximate value

$$-f_I(\pi)/f_R(\pi) = -f_I(\pi)/f_L(0).$$

Turning now to case 3), consider first the general situation, *i.e.*, $\alpha_3 \neq 0$. We find that the coefficient of the term $\nu = p_a$ tends to

$$\lim \frac{2f(\theta_{pa})}{kd \sin \theta_{pa}} = -\frac{\alpha_1}{\alpha_3} - \frac{2}{kd}\frac{\beta'(0)}{\alpha_3}. \tag{23}$$

Similarly, for $\nu = -p_b$

$$\lim \frac{2}{kd} \frac{f(\theta_\nu)}{\sin \theta_\nu} = -\frac{\alpha_2}{\alpha_3} - \frac{2}{kd}\frac{\beta'(\pi)}{\alpha_3}$$

which is again a finite result.

As resonance is approached, in the case $\alpha_3 = \alpha_2 = \alpha_1 = 0$ we get instead, for $\nu = p_a$

$$\lim \frac{2}{kd} \frac{f(\theta_\nu)}{\sin \theta_\nu} = -\frac{f_I(0)}{f_L(0)\,|\,1 + \sigma\,|}$$

[15] In cases 1), 2), and 3).

plus a correction term in $(kd)^{-1}$. Here σ is the limit approached by the ratio A_R/A_L, [cf. (13) and the subsequent text].

IV. Remarks on Energy Conservation

For any wave function possessing the periodicity suitable to the grating , and regular in the exterior of its elements, the total energy passing through the boundaries of a typical cell will be equal to the energy passing through the surface of the typical cylinder contained in that cell, as can be seen from direct applications of Green's theorem. Furthermore, due to the periodicity, the energy passing through the vertical boundaries of the cell is zero.

Consequently, energy is conserved in the correct solution just as well as in the incident field. For an incorrect solution, however, the degree of conservation of energy will be measured by the value of the surface integral of Poynting's vector, provided we are dealing with a suitably periodic wave function, which is regular in the exterior of the cylinders of the grating. Now, with regard to the single scattering solution, *according to which each cylinder contributes to the field as if in isolation*, it is easy to show that the boundary values are adopted with an error of order A_L, say. Energy is conserved to order zero, except in the resonance case. In that case A_L diverges so that energy is not conserved at all. To see this, we simply note for example that a cylinder at a distance nd to the right of a given "central" cylinder contributes a field of the order of

$$H_0(nkd)f_I(\pi)$$

to the boundary values on the cylinder selected as "central." On the other hand, in our analysis, *the contribution of a single cylinder is given by* (7a). It is easy to show that in this case, the surface energy integral vanishes to order $(kd)^{-1/2}$ and that the error is not only of higher order in $(kd)^{-1}$ for a noncritical case, but it is also uniformly bounded, *i.e.*, does *not diverge* as resonance is approached. Consequently in our result energy is conserved to the proper order, and this is independent of the "resonance."

It should be added that conservation of energy does not seem to guarantee that the boundary conditions are approximately fulfilled. Far from the vanishing of Im $\int u\partial\bar{u}/\partial n ds$ over a surface, only the orthogonality of the function and its normal derivative follows. For example the exact solution for a grating of perfect dielectric cylinders is useless as a substitute for the solution of the corresponding problem of conducting cylinders. Yet it certainly fulfills conservation of energy. While the energy law is useful as a check, proposed approximate solutions always require additional support.

V. Comparison with Other Theories

Since, as is well known, the theory of a grating of conducting cylinders implies a corresponding theory for the conducting reflection grating, it seems useful to compare the results obtainable from our solution with those by Artmann. Artmann's results are obtained under the assumption of protuberances small compared to wavelengths, without restriction as to spacing. By specializing his results to the case of large spacing, while specializing our results to the case of thin cylinders, a valid comparison is possible. However, we require explicit expressions for the quantities $f_L(0)$, etc., since Artmann's results are expressed in terms of the geometry of the surface. To this end, we have calculated, by the method of small perturbations, the pattern produced by diffraction by a thin strip of thickness $y=2\epsilon f(x)$ where $k\epsilon$ is small. The procedure is omitted here for brevity; only the results are given as follows.

We consider a symmetrical strip $y=\pm\epsilon f(x)$, for $|x|<l$. The incident magnetic field has a single component, which is perpendicular to the xy-plane and is given by $F_{\text{inc}}=\exp ikx$. Then if we write

$$H(x, y) = \exp ikx + F_L(x, y)$$
$$F_L(x, y) = \epsilon F_L^{(1)}(x, y) + \epsilon^2 F_L^{(2)}(x, y) + \cdots \quad (24)$$

we find

$$F_L^{(1)}(x, y) = \frac{k}{2}\int_{-l}^{l} \cdot e^{ikx_0} f'(x_0) H_0^{(1)}(k\sqrt{(x-x_0)^2+y^2})\,dx_0 \quad (25)$$

$$F_L^{(2)}(x, y) = -\frac{i}{2}\int_{-l}^{l}\left\{f'(x_0)\frac{\partial F_L^{(1)}(x^0{}_{,0\theta})}{\partial x_0} - f(x_0)\frac{\partial^2 F_L^{(1)}(x_{0,0})}{\partial y^2}\right\} \cdot \left\{H_0^{(1)}(k\sqrt{(x-x_0)^2+y^2}\right\}dx_0. \quad (26)$$

These results are obtained by expanding the boundary condition for F_L in a power series in ϵ. It is easily verified that the function $\exp ikx+\epsilon F_L^{(1)}+\epsilon^2 F_L^{(2)}$ fulfills the boundary condition to order ϵ^2. From (25) and (26) we find

$$f_L(\theta) = \frac{k\epsilon}{2}\int_{-l}^{l} f'(x_0) e^{ikx_0(1-\cos\theta)}\,dx_0 + 0(k\epsilon)^2. \quad (27)$$

The leading term vanishes for $\theta=0$, since $f(\pm l)=0$. This is natural since Re $f_L(0)$ is quadratic in ϵ by the forward amplitude theorem. To obtain $f_L(0)$ we use (26) together with (25). After various integrations by parts we obtain

$$f_L(0) = \frac{-k^2\epsilon^2}{4\pi}\int_{-\infty}^{\infty}\frac{|\phi(l)|^2}{\sqrt{1-t^2}}\,dt + 0(k\epsilon)^2 \quad (28)$$

where

$$\phi(l) = \int_{-l}^{l} f'(x_0) e^{ikx_0(1-t)}\,dx_0. \quad (29)$$

Here we have used the expression

$$H_0^{(1)}(|x|) = \frac{1}{\pi i}\int_{-\infty}^{\infty}\frac{e^{ixt}}{\sqrt{t^2-1}}\,dt \quad (30)$$

where

$$\sqrt{t^2-1} = -i\sqrt{1-t^2} \quad \text{for} \quad |t| < 1.$$

It is easy to verify that Re $f_L(0)$ is negative, while Im $f_L(0)$ is positive.

Let us now briefly discuss the solution of the reflection problem. It is well known that to obtain this solution from the cylinder solution we have to consider a grating of cylinders symmetric with respect to the plane $y=0$, and construct the function $u(x, y; \phi)\pm u(x, y; -\phi)$, where $u(x, y; \phi)$ is the solution corresponding to the incident wave $\exp ik(x\cos\phi+y\sin\phi)$. The upper sign is taken when we have $H\|$, while the lower sign refers to the case of $E\|$. In calculating by means of (7), (8), (9), (10) we have to consider the subscript I to refer to *both* the directions of incidence ϕ and $-\phi$. If ϕ is replaced by $-\phi$, then A_L and A_R are unaffected. Because of the symmetry, the quantity $f_I(\theta)$ for the direction of incidence $-\phi$ is equal to $f_I(-\theta)$ as calculated for the direction of incidence $+\phi$. Consequently also $f_I(0)$ and $f_I(\pi)$ remain unaltered under this transformation, whence the same is true of α_1 and α_2 of (10). It follows that in calculating with (7) for the direction of incidence $-\phi$, the first term, $f_I(\theta)$ is replaced by $f_I(-\theta)$ and the remaining terms are unaltered. Consequently, for $E\|$, the necessary subtraction leads to a simple value for the total $f(\theta)$ in the reflection problem, *i.e.*,

$$f_{\text{total}}(\theta) \cong f_I(\theta) - f_I(-\theta).$$

Since $f_I(\theta)$ is an analytic function of $\cos\theta$, it is easily verified that there is no divergence of the terms $f(\theta_\nu)/\sin\theta_\nu$ as $\theta_\nu\to 0$, in (5), so that there is no resonance phenomenon.

On the other hand, in the case of $H\|$, we have to add the terms $f(\theta)+f(-\theta)$. It is interesting to note in this connection that, if the *cylinders* are taken to be of rectangular cross section and of unit or integral wavelength thickness, then it follows from our discussion of the determinants α in a previous section that $f_I(\theta)+f_I(-\theta)=0$, if we choose $\phi=\pi/2$. In this case our result for the reflection grating is the trivial result $\exp iky+\exp(-iky)$, regardless of whether the spacing is critical. However this result is *easily verified for any collection of rectangular proturberances*, for any spacing whatever, if $\phi=\pi/2$ and the thickness is half a wavelength. A protuberance of half a wavelength corresponds to a cylinder of thickness equal to a wavelength.

We continue our discussion of the $H\|$ case by specializing to the case of *thin* cylinders. For strips of *zero* thickness the far field amplitude is well known to be odd in θ. Consequently the term $f_I(\theta)+f_I(-\theta)$ will be of order $k\epsilon$ where ϵ is the thickness. If we turn to the next term, however, in the case of resonance [cf. (17)]

we find a different order of magnitude. For the reflection grating this term becomes in fact

$$-\frac{f_I(0)}{f_L(0)}\,[f_L(\theta)+f_L(-\theta)].$$

Now $f_I(0)=f_R(\phi+\pi)$ by reciprocity. For zero thickness this quantity is identically zero and for a thin strip it is of order $k\epsilon$. The quantity $f_L(\theta)+f_L(-\theta)$ is also of order $k\epsilon$. But the denominator $f_L(0)$ is of order $(k\epsilon)^2$ [cf. (27)]. Therefore the total amplitude is a *finite* number, no matter how small $k\epsilon$ is, provided we have a critical combination of incidence angle and wavelength. This is in contrast to the situation for noncritical wavelengths.[16] Artmann has shown also that the maximum amplitude occurs at slightly larger wavelengths than critical, and that the shift is independent of the order of the spectrum. To see this from our result we return to the formula for $f(\theta_\nu)$ at a noncritical wavelength. Consulting (7) and (9), and neglecting terms of order A_R, we find, for a case when A_L is large but not infinite,

$$f(\theta_\nu)+f(-\theta_\nu)=f_I(\theta_\nu)+f_I(-\theta_\nu)+\frac{f_I(0)f_L(\theta_\nu)}{(1/A_L)-f_L(0)}. \quad (31)$$

From (12), $A_L\sim 2\cdot(kd\delta_a)^{-1/2}$, where, if δ is negative, the positive imaginary root is taken. Since $-\mathrm{Re}\,f_L(0)$ is positive by the forward amplitude theorem there can be no cancellation between $1/A_L$ and $f_L(0)$ if δ is positive. On the other hand, if δ is negative, then $1/A_L$ is positive imaginary. Comparing (28) we see that $\mathrm{Im}\,f_L(0)$ is also positive. Thus the imaginary part of the denominator will vanish at a certain negative value of δ_a, given by

$$\sqrt{2kd\,|\,\delta_a\,|}=\frac{k^2\epsilon^2}{2\pi}\int_1^\infty\frac{|\,\phi(t)\,|^2+|\,\phi(-t)\,|^2}{\sqrt{t^2-1}}\,dt. \quad (32)$$

Consequently [cf. (11a)], a maximum occurs for kd slightly less than critical, in general, since the numerator will only vary slightly with such a small variation in k. Eq. (32) shows that δ_a is independent of the order ν, in which the maximum is being observed, and is also[17] independent of the index p_a of the order which tends toward grazing. Furthermore it is easily seen that if f_c is the amplitude at the critical value, while f_m is the value at the maximum then $(f_c-f_m)/\delta$ is of the order of f_c/δ, *i.e.*, inversely proportional to δ. Consequently the maximum is very steep.

It is possible to show that all these results are in agreement with the results of Artmann [compare for example his equation (3.32)], provided we replace Artmann's sums by integrals, in accordance with the fact that kd is to be assumed large. Using our notation, Artmann's result can be rewritten

$$0=\sqrt{\delta_a(2kd-\delta_a)}+i\,\mathrm{Im}\sum_{\nu\neq p_a}d\left(\frac{2\pi k}{d}\right)^2\left(\frac{p_a-\nu}{d}\right)^2\cdot\left|\epsilon^2\int_{-l}f(x)\exp ix\left(\frac{\delta_a}{d}+k\cos\theta_\nu-k\right)dx\right|^2\sqrt{k\sin\theta_\nu}.$$

Using the fact that d is large we can replace the above sum by an integral, via the substitution $k\cos\theta_\nu=kt$, $2\pi/kd=dt$, $-\infty<t<\infty$. Since δ_a is small we have $2\pi(\nu-p_a)/d=kt-k$, while the term δ_a/d in the exponential can be neglected. This results precisely in our (32). On the other hand Artmann's theory is also valid for small thickness of protuberances, *even if the spacing is not large*, while our results, although restricted to large spacing ($kd\gg 2\pi$), *do not require* that the thickness is small compared to wavelength.

Having briefly compared our theory with that of Artmann we now turn to a brief comparison with new results of Twersky,[12] which appear to be in disagreement with ours. To summarize this disagreement, we note that a functional equation is obtained for the amplitude in the reflection grating. This functional equation is solved approximately by iteration, the justification for retention of the leading term (alone), being the assumption of *large spacing*.[18] Then the result is a quantity $\bar{f}_\nu\equiv\bar{f}(\theta_{\nu 0},\,\pi-\theta_0)$ which is in turn defined as the solution of a new integral equation [equations (60), (56)]

$$\bar{f}_{\nu 0}\equiv\bar{f}(\theta_\nu,\,\pi-\theta_0)=f(\theta_\nu,\,\pi-\theta_0)-\frac{1}{2\pi}\int_{-\pi/2}^{\pi/2}f(\theta,\,\pi-\phi)\bar{f}(\phi,\,\pi-\theta_0)\,d\phi,$$

in which the quantity f is the result based on single scattering theory, and $\bar{f}$ is to be solved for, with f as given data.[19] It is shown that $\bar{f}$ is, under certain circumstances, purely imaginary, and that consequently if one retains terms of higher order of magnitude in the specular amplitudes, while neglecting them in the other spectra, then energy is conserved exactly.[20] It is then emphasized[21] that the results (which according to page 29 and (70) are obtained for *large kd*) "differ significantly from a single scattering approximation in that they contain $\bar{f}$ instead of f." Arguments are given to show that the presence of f rather than $\bar{f}$ would be incorrect physically. The results insofar as they are explicit seem to be in disagreement with our own even before the passage to the limit of resonance, since our naive leading term is the single scattering term, in the noncritical case, and our principal result is the correction to this term so that in the limit of infinite spacing our results reduce to single scattering. We reserve further comment until Twersky's results have appeared in final form, but note that the discrepancy would be removed if the validity of Twersky's result were additionally restricted

[16] Then the leading term is $f_I(\theta)+f_I(-\theta)$, which tends to zero with the thickness.

[17] If we keep kd fixed, and vary the angle of incidence in order to vary p_a.

[18] Twersky, *op. cit.*, cf. (70) and p. 11.

[19] In this formula the superscribed bar does not mean complex conjugate.

[20] Twersky, *op. cit.*, pp. 29–30.

[21] *Ibid.*, p. 30.

to small scatterers, or at any rate to scatterers whose scattered amplitude is small, for then his integral equation shows that $\bar{f} \cong f$.

Appendix

In this appendix we give a brief intuitive derivation of (7) and (7a).

The nth element of the grating contributes an outgoing wave function $F(x-nd, y)$ to the total field [cf. (3) of the text]. The function $F(x-nd, y)$ is regular in the exterior of the nth cylinder. If r_n, θ_n are polar coordinates measured from the origin $(nd, 0)$, then we know that for large r_n the asymptotic form of F is

$$F(x - nd, y) \to (2/\pi k r_n)^{1/2} \exp ik\left(r_n - i\frac{\pi}{4}\right) f(\theta_n) \quad (33)$$

where $f(\theta_n)$ is unknown [cf. also (4) of the text]. Now if the spacing is large compared to both wavelength and dimensions of the cylinders, then the zeroth cylinder subtends an infinitesimal angle at the other cylinders. Hence, for cylinders to the left of the zeroth cylinder, (*i.e.*, n negative) $\theta_n \to 0$ in the neighborhood of the zeroth cylinder, while for n positive $\theta_n \to \pi$. On the other hand if (x, y) is a point in the neighborhood of the zeroth cylinder, then $r_n(x, y) \to |x - nd|$. Using these approximations in (33) and then evaluating (3) of the text in the neighborhood of the zeroth cylinder, we find that

$$u \cong u_{\text{inc}} + A_L f(0) e^{+ikx} + A_R f(\pi) e^{-ikx} + F(x, y).$$

Thus the effective excitation contains two plane waves in addition to u_{inc}). Now $F(x, y)$ is the sum of the responses to all these excitations, whence (7a) of the text follows. Eq. (7) is the far field form of (7a).

Line-of-Sight Wave Propagation in a Randomly Inhomogeneous Medium*

BOB M. FANNIN†

Summary—**Theoretical calculations have been made, using the single-scattering approximation, for propagation in a randomly inhomogeneous medium in which the deviations of refractive index from the mean are small. The statistical quantities considered were the variance, correlation function, and power spectrum for the phase and relative amplitude of the field at a point and their differences at two points. The emphasis in this paper is in indicating the transition from the ray treatment results to the scattering cross section results. The correlation function for the refractive index is taken to be time as well as space dependent so that the power spectrum can be computed from the original formulation.**

Introduction

THE DEGREE of inhomogeneity of the atmosphere constitutes the limiting factor in the ultimate accuracy of radar systems. The quantity which describes the propagation characteristics of the atmosphere at a given point is its refractive index (complex if absorption is considered), which is a function of the temperature and pressure of the air as well as the concentration of such constituents as water vapor, precipitation, and free electrons. The refractive-index distribution in the atmosphere is such a complicated function of space and time that, when making a theoretical study of atmospheric propagation phenomena, it is generally necessary to consider one at a time the different characteristic types of variations likely to be encountered. This study is concerned with the relatively small scale, random-type refractive index variations that are present in the atmosphere primarily due to its turbulent character. The stratified nature of the atmosphere and such phenomena as inversion layers are not considered in this paper.

The situation being considered is one in which the propagation path is line-of-sight and such that the earth and all other obstacles are far enough removed so that their effect can be neglected or considered separately. Computations of quantities associated with a wave traveling through a randomly inhomogeneous medium such as the atmosphere (in which the root-mean-square of the refractive-index deviations from the mean is very small) are usually carried out on the basis of a scattering mechanism[1] or a ray concept.[2] Not only are the fundamental physical mechanisms visualized

* Manuscript received by the PGAP, February 13, 1956. The research reported here has been sponsored by the AF Cambridge Res. Ctr., Air Res. and Dev. Com., under Contract AF 19(604)-494 and St. Louis Ordnance District, under Contract DA 23-072-ORD-763.

† Elect. Engrg. Res. Lab., University of Texas, Austin, Tex.

[1] C. L. Perkeris, "Note on scattering in an inhomogeneous medium," *Phys. Rev.*, vol. 71, p. 268; February, 1947, H. G. Booker and W. E. Gordon, "A theory of radio scattering in the troposphere," Proc. IRE, vol. 38, pp. 401–412; April, 1950, are references on basic scattering theory, while A. D. Wheelon and R. B. Muchmore, "Line-of-sight propagation phenomena—II. Scattered components," Proc. IRE, vol. 43, pp. 1450–1466; October, 1955, deals specifically with the line-of-sight problem.

[2] See, for example, R. B. Muchmore and A. D. Wheelon, "Line-of-sight propagation phenomena—I. Ray treatment," Proc. IRE, vol. 43, pp. 1437–1449; October, 1955.

quite differently in connection with these two approaches but the mathematical formulations involve different approximations which are valid for contrasting situations. In short, the ray concept is generally considered to be valid when the atmospheric "blobs" are relatively quite large so that the receiver is in the near (Fresnel) field of the blobs while the scattering cross section approach is appropriate when the blobs are small so that the receiver is in their far (Fraunhofer) field. The treatment employed here is that obtained by applying first order perturbation theory to the wave equation; *i.e.*, the single scattering approximation.[3] The scattering cross section concept generally employed evolves when the additional assumption is made that the blobs are sufficiently small compared with the range and wavelength. This last restriction will not be imposed in this development so that the results are equally valid for large as well as small blobs.[4] This approach thus has the advantage of presenting a unified treatment which furnishes results that, for the limiting cases of very large and very small blobs, coincide with those obtained by applying the usual ray or scattering cross section methods, respectively.

Refractive-Index Correlation Function

The following development incorporates a correlation function for the refractive index which is both time and space dependent. This makes it possible for power spectra calculations to be made directly from the original formulation.

The medium is taken to have small random variations about a mean, the statistical character of the fluctuations being homogeneous and isotropic except for a mean wind. Thus the refractive index (n) can be expressed as

$$n(x, t) = n_0 + \Delta n(x, t), \quad \Delta_n << n_0, \quad n_0 \approx 1 \tag{1}$$

in which n_0 is the mean value of refractive index, x denotes a position in space, and t denotes time. Also, using **boldface** symbols to denote vectors,

$$\overline{\Delta n(x_1, t)\Delta n(x_2, t+\tau)} = \overline{\Delta n^2} C(|\boldsymbol{r} - \boldsymbol{v}\tau|, \tau) \tag{2}$$

where $\boldsymbol{r}$ is the vector distance between x_1 and x_2, $\boldsymbol{v}$ is the mean wind velocity, C is the normalized time and space dependent correlation function for the refractive index, and the bars denote time averages. The effect of absorption is neglected so that Δn^2 is real.

In what follows the form of the correlation function will be taken as[5]

$$C = \exp\left[-\overline{|\boldsymbol{r} - \boldsymbol{w}\tau|^2}/l^2\right]$$
$$= \exp\left\{-[u^2\tau^2 + |\boldsymbol{r} - \boldsymbol{v}\tau|^2]/l^2\right\} \tag{2a}$$

in which $\boldsymbol{w}$ denotes the wind velocity composed of a mean component $\boldsymbol{v}$ and a component of magnitude u with random direction while l is a measure of the scale of turbulence and is frequently referred to as the mean blob size. Thus incorporated in (2a) is a Gaussian decrease with separation for $\tau = 0$, a drift with velocity $\boldsymbol{v}$, and a Gaussian decrease with τ to take into account the random movement and dispersion of the blobs. Undoubtedly (2a) is not an entirely adequate representation of turbulent atmospheres. There is, however, little direct data upon which to base a more appropriate correlation function and, in at least some respects, the results for the line-of-sight case are relatively insensitive to the exact form of C. The additional assumption that $l > \lambda$ is also made.

Mathematical Formulation

Let us consider an isotropic radiator (with wavelength λ) at point (a) in space and study the field at point (b), a distance R from (a). The wave equation for which a solution is sought is

$$(\nabla^2 + k^2 n^2)\boldsymbol{E} = 0 \tag{3}$$

where $k = (2\pi/\lambda)$. Neglecting terms in $(\Delta n)^2$, defining $\boldsymbol{E}_s$ by $\boldsymbol{E} = (\boldsymbol{E}_0 + \boldsymbol{E}_s)$ where $\boldsymbol{E}_0$ is the field that would exist if $\Delta n = 0$, and taking n_0 as unity, (3) then becomes

$$(\nabla^2 + k^2)\boldsymbol{E}_s = -2k^2 \nabla n \boldsymbol{E} \tag{4}$$

In this form the equation is immediately interpretable as expressing $\boldsymbol{E}_s$ as being composed of contributions from each differential volume (dv) in space radiating like an elementary dipole whose moment and orientation is given by $-2\Delta n \boldsymbol{E} dv$. $\boldsymbol{E}$ is not known so we take the single-scattering approximation by using $\boldsymbol{E}_0$ instead of the correct $\boldsymbol{E}$ for the field at the differential scattering volume. When the intuitive assumption is made that the important scattering volumes are relatively close to the straight-ray path (since $l > \lambda$) the sine of the angle between the direction of $\boldsymbol{E}_0$ at the scattering volume and the direction to the receiving point can be taken as unity. Also, only the component of the field at the receiver that is in the direction of $\boldsymbol{E}_0$ need be considered so that the vector notation can be dropped. Considering the E's (not boldface) to denote complex quantities in the customary convention for sinusoidally varying fields, the single-scattering expression for (E_s/E_0) becomes

$$(E_s/E_0) = (k^2 R/2\pi) \int_v \Delta(n/R_a R_b) \cdot \exp\left[-jk(R_a + R_b - R)\right] dv \tag{5}$$

in which R_a and R_b are the distances from dv to a and b, respectively. In keeping with the small perturbation approach employed throughout, the real and imaginary

[3] D. Mintzer, "Wave propagation in a randomly inhomogeneous medium. I," *J. Acous. Soc. Amer.*, vol. 25, pp. 922–927; September, 1953, or A. D. Wheelon, "Near-field corrections to line-of-sight propagation," Proc. IRE, vol. 43, pp. 1459–1466; October, 1955.

[4] L. A. Chernov, "Correlation of the amplitudes and phases in wave propagation in statistically-inhomogeneous media," *Doklady, Akad. Nauk USSR*, vol. 98, pp. 953–956; June, 1954, treats a very similar problem by almost the same methods presented in this paper.

[5] The author is indebted to K. A. Norton for pointing out the equivalence of the two expressions in (2a).

parts of (5) are taken as the deviations in magnitude and phase of E relative to E_0. Since $\overline{\Delta n}$ is defined to be zero the average value of (5) is also zero.

The fundamental quantities to be determined are

$$\rho_{m,p}(D, \tau) = \overline{\alpha_{m,p}(b_1, t)\alpha_{m,p}(b_2, t + \tau)} \tag{6}$$

in which $\alpha_p(b, t)$ and $\alpha_m(b, t)$ denote the phase of E/E_0 and the magnitude of $(E-E_0)/E_0$, respectively, at point b and at time t. Eq. (6) define two quantities, the comma between the subscripts indicating that either the first or the second subscripts may be taken. Both b_1 and b_2 are assumed to be a distance R from the transmitter at (a) and displaced one from the other a distance D, the assumption being made that $R \gg D$. The ρ's are thus the cross-correlation functions for the phase or relative amplitude variations of the field at point b_1 and b_2, D being a parameter. Of course, when $D=0$ the ρ's become autocorrelation functions.

From (5) it follows that

$$\rho_{m,p} = 1/2(2\pi R/\lambda^2)^2 \int_v \int_v \frac{\overline{\Delta n(x, t_1)\Delta n(x', t_2)}}{R_a R_b R_a' R_b'} \cdot [\cos k(R_a + R_b - R_a' - R_b') \pm \cos k(R_a + R_b + R_a' + R_b' - 2R)]dvdv' \tag{7}$$

the upper sign being taken for ρ_m and the lower sign for ρ_p, the primed and unprimed symbols referring to two different points in space. To evaluate this double volume integral, spheroidal coordinates were used and (2) and (2a) employed. Again presuming that the important scattering volumes are relatively near the straight-ray path and that $R \gg l$, it was assumed that for the correlation function in the integrand, approximations could be introduced that amount to taking the spheroidal coordinates as cylindrical over a volume of dimensions of the order of l. With these simplifying modifications (7) reduces to

$$\rho_{m,p}(D, \tau) = \overline{\Delta n^2}\pi^{5/2} l R \lambda^{-2}[P_1(D, \tau) \mp P_2(D, \tau)] \tag{8}$$

in which

$$P_1(D, \tau) = \exp[-(u^2 + v^2 \sin^2\phi)\tau^2/l^2] \cdot \int_{-1}^{1} \exp\{-[(1 + y)(D/2l) - (v\tau/l)\cos\phi]^2\} dy \tag{9a}$$

$$P_2(D, \tau) = \exp(-u^2\tau^2/l^2)\ \mathrm{Re} \int_{-1}^{1} Q^{-1} \exp\{-[1 + y)^2 D^2/4 - (1 + y)Dv\tau\cos\phi + v^2\tau^2]/l^2 Q\} dy \tag{9b}$$

and

$$Q = [1 - 2q(1 - y^2)j]. \tag{10}$$

The component of v along the propagation paths has been taken as zero and ϕ denotes the angle between v and the direction from b_1 to b_2. The parameter q is

$$q = R/4\pi l^2 = l_0^2/\pi l^2 \tag{11}$$

in which l_0 denotes the half-width of the first Fresnel zone at the midpoint of the path.

The variable of integration, y, in (9a) and (9b) is

$$y = (R_a + R_a' - R_b - R_b')/2R \tag{12}$$

so that these integrals denote the summing up of the contributions of different layers sliced normal to the propagation direction. Of course, in these spheroidal coordinates the layers are hyperbolic but they are approximately plane over the important region. Therefore, (9a) and (9b) are appropriate for considering the effect of a turbulent layer. Assumed variations along the path in the intensity or scale of the refractive-index fluctuations can be inserted into these equations. Also, the transition to the case of a plane wave incident upon a turbulent region ($R \to \infty$) is easily effected.

Continuing with the assumption that the statistical character of the refractive-index fluctuations is homogeneous throughout the whole region, (9a) simplifies to

$$P_1(D, \tau) = (l\sqrt{\pi}/D) \exp[-(u^2 + v^2 \sin^2\phi)\tau^2/l^2] \cdot \{\mathrm{erf}[(D - v\tau\cos\phi)/l - \mathrm{erf}[v\tau\cos\phi/l]\}. \tag{9a'}$$

The autocorrelation functions, $\gamma_{m,p}(D, \tau)$, for the differences in phase or relative amplitude at points b_1 and b_2, are given by

$$\gamma_{m,p}(D, \tau) = \overline{[\alpha_{m,p}(b_1, t) - \alpha_{m,p}(b_2, t)][\alpha_{m,p}(b_1, t + \tau) - \alpha_{m,p}(b_2, t + \tau)]} = [2\rho_{m,p}(0, \tau) - \rho_{m,p}(D, \tau) - \rho_{m,p}(D, -\tau)]. \tag{13}$$

Also of interest are the power spectra, $S_{m,p}(D, \omega)$, of the phase or relative amplitude differences,

$$S_{m,p}(D, \omega) = (1/\pi) \int_{-\infty}^{\infty} \gamma_{m,p}(D, \tau)\cos(\tau\pi)d\tau \tag{14}$$

in which $S_{m,p}(D, \omega)$ has been defined such that

$$\int_0^{\infty} S_{m,p}(D, \omega)d\omega = \gamma_{m,p}(D, 0).$$

The portion of (8) that involves P_1 is seen to differ from the expression for $\rho_p(D, \tau)$ derived using a ray concept only by a factor of one half.[6] Thus the functional form of P_1 is independent of q while P_2 is a function of q. A brief inspection of (9b) and (10) reveals that $P_2 \to P_1$ as $q \to 0$ and $P_2 \to 0$ as $q \to \infty$. Thus for very large blobs $\rho_m \approx 0$ while ρ_p has the value that would be calculated using a ray treatment. On the other hand, for very small blobs, $\rho_m \approx \rho_p$, the functional dependence upon l, R, and λ differing from that for ρ_p for large blobs only by a factor of one half. Since $\gamma(D, \tau)$ and $S(D, \omega)$ are defined

[6] Muchmore and Wheelon, *op. cit.*

in terms of the ρ's, the statements concerning the ρ's in this paragraph apply equally well to these quantities.

Also in (9a) and (9b) it is seen that the "dispersion" velocity, u, enters only in the form of the same Gaussian multiplying factor that appears in (2a), since this factor is not involved in the space integrations. Thus any other functional form involving u could be directly substituted. Likewise, if it was desired to let l in (2a) be a function of τ this time dependent could be substituted throughout.

Since $\rho_{m,p}(\infty, \tau) = 0$, (13) shows that $\gamma(\infty, \tau) = 2\rho(0, \tau)$ as would be expected. This simply indicates that the signals at b_1 and b_2 are uncorrelated when D is very large. Thus the spectra for the fluctuations of a single signal are given by $\frac{1}{2}S_{m,p}(\infty, \omega)$.

Numerical Results

Space limitations preclude the presentation of the numerical results for more than a few combinations of the values of the many parameters.

Single Path Results

The variance of the phase and relative amplitude of the field at a single point is just $\rho_{m,p}(0, 0)$. From (8), (9a′), and (9b) this is seen to be

$$\rho_{m,p}(0, 0) = 4\overline{\Delta n^2}\pi^{5/2} l R \lambda^{-2}\left[1/2 \mp 1/2\,\mathrm{Re}\int_0^1 Q^{-1}dy\right] \quad (15)$$

in which Q is defined by (10). The integral in (15) can be evaluated and the real part taken but the resulting expression is so lengthy that it will not be given here. The quantity in the brackets of (15) is plotted vs q (the q scale is logarithmic) in Fig. 1. The coefficient of the bracketed expression in (15) is the value of $\rho_p(0, 0)$ that is obtained using a ray approach. It is seen that $\rho_p(0, 0)$ agrees with the ray concept value for big blobs but differs from it by a factor of one half for small blobs. $\rho_m(0, 0)$ goes from zero to the same value as $\rho_p(0, 0)$ as the blob size goes from large to small as mentioned in the previous section. Fig. 1 shows the transitions as q goes from a small to a large value.

The square root of $\rho_p(0, 0)$, $(\alpha_p)_{\mathrm{rms}}$, thus varies directly as the square root of l and R inversely as λ when q is either much larger or much smaller than unity, with the dependence on these parameters shifting to $l^{-0.078}$, $R^{0.789}$, and $\lambda^{-0.711}$ for $q = 1$. The value of $(\alpha_m)_{\mathrm{rms}}$ also varies as the square root of l and R and inversely as λ for large q but approaches $(8\sqrt{\pi\overline{\Delta n^2}}/15)^{0.5}(R/l)^{1.5}$, independent of λ, for small q. That is, when a scattering mechanism predominates then $(\alpha_p)_{\mathrm{rms}}$ and $(\alpha_m)_{\mathrm{rms}}$ have the same value and dependence upon l, R, and λ but when a ray concept suffices then the value of $(\alpha_m)_{\mathrm{rms}}$ is much less than that for $(\alpha_p)_{\mathrm{rms}}$ and its functional dependence upon l, R, and λ is considerably different.

Eqs. (8), (9a), and (9b), with D taken to be zero, give the expression for the autocorrelation functions for phase and relative amplitude variations at a single receiving point. As mentioned above, the dispersion velocity, u, enters solely in the form of a Gaussian multiplier while the drift velocity, v, enters in a more complex manner which depends upon the value of q. This dependence of $\rho_{m,p}(0, \tau)$ upon v is shown in Fig. 2 for $q = 0$, 1, and ∞. The curves in this figure were normalized by dividing by $\rho_{m,p}(0, 0)$.

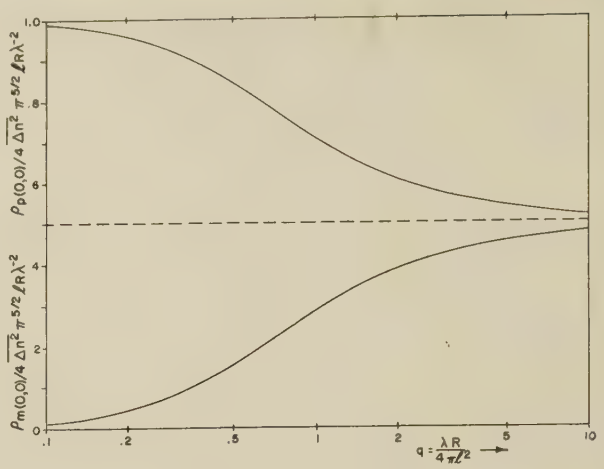

Fig. 1—Variance of phase and relative amplitude for a single path where unity on the ordinate scale corresponds to the ray theory value

The effect of the parameter q upon the power spectra for the phase and relative amplitude variations at a single point can be determined qualitatively by inspecting Fig. 2. The correlation functions for the phase for $q = 0$ and ∞ and for the amplitude for $q = \infty$ are Gaussian so the corresponding power spectra will also be Gaussian. The correlation function for the phase for $q = 1$ falls off less rapidly so that a larger portion of the power is contained in the lower frequencies. Likewise, as q decreases the correlation function for the amplitude variations falls off more and more rapidly so that a larger portion of the power is contained in the higher frequencies.

Cross-Correlation Functions of Signals at Two Receiving Points

Fig. 3 shows $\rho_{m,p}(D, 0)$ (normalized) vs (D/l), *i.e.*, a plot of the normalized cross-correlation functions for the phase and relative amplitude variation of the field at b_1 and b_2, for zero time difference, as a function of the separation between receiving antennas.

Signal Differences for Two Receiving Points

The power spectra for the phase and relative amplitude differences are plotted in Fig. 4 for a number of values of (D/l) for $q = \infty$, $u = 0$, and $\phi = 0$. That is, the curves are for the case when only the effect of a mean wind across the paths is considered. Naturally these curves apply equally well for phase differences when $q = 0$. It is seen that decreasing the antenna separation reduces the rms of the fluctuations but cuts out the lower frequencies more rapidly than the higher frequencies.

Fig. 5 indicates the effect of q upon the power spectra for the difference variations. These curves have been normalized and are for $(D/l) = 1$, $u = 0$, and $\phi = 0$.

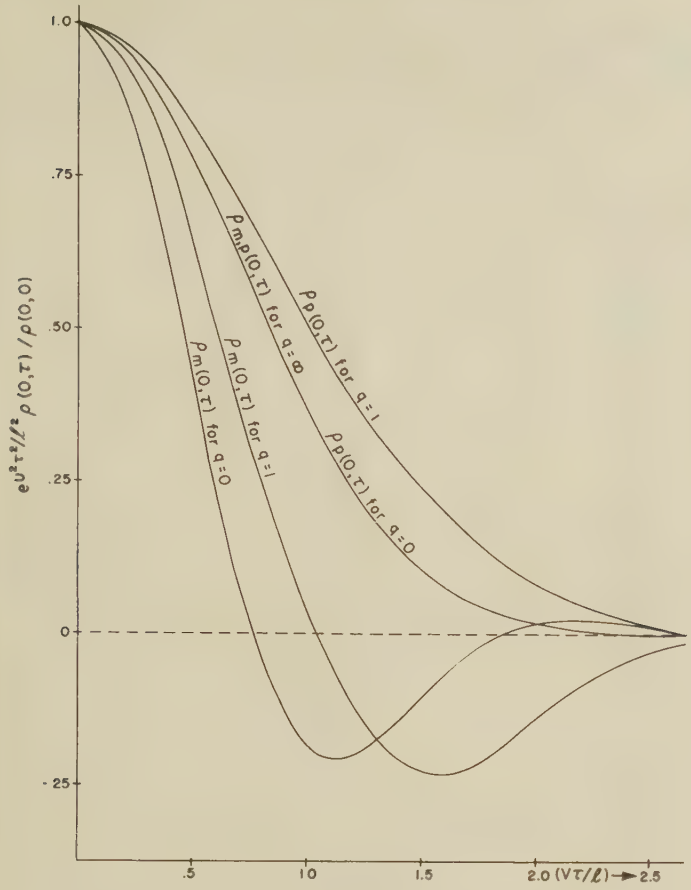

Fig. 2—Normalized autocorrelation functions for phase and relative amplitude variations for a single path.

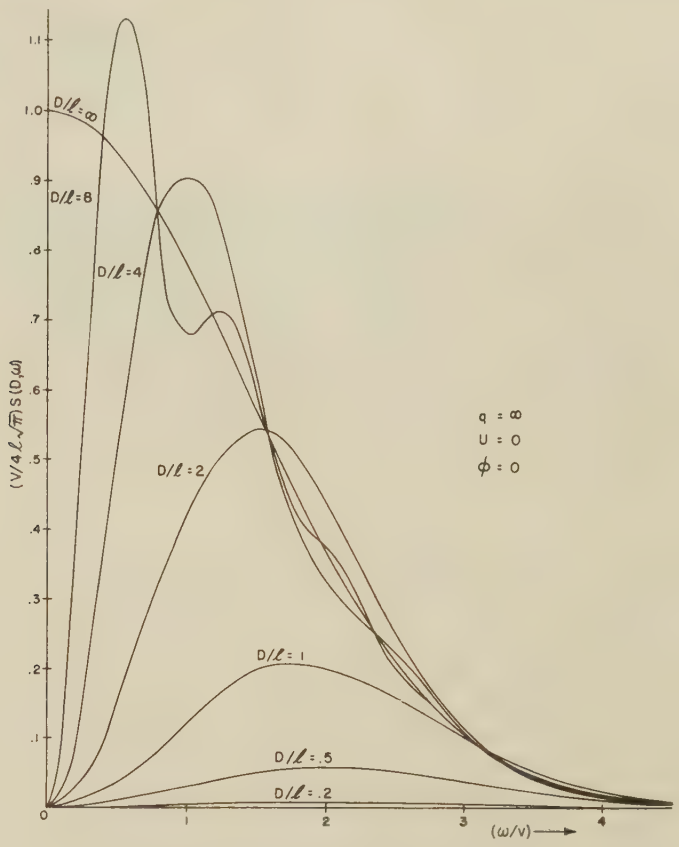

Fig. 4—Power spectra for phase and relative amplitude difference variations.

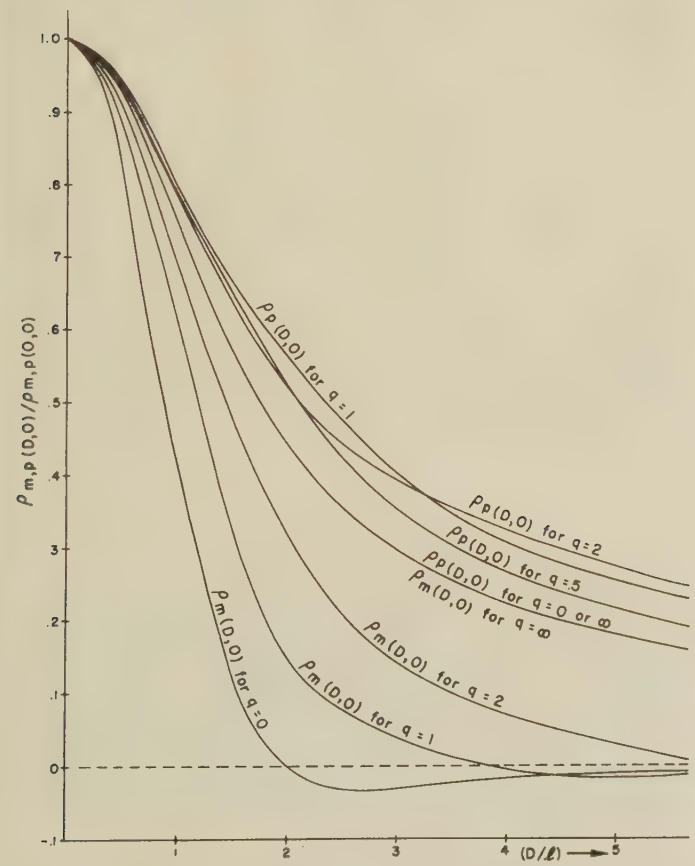

Fig. 3—Normalized cross correlation of the phase or relative amplitude at two points for zero time difference.

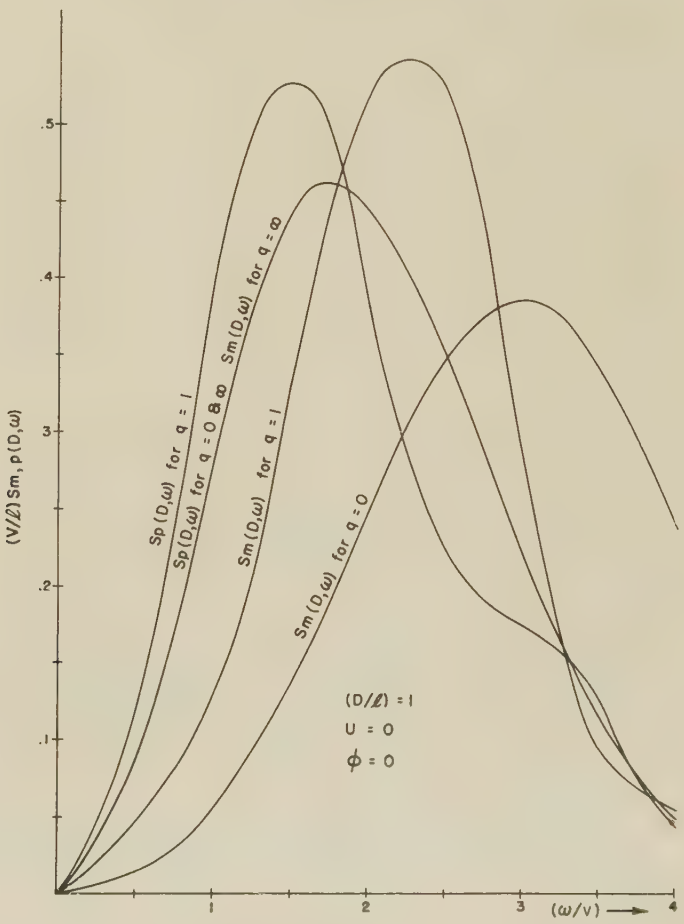

Fig. 5—Normalized power spectra for phase and relative amplitude difference variations.

Partially Reflecting Sheet Arrays*

GISWALT VON TRENTINI†

Summary—**Multiple reflections of electromagnetic waves between two planes are studied, and the increase in directivity that results by placing a partially reflecting sheet in front of an antenna with a reflecting screen is investigated at a wavelength of 3.2 cm. The construction and performance of various models of such arrays is discussed. Thus, for example, a "reflex-cavity antenna" with an outer diameter of 1.88 λ and an over-all length of only 0.65 λ is described which has half-power beamwidths of 34° and 41° in the *E* and *H* planes, respectively, and a gain of approximately 14 db. It is shown that larger systems produce considerably greater directivity but that their efficiency is poor.**

Introduction

A LARGE, plane, conducting screen placed behind an antenna serves as a shield against backward radiation and also affects, depending on its spacing, the forward pattern.[1] Improved directivity in the normal direction is possible only to a limited degree because the illumination of the reflecting screen is not optimum and the rays reflected from more distant zones produce, in part, out-of-phase contributions.

Improved illumination and an increase in directivity, and therefore in gain, can be obtained by adding a partially reflecting sheet in front of the antenna and parallel to the reflecting screen, causing multiple reflections between the sheet and screen. The distance between the sheet and screen must be such that the partial rays projected through the sheet into space have equal phases in the normal direction.

This paper presents the results of tests with various types of sheets and discusses a few simple forms of "reflex antennas." In order to work with small systems that are easy to construct and convenient to measure, the investigation was carried out at a wavelength of 3.2 cm. If adequately scaled, such arrays may also be used for longer wavelengths.

Derivation of the Radiation Pattern of an Antenna Between Screen and Parallel Sheet

If an antenna is located in front of, or in the plane of, a conducting screen, its radiation can be imagined as originating in a point P of the screen with element pattern $f(\alpha)$ (Fig. 1).

A partially reflecting sheet placed at a distance l from the completely reflecting screen introduces multiple reflections with decreasing amplitudes between these two planes. Let the reflection coefficient of the sheet be

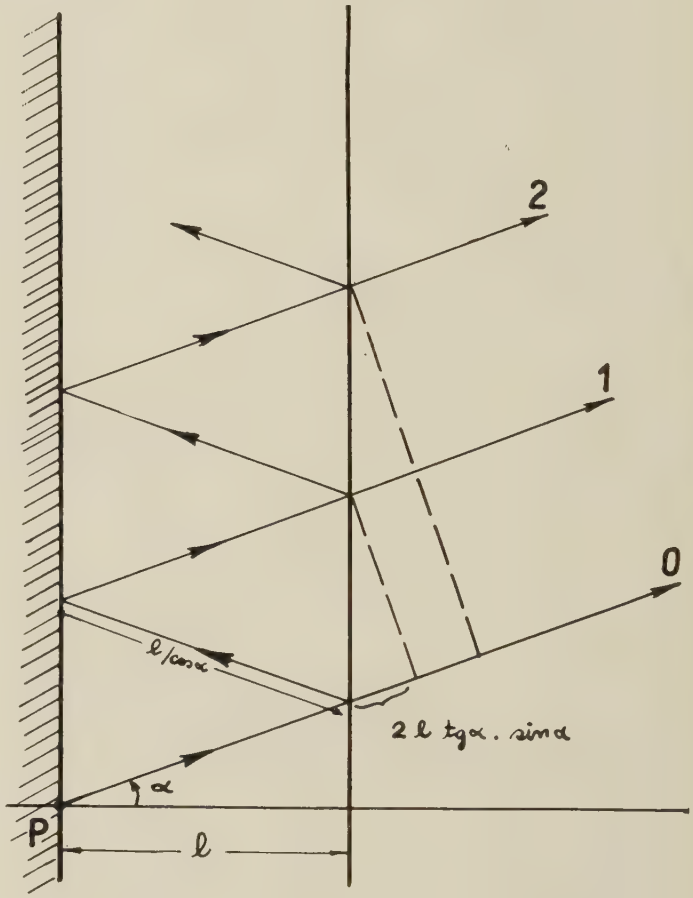

Fig. 1—Multiple reflections between screen and sheet.

$pe^{j\psi}$. Assuming no transmission losses, the amplitude of the direct ray 0 is proportional to $\sqrt{1-p^2}$; the amplitude of the once-reflected ray 1 is proportional to $p\sqrt{1-p^2}$; the amplitude of the twice-reflected ray 2 is proportional to $p^2\sqrt{1-p^2}$; etc. The electric field intensity in the Fraunhofer zone consists of the vector sum of these partial rays, and for an infinite screen and sheet we may write

$$E = \sum_{n=0}^{\infty} f(\alpha) E_0 p^n \sqrt{1-p^2}\, e^{j\Theta_n}. \qquad (1)$$

The phase angle Θ_n is composed of the phase variations during reflections from the completely reflecting screen and partially reflecting sheet, and also of the path differences of the partial rays. An additional phase shift occurs when a partial ray passes through the sheet, but since this is the same for all rays it need not be taken into account. From Fig. 1 we may derive the phase difference between ray 1 and ray 0 as

* Manuscript received by the PGAP, April 18, 1955; revised manuscript received, October 3, 1956.

† Starnberg, Oberbayern, Luitpoldweg, Germany.

[1] John D. Kraus, "Antennas," McGraw-Hill Book Co., Inc., New York, N. Y., ch. 12-2; 1950.

$$\Theta_1 = \frac{2\pi}{\lambda} 2l \tan\alpha \sin\alpha - \frac{2\pi}{\lambda} \frac{2l}{\cos\alpha} - \pi + \psi,$$

and between ray 2 and ray 0 as

$$\Theta_2 = \frac{2\pi}{\lambda} 4l \tan\alpha \sin\alpha - \frac{2\pi}{\lambda} \frac{4l}{\cos\alpha} - 2\pi + 2\psi$$

which, somewhat transformed, gives

$$\Theta_n = n\Phi = n\left[-\frac{4\pi}{\lambda} l \cos\alpha - \pi + \psi\right]. \tag{2}$$

Since $p<1$, we obtain

$$\sum_{n=0}^{\infty} (pe^{j\Phi})^n = \frac{1}{1 - pe^{j\Phi}}.$$

Inserting this in (1), the absolute value of field strength becomes

$$|E| = |E_0| f(\alpha) \sqrt{\frac{1 - p^2}{1 + p^2 - 2p\cos\Phi}},$$

and the power pattern is therefore

$$S = \frac{1 - p^2}{1 + p^2 - 2p\cos\left(\psi - \pi - \frac{4\pi}{\lambda} l \cos\alpha\right)} f^2(\alpha). \tag{3}$$

We must take into account, however, that the amplitude p and the phase ψ of the sheet reflection coefficient are a function of the angle of incidence α. Maximum power in the direction of $\alpha=0°$ is obtained when

$$\psi - \pi - \frac{4\pi}{\lambda} l = 0,$$

and hence the equation determining the resonance distance l_r of the sheet is

$$l_r = \left(\frac{\psi_0}{360} - 0.5\right)\frac{\lambda}{2} + N\frac{\lambda}{2}, \tag{4}$$

with ψ_0 expressed in degrees and $N=0, 1, 2, 3$, etc. The phase angle for a sheet with inductive field impedance is in the second quadrant, and for a capacitive sheet, in the third quadrant.

Results of Tests and Comparison with Calculations

An exact evaluation of (3) and (4) is difficult since the reflection factor of sheets is known for the case of a plane wave only. Using the plane wave value, however, an approximate, qualitative solution can be obtained that should be satisfactory in the Fraunhofer zone.

If the sheet consists of a grid of parallel equidistant wires running in the direction of the electric vector, the field impedance will be:[2]

$$jV = j120\pi \frac{d}{\lambda} \cos\alpha \left[\ln\frac{d}{2\pi\rho} + F\right]. \tag{5}$$

The factor F is itself again a function of α, but may be neglected if the wire distance d (grid constant) is small with respect to λ, and the wire radius ρ is very small with respect to d.

From the relation

$$pe^{j\psi} = \frac{-1}{1 + j\frac{V}{60\pi}} \tag{6}$$

we get

$$p = \frac{1}{\sqrt{1 + \left(\frac{V}{60\pi}\right)^2}} \tag{7}$$

and

$$\psi = \arctan\left(-\frac{V}{60\pi}\right). \tag{8}$$

For a grid with $2\rho=0.5$ mm and $d=9$ mm, and with $\lambda=3.2$ cm, we obtain $\rho_0=0.707$ and $\psi_0=135°$ in the normal direction ($\alpha=0°$). In other words, at the first reflection 50 per cent of the energy is reflected back to the screen. From (4) we find that the resonance distance l_r is 14 mm, and from (3) we obtain the radiation pattern in the H plane, as shown in curve 1 of Fig. 2. The element pattern of the antenna, $f_{(\alpha)}{}^2$, is taken from the measured values for a waveguide aperture with a large reflecting screen, as given in curve 1 of Fig. 3. The total pattern obtained in this way has no side lobes, a 3 db beamwidth of 35°, and a 10 db width of 58°. The calculation for a corresponding capacitive sheet gives a resonance distance of 18 mm and a slightly more directive radiation pattern. A much more considerable increase in directivity is obtained with larger reflection coefficients. Curve 2 of Fig. 2 was calculated for a $p_0=0.837$ (*i.e.*, 70 per cent energy reflection in the normal direction) and a decrease of capacitive field impedance proportional to $\cos\alpha$. Since $\psi_0=213.2°$, the resonance distance l_r becomes 17.47 mm. Curves 3 and 4 were correspondingly calculated for p_0 equal to 0.9 and 0.95, respectively.

Tests confirmed these theoretical results. A rectangular waveguide aperture ($1\times\frac{1}{2}$ inch) in a plane conducting screen (32×32 cm) was used as an antenna. The measured radiation pattern in the H plane is shown in curve 1 of Fig. 3. When a movable frame with a wire

[2] G. G. MacFarlane, "Surface impedance of an infinite parallel-wire grid at oblique angles of incidence," *JIEE*, Part IIIA, vol. 93, p. 1523; March–May, 1946.

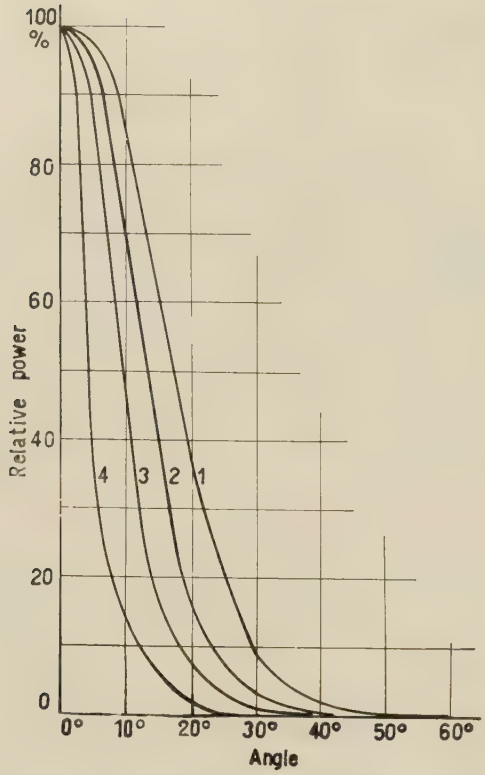

Fig. 2—Calculated radiation pattern of a sheet with a reflection coefficient of 1) $p_0=0.707$, 2) $p_0=0.837$, 3) $p_0=0.9$, 4) $p_0=0.95$.

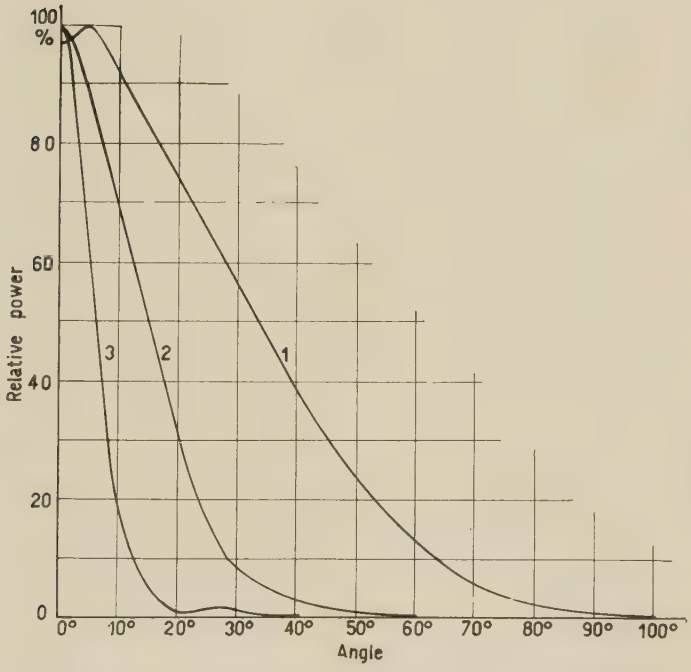

Fig. 3—Measured radiation pattern of a waveguide aperture with reflecting screen (1) and a wire grid (2) or strip-grating (3) disposed in front of it.

grid similar to the one calculated above was placed in front of the aperture, the resonance distance l_r was found to be 13.5 mm and a considerable increase in directivity was noted. The measured pattern in the H plane is shown by curve 2 of Fig. 3. This curve follows to a great extent the calculated curve (curve 1 of Fig. 2) but the directivity is somewhat greater.

If a homogeneous dielectric plateglass ($32\times32\times0.3$ cm) is used in place of the wire grid, a resonance distance of 15.9 mm results and the radiation pattern in the H plane corresponds almost exactly to that of a grid. From the resonance distance we obtain $\psi_0\simeq180°$, which corresponds to a plate thickness of one-fourth of the wavelength in the dielectric. Therefore, the relative dielectric constant would be approximately 7 and $p_0\simeq0.75$.

Patterns in the E plane are considerably different. In that place, the array with the dielectric plate has a 3 db beamwidth of 35°, and a 10 db width of 73°, and at an angle of $\pm72°$ there are side lobes of approximately -8 db. Apart from the considerably wider and more irregular individual pattern of the waveguide aperture with screen, the reflection factor of this sheet decreases with the increase in angle and passes through a minimum (Brewster angle).

The radiation pattern of the array with the wire grid is strongly lobed in the E plane. Side lobes are as high as 80 per cent at an angle of $\pm13°$, 40 per cent at $\pm26°$, and so on.

As the angle of incidence increases, the wires of the grid are no longer parallel to the electric vector and reflection decreases. Furthermore, in the finite grid, reflections of induced currents are noticeable at the ends of the wires. In order to calculate these, a radiation originating from the edges may be added in a manner similar to the case of a slot-excited ground-plane antenna.[3] Due to the great width of the screen (10 λ), a rapidly varying field is superposed which, when multiplied by (3), results in an irregular radiation pattern with pronounced ripples.

It is possible to obtain a considerably stronger reflection, *e.g.*, by means of a capacitive strip-grating placed vertically to the electric vector. The test arrangement consists of aluminum foil 12 mm in width, glued to the dielectric plate at intervals of 1 mm. Such a strip-grating in air gives a reflection factor of $p_0=0.89$ for a plane wave.[4] Due to the dielectric plate, the capacity and, consequently, the reflection factor are somewhat increased. With a resonance distance of $l_r=16.3$ mm curve 3 (Fig. 3) results. Directivity in the E plane is somewhat less and the main beam is slightly irregular. The absolute gain amounts to 19.6 db. The adjustment of the resonance distance is very critical, and the sheet as well as the screen must be perfectly plane and situated parallel to each other.

The influence of the edges on the main beam decreases when both sheet and screen are smaller. A re-

[3] A. Dorne and D. Lazarus, "Very High Frequency Techniques," Radio Res. Lab. Staff, McGraw-Hill Book Co. Inc., New York, N. Y., ch. 7-3 and 4, 1947.

[4] N. Marcuvitz, "Waveguide Handbook," Rad. Lab. Ser., McGraw-Hill Book Co., Inc., New York, N. Y., vol. 10, ch. 5–18; 1951.

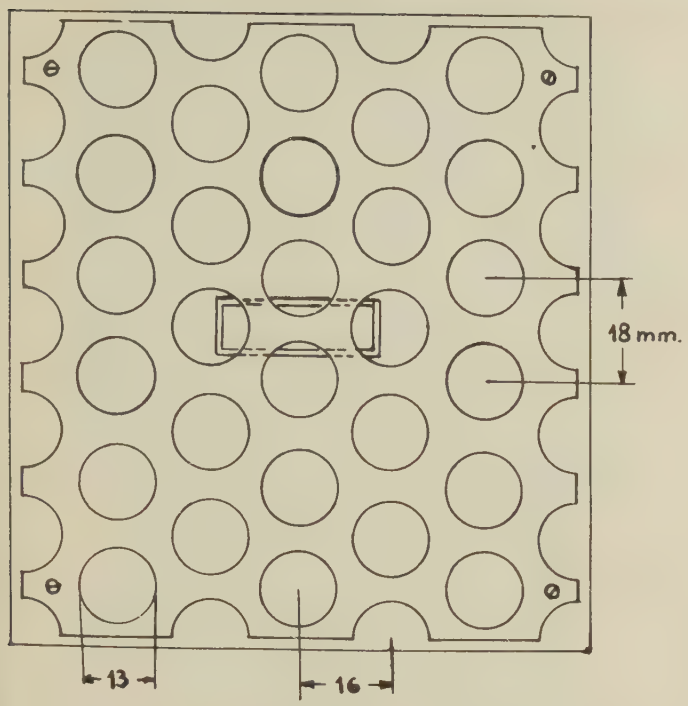

Fig. 4—Arrangement of the perforated grid in front of the waveguide aperture and screen.

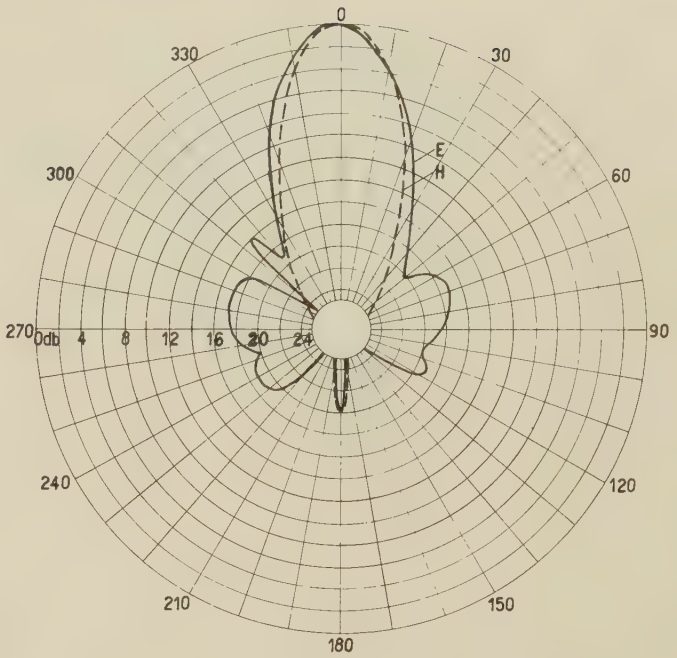

Fig. 5—Radiation pattern of the array of Fig. 4 in the H and E plane.

flecting sheet consisting of a conducting plate with equal holes uniformly spaced (13 mm diam), as shown in Fig. 4, gives a power gain of 18.5 db and a half-width of approximately 18° in both planes. Fig. 5 indicates the radiation pattern in polar coordinates. Sheet and screen measure 23×24 cm and have a resonance distance of $l_r = 14$ mm. The measured radiation pattern (main lobe) is similar to the calculated curve 3 in Fig. 2, and also corresponds approximately to the calculated reflection factor of such a perforated grid.[5]

As regards the second resonance distance $l_r = 30$ mm, directivity still increases but the side lobes become greater, as may be determined from (3).

Forms of Construction

In practice all forms of partially-reflecting sheets may be used. The choice depends to a great extent on the wavelength and use of the array. For decimeter and meter waves, reflecting sheets of perforated or wire grids with low wind resistance, may be used, whereas for centimeter waves closed sheets are preferable. These sheets can be made of low-loss insulating material and a sprayed, homogeneous, semipermeable metal coating, or with glued strips or disks of metal foil.

The reflection coefficient should lie between about $p_0 = 0.7$ and 0.9. Smaller values show little effect and larger values often produce the disadvantages of high loss, excessive tolerance, and great dependence on frequency. The reflection coefficient should increase for angles of incidence that deviate from the normal direction.

There are two possibilities of further improving array characteristics. Primarily, the amplitude distribution of the radiating sheet may be influenced by different reflection factors. Illumination is improved when the sheet produces strong reflection in its center and weaker reflection toward the margin. The choice of an appropriate taper depends on the nature of the sheet, its over-all size, and the excitation. The composition of inhomogeneous sheets is also important and diffraction can be used to improve directivity, for instance, on the capacitive strip-grating.[6]

Secondly, lateral radiation, which occurs principally in smaller systems, may be reduced by completely or partly covering the sides with metal. This produces a cavity which is excited by the antenna in its interior and which is coupled to free space by the partially reflecting front sheet. The number of modes excited in the enclosed space, and their configuration, depends on the nature and location of the exciting antenna (or antennas), and on the dimensions of the cavity.

Fig. 6 (a) is a sketch of a rectangular cavity excited in the principal TE_{10} mode by a waveguide aperture in the back screen. Fig. 6 (b) is a sectional view of a simplified distribution of the electric field corresponding to the second resonance distance of the sheet; the standing-wave distribution formed between back screen and front sheet is shown with a zero plane in the middle. Due to the presence of the metal side screens, the wave-

[5] J. C. Simon, "Etudes de la diffraction des ecrans plans et application aux lentilles hertziennes," *Ann. de Radioelect.*, vol. 6, p. 205; July, 1951.

[6] G. von Trentini, "Bündelung elektrischer wellen durch leitscheiben," *Z. angew. Phys.*, vol. 6, p. 462; October, 1954.

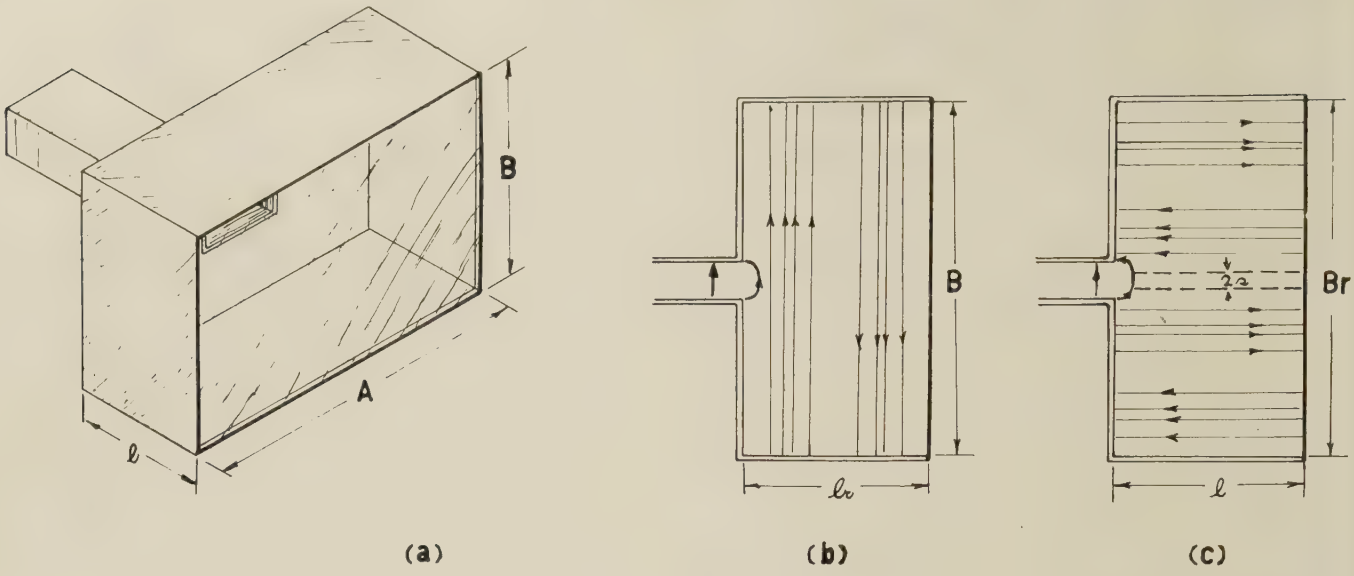

Fig. 6—Reflex-cavity antenna with approximated E-field distributions.

length within the cavity is somewhat larger than without walls, and the resonance distance l_r increases correspondingly. However, this influence is noticeable only with a small cavity in which the coupling of the waveguide also modifies the resonance distance to a slight extent.

As long as higher modes remain suppressed, the directivity of such a "reflex-cavity antenna" will increase with increasing distances of the side walls and with a consequent enlargement of the sheet and radiating aperture. Depending on the nature of excitation, other modes may however be excited along the dimension B. The TE_{10} mode distribution is to be preferred over the TE_{30} or TM_{11} mode. Fig. 6 (c) shows the approximate distribution of such a mode, the resonance of which has to be prevented for this affiliation. The resonance may be expected to occur at a side wall distance of

$$B_r \simeq n \frac{\lambda}{\sqrt{1-\left(\frac{\lambda}{2A}\right)^2}} + 2s, \quad n = 1, 2, 3, \cdots. \quad (9)$$

Depending on the field distribution, the exciting center is displaced a certain distance s (in this case about 1–2 mm) from the center of the waveguide. It should be noted also that one of the reflecting walls for a mode along B is the partially reflecting front screen, so that (9) is only approximately valid; fortunately, the reflection coefficient may be expected to lie close to -1 near grazing incidence.

In addition to affecting the resonance distance, B also affects the impedance at the waveguide aperture and thus the matching of the cavity. Consequently, radiation of the array is subject to a periodically-varying influence as B is increased and a favorable length must be found empirically.

Test Models and Results

In the test arrangements described in the beginning, sizes are large in comparison with wavelength and the gain is relatively small compared to geometric area. Smaller models that have higher efficiency are more important for practical use.

Fig. 7 (next page) presents three methods of construction which give an effective area of over fifty per cent.

The reflex antenna shown in the middle of Fig. 7 consists of a waveguide aperture (22.9×10.2 mm) in a reflecting screen (63×63 mm) and a grid of 6 parallel wires (58 mm long; $2\rho = 1.5$ mm; $d = 12$ mm). The resonance distance is $l_r = 14.5$ mm and two of the sides are closed by two adjacent wires ($A = 74$ mm; $2\rho = 1.5$ mm; $d = 6$ mm). The gain is approximately 14.3 db and the beamwidth in the H plane is 31.6° (3 db) and 58.5° (10 db), and in the E plane 37° and 63°, respectively. The side lobes in the two planes are -14 and -13 db. This system is also convenient for decimeter waves, excitation being produced by a dipole and the reflecting screen being replaced by slightly separated parallel bars, or by a fine mesh wire screen.

In the reflex antenna shown in the lower part of Fig. 7 reflection of the capacitive sheet is tapered. The antenna consists of a waveguide aperture, a reflecting screen (96×82 mm), and a polystyrene plate 1.8 mm thick with thin brass disks, 12 mm in diameter, glued to it. Their separation is around 15 mm in the center and 18 mm at the edge. Two side walls serve to hold the plate with the disks at a resonance distance of $l_r = 18.5$ mm. This reflex antenna has a gain of approximately 17.2 db. In the H plane the 3-db width is 20.5°, and the 10-db width is 39.9°. In the E plane the 3-db width is 22°, and the 10-db width, 42°. The side lobes amount to less than -14 db.

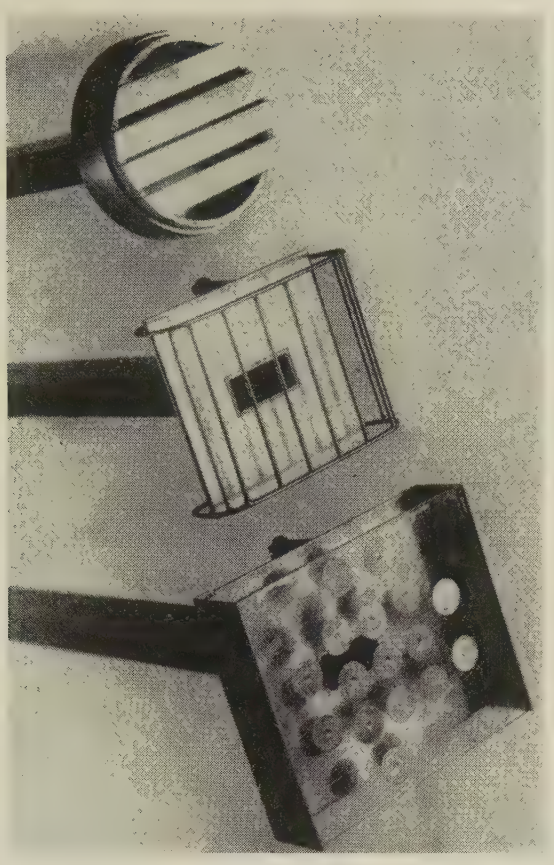

Fig. 7—Reflex antennas for $\lambda = 3.2$ cm.

The upper part of Fig. 7 shows a closed reflex-cavity antenna with tapered reflection. It consists of two telescoped brass tubes. The tube having the larger diameter (55/60 mm) is closed by a metal screen in the middle of which the waveguide ends. The tube having the lesser diameter (50/55 mm) is closed in front by four brass strips, 8 mm wide, placed perpendicularly to the electric vector; these brass strips are 0.8 mm thick and are spaced apart 1 mm and 2.8 mm, respectively. The (adjustable) resonance distance is $l_r = 18$ mm. This antenna has a gain of about 14 db and its radiation pattern is shown in polar coordinates in Fig. 8.

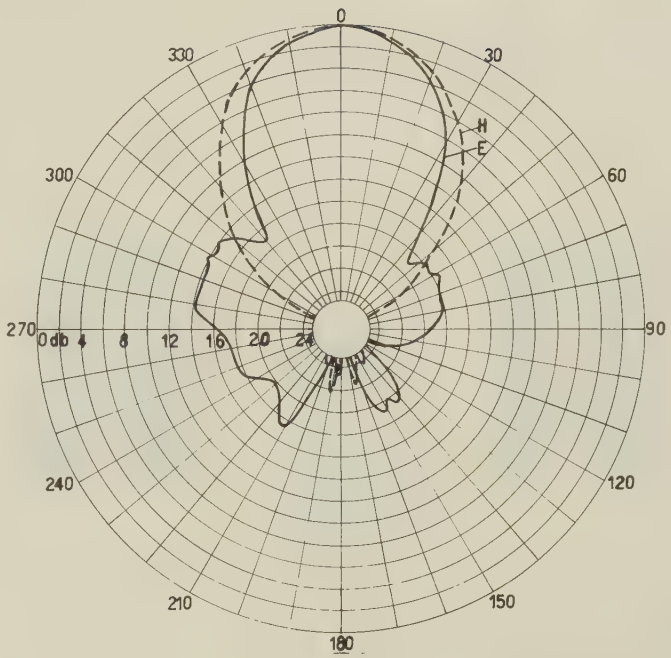

Fig. 8—Measured radiation pattern of the reflex-cavity antenna in the H and E plane.

To improve the match of the antenna to the waveguide, all models can be provided with an inductive diaphragm in the opening plane of the exciting waveguide. In the antenna just described, a diaphragm 14.8 mm wide gives a vswr of 1.05:1, and the antenna efficiency is comparable to that of a horn-type antenna. However, with an approximately equal aperture, the length of the reflex antenna is appreciably shorter than that of the horn antenna.

Of course, a group of these arrays may be fed from a common transmission line, or several distributed antennas may excite a single reflecting sheet. If radiation is to be effected in different directions, various partially-reflecting sheets may surround the antenna. Finally, the possibility exists of exciting other modes, thus producing additional radiation and polarization properties of the reflex-cavity antenna.

Contributors

Leroy R. Alldredge (M'46) was born in Mesa, Ariz., on February 6, 1917. He received the B.S. and M.S. degrees in physics from the University of Arizona in 1939 and 1940, the M.S. degree in engineering science from Harvard University in 1953, and the Ph.D. degree in physics from the University of Maryland in 1955.

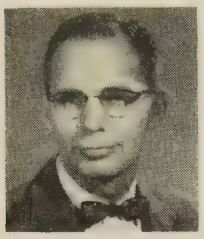

L. R. Alldredge

He served as instructor in physics at the University of Arizona in 1940 and 1941. He was a federal radio inspector for the F.C.C. from 1941 to 1944, and a radio engineer for Carnegie Institute of Washington, D.T.M., in 1944–1945. From 1945 to 1955 he was a physicist and division chief at the Naval Ordnance Laboratory. He joined the staff of the Communications Group, Intelligence Division of ORO, in July, 1955.

Dr. Alldredge is a member of Phi Kappa Phi, Sigma Xi, and the Terrestrial Magnetism and Electricity Section of the American Geophysical Union.

❖

David Carter (A'51) was born in New York, N. Y., in 1920. He received the B.E.E. degree, cum laude, from the College of the City of New York in January, 1945, and the Ph.D. degree in physics from Stanford University in March, 1951. During 1949–1951 he was awarded an RCA Fellowship for research at the Microwave Laboratory, Stanford University. At Stanford, he also worked as a teaching assistant in the physics department from 1947–1949.

D. Carter

During 1945–1947 he worked as electronics engineer at the Argonne National Laboratory and Hallicrafters Inc., Chicago, Ill., and taught at the Radio-Television Institute in New York City.

Dr. Carter was assistant professor of electrical engineering at New York University throughout 1951 and 1952, and also taught, part-time, at the Illinois Institute of Technology and UCLA extension in San Diego, Calif.

From 1952 to 1955 he worked on microwave antennas and operations analysis for Convair, San Diego, as senior research engineer and then as design specialist. Since 1955, he has been associate professor at San Jose State College. Concurrently he is consultant to the Antenna Systems Laboratory of Stanford Research Institute.

Maurice G. Chernin was born on June 21, 1923 in El Paso, Texas. He received the B.S. degree in electrical engineering from the University of Texas in 1944, and the M.S. degree, also in electrical engineering, from Stanford University in 1947.

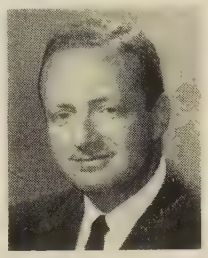

M. G. Chernin

He served in the United States Navy during World War II, working primarily on navigation, tactical radar, and attack boats. From 1947 through 1951, he was employed by the Airborne Instruments Laboratory, Inc. In 1951, he worked for the Armed Forces Security Agency. Since 1952 he has been employed by the Hughes Aircraft Company.

Mr. Chernin's main fields of experience have been in ground control intercept radar, moving target indicator, strategic bombing radar, and microwave antenna research. During the Airlift of 1948, he participated in establishing radar traffic control of allied aircraft entering and leaving Berlin, Germany. This was accomplished by the use of both a long range MTI ground radar and a radar flight control room.

❖

Robert S. Elliott (A'51–SM'53) was born in Brooklyn, N. Y., on March 9, 1921. He was a Pulitzer Scholar at Columbia University, New York, N. Y., where he received the A.B. degree in 1942 and the B.S. degree in 1943.

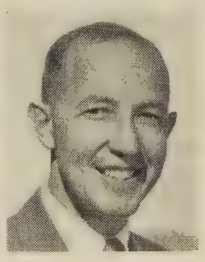

R. S. Elliott

From 1943–46, he was employed by the applied physics laboratory at Columbia, serving as a junior engineer on problems in radar, guided missiles, and the proximity fuse. In 1946 he became a member of the electrical engineering staff at the University of Illinois, where his duties included undergraduate and graduate teaching and research in antennas and microwave tubes. While at Illinois he received the M.S. degree in 1947 and the Ph.D. degree in 1952.

Summer employment in the antenna groups at Sperry in 1949 and North American in 1950 supplemented his Illinois employment. Upon leaving Illinois in 1952, Dr. Elliott served one year of active duty in the U. S. Navy and then joined the technical staff of the Hughes Aircraft Company, where he was in charge of the antenna research section of the microwave laboratory. At Hughes, Dr. Elliott specialized in surface wave antennas and uhf arrays. He is presently Technical Director and Vice-President of Rantec Corporation.

He is a member of Tau Beta Pi and Sigma Xi.

❖

Mohamed A. H. El-Said (SM'48) was born in Aga, Egypt, in May, 1916. He was graduated from Fouad University in Cairo in 1938, and was appointed to the faculty of engineering. In 1943, he received the M.Sc. degree and in 1944, the Ph.D. degree.

M. A. H. El-Said

Dr. El-Said was engaged in an engineering mission to England and the United States for the Egyptian government through a fellowship from 1945 to 1948. This project was jointly sponsored by the Marconi Wireless Telegraph Company in England, and the Westinghouse Electric Corporation in the United States. His main interest was theory and practice of electronic instrumentation in which he contributed a new type of electronic wattmeter.

Since 1949, he has occupied the position of assistant professor of radio engineering at Cairo University, and was recently assigned by the National Research Council to investigate the geophysical prospection of underground water by radio methods.

❖

Bob M. Fannin (A'49–SM'55) was born June 9, 1922, in Midland, Tex. He received the B.S. and M.S. degrees in electrical engineering from the University of Texas in 1944 and 1947, respectively. From March, 1944, until July, 1946, he served as an electronics officer in the U. S. Navy.

B. M. Fannin

In 1948, he became a research associate in the Electrical Engineering School of Cornell University. From 1951 until July, 1956, he was with the Electrical Engineering Research Laboratory, University of Texas, as a research engineer. At both Cornell University and the University of Texas, he was engaged primarily in tropospheric propagation studies.

In 1956, he received the Ph.D. degree from the University of Texas, and became a member of the teaching and research staff of the electrical engineering department of the University of New Mexico, August that year.

Coleman Goatley (A'55) was born in Tell City, Ind., on November 27, 1927. He served in the U. S. Navy from 1945 to 1950. In 1950 he re-entered the University of the South and in 1952 received the B.S. degree in physics.

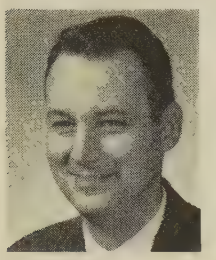

C. Goatley

Following graduation he joined the research department of the International Harvester Company, Refrigeration Division, where he was engaged in instrumentation of facilities for ballistic measurements and the evaluation and application of measurement data to trajectory computation.

In 1953 Mr. Goatley joined Melpar, Inc., Falls City, Va., where he has been primarily engaged in research and development work on microwave antennas. He is at present serving as staff assistant to the chief engineer.

❖

Francis D. Green, Jr. was born in Rockville, Conn., on October 26, 1930. He attended the University of Connecticut from 1948 to 1949, the George Washington University in 1955, and the University of Virginia in 1956.

F. D. Green, Jr.

He entered the United States Air Force in 1950 and received electronic training at this time. He maintained G.C.A. Radar Equipment until January, 1954. He joined the staff at Melpar, Inc., Falls Church, Va., in February, 1954, where, since, he has been engaged in antenna research and development.

❖

Paul T. Hutchison (S'47–A'49) was born in Tupelo, Miss., on November 2, 1922. He graduated from Mississippi State College with the B.S. degree in electrical engineering, and from the California Institute of Technology in 1947.

P. T. Hutchison

During World War II, Mr. Hutchison attended the Navy radar school at the Massachusetts Institute of Technology. From 1947–1954 he taught electrical engineering at Mississippi State College and also worked in the the microwave section in the Raytheon Manufacturing Company. At present, he is serving as assistant professor of electrical engineering at the Georgia Institute of Technology, while pursuing a course toward the Ph.D. degree in electrical engineering.

Samuel N. Karp was born in Brooklyn, N. Y., on February 13, 1924. He received the A.B. degree from Brooklyn College in 1944, and the M.Sc. and Ph.D. degrees in 1945 and 1948 from Brown University.

S. N. Karp

During his stay at Brown University he served as a research assistant and later as a research associate working in compressible fluid theory, especially the theory of oscillating airfoils. In 1948 he joined the Mathematics Research Group at New York University as a senior research scientist working on problems of electromagnetic theory. He is now a research assistant professor in the Division of Electromagnetic Research of the Institute of Mathematical Sciences at N.Y.U.

Dr. Karp is a member of Pi Mu Epsilon, Sigma Xi, and the American Mathematical Society.

❖

Phyllis A. Kennedy was born in Needham, Mass., on March 13, 1928. She received the A.B. degree in physics from Mount Holyoke College, South Hadley, Mass., in 1949 and became associated with the Division of Engineering and Applied Physics at Harvard University, Cambridge, Mass., where she is currently a member of the research staff.

P. A. Kennedy

She has been working on antenna problems under the direction of Prof. Ronold King, and has published several reports.

Miss Kennedy is a member of the Federation of American Scientists.

❖

Louis A. Kurtz (S'44–A'46–M'55) was born on March 13, 1923 in Long Beach, Calif. He received the B.S. degree in 1945 and the M.S. degree in 1951 from the University of California in Berkeley. He was a teaching assistant at the University of California from 1947 to 1949, as well as a research engineer for the U. S. Navy Antenna Project at the University.

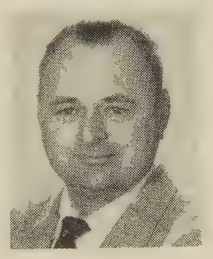

L. A. Kurtz

In 1949 Mr. Kurtz was employed by the Dalmo Victor Company as a development engineer. Following this, he became a member of the technical staff of the Microwave Laboratory, Hughes Aircraft Company, where he was engaged in the development of linear and two-dimensional slot arrays, phase shifters, hybrid junctions, and other microwave antennas and components. Mr. Kurtz is presently head of the microwave Antenna Department of Rantec Corporation.

He is an associate member of Sigma Xi.

❖

Alfred Leitner was born in Austria, on November 3, 1921. He came to the United States in 1938. He received the B.A. degree in physics from the University of Buffalo in 1944, and the Ph.D. degree in mathematical physics from Yale University in 1948.

A. Leitner

He spent four years as a research scientist with the Electromagnetic Division of the Institute of Mathematical Sciences at New York University. In 1951 he joined the department of physics at Michigan State University, where he is an associate professor.

Dr. Leitner has worked in the theory of special functions, such as the spheroidal wave functions and certain boundary value problems involving disks and prolate spheroidal structures; and in methodology of solving boundary value problems with a bent for applications, such as to the mathematical theory of antenna radiation.

Dr. Leitner is a member of the American Physical Society.

❖

Joe G. McCann (A'48–M'54) was born in Columbus, Ohio, in 1919. He received the B.A. degree in 1940 and the M.Sc. degree in physics in 1942, both from Ohio State University.

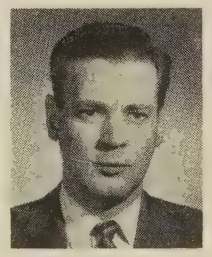

J. G. McCann

From 1942 to 1945 he was employed in the Centimeter Wave Section of Naval Research Laboratory. From 1945 to 1947 he was a design engineer at Submarine Signal Company, where he engaged in development work on search radars, microwave lens antennas, and automatic pattern recording equipment.

From 1947 to 1949 Mr. McCann was with Convair, working on microwave antennas and components for missile guidance projects. From 1949 to 1953 he was an engineering supervisor at Gilfillan Bros., Inc., where his duties included the supervision of design, production, and testing of all microwave equipment for GCA systems. Since 1953 he has been with Canoga Corporation in Van Nuys, Calif., where he is now chief engineer. In this capacity he is in charge of the engineering activities associated with the development of automatic tracking radar equipment used for missile range instrumentation and guidance.

James Radlow was born in 1925, in New York, N. Y. From 1940 to 1943, he attended City College of New York, and from 1943 to 1945, Brown University, in Providence, R. I. At the present time, he is completing work for the Ph.D. degree in applied mathematics at New York University.

JAMES RADLOW

Since 1953, Mr. Radlow has been a member of the electromagnetic research division at the Institute of Mathematical Sciences, New York University, where he is currently occupied with problems of diffraction by unidirectional screens.

He is a member of Phi Beta Kappa.

❖

O. J. Snow was born in Carrizozo, N. M., on March 11, 1919. He received the B.S. degree in physics from the Texas Technological College in 1940, and the M.S. degree in physics from the University of Pennsylvania in 1946. In 1940–41 he was engaged as laboratory instructor and graduate student in the physics department of Purdue University.

O. J. SNOW

From 1941 to 1943 he was employed by the Western Cartridge Company, in the field of spectrographic analysis, after which he moved to the Research Department of Philco Corporation, where he specialized in microwave research. He continued in the same field at the Frankford Arsenal and the Naval Research Laboratories in 1947 and 1948. In 1948, he joined the Naval Air Development Center, engaging in theoretical analyses related to guided missile systems, in particular, with contributions in the electromagnetic theory of radome performance. In 1955 he transferred to the Air Warfare Research Department of the same Center, where he is now participating in operational research.

❖

Robert J. Stegen (A'53) was born in Peru, Ill., in 1921. He received the B.S. degree in electrical engineering from the University of Illinois in 1942 and attended the California Institute of Technology during the summer of 1942. From 1942 to 1946 he was an engineering officer in the United States Naval Reserve. Following his discharge, he became a staff member and graduate student at the Electrical Engineering Research Laboratory, University of Illinois, and received the M.S. degree in electrical engineering in 1937. While at the University of Illinois, he was engaged in research at the higher microwave frequencies.

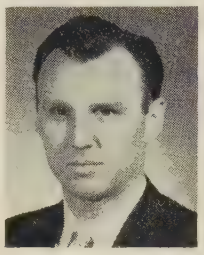

R. J. STEGEN

From 1947 to 1949 he was employed by Convair, San Diego, Calif. As head of the antenna development group, he did research design and development work on airplane, missile, and radar antennas and related microwave circuitry.

From 1949 to 1953 he was a member of the technical staff of Hughes Research and Development Laboratories, Culver City, Calif., and headed the antenna section development group. During this time he conducted research and development projects on slot arrays and antenna feed systems.

In 1953 he joined Canoga Corporation, where he is presently chief microwave and antenna engineer, concerned with the design, development, and production of microwave antennas and components, chiefly in the automatic tracking radar field.

Mr. Stegen is a member of Eta Kappa Nu, Honorary Electrical Engineering Society.

Giswalt von Trentini was born on April 21, 1913, in Munich, Germany. He graduated as Engineer-Physicist from the University and Institute of Technology in Munich in 1939. From 1940–1945 he was with the "Drahtlose Versuchstation Graefelfing," and later he was group engineer with E. N. K. Konstanz, where he specialized in the development of submarine radar camouflage and navigation systems.

G. VON TRENTINI

For a year and a half Mr. von Trentini was on the staff of the "Centre National D'Études des Telecommunicationes, Section Radio Marine," Grenoble, France. In 1948 he joined the "Labe, Instituto de Investigaciones Scientificas Y Tecnicas de Las Fuerzas Armadas," Buenos Aires, Argentina. There he works on radar antennas, waveguide design, and microwave research. Since 1953 he has also been a lecturer in the "Escuela Superior Tecnica del Ejercito," at Buenos Aires.

❖

Charles P. Wells was born January 23, 1909, in Tabor, Iowa. He received the B.A. degree with a major in mathematics from Simpson College, Indianola, Iowa, in 1930 and the Ph.D. in applied mathematics from Iowa State College in 1935.

C. P. WELLS

He served as instructor in mathematics at North Dakota State College from 1934 until 1938, when he went to Michigan State University, where he is now professor of mathematics in charge of applied mathematics.

During World War II, he was an operations analyst with the U. S. Air Force.

His primary interests are boundary value problems, electromagnetic theory, and in particular, antenna radiation problems.

Index to

IRE TRANSACTIONS

ON

ANTENNAS AND PROPAGATION

Volume AP-4, 1956

IRE Transactions on Antennas and Propagation

Index to Volume AP-4—1956

Contents

Forward and Multiple Scattering

Antenna Theory and Microwave Optics

Propagation in Doubly-Refracting Media

Summaries of the Panel Discussions

Appendix: Abstracts of the Contributed Papers

A-1 Contributed Papers—Scattering, Diffraction, and General Mathematical Papers

A-2 Contributed Papers—Multiple Scattering, Scattering from Rough Surfaces, and Transmission and Reflection Problems

Volume AP-4, Number 4, October, 1956

Index to Authors

Numbers refer to index numbers in contents listing.

Index to Technical Subjects

Nontechnical Index